Study of extensive air showers at sea level

Abdullah, Muzahim Mohammed

STUDY OF EXTENSIVE AIR SHOWERS AT SEA LEVEL

By

Muzahim Mohammed Abdullah, B.Sc. (Basrah), M. Sc. (Durham)

A thesis submitted to the University of Durham
for the degree of Doctor of Philosophy

Department of Physics,
Durham University, U.K.

JUNE, 1982

TO MY PARENTS

CONTENTS

ABSTRACT

Methods of determining the age parameter of air showers of size 10^4 - 10^7 particles which trigger the Durham E.A.S. array are discussed. The average age parameter of showers and their dependence on shower size and zenith angle have been studied. The result for the mean age parameter shows consistency with some previous work. Also, the data was used to determine the size spectrum in the range of shower size 2.10^4 - 2.10^7 particles in both differential and integral form. The results are then compared with other measurements. Except at very small and large shower size, the spectrum shows a close agreement with previous work assuming all showers obey the Greisen lateral structure function. Possible source directions of cosmic rays have been studied. A study of the arrival directions of showers in galactic coordinates has been carried out and in general indicates an isotropic distribution in arrival directions. In one particular direction an excess of events is observed at the level of 3.4 standard deviations. More experimental data is required to determine whether this is a real source or not. A search for particles that travel faster than light (tachyons) using an unshielded plastic scintillation detector has also been carried out. No evidence for the existence of tachyons has been found.

PREFACE

This thesis is an account of the work carried out by the author under the supervision of Dr. F. Ashton. He has shared, with his colleagues, in analysing and interpreting data concerning the average age parameter, size spectrum and arrival direction of extensive air showers. The author has also shared in the calibration of detectors, construction of electronics units and collecting, analysing and interpreting data from the tachyon experiment. Basic data concerning the sampled electron densities in individual extensive air showers was supplied by the group of Dr. M.G. Thompson.

Some preliminary results described in this thesis have been reported by Abdullah et al (1978, 1981).

ACKNOWLEDGEMENT

I am indebted to Professor A.W. Wolfendale, F.R.S., for the privilege of working in his laboratories and for his interest and support.

It is a pleasure to record a deep gratitude to my supervisor, Dr. F. Ashton, for his advice, guidance and many invaluable suggestions throughout this work. I wish to thank Dr. M.G.Thompson group for supplying Extensive Air Shower Data. I would like to thank all the members of Cosmic Ray Research group, both past and present, for their friendly co-operation and assistance, it has been a pleasure to work with them. In particular, I wish to express my sincere thanks to Dr. J. Fatemi and Mr. M. Enderby for many constructive discussions and valuable suggestions. I wish to extend my thanks to the Durham Computing Unit for the provision of computing facilities as well as for advice at various times. Thanks are due to Miss J. Morgan and Mr M. Spalding for their invaluable help in drawing the diagrams. Mrs. M. Bell is thanked for her careful typing of this thesis.

Finally, I am extremely grateful to my parents for their moral and financial support.

CHAPTER 1

THE COSMIC RADIATION

1.1 INTRODUCTION

Particles travelling at nearly the speed of light fall on the earth at all times and from all directions. These particles, the cosmic rays, have attracted the attention of investigators for more than six decades. The discovery of them activated man's resources to obtain an understanding of what they are, their physical properties and where they come from. Answers to such questions might lead us to a better understanding of the solar system and galaxy and perhaps even the Universe.

1.2 THE DISCOVERY OF THE RADIATION

The discovery of the existence of a naturally occurring penetrating radiation of unknown origin was demonstrated at the turn of the century by certain experiments on the conductivity of gases. The most likely explanation of the observed phenomena seemed to be that the radiation was due to radioactive materials in the earth. However, the balloon flights of Hess (1912) led him to conclude that the radiation was of extraterrestrial origin and the absence of significant changes in the ionization between day and night indicated that it did not emanate from the sun. At first it was assumed that the radiation was γ-rays due to its high penetrating power. In 1928-1929 however, Bothe and Kalhorster using a Geiger Muller counter, showed that a large proportion of the cosmic radiation in the lower atmospheric levels consisted of charged particles. The discovery of the latitude and east-west effect by Clay (1927), Johnson (1933) conclusively showed that the cosmic ray intensity coming from the east

was less than that coming from the west. With the advent of high altitude balloon flights the presence of a significant proportion of protons were observed in the primary flux (about 90%) in 1948. It was found later that heavy nuclei were also present. The development in particles detectors led to the discovery of many new particles such as the positron, Anderson (1932), which had been predicted by Dirac and the pion by Powell and his co-workers in 1947, which proved to be the particle proposed by Yukawa. Further searches disclosed the existence of both charged and neutral kaons and various hyperons. Primary electrons were discovered in 1961 in balloon experiments. Their existence in the galaxy and radio sources had already been inferred from the synchrotron nature of radio-emission.

Cosmic X-rays and discrete X-ray sources were discovered in 1962, first in rocket experiments and later with balloons. Investigation of the deep underground muon intensity at a depth of 3 Km below ground led to the setting up of high energy cosmic ray neutrino experiments. The first neutrino interactions were observed in 1965. A great many possible sources and acceleration processes of cosmic rays have been identified. Their relative importance for generating different cosmic ray components is still not clear. It also appears now that the highest energy cosmic ray particles may be of extragalactic origin.

1.3 SIGNIFICANCE OF COSMIC RAY STUDIES

For several decades cosmic ray research concentrated on the nuclear physics aspects of the particle beam and many important discoveries were made. Notably, the identification of the positron, the muon, the pion and the strange particles. More recently, cosmic ray studies have expanded so as to cover both elementary particles physics and astrophysics. Current fundamental problems in particle physics are whether quarks, magnetic monopoles or tachyons exist as

real entities. If they do exist then it is likely that any of these objects would be either incident on the earth in the primary cosmic ray flux or be produced in the atmosphere in very high energy primary cosmic ray interactions. Recently Fegan (1981) has presented evidence that a finite flux of tachyons may be produced in high energy cosmic ray interactions. A search for tachyons in the sea level cosmic ray flux is described by the author in Chapter 7. Astrophysicists are concerned with the origin of primary cosmic rays, the processes required in possible sources and the interstellar medium to explain the energy spectrum, mass composition and the variation of primary cosmic ray flux incident on the earth. Perhaps the most interesting problem is the study of mechanisms by which primary particles can be generated and accelerated to such energies as seen in cosmic rays.

1.4 INTENSITY OF PRIMARY COSMIC RAYS

Despite the difficulties of measuring the primary cosmic ray flux, a wealth of data has been acquired. Because of the wide range of energy and intensities of the cosmic ray primaries, it is not possible to measure the whole range of the energy spectrum in a single experiment. Wolfendale (1973) summarised measurements of the primary cosmic ray spectrum and the result of this summary is shown in figure 1.1. There are four different ranges of the spectrum to be considered. Measurements in the energy range from a few hundred MeV to $\sim 10^3$ GeV have been mainly undertaken using satellites and balloons (figure 1.1). In this range the spectrum is strongly influenced by modulation in the solar system. The lowest intensities are observed at times of high solar activity and this may impose an asymmetry in the arrival direction of these particles. The spectral form of the incident cosmic radiation can be expressed as a power law, Greisen (1965),

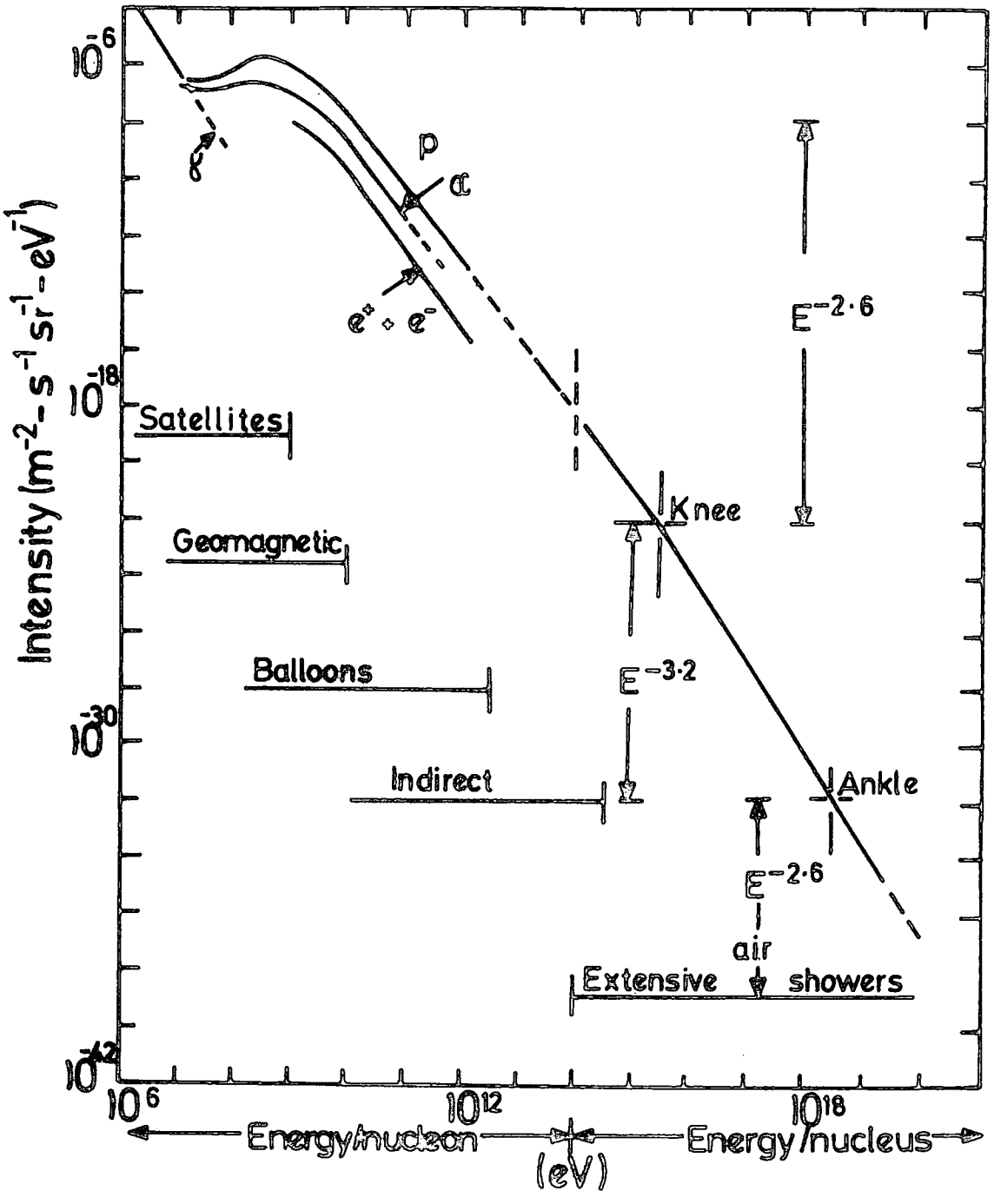

Figure 1.1 : Summary of measurements of the primary spectrum of protons and nuclei in the cosmic radiation (After Wolfendale, 1973).

Wolfendale (1973). In the energy range $10^{10} < E < 10^{15}$ eV, it has the form

$$I(>E) = K E^{-\gamma}$$

$$= A E^{-2.6} \quad m^{-2} \text{ sec}^{-1} \text{ sr}^{-1}$$

where E is measured in eV. In the range 10^{15} eV $< E < 10^{18}$ eV

$$I(>E) = B E^{-3.2} \quad m^{-2} \text{ sec}^{-1} \text{ sr}^{-1}$$

and for $E > 10^{18}$ eV

$$I(>E) = C E^{-2.6} \quad m^{-2} \text{ sec}^{-1} \text{ sr}^{-1}$$

Direct measurements have been carried out only to 10^{14} eV but have not met with universal acceptance. Above this value of 10^{14} eV, existensive air showers have provided all the information. At these energies, the atmosphere becomes a part of the detector system and makes it feasible to extend the energy measurements out to 10^{20} eV. The breaks occurring in the spectrum at 10^{15} eV and 10^{18} eV where the position of what are called the "knee" and "ankle", are generally interpreted as being caused by the escape of the galactic component from the galaxy and the penetration of the extragalactic component into the galaxy respectively. Figure 1.2 shows the integral spectrum of cosmic ray primaries as summarised by Kempa et al (1974) from available EAS studies. The most important aspect of this spectrum is the evidence of a "bump" in the region 10^{14} - 10^{15} eV as shown in the figure. The existence of the ankle in this summary is unclear. The best fitted line to the spectrum has been plotted in the differential form as seen in Figure 1.3 and compared with the results of other workers, as indicated in the figure. For the cosmic ray energy specturm $\geq 10^{19}$ eV, Berenzinky and Zatsepin (1969, 1971) have suggested that the cosmic rays are affected by their interaction with the isotropic flux of microwave photons that fill the

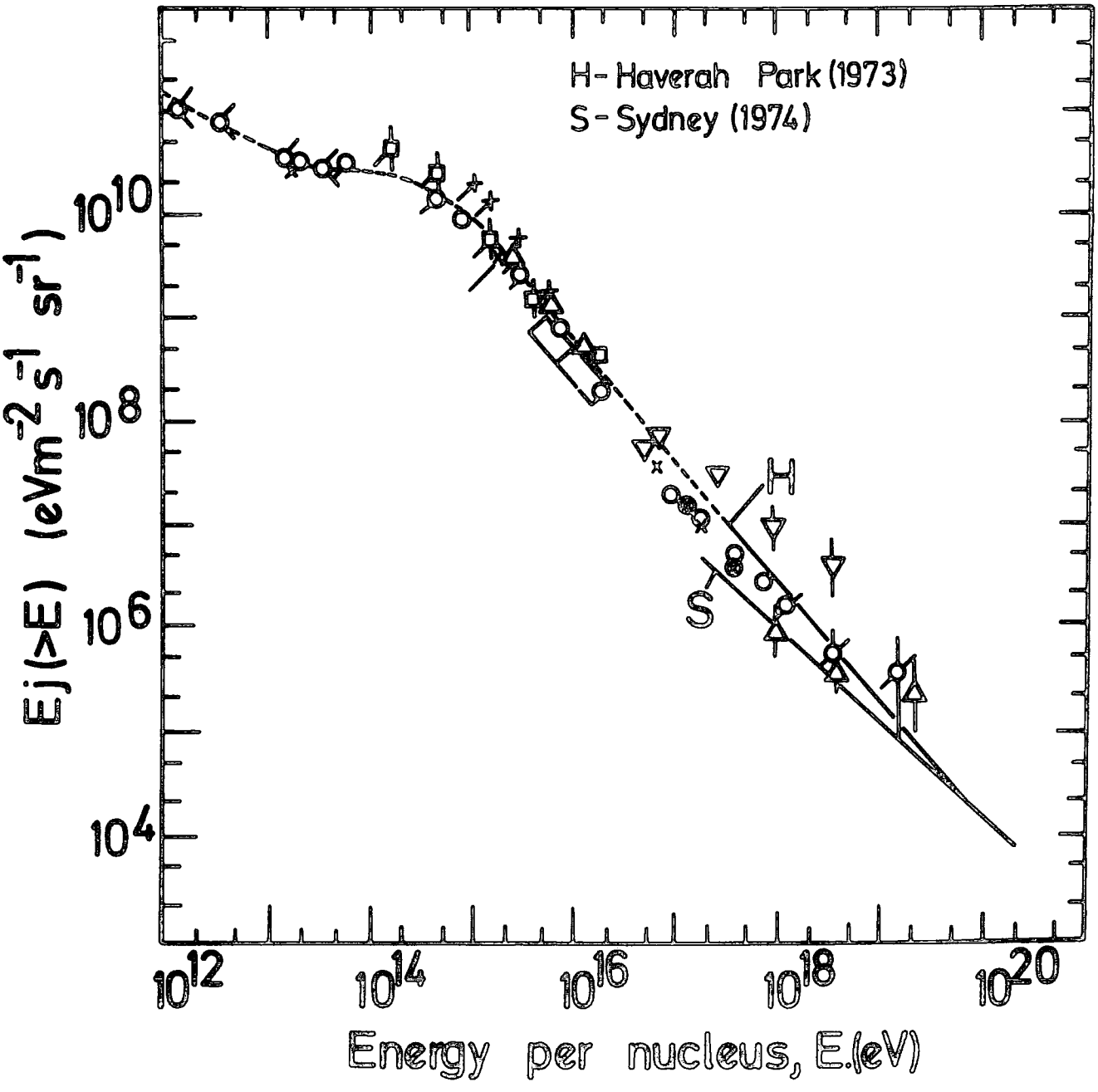

Figure 1.2: The integral primary cosmic ray spectrum. (After Kempa et al. (1974))

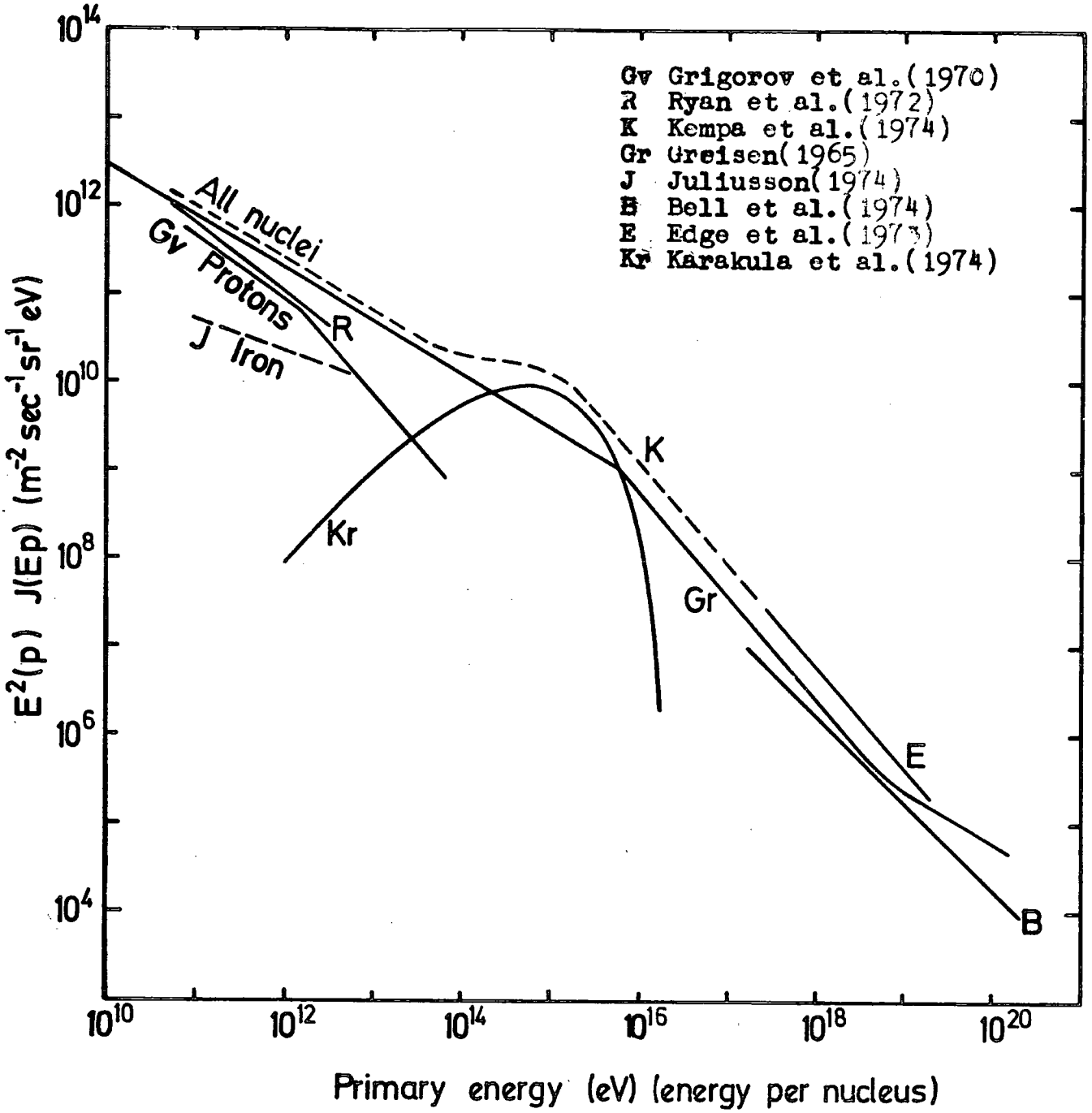

Figure 1.3: The differential energy spectrum of primary cosmic rays obtained from the results of various workers.

metagalaxy. After the discovery of the 2.7K^0 black body radiation in space, Greisen (1966) suggested that there should be a cut-off in the cosmic ray spectrum at about 6 x 10^{19} eV. However, this has not been confirmed. Hillas, in his summary (1975), pointed out that there is no such discontinuity in the spectrum up to approximately 10^{20} eV.

1.5 THE NATURE OF THE COSMIC RADIATION

Measurements of primary cosmic rays now extend up to about 10^{20} eV. In order to find out the origin of these particles, we must know their composition. Direct measurements of the composition have been made in the energy range 10^{10} - 10^{13} eV by using balloon's and satellites carrying emulsion stacks and ionisation calorimeters. The composition of the primary flux for $E_p \leqslant 100$ GeV is given in table 1.1 after Juliussen (1975) normalised to a percentage of the total. These figures depart from those of Ginzburg and Syrovatskii (1964) in the respect that the abundances clearly depend on energy. The increase in the abundance of iron with energy is probably due to the production mechanism of iron at the source. For higher energies the chemical composition is not certain. At lower energies the cosmic radiation is strongly modulated by the outward flowing hot solar plasma called the "solarwind". Figure 1.4 shows the abundance of elements in cosmic rays in the range of a few hundred MeV per nucleon to about one GeV per nucleon for hydrogen up to iron as given by Meyer et al (1974). For comparison the solar system abundance are also shown in figure 1.4. A comparison between abundances in cosmic rays and the Universe shows that there is an excess of light (L) nuclei (Li, Be, and B), in cosmic rays which are believed to come from the fragmentation of heavy cosmic ray nuclei during their passage from the source through the interstellar medium. The observed relative abundance of L nuclei suggests that cosmic rays at least in the energy range where relative abundances have

TABLE 1.1 : Composition of cosmic rays at different primary energies (After Julliussen, 1975)

Atomic Number (Z)	Element	Primary kinetic energy per nucleus (eV)			
		10^{10}	10^{11}	10^{12}	10^{13}
1	Hydrogen	58 ± 5	47 ± 4	42 ± 6	24 ± 6
2	Helium	28 ± 3	25 ± 3	20 ± 3	15 ± 5
(3-5)	(Lithium-Boron) Light nuclei	1.2 ± 0.1	1.1 ± 0.1	0.6 ± 0.2	
(6-8)	(Carbon-Oxygen) Medium nuclei	7.1 ± 0.4	12.2 ± 0.8	14 ± 2	
(10-14)	(Neon-Silicon) Heavy nuclei	2.8 ± 0.2	6.7 ± 0.5	10 ± 1	
(16-24)	(Sulphur-Chromium) very heavy nuclei	1.2 ± 0.2	3.6 ± 0.4	4 + 1	
(26-28)	(Iron-Nickel) Iron group nuclei	1.2 ± 0.2	4.5 ± 0.5	10 ± 2	24 + 7
30	(Zinc) very very heavy nuclei		0.007±0.004		

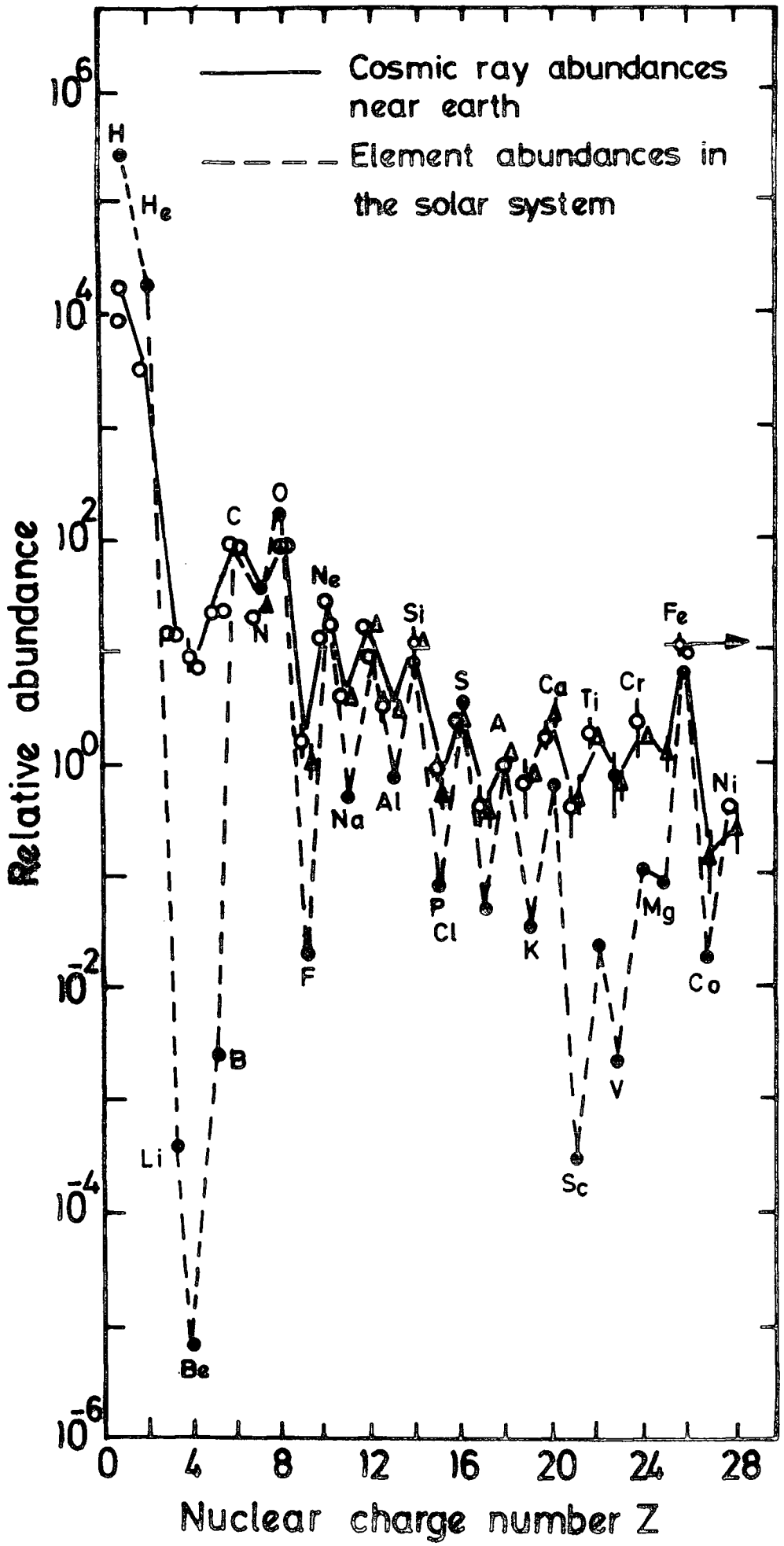

Figure 1.4 : Relative abundance of the elements from hydrogen to the iron group normalized to that of carbon (c = 100) (After Meyer et al, 1974).

been measured, have traversed ~ 2.5 g/cm^2 of interstellar hydrogen which corresponds to an average age for the cosmic rays of a few million years. The ratio of He^3 to all helium nuclei may also be used to estimate the amount of interstellar material traversed by cosmic rays.

1.6 PROPAGATION OF COSMIC RAYS THROUGH THE ATMOSPHERE-EXTENSIVE AIR SHOWERS

When a primary cosmic ray proton enters the atmosphere, on average it travels 70-80 g/cm ^{2} of air before it interacts with an air nucleus and then loses about 50% of its energy in the interaction. This means that the first interaction takes place on the average 10-30 Km above sea level. A series of interactions of the surviving primary particle with air nuclei produces many secondary particles. These in turn are capable of multiplying as they pass down through the atmosphere so that the total number of particles in the shower at sea level can be very large. Not only is the number very large but the particles are scattered over a wide area. The majority of the secondaries are pions. On average equal numbers of positive, negative and neutral pions are produced. Other particles such as K-mesons, hyperons, nucleons and antinucleons may also be produced. All the particles continue to travel on in direction very close to the original direction of the primary and can interact with air nuclei lower in the atmosphere, thus giving rise to more pions etc. at different depths. It is now known that this series of nuclear interactions produced by the surviving primary proton and produced pions largely controls the development of a shower and can be considered as its "backbone". The neutral pions decay almost instantaneously (mean life time $\simeq 10^{-15}$ sec) into two gamma-rays. From these photons, by the repeated operation of the processes of pair-production and of bremsstrahlung, the well known electron-photon cascade is built-up.

This large lateral spread of electrons produced by multiple Coulomb scattering enables a reasonably sized detector near sea level to respond to primaries incident on the top of the atmosphere over a large area, and the rate of detection of even the highest energy primaries is tolerable. This is in fact the only way of detecting primaries with energies in excess of 10^{15} eV. As the energy of the primary particles increases, the number of particles in the shower and the lateral extent of the shower increase and by measuring the number of particles in a shower, an estimate of the primary energy can be made. The charged pions also play an important role in EAS. Their longer lifetime (2×10^{-8} sec), means that at high energy they have a large probability of interacting with an air nucleons rather than decaying into a muon and a neutrino. The results of a pion-nucleons interaction are similar to those of proton interactions and more secondary pions, nucleons etc. are produced. The muons resulting from the decay of the charged pions have an even longer lifetime (2×10^{-6} sec), means that the muons have a high chance of reaching sea level without decay or interaction. Their greater mass than that of an electron (207 times) means that they are not scattered to such a large extent.

1.7 ORIGIN OF COSMIC RADIATION

Since the discovery of the cosmic radiation, the problem of the origin and the acceleration mechanism of these very high energy particles has been studied. There are basically three major regions in which the cosmic rays could be contained and be presumed to originate:-

(a) Solar Origin

(b) Galactic Origin

(c) Universe

In addition, one can consider sources that were, but are no longer, active. Contributions to the cosmic ray flux observed at the earth probably

come from all these mechanisms, but the identification of which is most prominent in different ranges of primary energy is of astrophysical importance. Energy requirements, mass composition, energy spectrum, gamma ray astronomy and arrival directions (see Chapter 6) studies, all provide pointers to the source regions.

(a) Solar Origin : It has been known for a long time that the sun can accelerate particles and sometimes it has been seriously suggested that most of our cosmic rays may be of solar origin and their intensity may be built up over long periods of time by storage around the planetary system. The idea started after an increase of cosmic ray intensity at the time of solar activity was observed. It indicated that there is an acceleration mechanism available on the sun which can produce particles with energies up to 10 GeV. Later, it was suggested by some workers that particles of higher energies also originate from the sun where their energies are acquired from the interplanetary magnetic field in a storage time of 10^3 -10^8 years before arriving at the earth. However, now one can give several obvious arguments against such a possibility. Solar particle events are associated mostly with visible flares and the chemical composition of the solar rays is different from that of galactic cosmic rays. Not only that, the magnetic fields of the solar system cannot contain the highest energy particles, that is above 10^2 GeV/nucleon. This would result in an anisotropy of the radiation and it is not observed. Therefore, the sun cannot be the only cosmic ray source and a powerful mechanism of particle acceleration is required.

(b) Galactic Origin : The assumption is that other stars like the sun in the galaxy (containing 10^{11} stars) generate cosmic rays. The required total observed flux would not be possible to produce. Therefore, we have to look for additional sources in other types of star. Several suggestions have been made. For example, stars such as magnetic variable

stars as well as novae and supernovae are considered. Current theories seem to favour supernovae because they seem to be capable of supplying the necessary energy. Supernovae are also believed to be rich in heavy elements and this is consistent with the measured cosmic ray composition. However, the energies reached by particles accelerated at their source of origin is likely to be less than the highest energy particles observed. A possible explanation for the highest energy particles observed is than an additional acceleration process is operative. This probably comes from the collision of cosmic ray particles with randomly moving magnetised gas clouds as they stream through the arms of the galaxy.

(c) Universe : In general the existence of the knee in the energy spectrum plot has been explained by the escape of the galactic component and the penetration of the extragalactic component. It has been suggested that extragalactic component may have an intensity of 10^{-3} 10^{-4} times that of the galactic component. It has also been suggested that very high energy cosmic ray particles producing EAS of size $> 10^6$ have an extragalactic origin, because their energies are too high to be confined within the galaxy by the galactic magnetic field. The galactic component may be limited at high energy by the size of the accelerating region and/or containment volume, to about 10^{15} eV. Therefore, they leak out from one galaxy into space and then enter other galaxies to contribute an extra galactic component to the cosmic ray flux.

1.8 SUMMARY

Starting with the investigation of the conductivity of gases in closed chambers, the subject of cosmic rays has, over the last six decades, come to have links with such diverse fields as nuclear physics, elementary particles physics, geophysics, astronomy, astrophysics

and solar physics. In cosmic ray studies fundamental contributions have been made in each of these fields. Most of the metastable fundamental particles and their important properties were discovered; important characteristics of high energy electromagnetic and nuclear collisions were established; an insight into the solar surface phenomena and the sun-earth relationships was obtained; information on the chemical composition of the sun and supernovae and on the matter and magnetic field distribution in the galaxy was provided and some important new aspects governing the basic stability of the galaxy were discovered. Cosmic rays will be studied for many years to come simply because they form a cheap high energy beam of particles, their continuing studies having two main aspects, nuclear physics and astrophysics. The study of the primary and secondary radiation provide a good opportunity for nuclear physics to investigate the characteristic of particles and the nature of high energy interactions. For astrophysics the origin of cosmic rays and the mechanism in which these particles are accelerated to such energies are their interest.

CHAPTER 2

DURHAM EXTENSIVE AIR SHOWER ARRAY

2.1 INTRODUCTION

An extensive air shower array of characteristic radius 60 m has been built around the Physics Department of Durham University. The array consists of 14 electron density sampling scintillation detectors which are classified according to the purpose each has been designed to perform :-

(a) The combined timing and shower density detectors.

(b) The shower density detectors.

Figure 2.1 shows the location of the particle detectors in the array. The areas and exact coordinates of the detectors are shown in table 2.1, using the centre of detector C as the origin and the line which goes through detector C and detector 52 is defined as the y-axis. Also, figure 2.1 shows the detectors are grouped according to their areas. The variation in detector area (0.75 m^2, 1.0 m^2, 1.6 m^2, 2.0 m^2) is mainly due to availability. The array has a triangular geometry and, wherever possible, detectors with the same areas have been placed at equivalent positions within the array to enhance the symmetry. Characteristic of all of the detectors is the similarity in how the scintillators are housed and figure 2.2 shows this. The boxes that contain the scintillators, photomultiplier tubes and associated electronics are made from wood and are weatherproofed. At one edge of each box containing a scintillator are situated the E.H.T. unit (section 2.5), the head amplifier (section 2.6) and the services box (section 2.7). In general, every detector consists of four photomultiplier tubes, viewing the plastic scintillator and in the case of the central and 2.0 m^2 detectors an additional fast photomultiplier

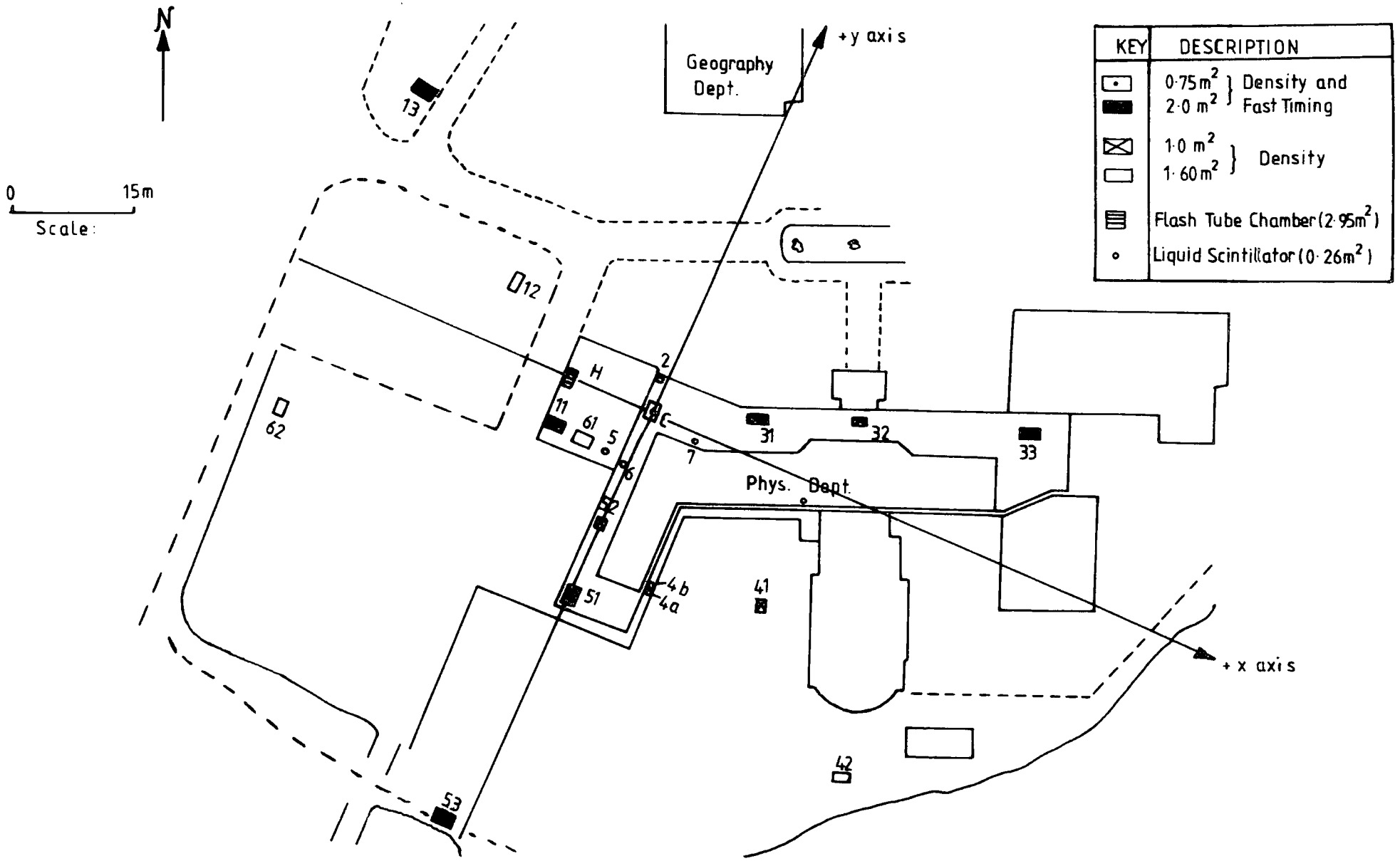

Figure 2.1 : Scale diagram of the Durham Extensive Air Shower Array.

Detector	C	Flash Tube Chamber H	11	13	31	33	51	53	12	42	61	62	32	41	52
x Coordinate (m)	0	-12.9	-12.1	-41.8	13.2	45.1	1.0	- 3.6	-22.9	39.1	- 8.7	-43.1	25.2	23.2	0
y Coordinate (m)	0	- 1.30	- 6.0	26.3	4.0	14.9	-27.1	-57.3	8.3	-33.1	- 5.8	-18.3	8.3	-16.6	-16.2
z Coordinate (m)	0	-12.2	- 4.9	-13.3	0.20	0.20	0.20	- 9.3	-13.1	- 9.1	- 4.9	-10.3	0.5	-11.3	0.5
Area (m^2)	0.75	2.95	2.0	2.0	2.0	2.0	2.0	2.0	1.60	1.60	1.60	1.60	1.0	1.0	1.0

Table 2.1 : Coordinates and areas of all detectors in the array; Z coordinate of flash tube chamber refers to the bottom of the chamber.

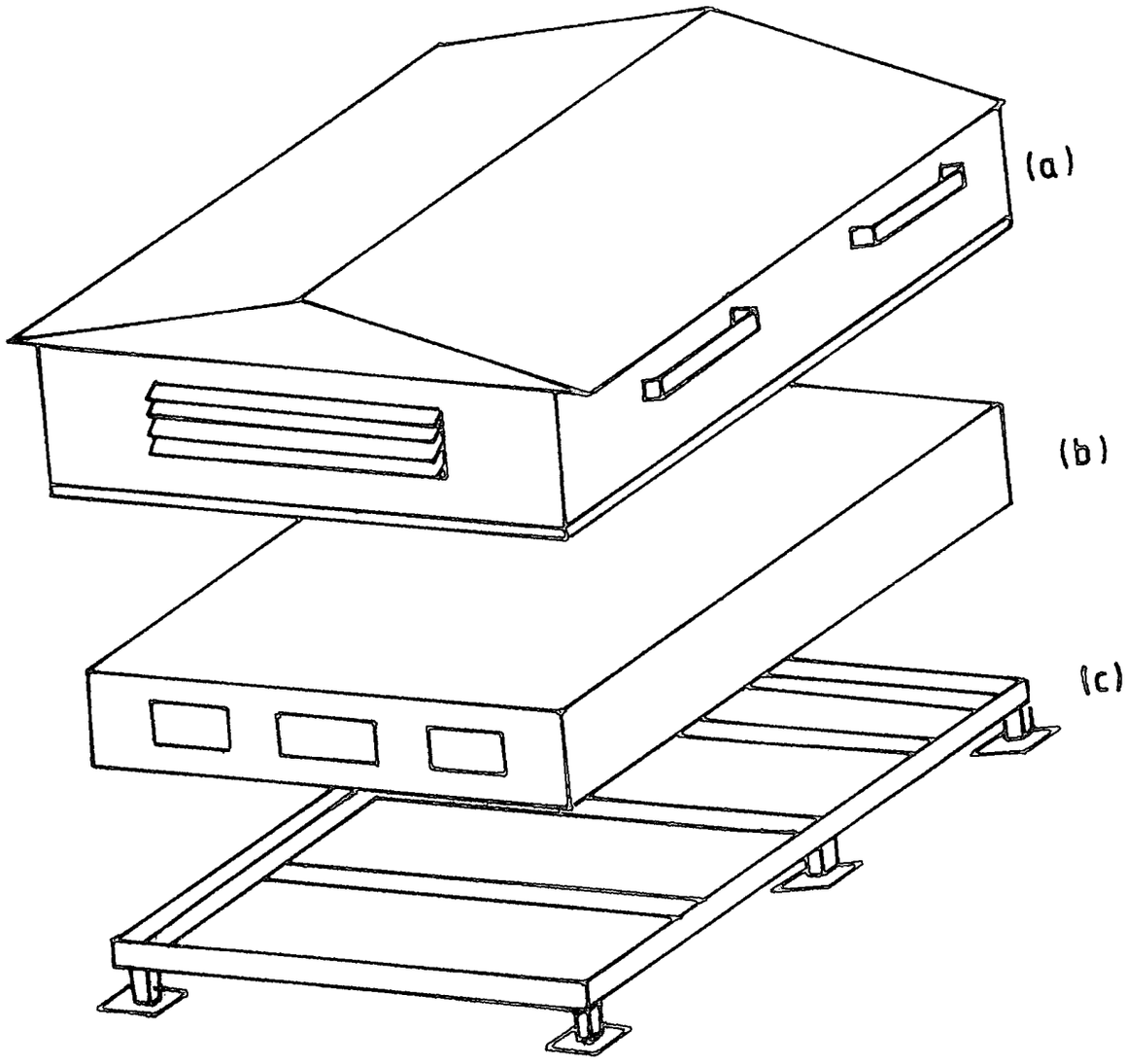

Figure 2.2 : A typical detector arrangement

(a) Weatherproofed Wooden hut

(b) Weatherproofed Wooden box containing scintillator and associated electronics.

(c) angle iron bed.

for timing measurements which enable the air shower arrival direction to be determined. All output pulses from the photomultiplier are sent to a four input adder, which sends the summed output pulse via 50 Ω coaxial cable to the cosmic ray laboratory. Once the signal has been returned to the laboratory, it is then passed to an analogue multiplexer and on to an oscilloscope where the output is photographed. The output of seven of the plastic scintillators are discriminated and passed to a coincidence unit which produce a trigger pulse for operation of the recording equipment and other apparatus.

2.2 TIMING AND SHOWER DENSITY DETECTORS

(a) The 2 m^2 Detectors (11, 31, 51, 13, 33, 53).

There are six 2 m^2 detectors in the array forming two triangle arrangements. One of them consists of detectors (11, 31, 51) and a coincidence between them and the central detector C is called the inner ring trigger. A coincidence between detectors (13, 33, 53) and the central detector C is called the outer ring trigger. Each detector is installed at the corner of an equilateral triangle forming the main array design. The three inner and outer timing detectors are on the circumference of a circle whose centre is detector C. Events could never have been established without them, they are the only detectors that have been designed to send timing measurement pulses to the laboratory. Each individual detector consists of a sheet of plastic scintillator coplanar with four photomultiplier tubes having five inch diameters. Two of the tubes are placed at one side of the plastic scintillator and the other two at the opposite side. In each detector a fast photomultiplier tube, having two inch diameter, is attached to one side of the plastic scintillator, halfway between two five inch tubes. Figure 2.3a shows these detector features.

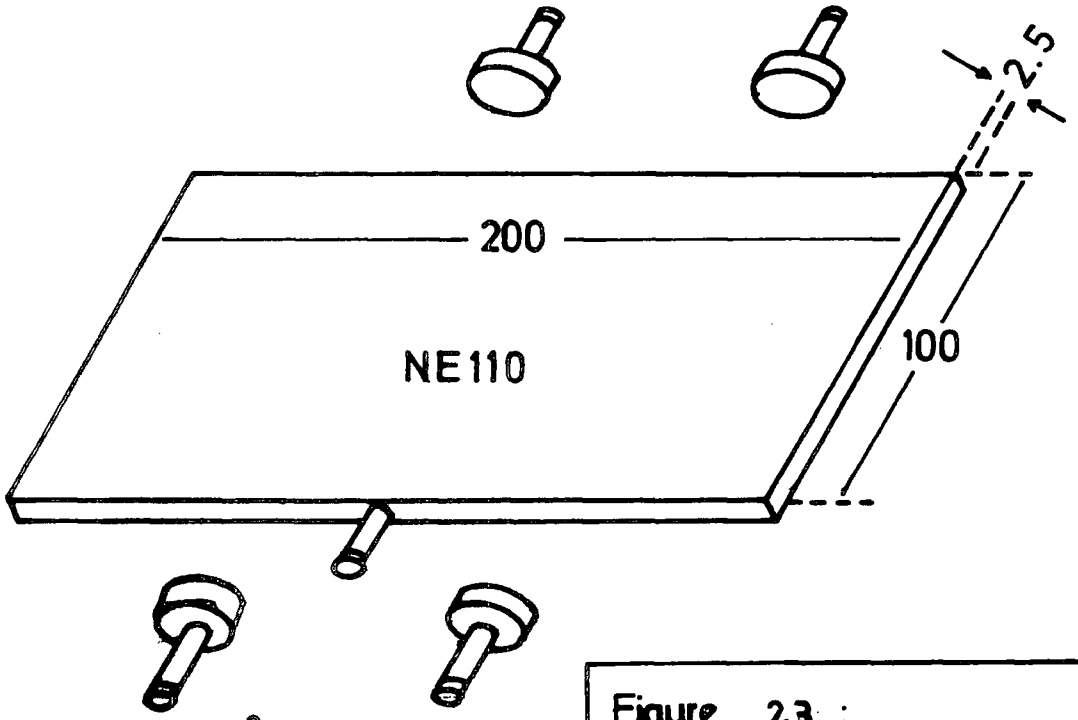

A $2m^2$ detector

(d)

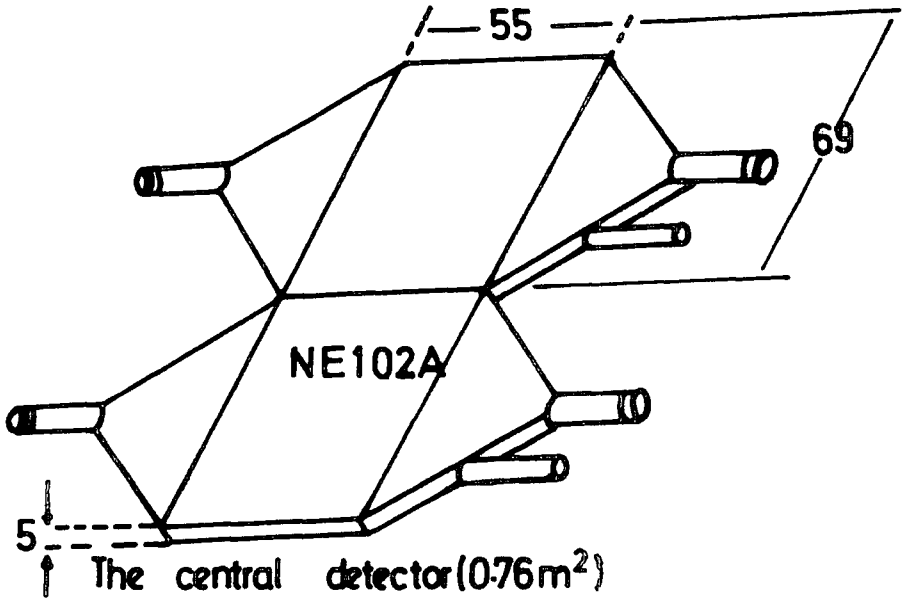

The central detector ($0.76m^2$)

Figure 2.3 :
The Array Scintillation Detectors
(All Dimensions in cm.)

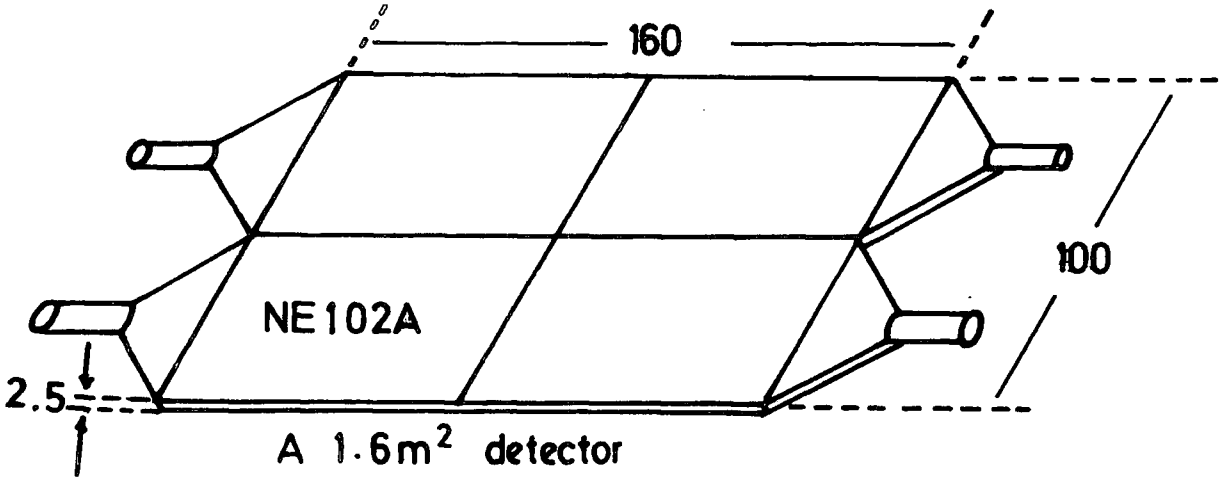

A $1.6m^2$ detector

(c)

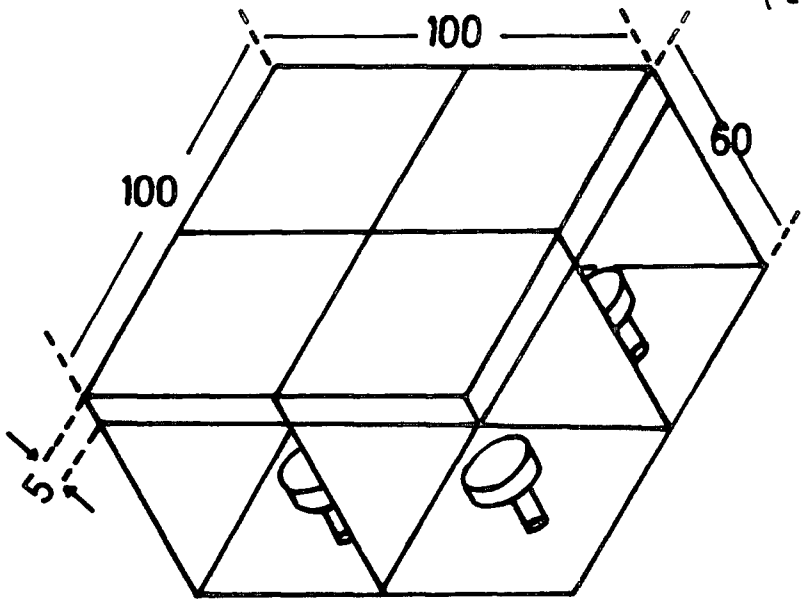

A $1m^2$ detector

(b) The Central Detector (C).

The central detector has a geometrical area of 0.75 m^2, and is located at the central position of the array. As shown in figure 2.3b, it consists of two separate rectangular slabs of 5 cm thick NE102A plastic scintillator viewed by two Phillips 53 AVP photomultipliers for density measurements. Also a fast timing tube Phillips 56 AVP is attached to the perspex light guide and gives the zero timing pulse with which the fast timing pulses from other detectors are referenced. These pulses are sent to the laboratory via a 50 Ω cable. The lengths of cable from the fast timing detectors are such that the fast timing signal from the central detector always arrives at the recording equipment before the fast timing pulses from the other detectors.

2.3 THE SHOWER DENSITY DETECTORS

Seven detectors are available to measure the particle density. Three of the seven shower density measuring detectors have an area of 1 m^2 each, the other four having an area of 1.6 m^2.

(a) The 1 m^2 Detectors (41, 52, 32)

Detectors of this area are located at about 25 m from the central detector. They are different from the other detectors in the respect that the photomultiplier tubes view the broad face of the 0.25 m^2 area of slab of scintillator. Figure 2.3c shows they consist of four individually light proofed quarters viewed by four photomultipliers. Pulses from independent quarters are summed in a mixer amplifier at the detector and are sent to the laboratory via a 50 Ω cable.

(b) The 1.6 m^2 Detectors (42, 12, 62, 61)

These are the detectors represented by numbers 42, 12, 62 and 61. The first three of these detectors are located outside the building,

while the last one is on the roof of the gallery inside the cosmic ray laboratory. Individual quarters of this type of detector consist of 0.4 m^2 area rectangular slabs of plastic scintillator with a photomultiplier tube (Phillips 53 AVP) joined to the NE102A scintillator plastic by way of a perspex light guide. Like the 1.0 m^2 detectors, each quarter operates independent of the other three. One single output from the four quarters is achieved using a mixer amplifier. Figure 2.3d shows how the scintillators are situated in relation to each other.

In the above detectors an extensive air shower event is recorded when particles in the shower simultaneously traverse the scintillators in the array. The particles (mainly electrons) lose energy in ionisation and excitation of molecules in their passage through the phosphor. Some of this energy is converted into photons and then into electrical signals which are summed and amplified in a head unit. There are two sets of pulses to represent each air shower event. One set comprises information of air shower density, the second set represents the timing information. The two sets are sent to the laboratory via 50 Ω coaxial cable. At this stage, after discriminating and shaping the pulses from all detectors, events are stored and recorded on an appropriate recording system (either a photographic film or magnetic disc) to be analysed and eventually evaluated in terms of arrival direction, core location and shower size.

2.4 PHOTOMULTIPLIER TUBES IN THE ARRAY

Photomultiplier tubes in all the detectors serve to convert the light output of the scintillator into electrical signals which can be interpreted in terms of particle densities at the detectors. The three types of photomultipliers have been used in the array detectors, E.M.I. 9579B have a five inch diameter photocathode, and Phillips 53 AVP and Phillips 56 AVP, both having two inch diameter photocathodes. The first

two types have been used for density measurements whereas the type 56 AVP has been used for fast timing purposes. The tubes run off a negative E.H.T. supply and the outputs of the density measuring tubes are negative with an exponential decay time constant of 20 μs. The output of the fast tubes are also negative pulses of time duration 5 nsec (full width at half maximum). The base circuit of different types of photomultiplier (figure 2.4) have been fully checked before constructing the array, in terms of their linearity of responses, gain variation with high tension supply voltage and temperature dependence stability (for further information see A. Smith, Ph.D. Thesis, 1976, Chapter 4).

2.5 E.H.T. SUPPLY UNITS

There are two E.H.T. units which supply the negative high voltage. The first supplies the voltage to photomultipliers used for the density measuring detectors, and is set at 2.4 kV. The other power supply unit supplies the fast timing photomultiplier tubes, and this is set at 2.7 kV. Due to the different values of working voltages needed by each photomultiplier the voltage supplies were fixed at the above mentioned values and these are adjusted appropriately amongst the four tubes in the detector using a resistor chain. This is shown in figure 2.5 and enables each tube voltage to be adjusted independently of the other. In the case of a detector "fast tube" there is a similar resistor chain to adjust the voltage across the tube as required.

2.6 THE DETECTOR HEAD AMPLIFIERS

The output pulses from each of the four density measuring photo-tubes are summed in a mixer-amplifier at the detector. The amplifier, figure 2.6, consists of four emitter followers with their outputs connected to an operational amplifier. These outputs are summed and

Base circuit for EMI 9579B PMT

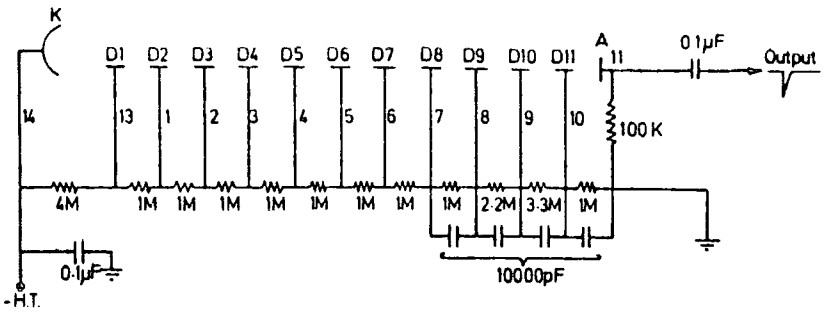

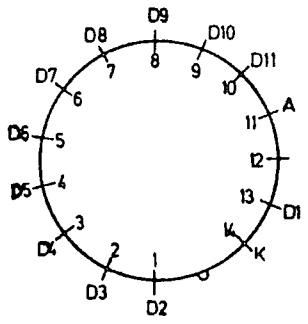

Base: 14pin Mullard FE1001
EMI B14A
Viewed from beneath.

Base circuit for PHILIPS 53 AVP P.M.T.

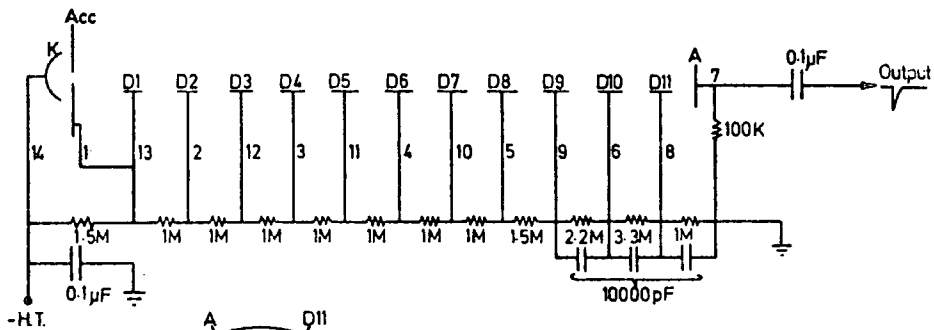

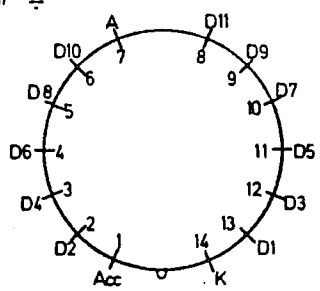

Base: 14pin Mullard FE1001
EMI B14A
Viewed from beneath.

Base circuit for PHILIPS 56 AVP P.M.T.

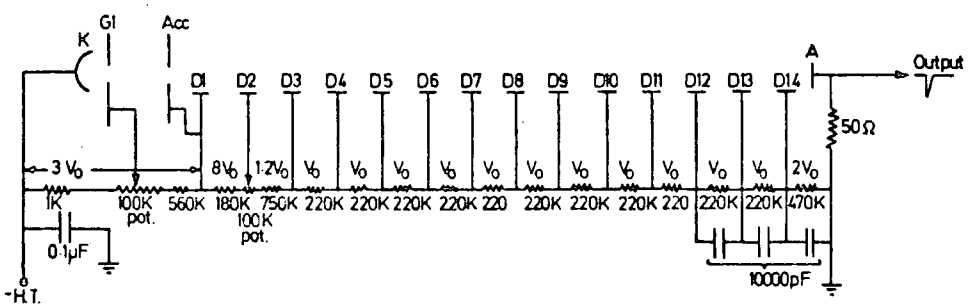

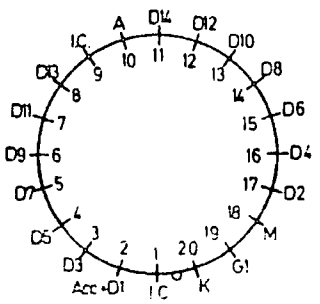

Base: 20pin Mullard FE1003
Viewed from beneath.

Figure 2.4 : The Array photomultiplier base circuits.

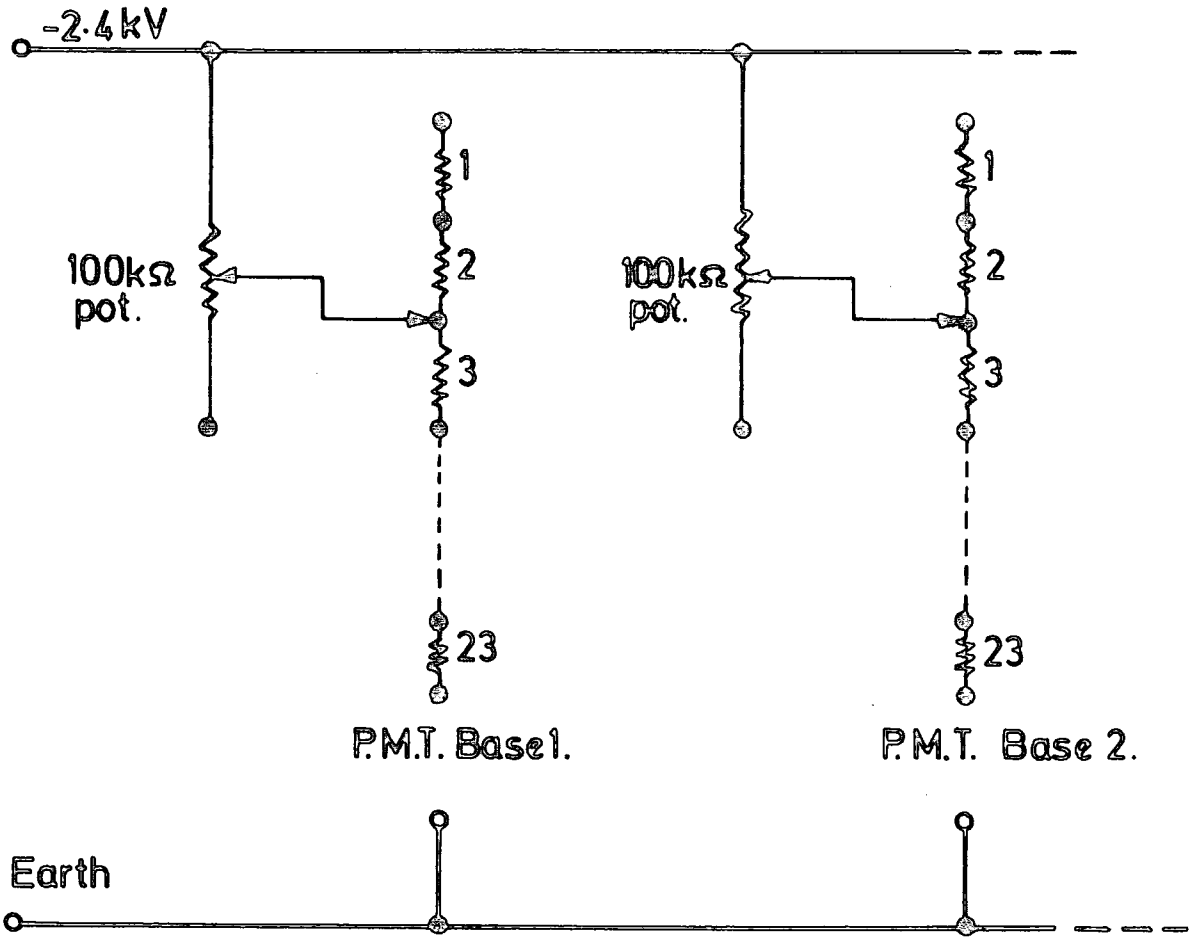

Figure 2.5 : The sections of the four E.H.T. distributions at each detector. All resistors are 100kΩ.

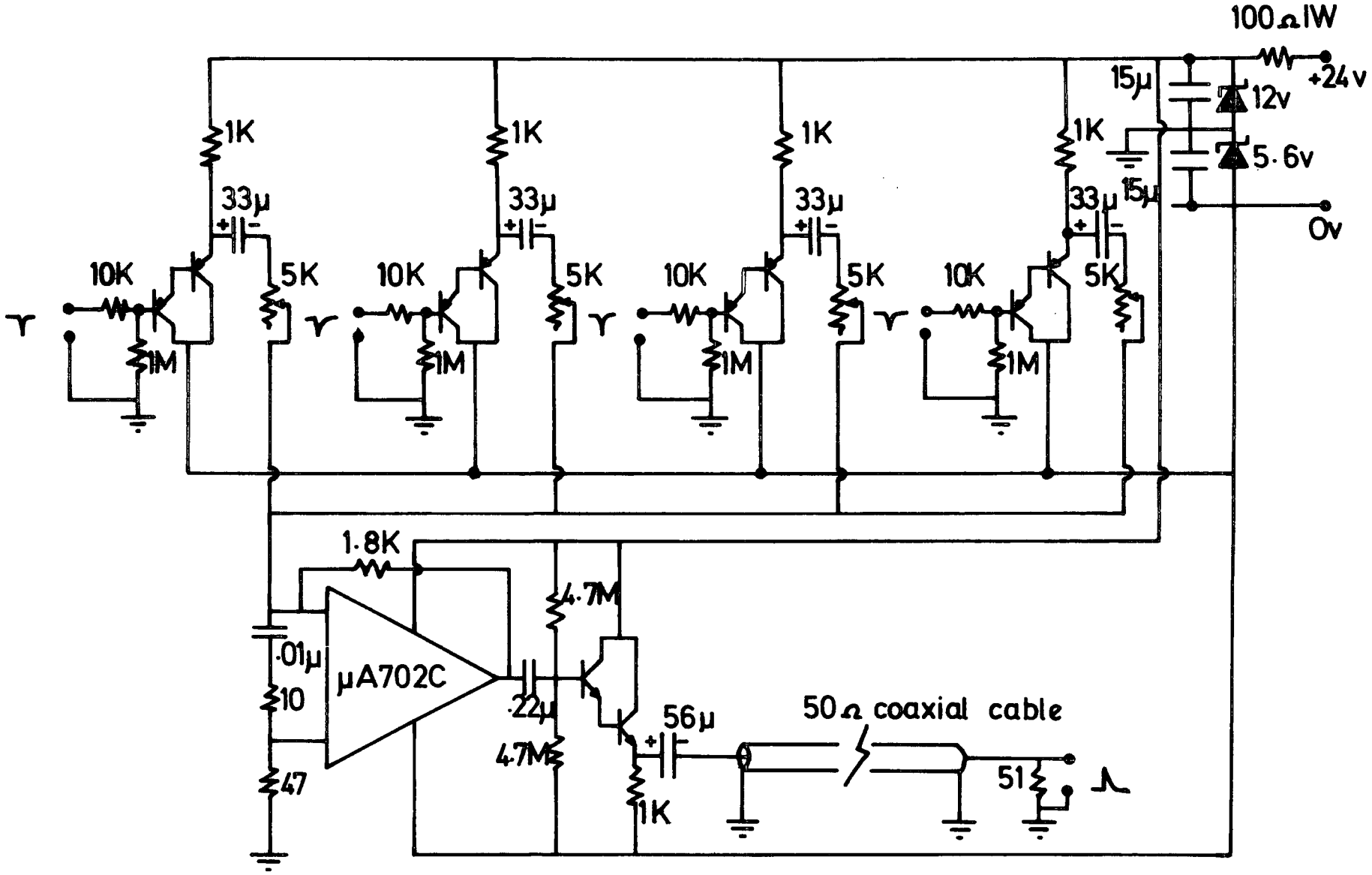

Figure 2.6 : Four input gain five mixer-amplifier.
(Transistors: PNP ZTX501, NPN ZTX301)

amplified and then fed into another emitter follower circuit such that the now positive signal can be driven down the long lengths of cable into the laboratory. A 24V voltage supply was used to supply the power to all of the amplifiers in the array.

2.7 THE SERVICES BOX

At each detector telephone and soldering iron facilities are provided to enable audio contact between the detectors and the laboratory and also to assist in electrical repairs.

2.8 CALIBRATION TELESCOPE

In order to calibrate individual detectors, a telescope, figure 2.7, is used for checking the density measuring detectors. It consists of a 23 cm x 23 cm x 3 cm slab of NE102A plastic scintillator, viewed from one edge by two Phillips 53 AVP photomultipliers. Each of them is supplied with 1.9 kV from the laboratory through a charge sensitive amplifier (C.S.A). This enables the cable requirement to be reduced, only 2 cables (one for each tube) being installed for each arm of the array as the photomultiplier pulse travels along the same cable as the high tension supply. The scintillator and tubes are sealed in an aluminium box to which is affixed wheels and a handle for ease of handling. In use, the telescope is placed above a detector to be calibrated and a coincidence requirement between pulses from the two photomultiplier tubes is used to indicate the passage of a cosmic ray particle. The output pulses from the detector to be calibrated are fed to a pulse height analyser and the telescope coincidence pulse is used to gate it. The pulse height distribution from the detector to be calibrated is thus displayed on a pulse height analyser.

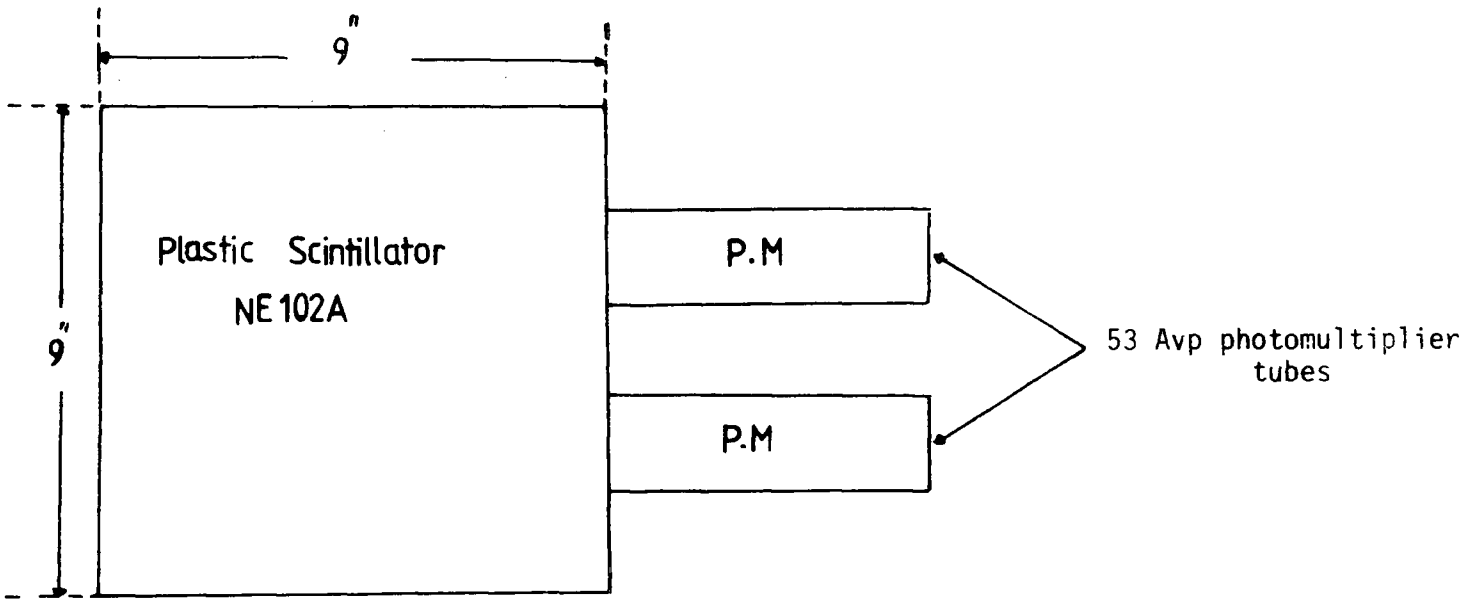

Figure 2.7 :The calibration telescope

2.9 CALIBRATION OF DENSITY MEASURING DETECTORS

The density detectors were calibrated so that they had a standard response to the passage of a single cosmic ray particle. The calibration procedure was carried out on each scintillation detectors as all the detectors differ in design, geometry and consequently in their response towards cosmic ray particles. Contour maps of the detectors response have been obtained, (A.C. Smith, 1976) and from these maps calibration points have been obtained, figure 2.8. The pulse height obtained at this point is then used in the calibration, knowing the relationship between this and the required mean pulse height of 100 mV per particle. The telescope described in the last section was used for the calibration. The output pulses from the two tubes of the telescope go through NE4675 charge sensitive amplifiers, figure 2.9. The signals from ($C.S.A_s$) are then passed through a dual discriminator to remove a large proportion of noise and from these into a coincidence unit which produce a 2 μs - 5V pulse for gating the P.H.A. In this way the majority of the pulses recorded by the P.H.A. are particle pulses. After some tens of minutes, a sufficiently accurate distribution is obtained to decide whether the photomultiplier E.H.T. supply was too low, too high. The E.H.T. was then adjusted using the potential divider across the specified photomultiplier such that the peak of the distribution coincided with the chosen calibration value. When this was reached the tube was calibrated overnight to obtain a more accurate distribution. The resulting distribution could then be drawn and the mode recorded.

2.10 CALCULATION OF THE CALIBRATION PULSE HEIGHT

The aim of the calibration is to adjust the E.H.T. supply to the photomultipliers in a detector so that the output, in mV at the laboratory, when divided by 100 will give the number of particles per square meter

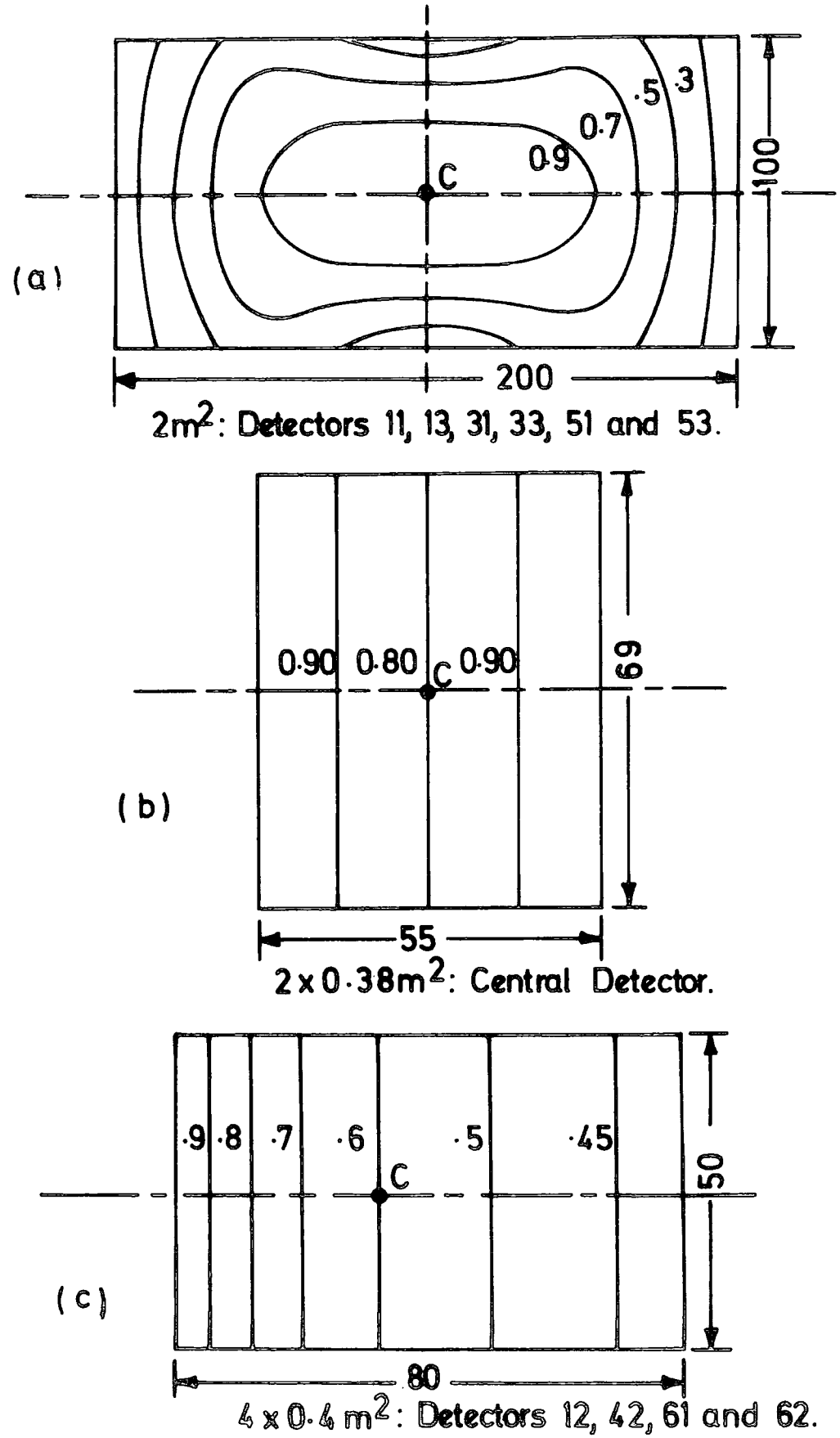

Figure: 28 : Pulse height contour map of the Array's Scintillators.
Dimensions in centimetres.
C represents the calibration points.
(After Smith, 1976)

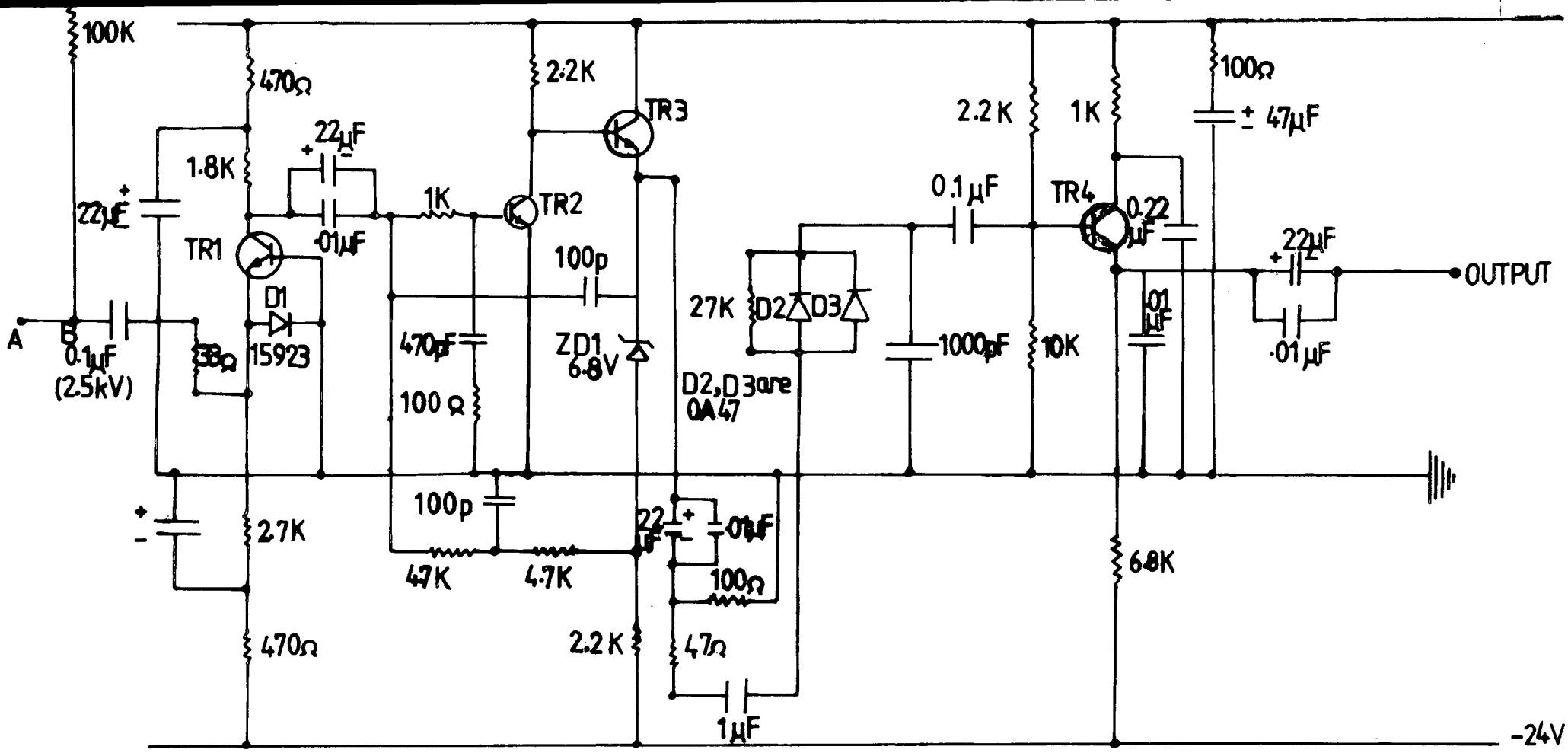

Figure 2.9 : Circuit diagram of the charge sensitive amplifiers(C.S.A)used in the calibrated telescope.
AB represents the 50m of coaxial cable connecting the CSA to the photomultiplier of the calibation telescope.

at the detector, i.e. the particle density at the detector. For detectors that consist of a single piece of plastic scintillator of sensitive area S viewed by a number of photomultipliers n, the calibration will be on a mean pulse height of (100 mV)/(nxS) per particle per m^2. For practical reasons, it is quicker to measure the peak (mode) of the pulse height distribution obtained rather than the mean, this required the introduction of a factor (R) into the calibration of the detectors. This factor is the ratio of the value of the mean to the mode of the measured pulse height distributions averaged over the sensitive area of the detector. Another parameter has been included in the calibration procedure, this parameter (g), is given by the pulse height at the calibration point divided by the pulse height at the mean pulse height coordinate and has been determined by A.C. Smith (1976). The calibration telescope used for day to day calibrations consisted of a single slab of phosphor viewed by two photomultipliers (figure 2.7). This telescope gave a high rate of single particles traversing its area but with the disadvantage that particles traversing it covered the whole range of zenith angles from 0 to 90^{o}. The relationship between the average of the pulse height distribution for particles traversing the detector to be calibrated using this telescope and average pulse height that would have been recorded if a vertical beam of single particle was used was determined in a subsidiary experiment. This was done using a narrow angle vertical telescope using two separate small area scintillators to define the beam direction.

2.11 PERFORMANCE OF THE ARRAY

In the work described in this thesis, extensive air showers (E.A.S.) selected by an inner ring trigger $\Delta_C(\geqslant 4m^{-2})$. $\Delta_{11}(\geqslant 2m^{-2})$. $\Delta_{31}(\geqslant 2m^{-2})$. $\Delta_{51}(\geqslant 2m^{-2})$ and on outer ring trigger $\Delta_C(\geqslant 4m^{-2})$. $\Delta_{13}(\geqslant 2m^{-2})$. $\Delta_{33}(\geqslant 2m^{-2})$. $\Delta_{53}(\geqslant 2m^{-2})$ have been investigated. Figures

2.10 and 2.12 show the measured size distribution of E.A.S. falling in annular rings at different distances from the central detector C using these two triggers where the radii of the annular rings are measured in the horizontal plane (X,Y,0) of the array. Figures 2.11 and 2.13 are similar plots to figures 2.10 and 2.12 except that the radii of the annular rings are measured in the plane of the shower front (i.e. they are orthogonal distances from the central detector C to the shower axis direction). It is seen from these figures that the minimum shower size detected by the inner ring trigger is 10^4 particles and by the outer ring trigger 10^5 particles respectively. Using the calculations of Kempa (1976) relating the number of particles to primary energy, these figures correspond to threshold energies of 10^{14} eV and 8.10^{14} eV respectively.

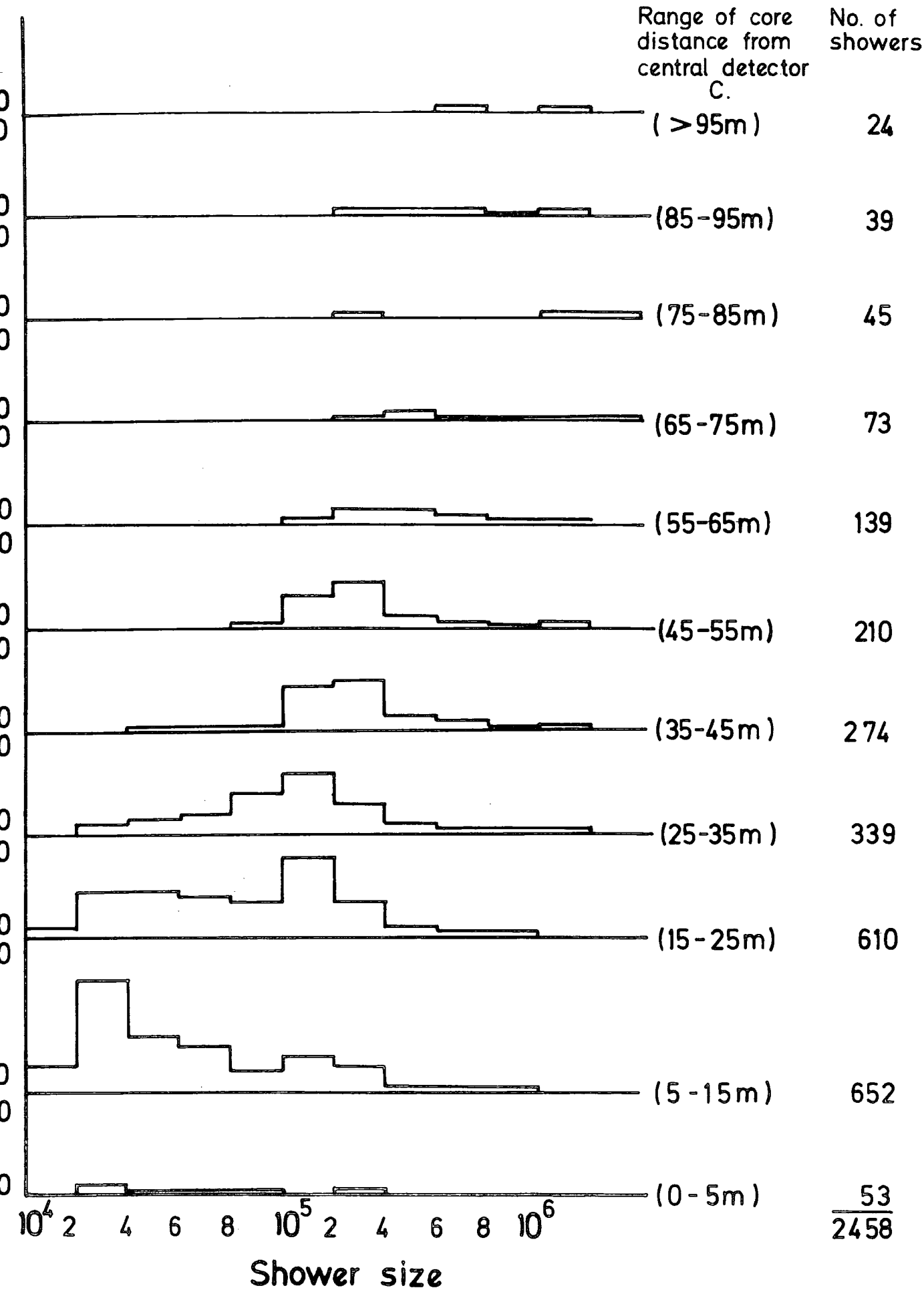

Figure 2.10 : Inner ring trigger $\Delta_C(\geq 4m^{-2})$. $\Delta_{11}(\geq 2m^{-2})$. $\Delta_{31}(\geq 2m^{-2})$. $\Delta_{51}(\geq 2m^{-2})$. Size distribution of E.A.S. falling in annular rings at different distances from the central detector C. The radii of the annular rings are measured in the horizontal plane (X,Y,0) of the array. Total number of showers = 2458.

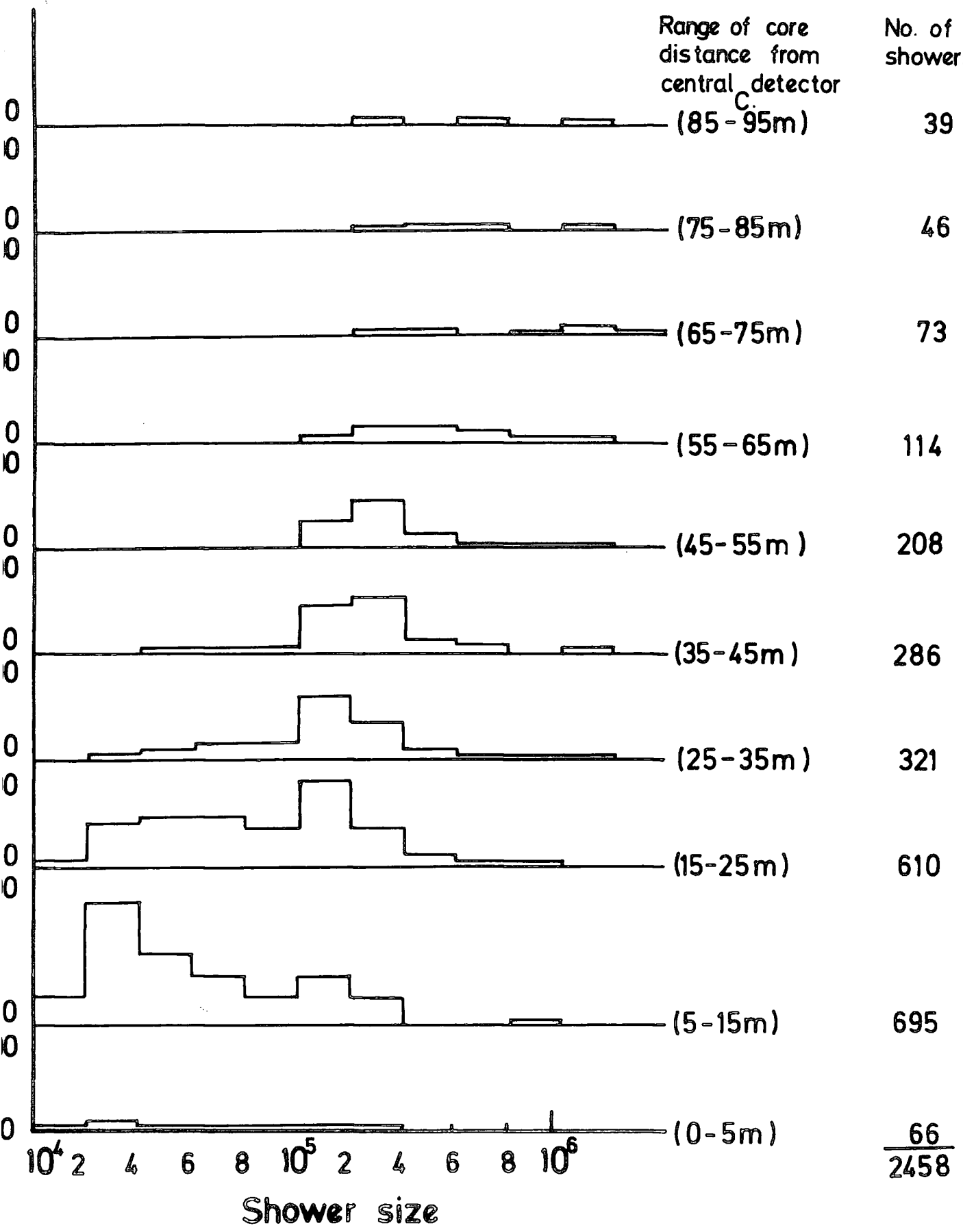

Figure 2.11 : Inner ring trigger. Same as figure 2.10 except that the radii of the annular rings are measured in the plane of the shower front (i.e. they are orthogonal distances from C to the shower axis direction). Total number of showers = 2458.

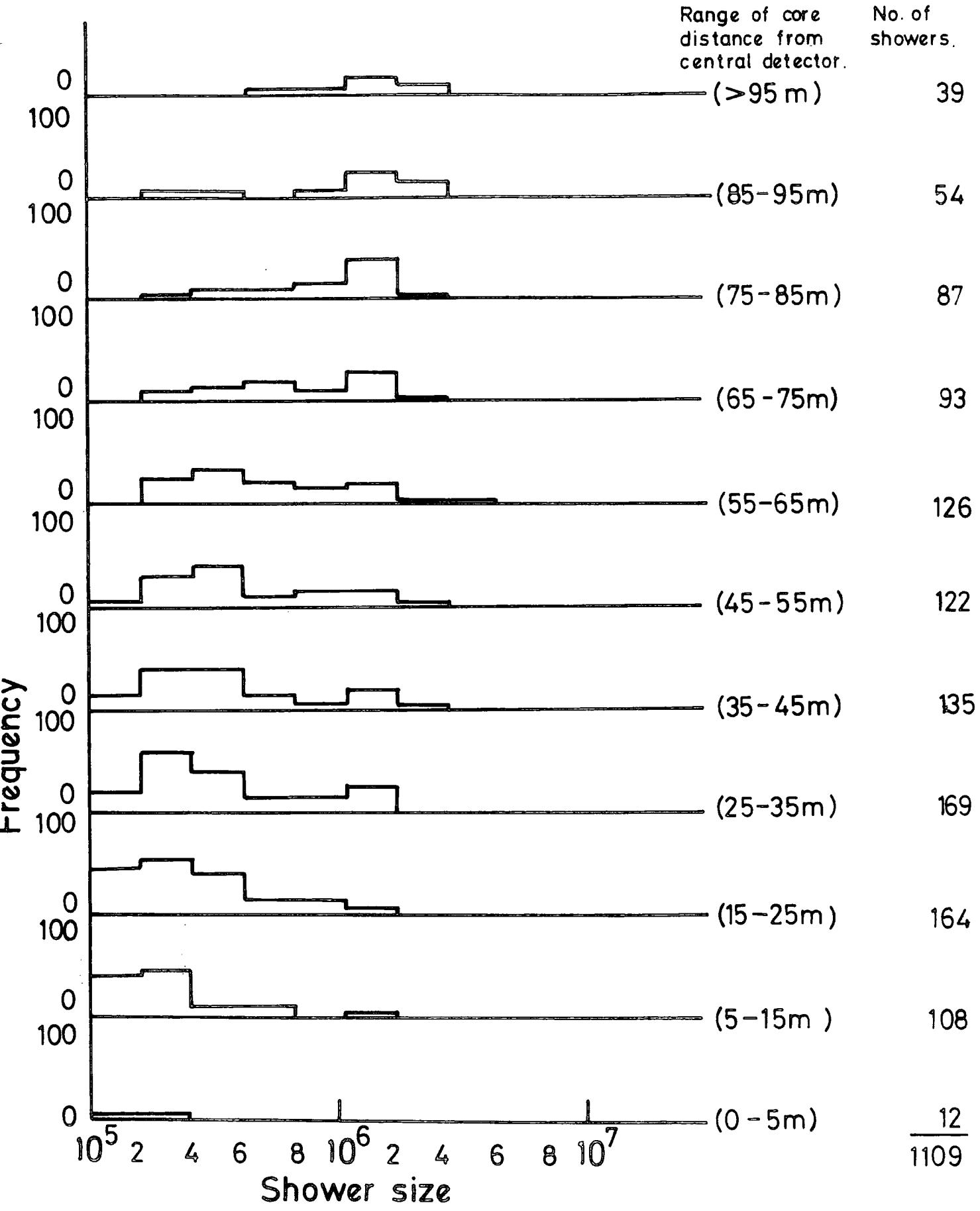

Figure 2.12 : Outer ring trigger $\Delta_C(\geq 4m^{-2})$. $\Delta_{13}(\geq 2m^{-2}).\Delta_{33}(\geq 2m^{-2}).\Delta_{53}(\geq 2m^{-2})$.
Size distribution of E.A.S. falling in annular rings at different distances from the central detector C. The radii of the annular rings are measured in the horizontal plane (X,Y,0) of the array. Total number of showers = 1109.

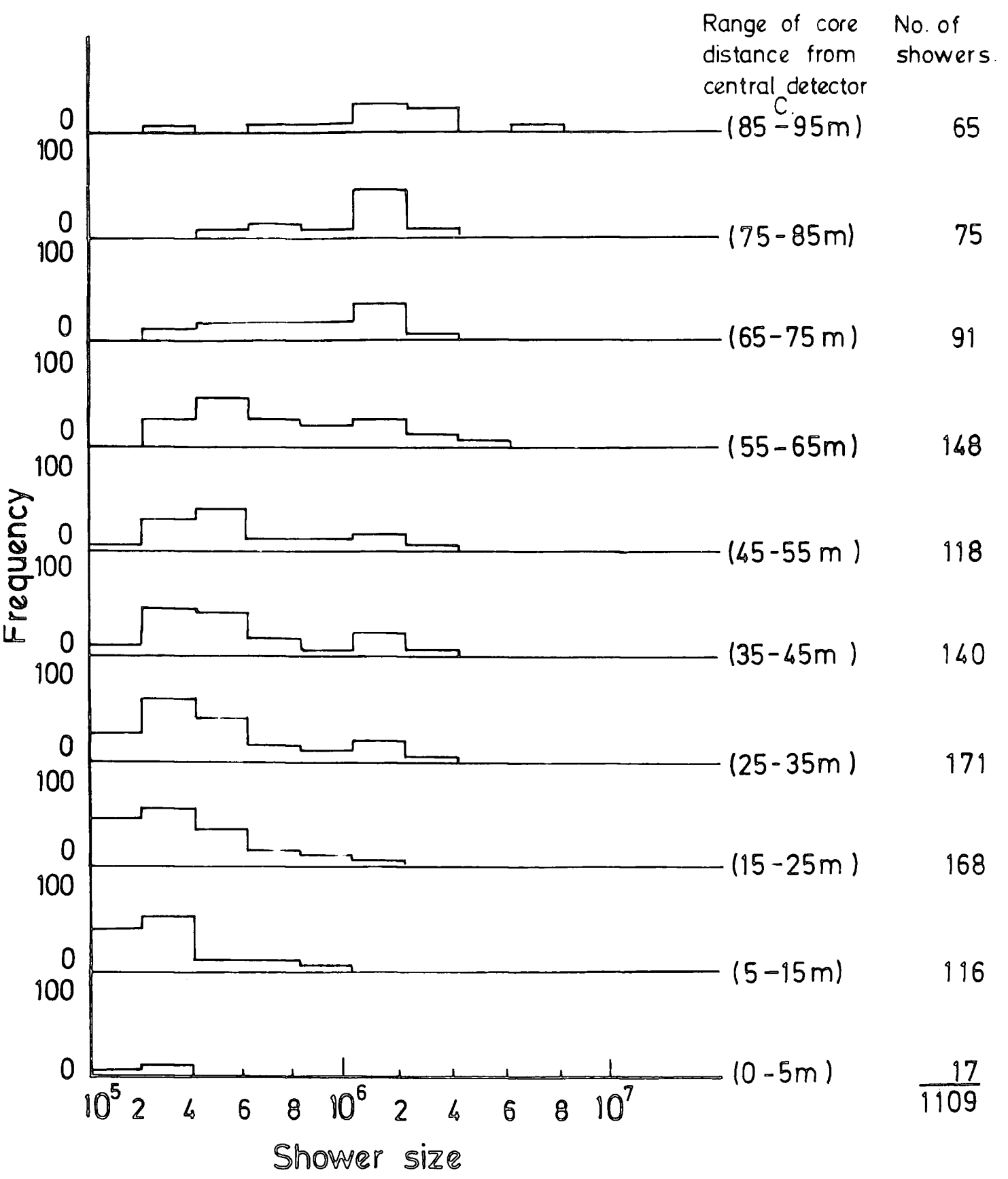

Figure 2.13 : Outer ring trigger. Same as figure 2.12 except that the radii of the annular rings are measured in the plane of the shower front (i.e. they are orthogonal distances from C to the shower axis direction). Total number of showers = 1109.

CHAPTER 3

METHODS OF AIR SHOWER DATA ANALYSIS

3.1 INTRODUCTION

Shower data are collected under the triggering of the air shower array corresponding to a four-fold coincidence between the central detector C and the 2 m^2 detectors 55, 33 and 13 for the inner ring trigger whereas for the outer ring trigger, a coincidence between C and the detectors 51, 11 and 31 each of area 2 m^2 is required. The triggering threshold levels for these detectors were calibrated at particle density levels of (4 P/m^2 for the central detector and 2 P/m^2 for the 2 m^2 detector). The experimental data is a number of density and timing measurements which may be classified as independent variables. The aim of the analysis is to determine :-

(1) The core distance from the central detector, measured in the plane of the shower front.

(2) The zenith and azimuthal angles of the arrival direction of the shower.

(3) The shower size (N).

Measurements of the radius of curvature of the shower front cannot be obtained due to the inaccuracy in the relative time difference measurements.

3.2 METHODS OF SHOWER PARAMETER ANALYSIS

Methods of air shower analysis vary but in general their aims are to find the best estimate of the above parameters from the data available. In every case accuracy is the main concern. Various shower parameters can be considerably improved by employing more detectors other than the ones mentioned earlier since fluctuations in particle density or timing

measurements at individual detectors severely bias the eventual calculated quantities. Numerical minimization methods are techniques most widely used in the analysis of air shower data and in particular achi-squared minimization is most often employed.

3.2.1 Methods of Core Location

There are two methods available, the first which is called the loci curve method, and the second method which uses a computer when a large amount of data is involved. For both methods, the sampled particle densities are used to locate the core position.

3.2.2 The Method of Intersecting Loci

This method was first introduced by Williams (1948) to determine the core position. The ratio of the electron densities from any two detector is used to determine a locus on which the axis of the incident E.A.S. must have fallen. A minimum of three detectors give two independent density ratios and the intersection point of the two corresponding loci defines the core position. In practice at least four detectors are required so that the third available density ratio can be used to define a locus which should intersect the core position determined by the other two loci for consistency. In general the produced loci curves do not intersect at a single point (see section 3.3) due to density fluctuation and the non-uniqueness of the lateral electron structure function. However the centre of gravity of the overlapping area provides a good estimate of the core position and once the core position has been determined, it is a matter of substituting the relevant core distances in the assumed lateral distribution function to find the shower size. The method depends on assuming that the lateral distribution of electrons in an air shower can be expressed as an explicit function of shower size N and core distance r. The lateral distribution

used in the present analysis is known as the Greisen function. For an E.A.S. core that falls at a distance r_1 from a detector which records a density Δ_1 and at a distance r_2 from a detector which records a density Δ_2 then assuming the electron lateral distribution is that given by Greisen

$$\frac{\Delta_1}{\Delta_2} = \left(\frac{r_2}{r_1}\right)^{2-s} \left(\frac{r_2 + r_0}{r_1 + r_0}\right)^{4.5-s} \left(\frac{1 + \frac{r_2}{11.4 r_0}}{1 + \frac{r_1}{11.4 r_0}}\right)$$

where $s = 1.25$ is the age parameter of the shower. For different values of r_2 the density ratio $\frac{\Delta_1}{\Delta_2}$ is plotted as a function of r_1 and the result is shown in figure 3.1. Hence for any pair of detectors a series of loci of possible core positions corresponding to different electron density ratios between the two detectors can be constructed. Examples of such curves for some pairs of detectors used in the Durham air shower array are shown in figures 3.2a and 3.2b. The loci method is accurate provided the shower core has fallen within or near the array boundary and the arrival direction of the shower is close to the vertical direction.

3.2.3 Computer Method of Core Location (χ^2-minimization)

In this method a computer programme is used to search over a lattice of points and the best fit to the core position and shower size is determined corresponding to a minimum χ^2 defined by

$$\chi^2 = \sum_i K_i \left(n_{i_{obs}} - n_{i_{calc}}\right)^2$$

where K is the weight function given by σ_i^{-2} and σ_i is the standard deviation of the density measurements. $n_{i_{obs}}$ is the measured number of particles at the i^{th} detector and $n_{i_{calc}}$ is the calculated number of particles at the i^{th} detector. The prediction of n_i were

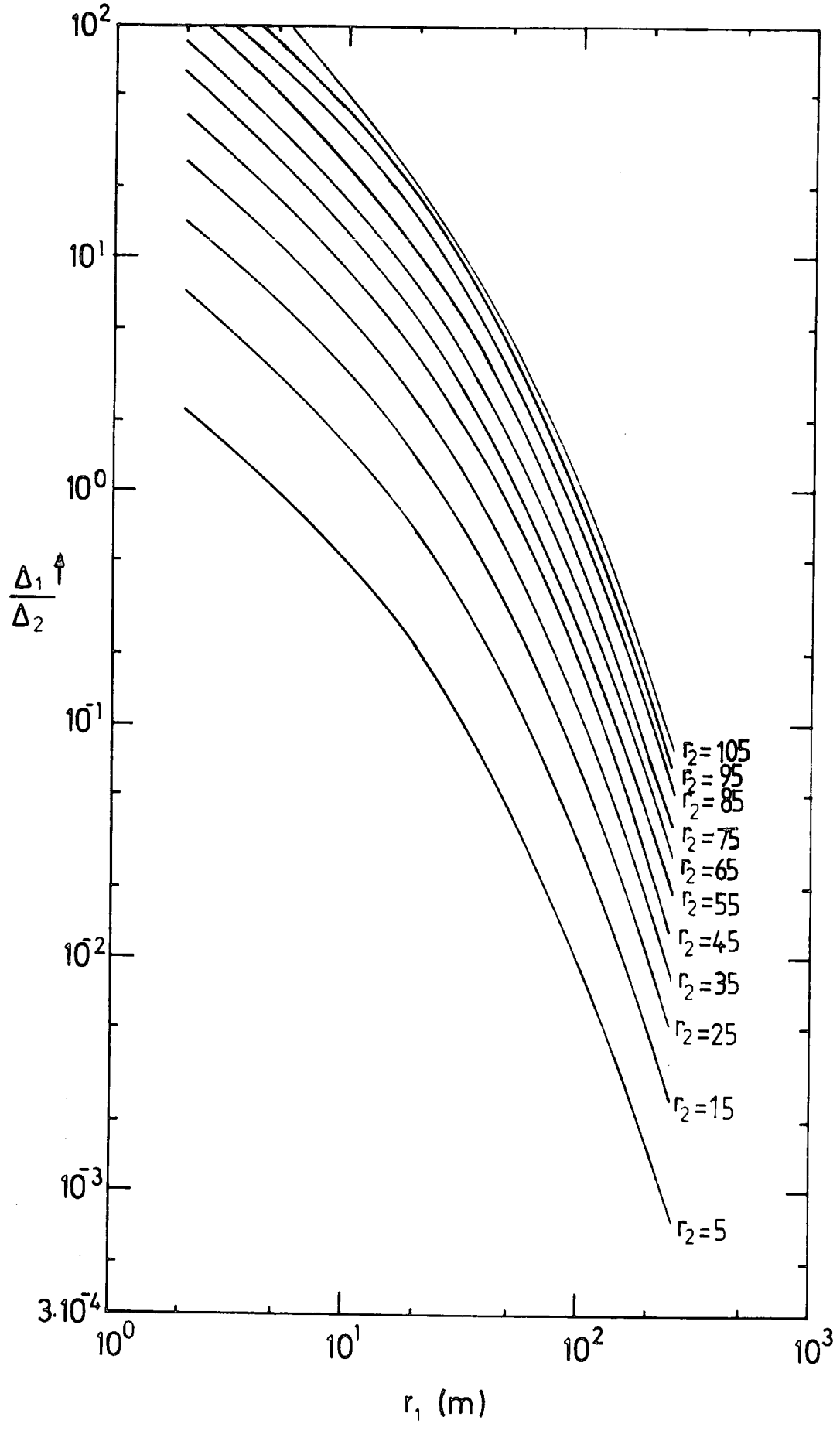

Figure 3.1 : The ratio of densities in detectors 1 and 2, $\frac{\Delta_1}{\Delta_2}$ as a function of r for fixed values of r
r_1 = core distance from detector 1 in metres
r_2 = core distance from detector 2 in metres.

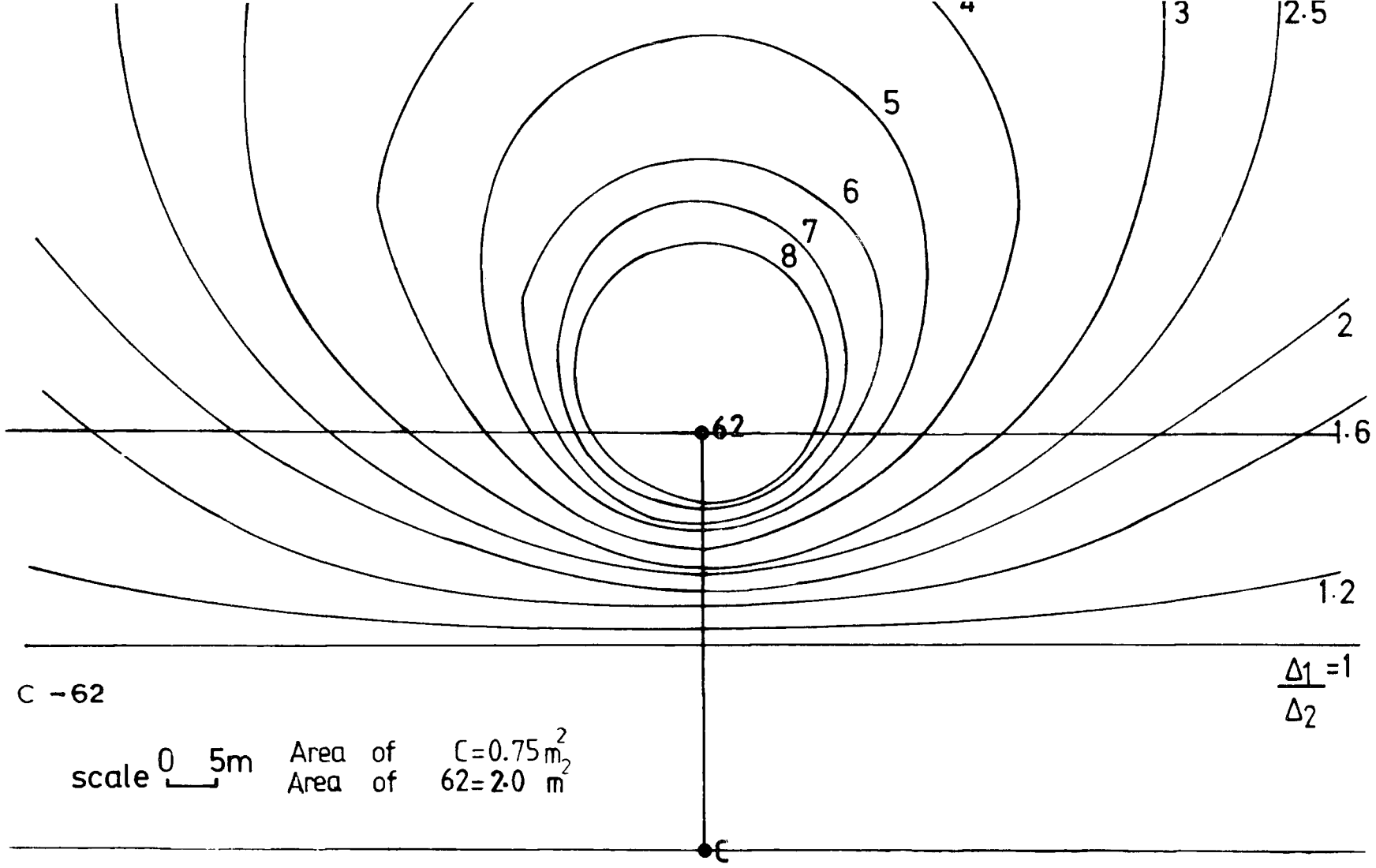

Figure 3.2a : Loci curves on which the core of an air shower must have fallen to give the density ratio, $\frac{\Delta_c}{\Delta_{62}}$, indicated on each curve.

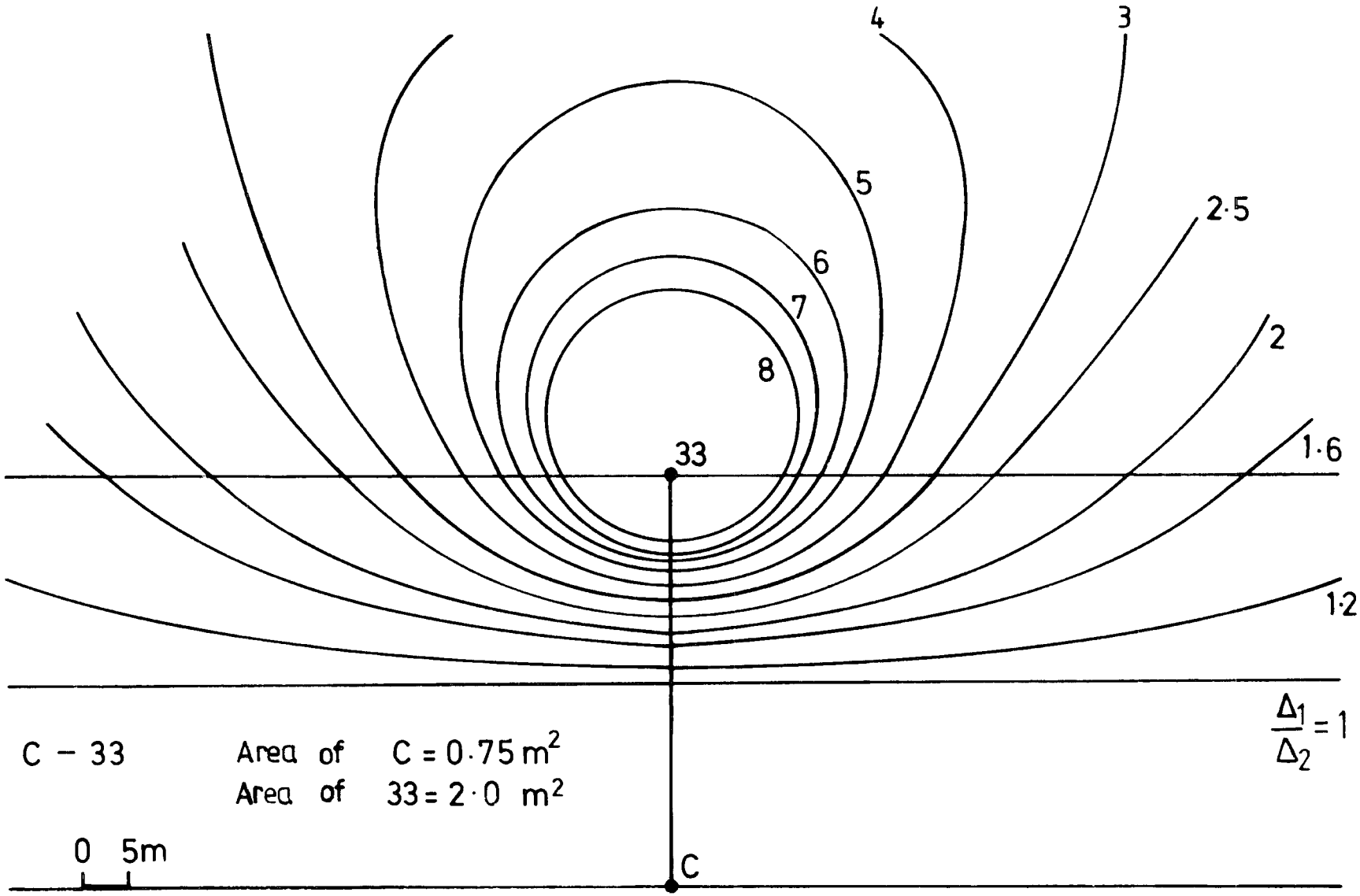

Figure 3.2b : Loci curves on which the core of an air shower must have fallen to give the density ratio, $\frac{\Delta_c}{\Delta_{33}}$, indicated on each curve.

based on employing an assumed structure function. The programme procedure started from a point chosen near to the highest recorded density in the array. The process is repeated for different lattice points that cover the array and for different random points chosen uniformly around the starting points (x_s, y_s). The lattice point giving the minimum value of χ^2 is taken as the best estimate of the core position. Clark et al (1958), Evans (1971) and more recently Smith (1976) have described this method.

3.3 ERRORS AND FLUCTUATIONS

3.3.1 Loci Curve Method of Core Location

Intersecting loci curves should in principle meet each other in one point where the core position is located. However, because of sampling density fluctuations this is not necessarily the correct core position. To account for fluctuations the error on the ratio of two detector densities involved in determining the locus of the loci curve is required. The result is given by the formula

$$\sigma_y = \frac{1.2\,\Delta_1}{\Delta_2}\sqrt{\frac{1}{\Delta_1 A} + \frac{1}{\Delta_2 B}}$$

where Δ_1 and Δ_2 are the densities at any two detectors with area A and B respectively and $Y = \Delta_1/\Delta_2$. The loci corresponding to $Y = \Delta_1/\Delta_2$ and the error defining loci corresponding to $\dot{Y} = \Delta_1 / \Delta_2 \pm \sigma_y$ can thus be found.

Figure 3.3 and 3.4 illustrate the procedure used in practice. Figure 3.5 shows a case in which three intersecting loci curves define a core position unambiguously and in this case sampling density fluctuations are of minor importance.

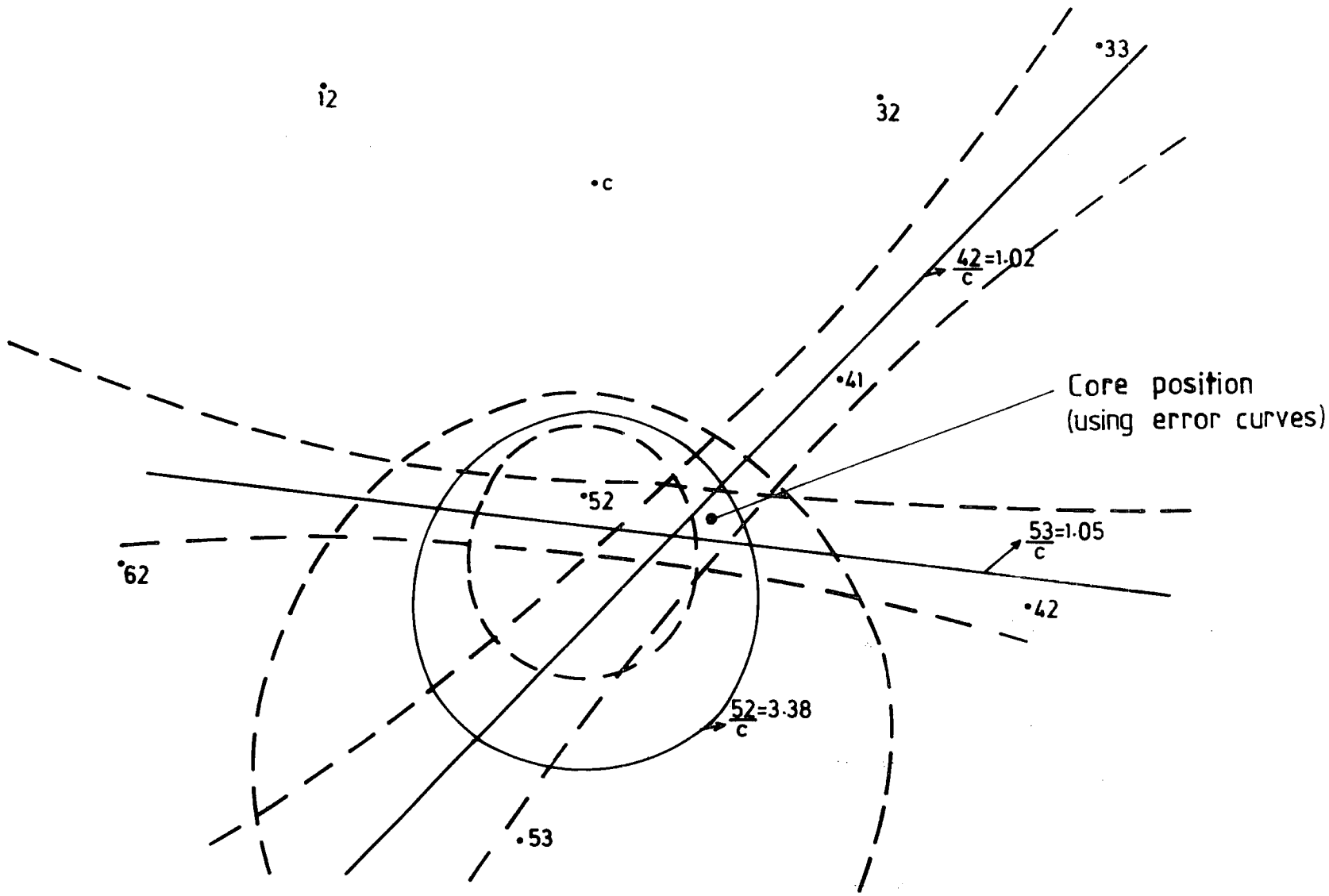

Figure 3.3 : An example of a shower core located by the loci curve method.

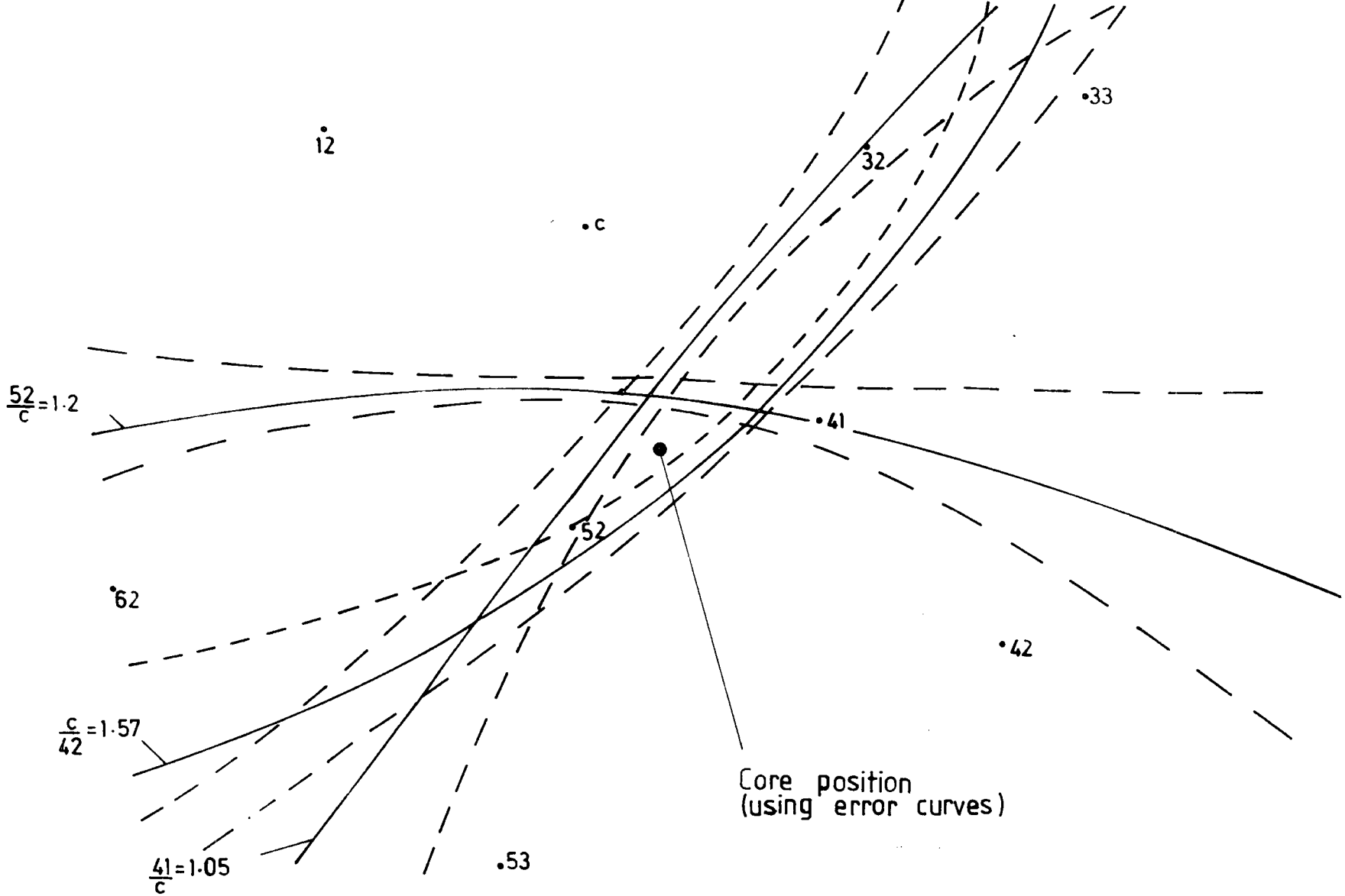

Figure 3.4 : An example of a shower core located by the loci curve method.

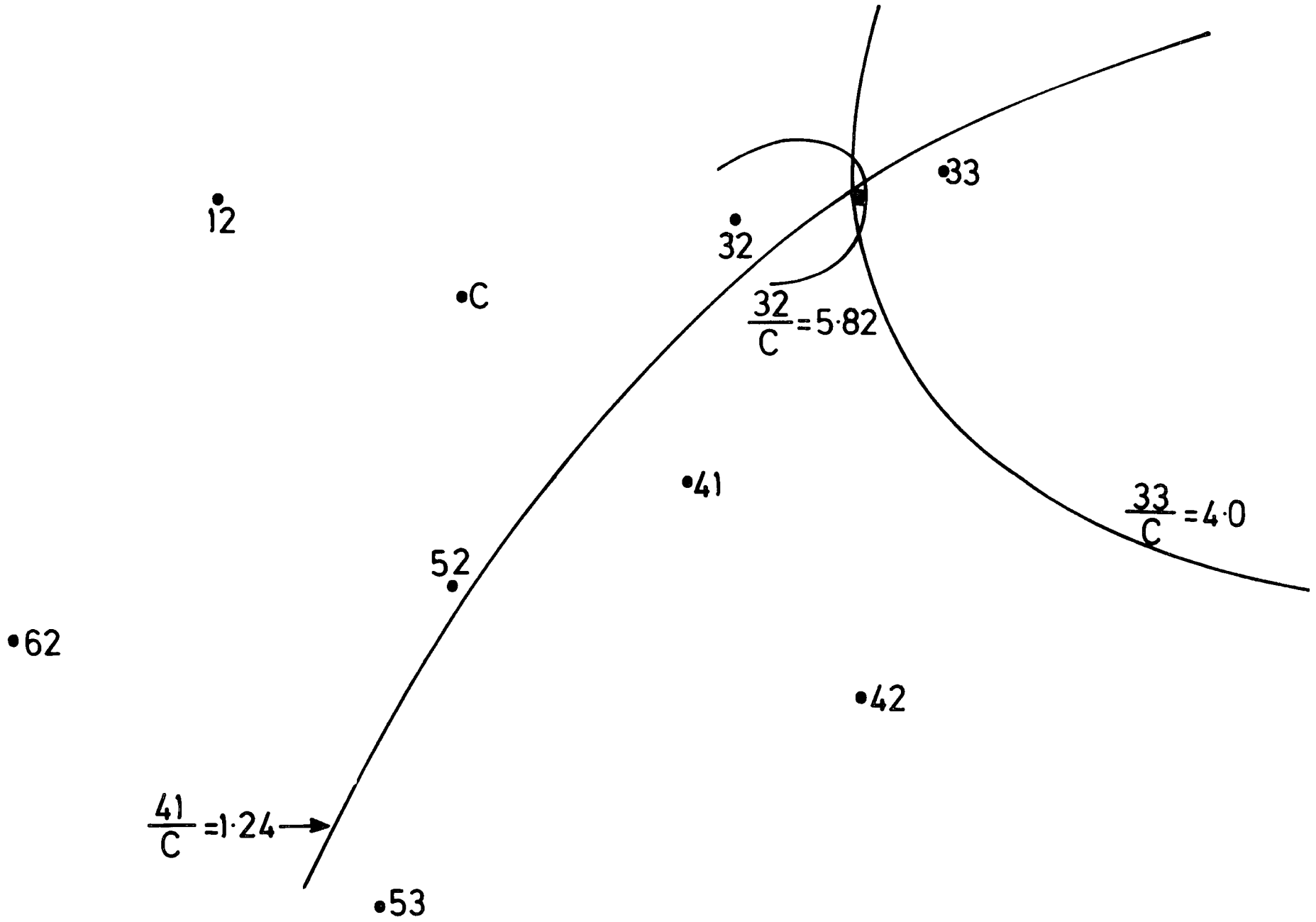

Figure 3.5 : An example of a shower where core position is found without referring to error curves.

3.3.2 Statistical Fluctuations in Sampled Particle Number

The majority of particles detected in an extensive air shower detector are electrons which are the result of superimposed electron photon cascades. All these cascades are past the maximum of their development so that the electrons behave independently of one another. Thus if the expected number through a given detector is n then an estimate of the shower fluctuations is that n is distributed as a Poisson distribution. In practice, the observed fluctuations are usually broader than purely Poissonian. In order to characterise the broader distributions that are observed, they can be considered as roughly Poissonian in shape but with a broader width and the width can be described by some factor $k > 1$ times the standard deviation of a normal Poissonian distribution, i.e. $k\sqrt{n}$. Experimental analysis (J. Fatemi, Ph.D. thesis, 1981) shows that in a sample of 100 showers in which their core position and shower size were determined by the intersecting loci method that the average width of the fluctuations for shower sizes in the range of $7.4.10^4$ to $2.7.10^6$ particles) was found to be $1.2\sqrt{n}$ (i.e. $k = 1.2$). This means that in a plot of measured particle number against predicted particle number, 68% of the points fell within $\pm 1.2\ n^{\frac{1}{2}}$ of the mean. Smith (1976) has looked at the same problem and reached the same conclusion. Clark et al (1961) made a similar study and found that for showers in the range $5.10^5 < N < 10^8$ particles that $k = 1.15$ at distances >50 m from the shower core. For $n_e > 33$ particles and for near vertical showers ($\theta < 30^o$) at distances of 30 m from the core of the shower, Kitajima et al (1979) found the fluctuations are broader than Poissonian.

3.4 METHODS OF ARRIVAL DIRECTION DETERMINATION

In the Durham E.A.S. array where the measurements of arrival direction of extensive air shower are involved, there are two methods using seven detectors (C,11,31,51,13,33 and 53) see figure 2.1, by which the zenith and azimuthal angles can be determined.

Consider a fast timing detector X where the central timing detector C is placed at the origin of a right-hand set of Cartesian coordinates and X represents any detector of fast timing measurements placed at point (α, β, γ) as shown in figure 3.6. In the analysis the normal to the shower front has the zenith angle θ and azimuthal angle ϕ and the shower front passing through X contains a line XS which is normal to CS. To calculate the time for the shower front to pass through detector C after having passed through a detector at X, it is necessary to calculate the distance CS = ℓ. For any position of the points S on the line CS.

$$R = \{ (X_\ell - \alpha)^2 + (Y_\ell - \beta)^2 + (Z_\ell - \alpha)^2 \}^{\frac{1}{2}}$$

$$= \{ (\ell \sin\theta \cos\phi - \alpha)^2 + (\ell \sin\Theta \sin\phi - \beta)^2 + (\ell \cos\Theta - \gamma)^2 \}^{\frac{1}{2}}$$

As ℓ varies in magnitude XS will be orthogonal to CS when R is a minimum. R becomes a minimum when $\frac{dR}{d\ell} = 0$ and consequently

$$\ell = \alpha \sin\theta \cos\phi + \beta \sin\theta \sin\phi + \gamma \cos\theta \qquad (1)$$

$$R = \{(\alpha^2 + \beta^2 + \gamma^2) - (\alpha \sin\theta \cos\phi + \beta \sin\theta \sin\phi + \gamma \cos\theta)^2\}^{\frac{1}{2}} \qquad (2)$$

It is seen that equation (2) can be used to determine the orthogonal shower axis distance for a detector situated at (α, β, γ). Using equation (1) and the coordinates of the fast timing detector, the time difference t between an E.A.S. shower front traversing a given detector

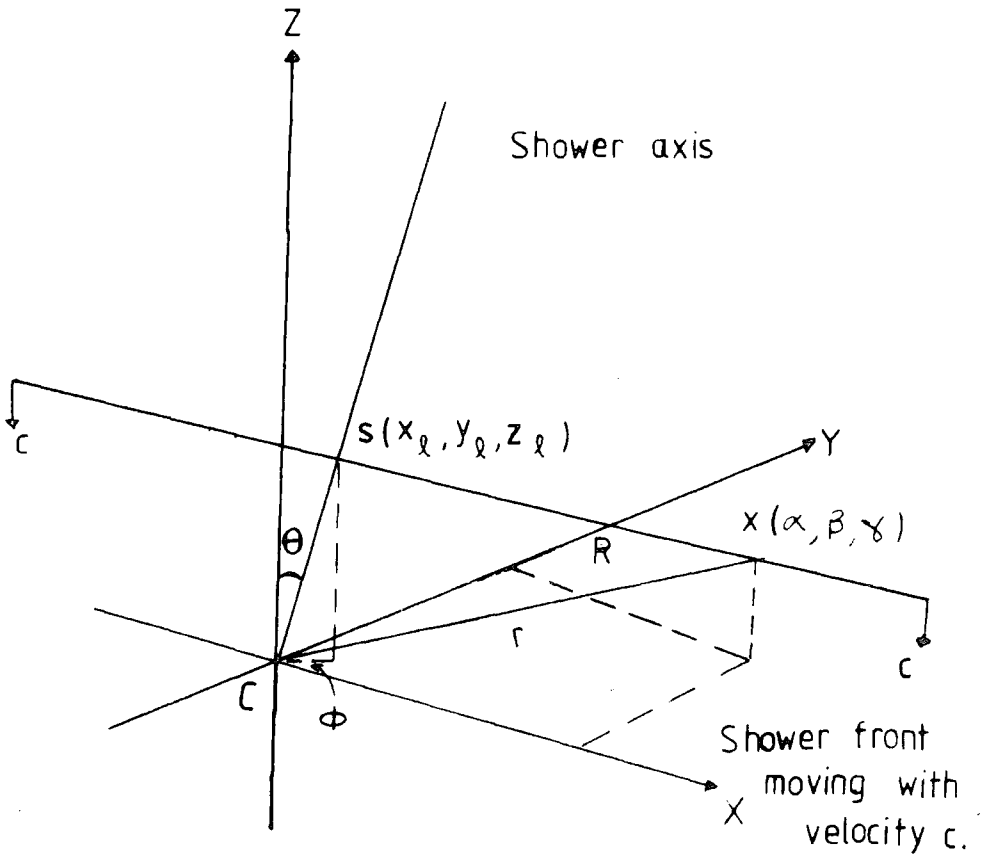

Figure 3.6 : Diagrams showing a shower whose axis has zenith angle θ and azimuthal angle ϕ . The shower front is a plane containing XS which is normal to the shower axis direction CS. CS = ℓ, SX = R and CX = r.

and detector C can be measured such that $Ct = \ell$. Where $C = 3.10^8$ m sec^{-1} is the velocity of light. Figure 3.7 shows how t depends on θ and ϕ for detector C and 13. It is seen that the maximum value of t = +180 ns (corresponding to a shower with $\theta = 90^0$, $\phi = 330^0$ which sweeps through C before 13) and the minimum value of t = -180 ns (corresponding to a shower with $\theta = 90^0$ and $\phi = 150^0$ which sweeps through 13 before C). Curves similar to those shown in figure 3.7 have been evaluated for detector C and each timing detector. In the present array fast timing is achieved using time to amplitude converters which are started when a pulse arrives from detector C and stopped by pulses from the timing detectors. Known cable delays must be inserted in the timing channels 13, 33, 53, 11, 31 and 51 to ensure that the pulse from C always arrives at the time to amplitude converters before the pulses from the 6 outer-timing detectors. In all cases the cable delays used are ample to efficiently record all showers with zenith angles in the range 0 to 90^0.

Consider the inverse problem where the values of t are measured and the problem is to find θ and ϕ. Suppose a shower with zenith and azimuthal angles (θ and ϕ) passes through two timing detectors D_1 and D_2 located at (X_1, Y_1, Z_1) and (X_2, Y_2, Z_2) at time differences t_1 and t_2 relative to the time it passes through C which is situated at the origin. t_1 and t_2 are counted positive if the shower front traverses C first and negative if it traverses them before it traverses C. Equation (1) can be written for the two detectors.

$$Ct_1 = X_1 \sin\theta\cos\phi + Y_1 \sin\theta\sin\phi + Z_1 \cos\theta$$

$$Ct_2 = X_2 \sin\theta\cos\phi + Y_2 \sin\theta\sin\phi + Z_2 \cos\theta$$

Writing $Ct_1 = T_1$ and $Ct_2 = T_2$ and using the direction cosing of the unit

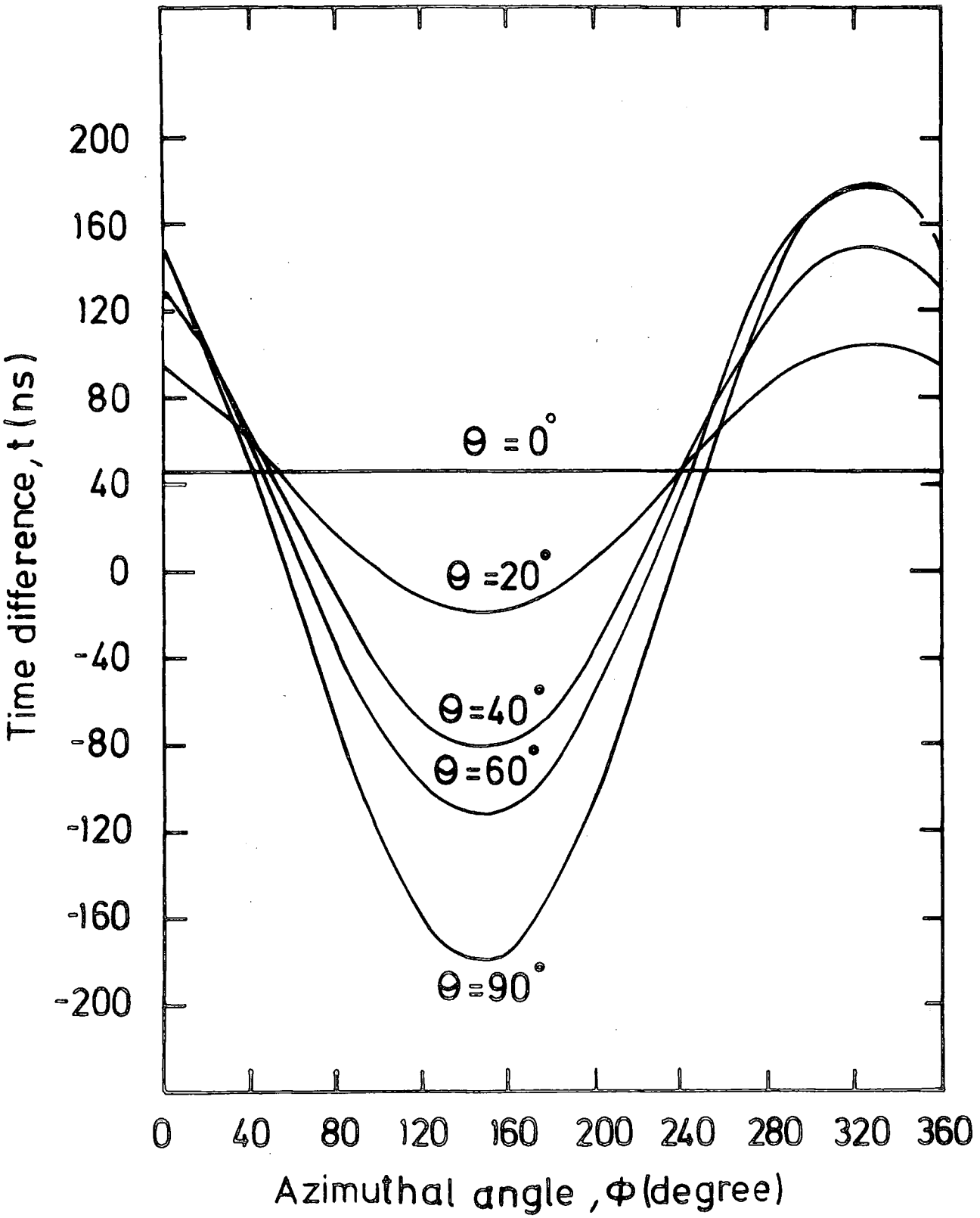

Figure 3.7 : Time difference t(ns) between a shower front traversing detectors C & 13 as a function of the azimuthal angle ϕ for different zenith angles θ of the E.A.S. t is counted + V_e if the shower front traverses C before 13 and -V_e if it traverses 13 before C.

vector normal to the plane of the shower front which are given by

$$\ell = \sin\theta\cos\phi$$

$$m = \sin\theta\sin\phi$$

$$n = \cos\theta$$

and using the above equations one can work out the zenith and azimuthal angles of arrival of E.A.S. and they are given by

$$n = \cos\theta = \frac{-(AB+CD) \pm \sqrt{(AB+CD)^2 - (B^2+D^2+1)(A^2+C^2-1)}}{(B^2+D^2-1)}$$

and $$\tan\phi = \frac{C + Dn}{A + Bn}$$

$$A = \frac{Y_2T_1 - Y_1T_2}{Y_2X_1 - Y_1X_2}$$

$$B = \frac{Y_1Z_2 - Y_2Z_1}{Y_2X_1 - Y_1X_2}$$

$$C = \frac{X_1T_2 - X_2T_1}{X_1Y_2 - X_2Y_1}$$

$$D = \frac{X_2Z_1 - X_1Z_2}{X_1Y_2 - X_2Y_1}$$

Thus, in principle, the arrival direction of an air shower can be determined with a minimum of 3 timing detectors (i.e. the central detector C and two outer detectors). In practice at least 4 detectors are required so that the extra information can be used to check that the result obtained from all possible pairs are consistent. If a large number of timing detectors are used then a numerical minimizing procedure can be used to find θ and ϕ. The following function is minimized, the summation is overall timing detectors -

$$T = \sum_{\text{all timing detectors}} (t_{i_{obs}} - t_{i_{calc}})^2$$

where $t_{i_{obs}}$ is the observed time of arrival measured by the i^{th} timing detector relative to the central detector ($t_c = 0$) and $t_{i_{calc}}$ is the predicted time at the i^{th} detector calculated by assuming a shower is incident on the array at zenith angle (θ) and azimuthal angle (ϕ). The most significant value of θ and ϕ are those when the function T is a minimum. The procedure used here is the same as the one used in core position determination. This method, to determine the zenith and azimuthal angles using fast timing between scintillation counter detector was first used by Bassi et al (1953). These authors also showed that the thickness of the electron shower front is $\sim$1.5 m with a radius of curvature of 2.6 Km for showers of size 10^5 - 10^6 particles at sea level.

In order to have any confidence in the result obtained in this work it is important to determine the input parameter to a degree of accuracy which makes the errors of these parameters too small to markedly affect the final result. A comparison between input and output parameters to determine any shift in them due either to the experimental technique or the analysis procedure has been made. A Monte Carlo analysis on the accuracy of the measured air shower parameters has been carried out by Smith (1978). The simulation programme used comprised three distinct parts : the shower simulation, the array simulations and the analysis programme which was mentioned previously. Showers have been simulated and fired at the array with random core location, shower size, zenith and azimuthal angles. It is concluded that for 800 showers triggering the array at zenith angles $\leq 30^0$ falling 50 metres from the central detector, the overall uncertainty in zenith angle is $\pm 2.0^0$ and that of the azimuthal angle is $\pm 6.0^0$. For showers in the size range $10^5 < N < 10^6$ particles falling at core distances < 72 m from the centre of the array, the error in core position determination is reasonably well represented by a Gaussian distribution of standard deviation 6.0 m (Ashton et al, 1977).

CHAPTER 4

EXTENSIVE AIR SHOWERS AND THE DEPENDENCE OF THEIR AGE PARAMETER ON SHOWER SIZE AND ZENITH ANGLE

4.1 INTRODUCTION

An extensive air shower (E.A.S.) is produced as a result of a complicated chain of events initiated when a high energy ($>10^{14}$ eV) cosmic ray particle enters the earth's atmosphere. Many secondary particles are produced as the primary nucleon or nucleons in the case of heavy primaries propagate through the earth's atmosphere, on the average each nucleon making collisions with air nuclei every 80 $g.cm^{-2}$. The secondary particles move through the atmosphere in almost the same direction as the primary particles and give rise to a cascade of particles, some of which penetrate to sea level. Consequently, the total number of particles in the shower can be very large and the particles are scattered over a very large area at sea level. The nature of E.A.S. depends upon the nuclear interaction characteristics such as the multiplicity of secondaries and the inelasticity of nucleon-nucleon and pion-nucleon collisions. Also, the size of the E.A.S. produced (the total number of particles in the shower) depends on the level of the first interaction and the level of observation. The lateral extension of showers ensures the detection near sea level of showers initiated by primaries which are incident on the top of the atmosphere over quite a large area. The observation of E.A.S. provide a unique method of detecting ultra high energy particles ($\geqslant 10^{14}$ eV). By studying various parameters of the different components of E.A.S. and the relationship between them, then in principle the primary spectrum, mass composition and the characteristic of high energy interactions can be deduced. There are four principal components of cosmic rays in the atmosphere :

(i) A nuclear component containing particles capable of producing nuclear collisions. It is attenuated strongly in passing through the atmosphere. It consists of surviving primary nucleons and secondary charged pions produced by the hadron cascade.

(ii) An electron-photon component which owes its origin mainly to the production of neutral π mesons in nuclear collisions which decay into two γ-rays which then multiply by pair production and bremsstrahlung processes. It reaches a broad maximum at about 5 km altitude, and is then attenuated by absorption processes before it reaches the earth's surface (see section 4.2).

(iii) A muon component which owes its origin to the decay ($\pi \rightarrow \mu + \nu$) of charged pions. Muons are weakly interacting particles and in general propagate directly to sea level from their point of production.

(iv) A neutrino component which arises from the decay of unstable particles in the atmosphere, mostly pions and muons. Neutrinos undergo only weak interactions with matter and are capable of passing through the earth without any sensible attenuation.

4.2 THE ELECTRON-PHOTON CASCADE

Neutral π-mesons decay, within a very short time ($\sim 2 \times 10^{-16}$ sec). predominantly into two photons which by creation of electron-positron pairs initiate an electromagnetic cascade. The number of particles in the cascade continues to multiply until the energy of the electrons is degraded to such an extent that ionization loss dominates the energy loss by bremsstrahlung and until the photon energies have been reduced to the point where Compton scattering and photoelectric absorption dominate the pair-production process. As the shower propagates through the atmosphere the number of shower particles reaches a maximum and

subsequently decreases with increasing atmospheric depth. The development of an air shower can be understood by studying the shower cascade curve which shows the dependence of shower size on the depth in the atmosphere for a fixed primary energy. The cascade curve is investigated by plotting the shower size as a function of depth for equal shower intensity. Figure 4.1 shows the experimental results obtained for many showers recorded by different experiments at various observational levels. Information on the character of nuclear interactions at high energies ($>10^{14}$ eV) can be obtained from such longitudinal development curves.

Gaisser (1974) has studied the longitudinal development curves using the Chacaltaya results of Bradt et al (1965) and La Pointe et al (1968) and has found that they are consistent with iron primaries when the scaling hypothesis is modified to allow for an increase in the production cross section with energy and some allowance for the intranuclear cascading is introduced. Khristiansen (1975) has pointed out that the experimental data at mountain altitudes are inconsistent with the extrapolation of the scaling hypothesis to the high energy region (10^{14}-10^{17} eV).

4.3 LATERAL DISTRIBUTION OF CHARGED PARTICLES

The lateral distribution of shower particles, i.e. the dependence of the particle density on the distance from the shower axis, is of interest for two reasons. Firstly, the shower-particle distribution relative to the direction of motion of the primary particle, or the shower axis, reflects the development of the shower during its passage through the atmosphere. Comparison of the experimental lateral distribution of particles in showers with different total numbers of particles, and at different depths in the atmosphere, with theoretical distributions obtained on the basis of different models, yields some information about the process which gave rise to the deflection of the particles from the

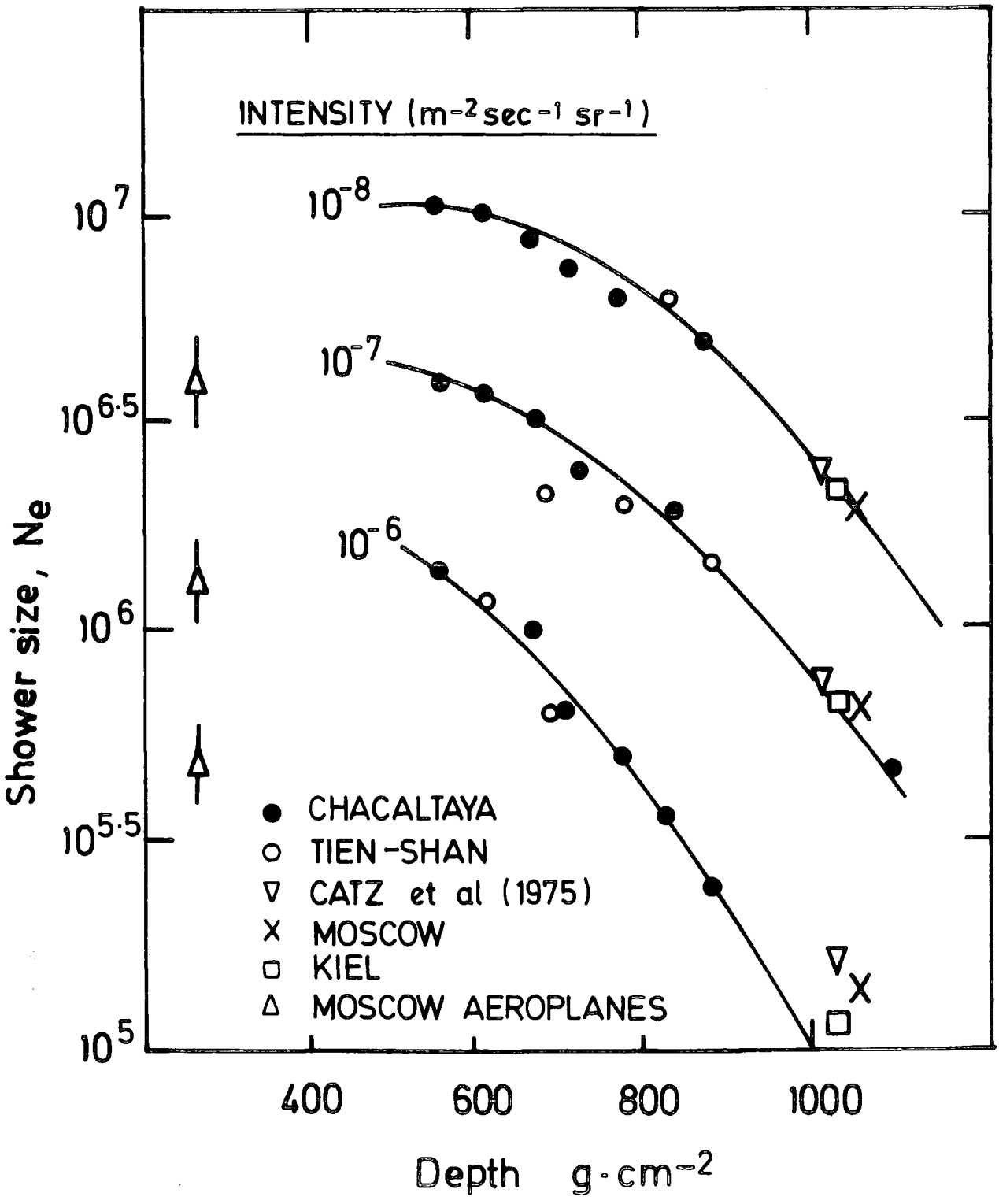

Figure 4.1 : The longitudinal development of air showers. The experimental data shown are derived from equi-intensity cuts of size spectra (After Catz et al, 1975).

shower axis. Secondly, a knowledge of the lateral distribution of shower particles may be used to determine the total number of particles crossing the plane of observation. The latter number can in turn be employed to estimate the energy of the primary particle initiating the shower, which is important in the analysis of experimental data on extensive air showers. Nishimura and Kamata (1952, 1958) have derived the expected lateral structure function of E.A.S. particles. Their derivation was based on a purely electromagnetic cascade shower theory taking into account the multiple scattering of electrons. Greisen (1956) produced a simplified formula representing the lateral distribution of all charged particles in E.A.S. of size N_e at sea level (known as the N.K.G. formula, i.e. Nishimura, Kamata, Greisen) which is given as

$$\rho_e(N_e,r) = \frac{N_e}{r_1^2} f\left(\frac{r}{r_1}\right) \qquad (4.1)$$

where $$f\left(\frac{r}{r_1}\right) = C(s) \left(\frac{r}{r_1}\right)^{s-2} \left(1 + \frac{r}{r_1}\right)^{s-4.5} \qquad (4.2)$$

s is the shower age parameter and is a measure of the stage of development for the shower, r is the distance to the shower axis, r_1 is the Moliere unit having a value of 79 metres at sea level and C(s) is normalization factor related to the cascade age parameter as follows :

$$C(s) = 0.443\ s^2\ (1.9-s) \quad \text{for } s < 1.6$$

$$C(s) = 0.366\ s^2\ (2.07-s)^{5/4} \quad \text{for } s < 1.8$$

An empirical formula representing the lateral electron shower density has been suggested by Greisen (1960) which is based on experimental measurements done over a wide range of shower sizes (10^3-10^9) at core distances ranging from 5 cm to 500 m and at various atmospheric depths of observation varying from 537 g.cm^{-2} to 1800 g.cm^{-2}. This formula is

given as:-

$$\rho_e(N_e,r) = \frac{0.4N_e}{r_1^2}\left(\frac{r_1}{r}\right)^{0.75}\left(\frac{r}{r+r_1}\right)^{3.25}\left(1+\frac{r}{11.4\,r_1}\right) \qquad (4.3)$$

for s = 1.25. Measurements of the lateral structure function have been carried out by many workers using different measuring techniques and it has been found that the shape of the structure function is dependent slightly upon the type of the detectors employed. The measurements done with Geiger tubes give a good representation of the actual density distribution of the shower particles, while measurements with scintillation counters give a slightly steeper distribution. This is attributed to the sensitivity of the scintillator to the photon component of the shower. Figure 4.2 illustrates this fact, and shows a comparison of various electron lateral distributions (normalized to a common shower size of 10^5 particles) measured by different groups. The measurements of Hasegawa et al (1962), who used an array of scintillation counters, show a steeper density distribution than that of Greisen (1960), for an age parameter of 1.25. Hasegawa et al found that their data could be represented by the following expression :

$$\rho(N_e,r) = \frac{N_e}{2\pi\sqrt{120\pi}}\,\frac{\exp(-r/120)}{r^{1.15}} \qquad (4.4)$$

Detailed analysis of the experiment of Catz et al (1975) has shown that the lateral distribution of particle densities recorded by scintillation counters can be described by the following relation :

$$\rho_e(N_e,r) = \frac{1.57 \times 10^{-2} \times N_e}{(1+r)^{1.62}}\exp(-r/120) \qquad (4.5)$$

where r is the distance from the shower axis, and varies from about 2 metres to about 70 metres. The lateral distribution of electrons in E.A.S. obtained by Catz et al (see figure 4.2) seems to agree well with

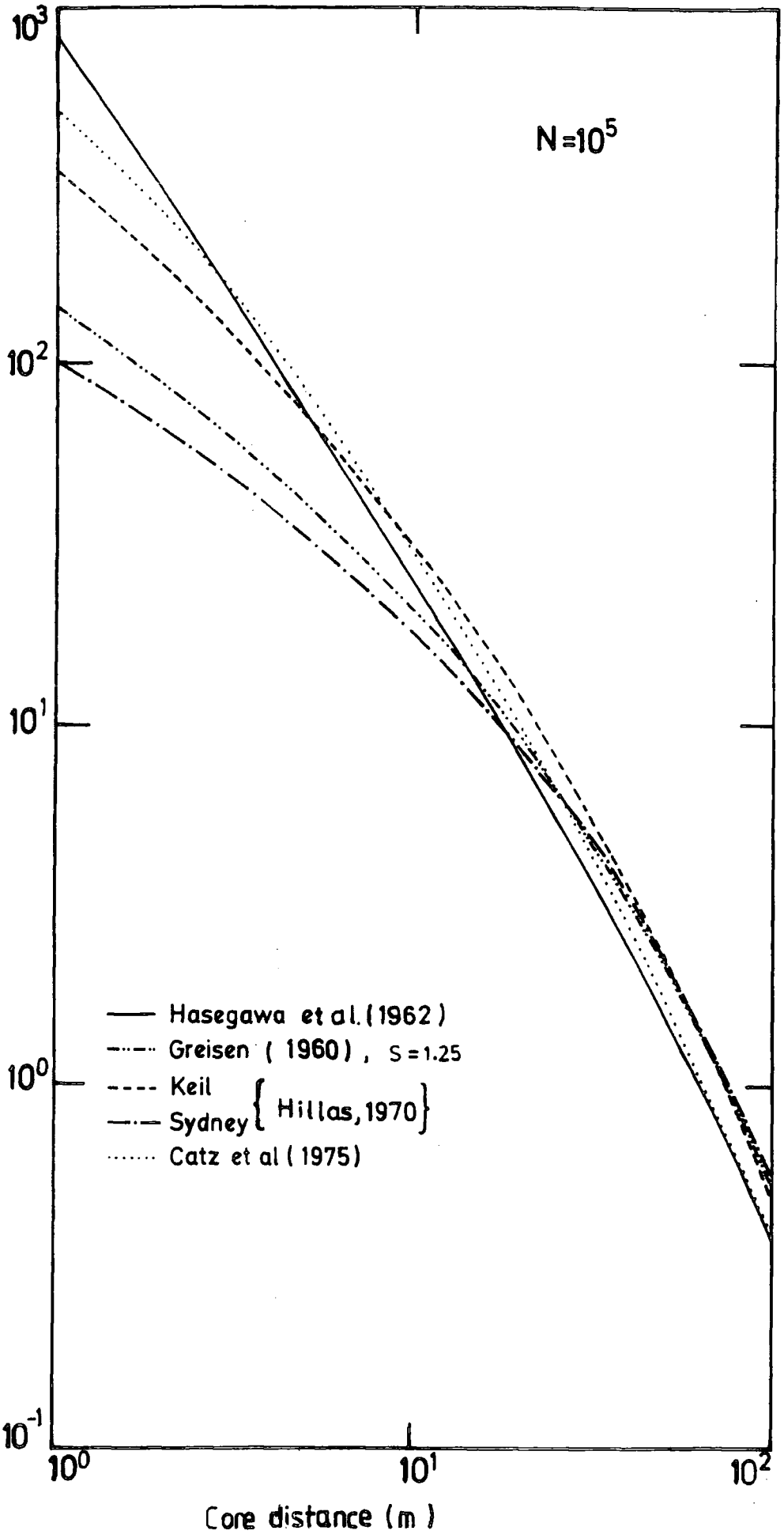

Figure 4.2 : Measurements of the electron lateral distribution function obtained by different workers at sea level and normalized to a common shower size of 10^5 particles.

the N.K.G. relation for an age parameter of 1.25. It is also clear from the figure that this distribution is steeper than that suggested by Greisen (1960) in the region below 20 metres from the shower core. The distribution of particle densities observed by the Sydney group (Hillas, 1970) for large air showers gives a much flatter distribution. The flattening of the distribution can possibly be attributed to the detection of multi-cored showers induced by primaries of energies greater than 10^{15}eV. Nevertheless, it can be concluded from figure 4.2 that there is general agreement between the above mentioned distributions in the region 20-100 metres from the shower axis. There is some discrepancy between the measurements at distances near to the shower axis and at large distances ($\geqslant$100 metres). This discrepancy could be due partly to inaccurate shower core determination and partly to the effect of the dependence of the measured lateral distribution on the type of particle detector used in the apparatus.

4.4 THE SHOWER AGE PARAMETER

The behaviour of the electron-photon cascade is well described in terms of cascade shower theory (Nishimura and Kamata, 1958). According to this theory, the stage of shower development is characterised by an age parameter (s) which is defined approximately as :

$$s = 3t/(t + 2y_0 + 2x) \qquad (4.6)$$

where $y_0 = \ln (W_0/\varepsilon_c)$, W_0 being the energy of the photon that initiated the shower cascade and ε_c is the electron critical energy in air, 84 MeV. Further, $x = \ln(r/r_1)$, r and r_1 are defined as in equation 4.1 and t is the atmospheric depth ($g.cm^{-2}$). If the age parameter is less than one, then the shower is in the early stages of development and is called a "young" shower. At maximum development the age parameter is assigned a

value of unity while for age parameter larger than one, the shower has passed its maximum development and is decreasing in size, it is now defined as an "old" shower.

Equation (4.6) shows the dependence of the age parameter on radial distance. In practice, this dependence is rather weak. Figure 4.3 shows the effect of the age parameter on the lateral electron density distribution obtained using the N.K.G. distribution function. From the experimental observation on E.A.S. at sea level, Vernov et al (1970) have suggested that, as the shower size increases, the average age parameter increases. The mountain altitude observations of Miyake et al (1973) support this increase. Figure 4.18a shows the shower age parameter for various shower sizes as predicted by Karakula, (1968) (see Wdowczyk, 1973) on the basis of the so-called standard model of high energy interactions of De Beer et al (1966).

4.5 EXPERIMENTAL ARRANGEMENT AND ANALYSIS

The Durham E.A.S. array was previously described in Chapter two and a scale diagram of it is shown in figure 2.1. Air showers were selected by inner ring and outer ring triggers; a 2 particles m^{-2} coincidence in detectors 11, 31, 51 and 13, 33, 53 with a further requirement of 4 particles m^{-2} in the central detector C. The areas of the detectors vary from 2 m^2 to 0.75 m^2 . For each event the sampled electron densities were used to measure the age parameter of the shower (s was determined by assuming the core position was as found assuming the Greisen structure function was correct and the best s and N that fitted the measured electron densities in E.A.S. detectors was then found). This was achieved by computer using the CERN MINUIT programme which is a package for minimizing a function of n parameters. Table A.1 shows values of C(s) corresponding to given age parameters that were used in the

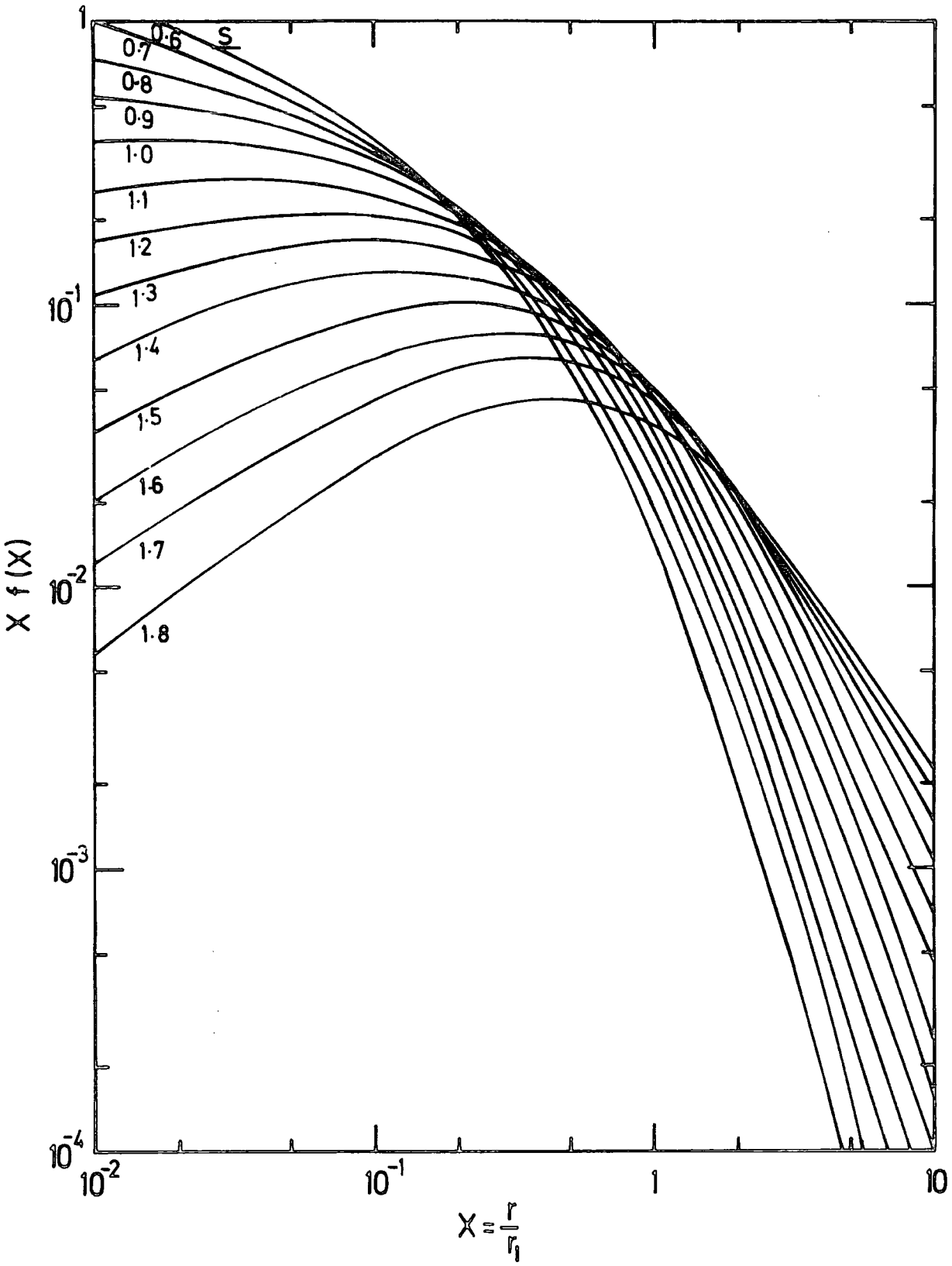

Figure 4.3 : The dependence of the electron structure function on the age parameter for a fixed shower size. The curves are obtained by using the N.K.G. structure function.

data analysis (see Appendix A). In deriving the age parameter distribution, we have to consider the fact that the efficiency of triggering depends on age for a given shower size. The requirement for an E.A.S. trigger is that the density of particles in each triggering detector exceeds a certain level. Since the density given in equation 4.1 depends on s, the distance from the axis r is a function of N and s for a given ρ. Hence the collecting area depends on s as $\pi r^2(N,s)$ for a given triggering level of ρ. For the present triggering level, the minimum shower size to produce an inner ring and outer ring trigger as a function of age is given in figure 4.4. For that reason showers of size $7.1.10^4$ particles for inner ring and $2.3.10^5$ particles for the outer ring were chosen to be minimum analyzable shower sizes. The curves of collecting area as function of size were calculated for different age and are shown in figures 4.5 and 4.6 and were used in the data analysis. The age parameter distribution, core distance, zenith angle and the shower size distributions for all the data, the inner ring trigger data and the combined inner and outer ring trigger data, are given in figures 4.7 to 4.9. The data were grouped into different ranges of shower size as shown in table 4.1, where in each size range the measured distribution of age for showers having orthogonal core distances $\leq$95 m for the inner ring and $\leq$105 m for the outer ring triggers from C were obtained. The resulting data was further sub-divided into two ranges of zenith angle ($\theta < 22^0$ and $\theta \geq 22^0$) the results are shown in figures 4.10 to 4.16). The distributions (full lines) are for the showers triggered by the array. The measured age distributions were corrected for the variation of collecting area with shower age and the result is shown by the dashed lines in figures 4.10, 4.13 and 4.16. This was done by using the curves of figures 4.5 and 4.6 which for showers of fixed size shows the variation of collecting area with age. Using this

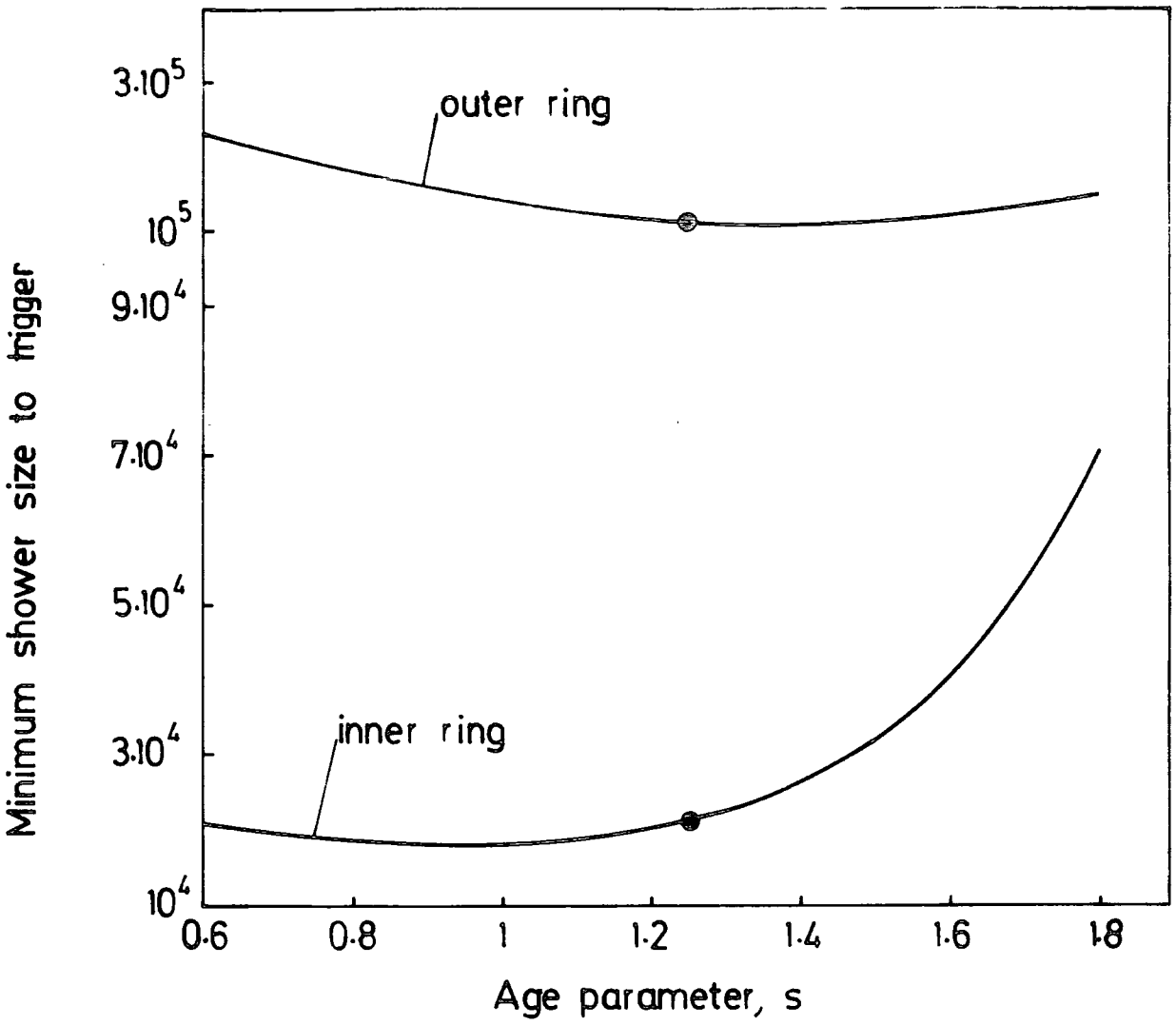

Figure 4.4 : Variation of the minimum shower size as a function of age parameter to produce the inner ring and outer ring triggers.

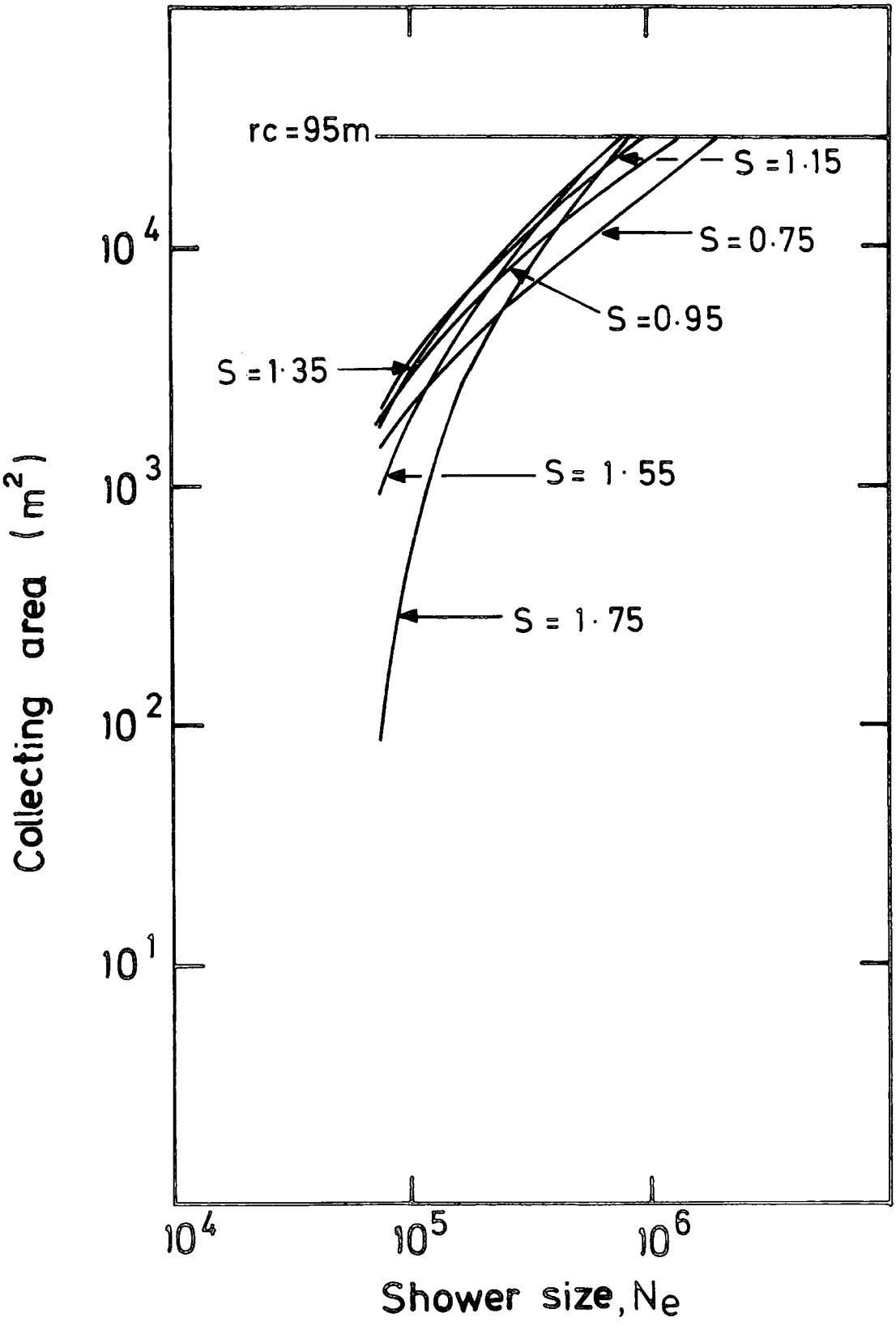

Figure 4.5 : Collecting area as a function of shower size for showers with different age parameter detected by the inner ring trigger Δ_C ($\geq 4m^{-2}$), Δ_{11} ($\geq 2m^{-2}$), Δ_{31} ($\geq 2m^{-2}$), Δ_{51} ($\geq 2m^{-2}$).
All showers have core distance $\leq$95 m from the centre of the array.

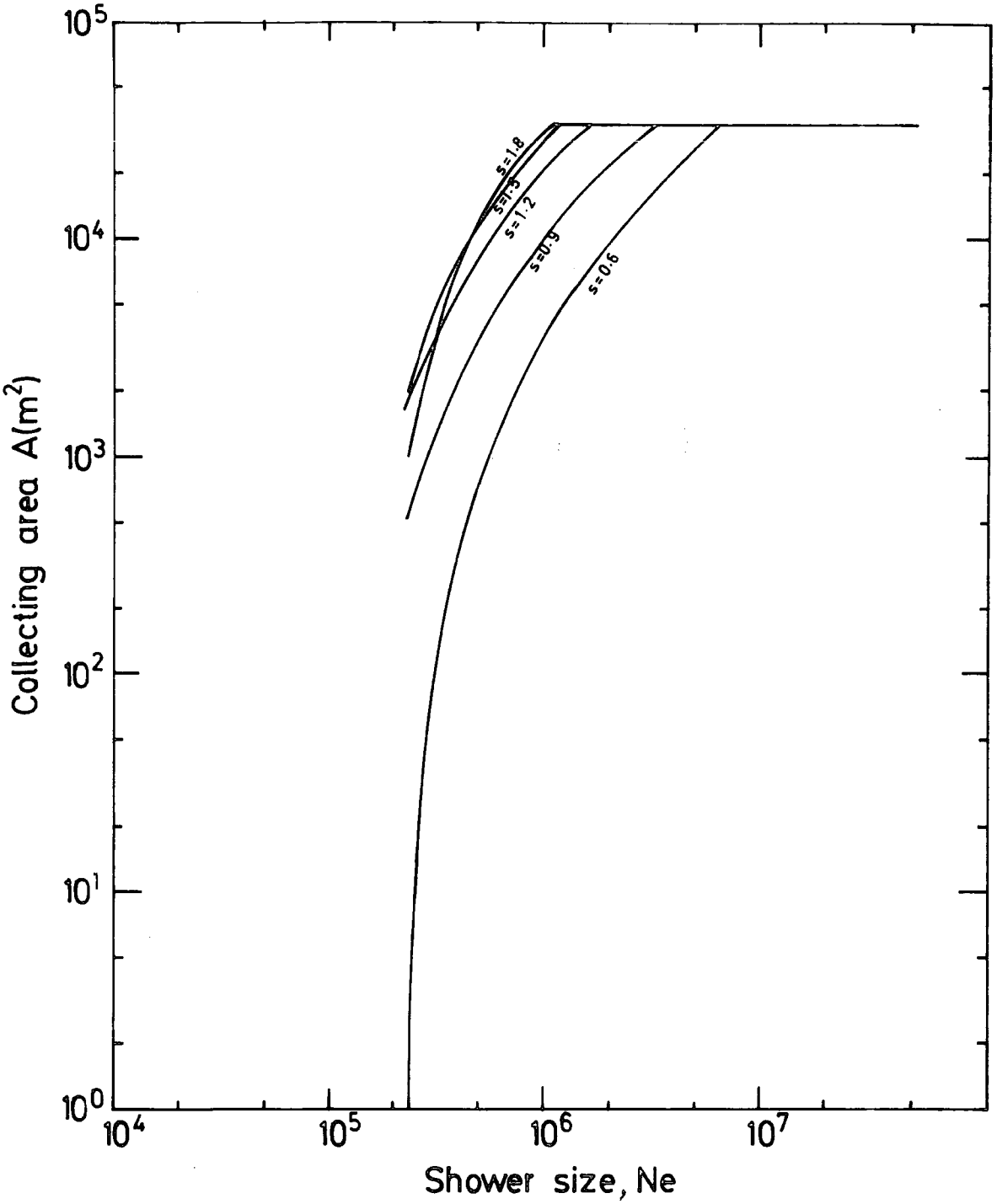

Figure 4.6 : Collecting area as a function of shower size for showers with different age parameter detected by an outer ring trigger, $\Delta_C(\geq 4\ m^{-2})$, $\Delta_{13}(\geq 2\ m^{-2})$, $\Delta_{33}(\geq 2\ m^{-2})$, $\Delta_{53}(\geq 2\ m^{-2})$. All showers have core distance ≤ 105 m from the centre of the array.

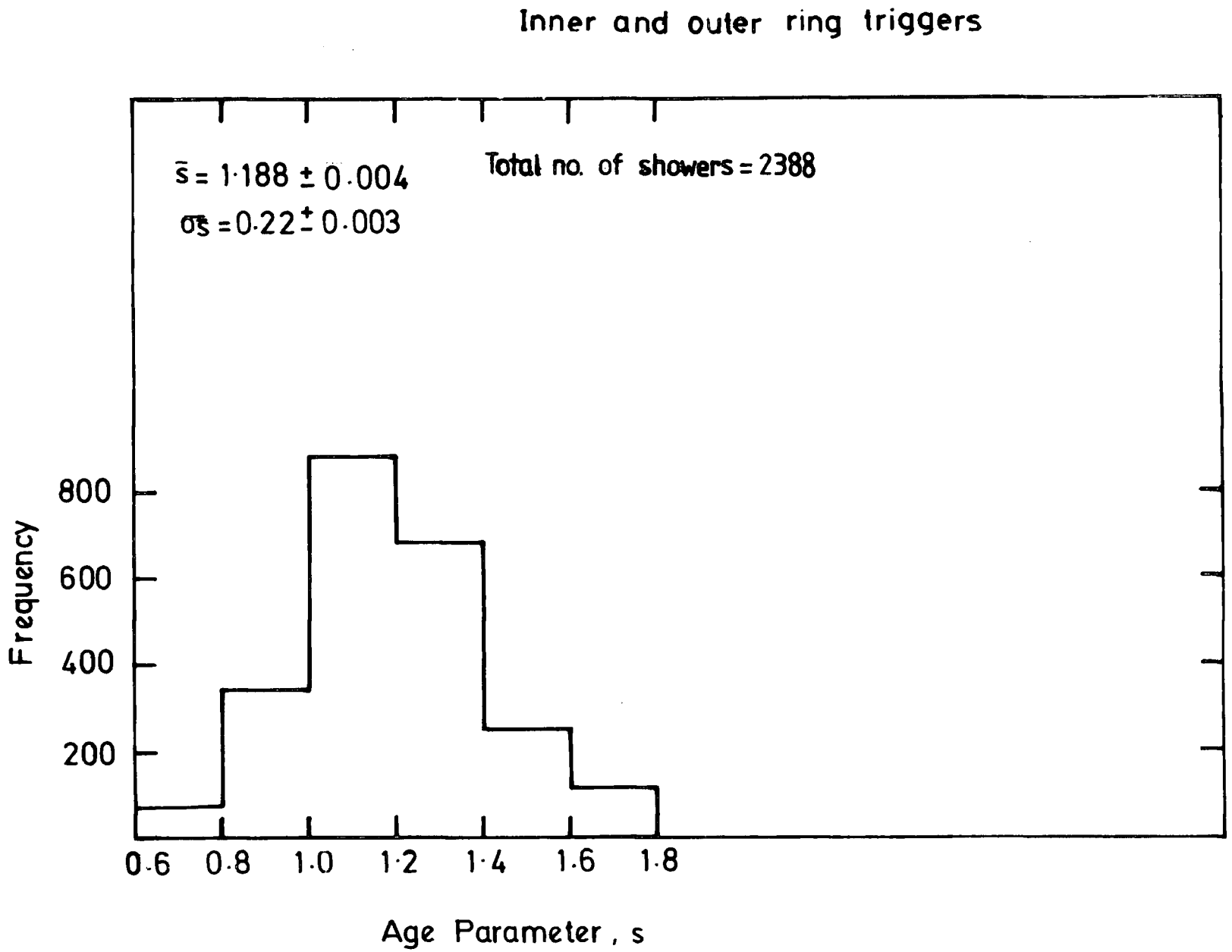

Figure 4.7 : The age parameter of showers detected by the inner and outer ring triggers.

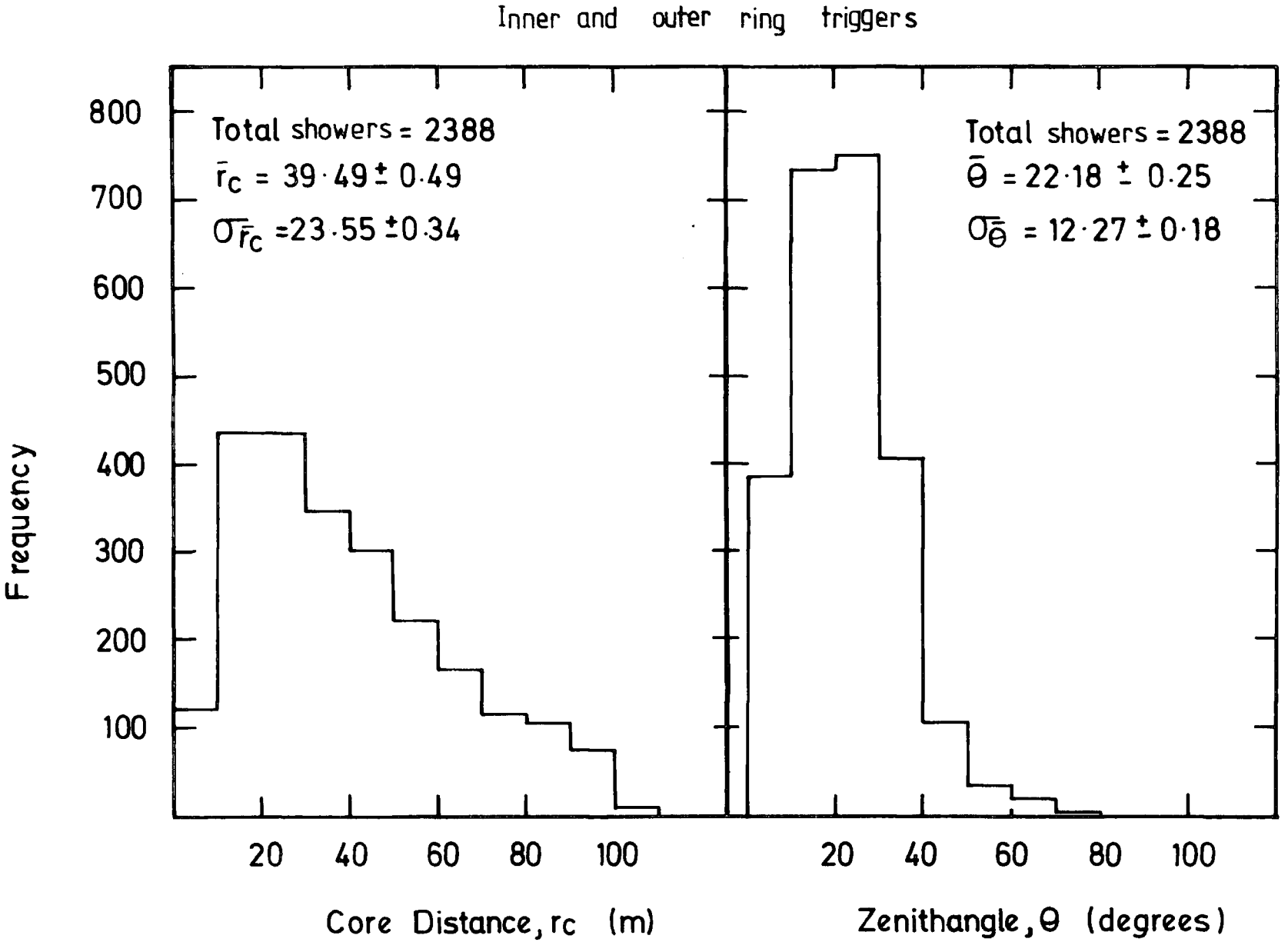

Figure 4.8 : The core distance and zenith angle distributions of showers detected by the inner and outer ring triggers.

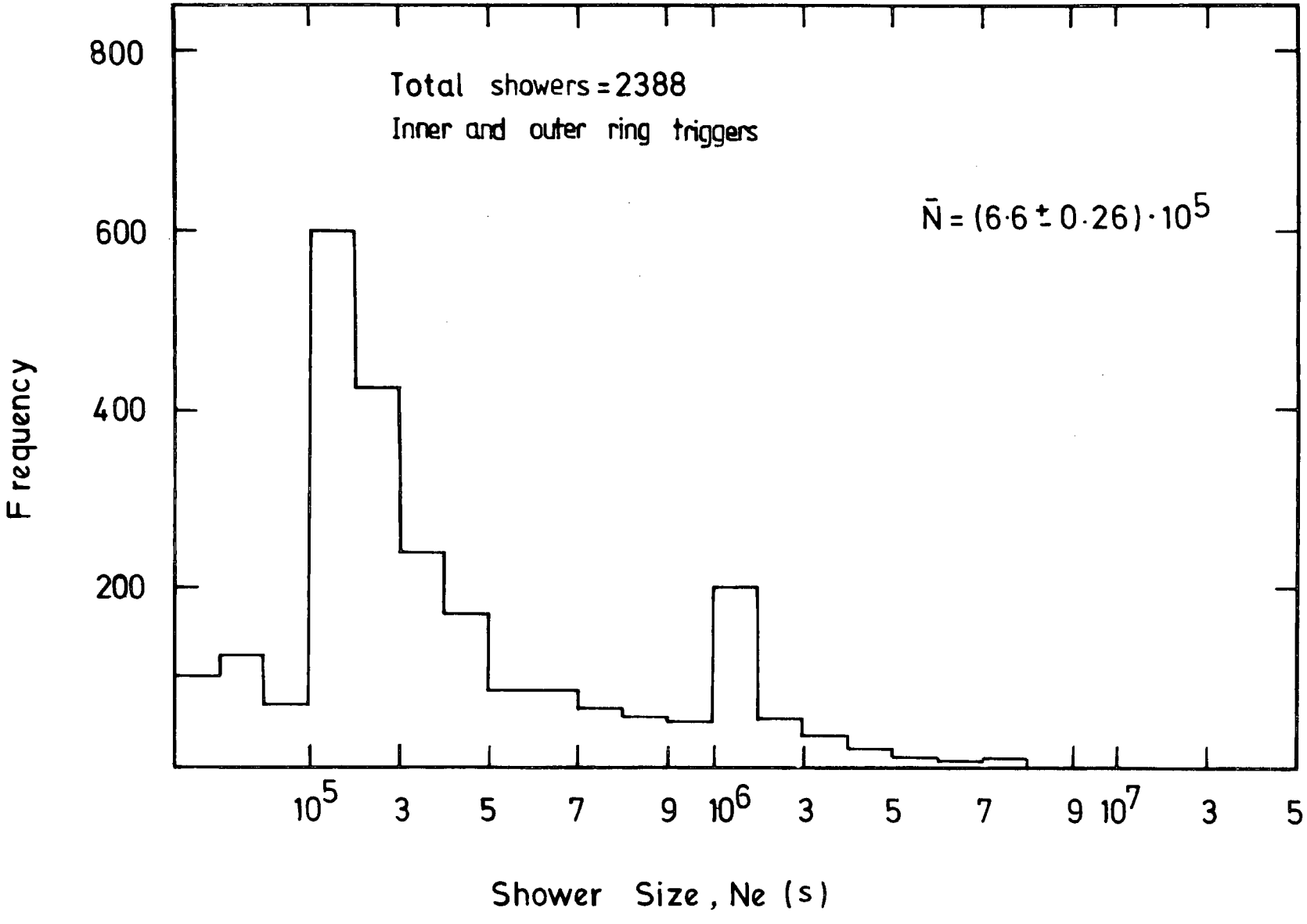

Figure 4.9 : The shower size distribution of showers detected by the inner and outer ring triggers

(a) Inner ring trigger

Size range	$7.1.10^4$-10^5	10^5 -6.10^5	6.10^5 -8.10^6	Total
Total no. of events for $\theta < 22^o$	133	659	125	917
Total no. of events for $\theta \geq 22^o$	165	539	111	815
Total	298	1198	236	1732

(b) Outer ring trigger

Size range	$2.3.10^5$-5.10^5	5.10^5-5.10^6	5.10^6-5.10^7	Total
Total no.of events for $\theta < 22^o$	134	186	21	341
Total no.of events for $\theta \geq 22^o$	123	182	10	315
Total	257	368	31	656

Table 4.1 : The total number of analysed events detected by the (a) Inner ring, (b) Outer ring triggers for two ranges of zenith angle ($\theta < 22^o$ and $\theta \geq 22^o$) and for the different ranges of shower size. r_c, the core distance from the central detector was taken to be $\leq$ 95 m for inner ring and $\leq$ 105 m for outer ring triggers.

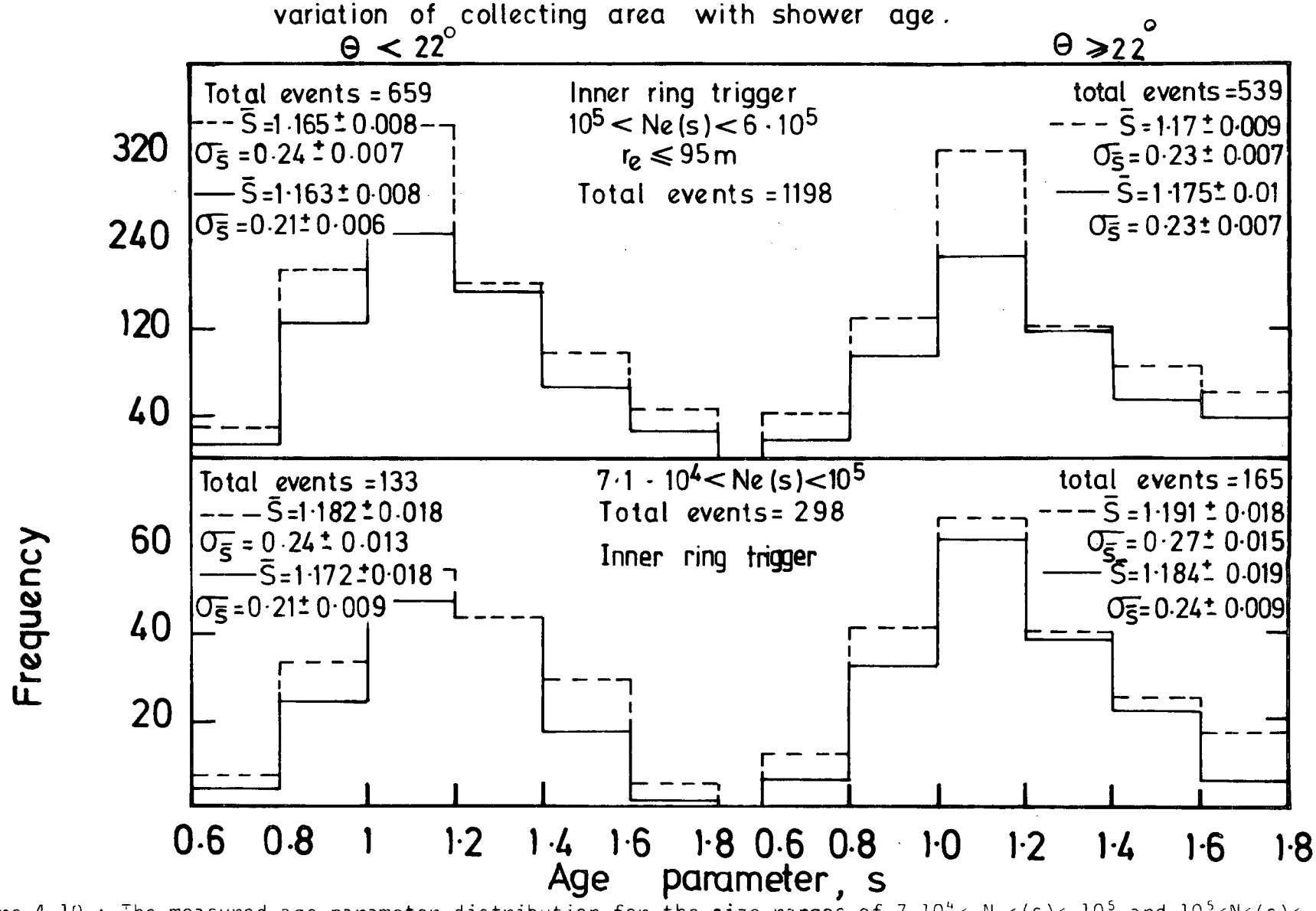

Figure 4.10 : The measured age parameter distribution for the size ranges of $7.10^4 < N_e(s) < 10^5$ and $10^5 < N_e(s) < 6.10^5$ particles and for two zenith angle ranges ($\theta < 22^0$ and $\theta \geq 22^0$). The dotted lines are the distributions corrected for variation of collecting area with age parameter.

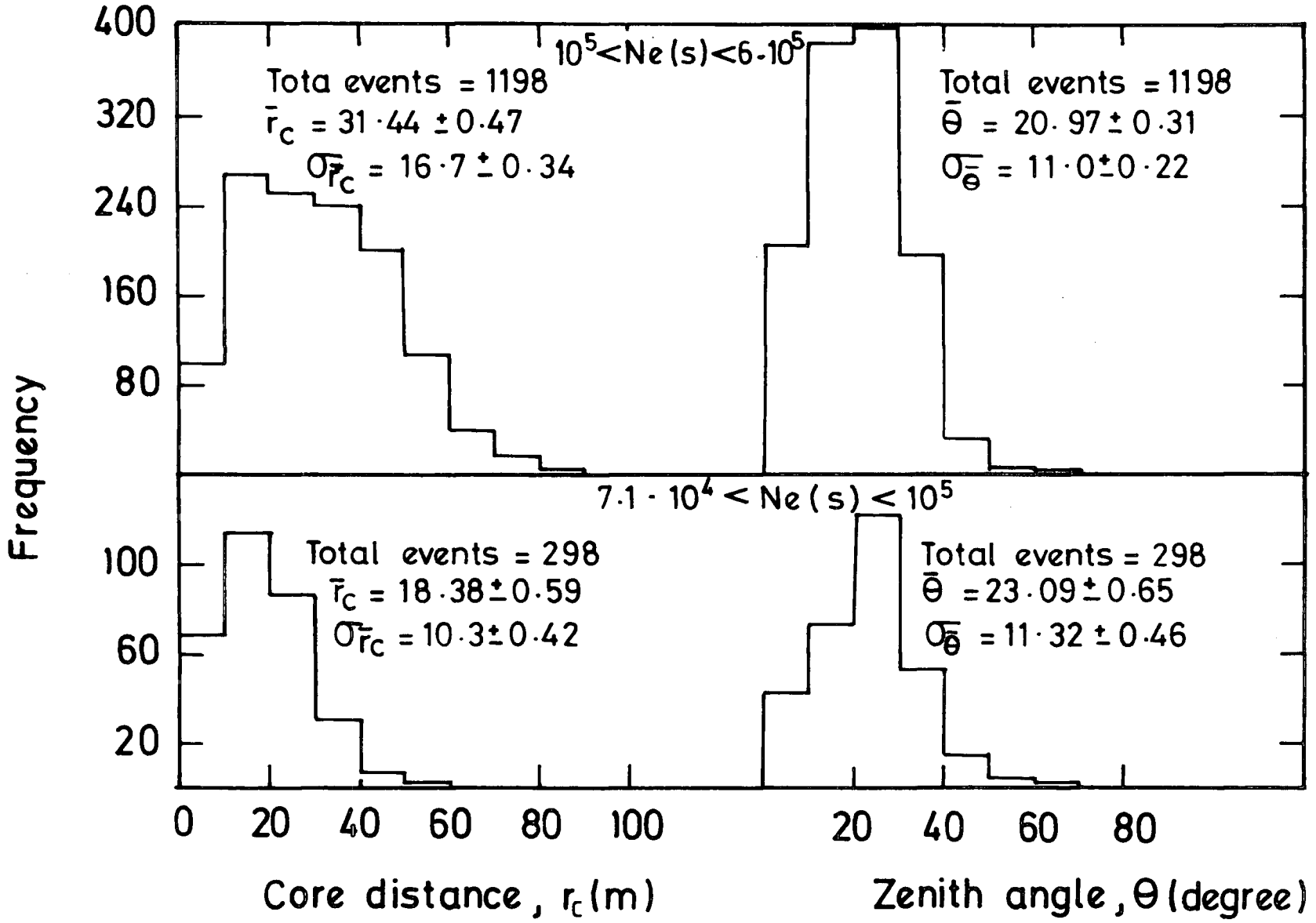

Figure 4.11 : The core distance and zenith angle distribution of events in the size ranges of $7.1.10^4 < N_e(s) < 10^5$ and $10^5 < N_e(s) < 6.10^5$ particles for inner ring triggers.

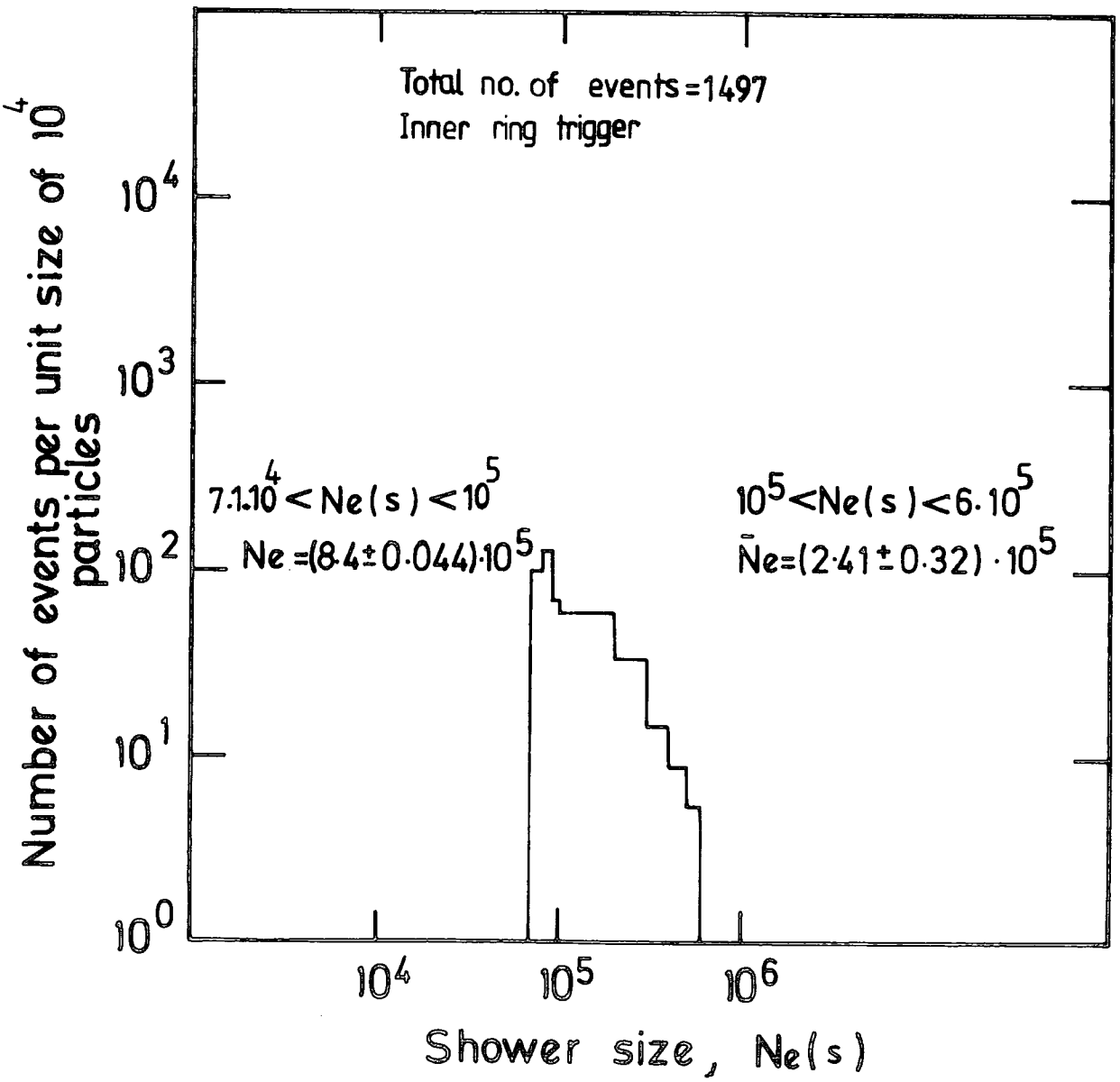

Figure 4.12 : The shower size distribution for the ranges of $7.1.10^4 < Ne(s) < 10^5$ and for $10^5 < N_e(s) < 6.10^5$ particles for inner ring triggers.

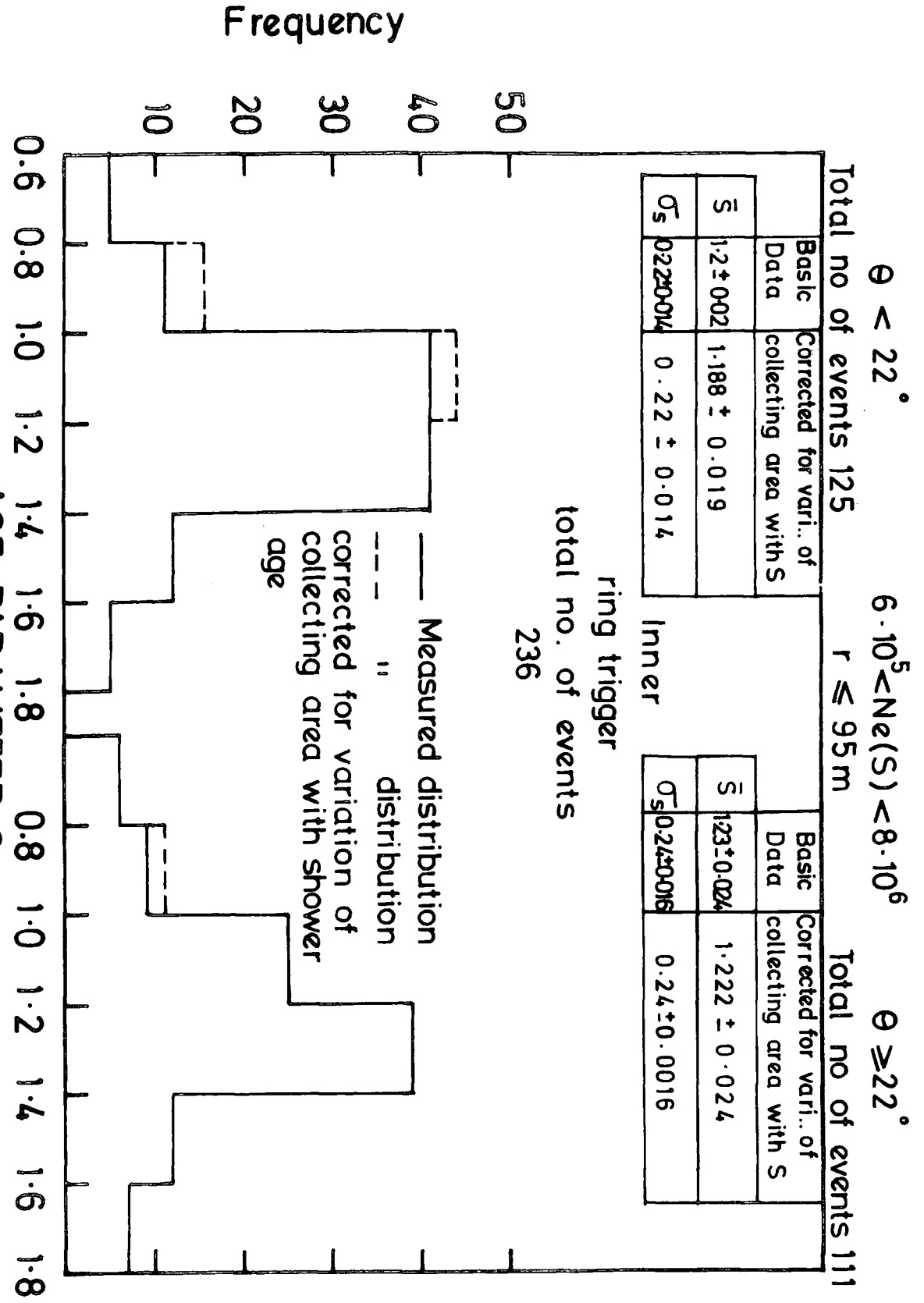

Figure 4.13 : The measured age parameter distribution for the size range of $6.10^5 < N_e(s) < 8.10^6$ particles and for two zenith angle ranges ($\theta < 22^0$ and $\theta \geq 22^0$). The dotted lines are the distributions corrected for variation of collecting area with age parameter.

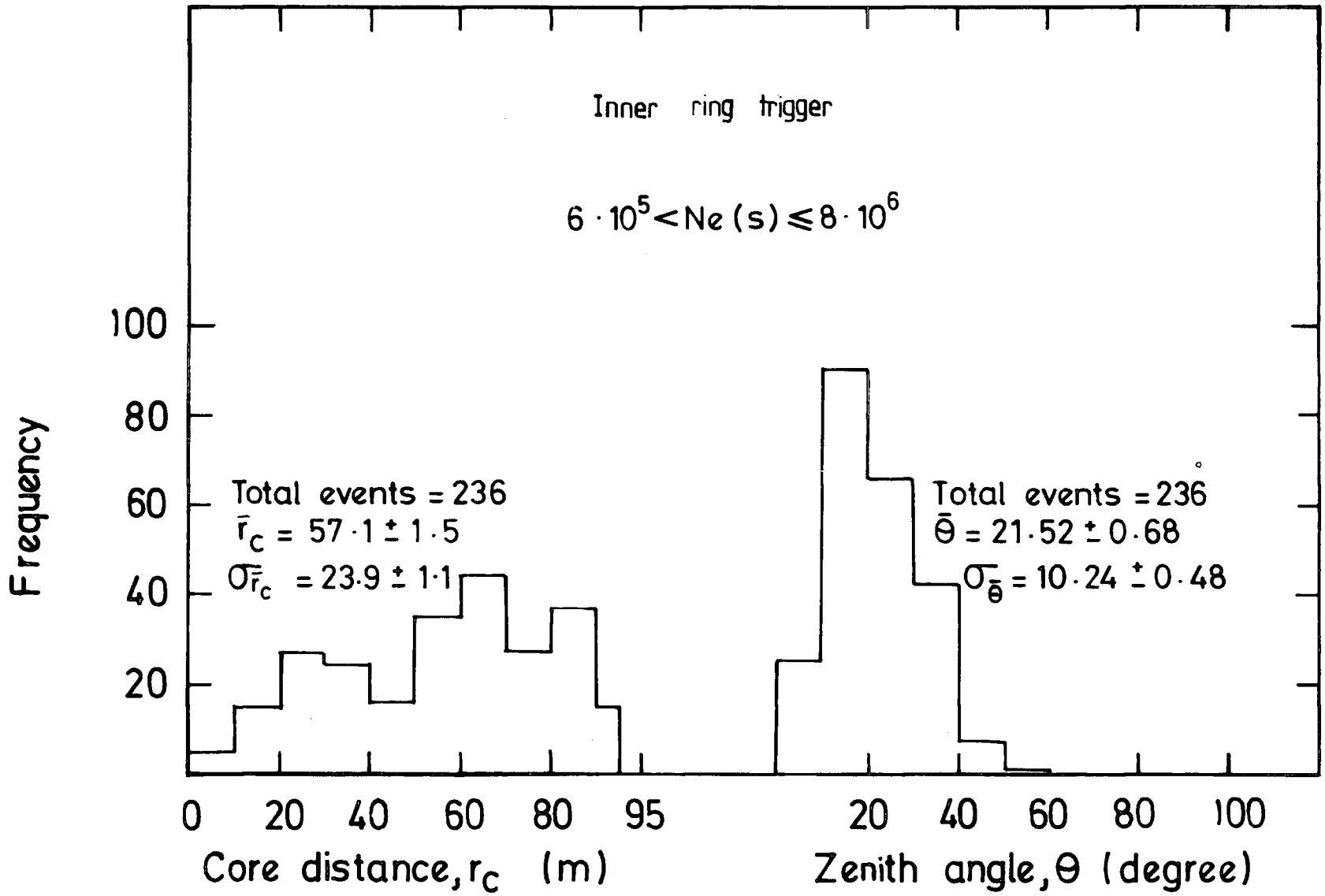

Figure 4.14 : The core distance and zenith angle distribution of events in the size range of $6.10^5 < N_e(s) \leq 8.10^6$ particles for inner ring trigger.

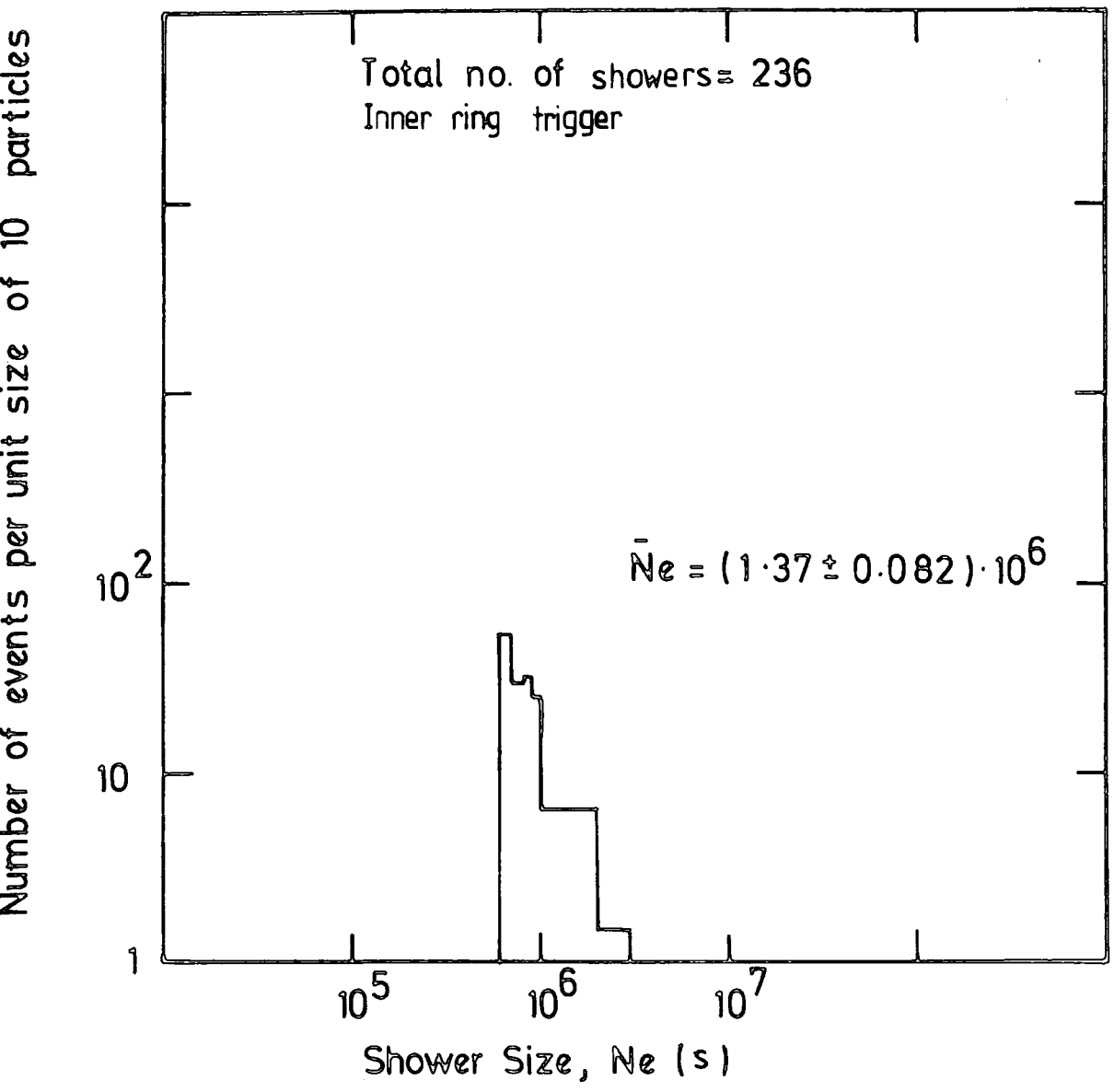

Figure 4.15 : The shower size distribution for the range of $6.10^5 < N_e(s) < 8.10^6$ particles for inner ring trigger.

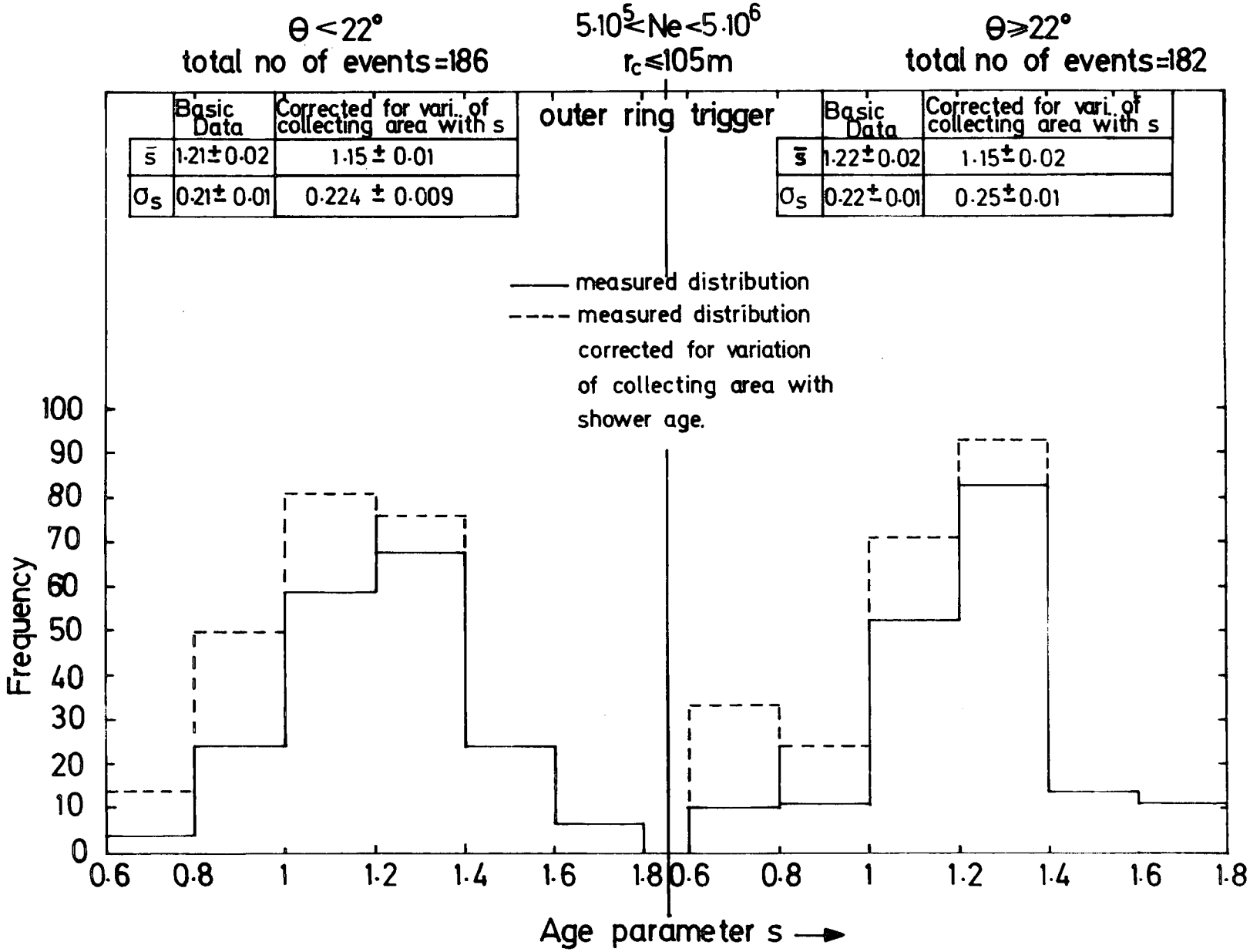

Figure 4.16: The measured age parameter distribution for the size range of $5.10^5 < Ne < 5.10^6$ particles and two zenith angle ranges ($\theta < 22°$ and $\theta \geq 22°$). The dotted lines are the distribution corrected for variation of collecting area with age parameter.

information the relative collecting probabilities for showers of various ages can be found. For every interval of age its average age, $\bar{s}$ and size $\bar{N}_e$ were calculated and by using figures 4.5 and 4.6 the corresponding collecting areas $A(\bar{s},\bar{N}_e)$ were obtained. These areas were used to get the relative collecting proabilities for all intervals which were the ratio of their collecting area to a given area, i.e. for the inner ring trigger area (πr_c^2 : r_c = 95 m) = $2.84.10^4 m^2$. These ratios, or collecting probability factors, have been multiplied by their corresponding frequency of measured age intervals to obtain the corrected frequency of every interval which are shown by the dashed lines. These dashed lines form the corrected distribution of age parameter for the different mentioned ranges of shower size. Examples of showers with different age parameter are given in figures 4.17a and b.

4.6 RESULTS AND COMPARISON WITH PREVIOUS MEASUREMENTS

4.6.1 Dependence of the Age Parameter on Shower Size and Zenith Angle

The expected variation of average age parameter with shower size was calculated by Karakula (1968), where the standard model of E.A.S. development was used. The results are given in figure 4.19, as reported by Wdowczyk (1973), which shows a small decrease of age parameter with increasing shower size, where the decrease is more pronounced for less inclined showers. The simulation work of Acharya et al (1979) on the size-age dependence of E.A.S. is also shown in the figure where a greater average age parameter for primary iron showers than primary proton showers is found. For comparison they presented their experimental results for small showers ((1-4).10^4 particles) at an atmospheric depth of 920 $g.cm^{-2}$ which are consistent with primary protons.

Experimentally it is of interest to note that while most of the

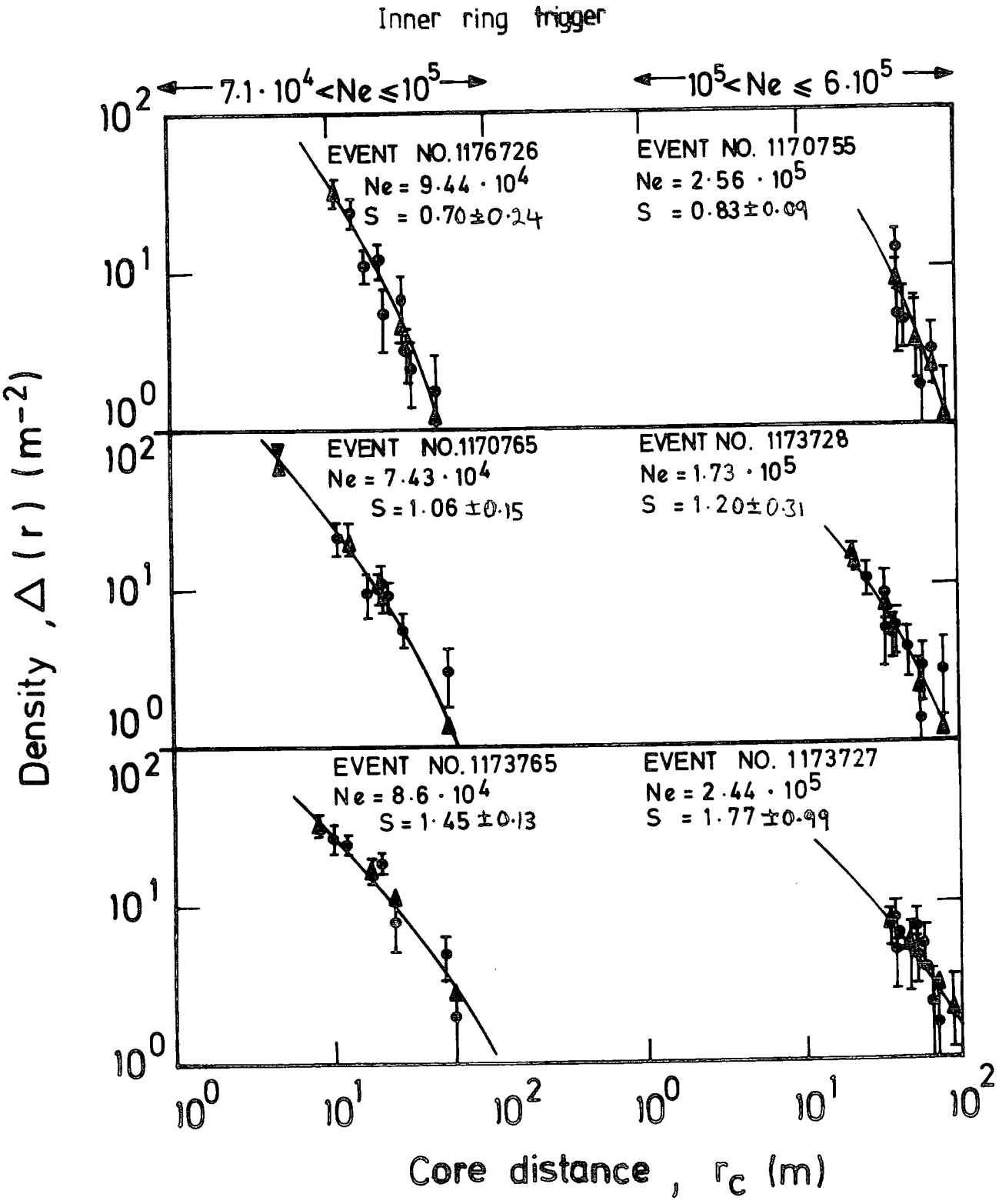

Figure 4.17a : Examples of the lateral structure of typical E.A.S. events (Inner ring triggers)

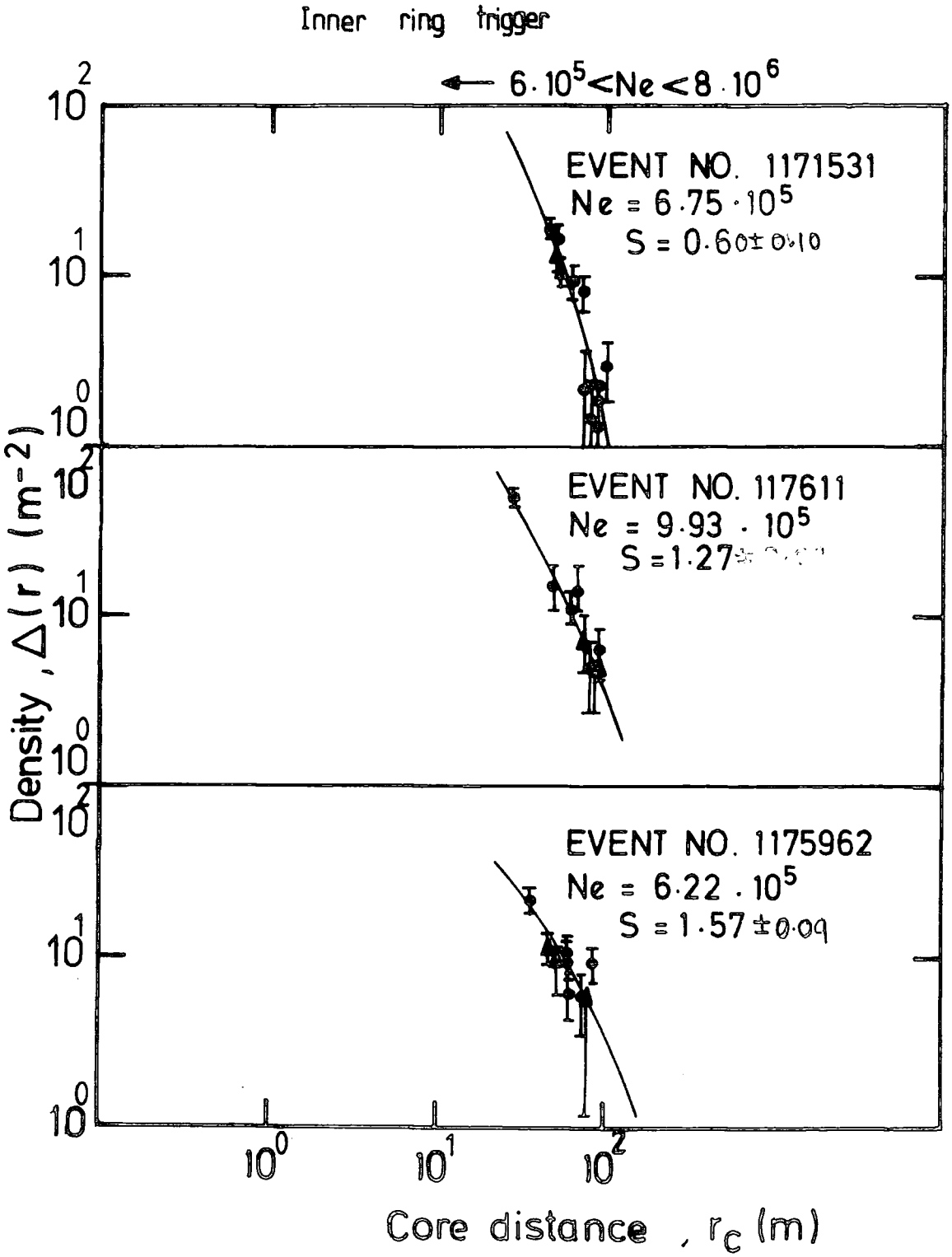

Figure 4.17b : Example of the lateral structure of typical E.A.S. events (inner ring trigger)

measurements do not show any size dependence of the average age parameter (Greisen, 1960) for sizes $<10^6$ particles at sea level there is some evidence which suggests that for larger shower sizes the average age parameter increases with shower size. The experimental points of Vernov et al (1970) at sea level and Miyake et al (1973) at mountain altitude, show this dependence which is shown in figure 4.18. These results indicate that the average age parameter at sea level and mountain altitude increases at an equivalent primary of about 3.10^{16} eV. Miyake et al (1973) suggested that the increase of age in this energy region could be due to a change in the composition of the primary cosmic rays in the properties of high energy nucleon-nucleon collisions.

A more detailed age parameter study is the work of Chuderkov et al (1979) in which they studied the correlation of age parameter with core distance for two core distance ranges of (1-15)m and (6-45) m for $N_e \geqslant 2.10^5$ particles. On the average they found no significant increase of age with core distance, where the mean lateral distribution function is well approximated by a single N.K.G. function.

The present results of the shower size-age parameter dependence is shown in figure 4.19 and table 4.2 and is for six ranges of shower size for both data obtained using the inner and outer ring triggers. The average age parameter for the first two size ranges decreases from 1.182 to 1.165 for the inner ring trigger data and from 1.17 to 1.15 for the outer ring trigger data as predicted by theory, since the maximum development of a shower moves closer to the observation level as the primary energy increases. In general the present measurements are not too inconsistent with expectation except at the largest shower size where a significant increase in the value of the age parameter is observed. The increase is in the same range of primary energy as the increase observed by Vernov et al (1970) and Miyake et al (1973). The dependence of age

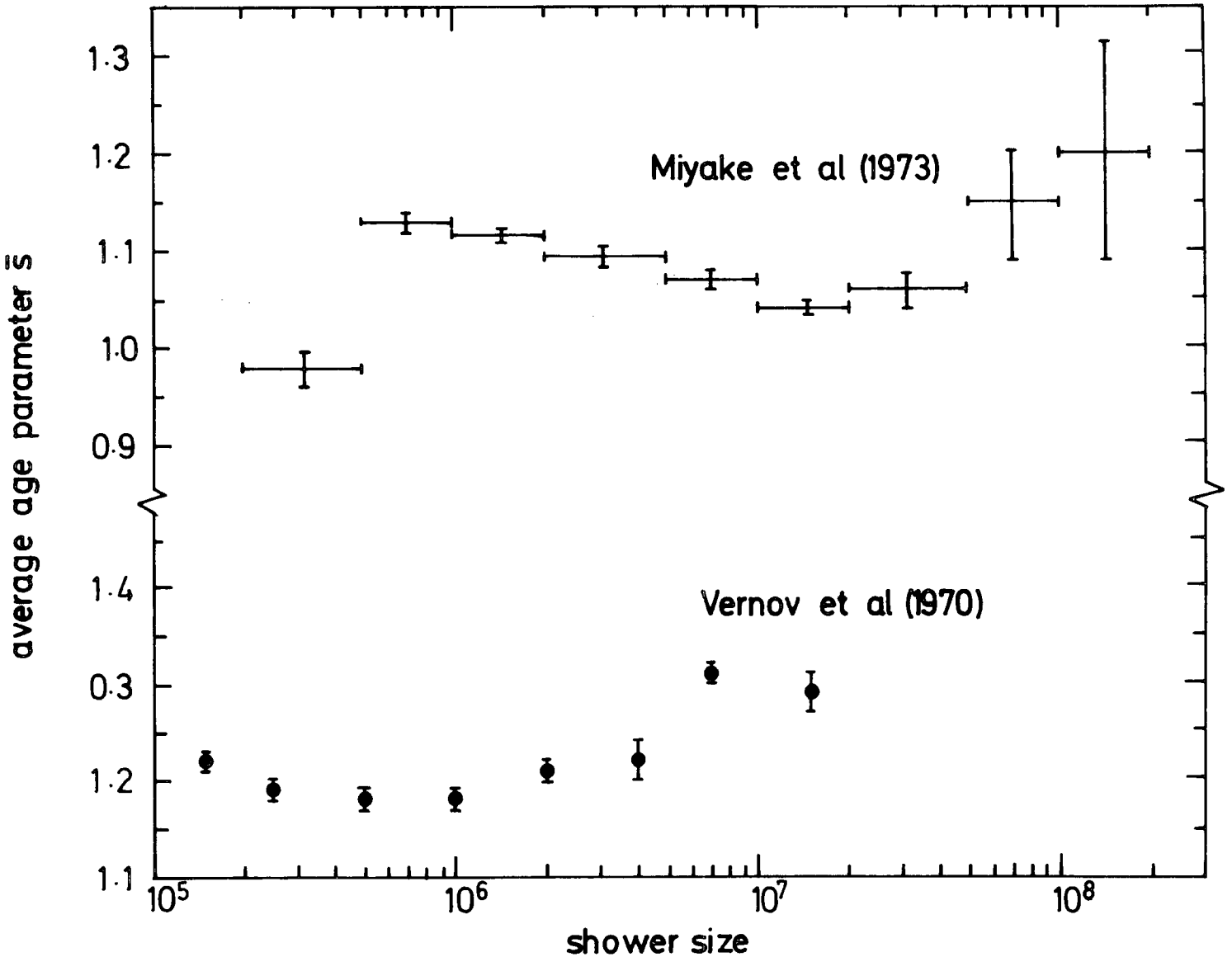

Figure 4.18 : The dependence of average age parameter as a function of shower size measured by Vernov et al (1970) at sea level and by Miyake et al (1973) at 2770 m. elevation.

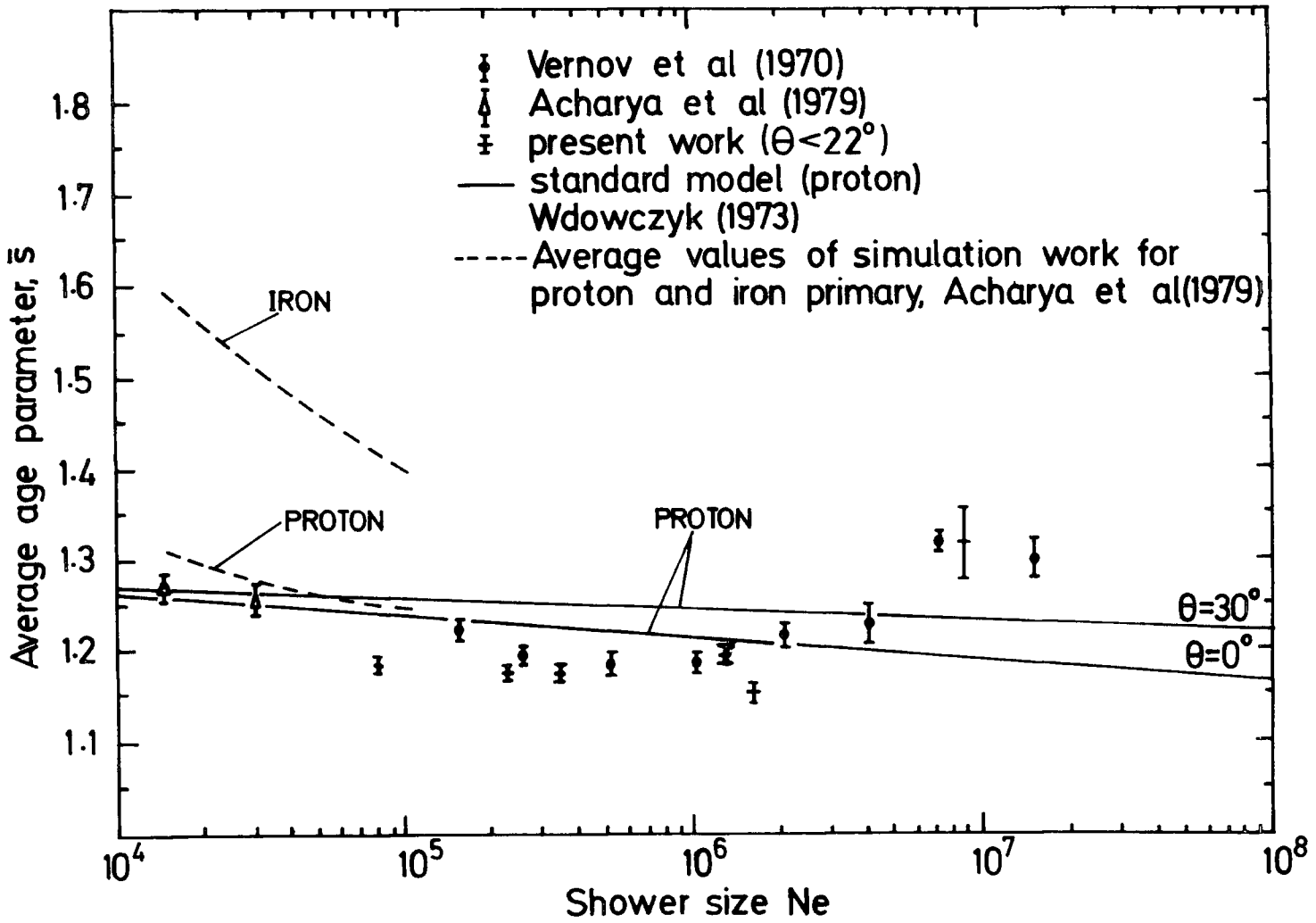

Figure 4.19a : Dependence of the average age parameter on shower size. The experimental points of Acharya et al (1979) are the averages of their raw data uncorrected for bias.

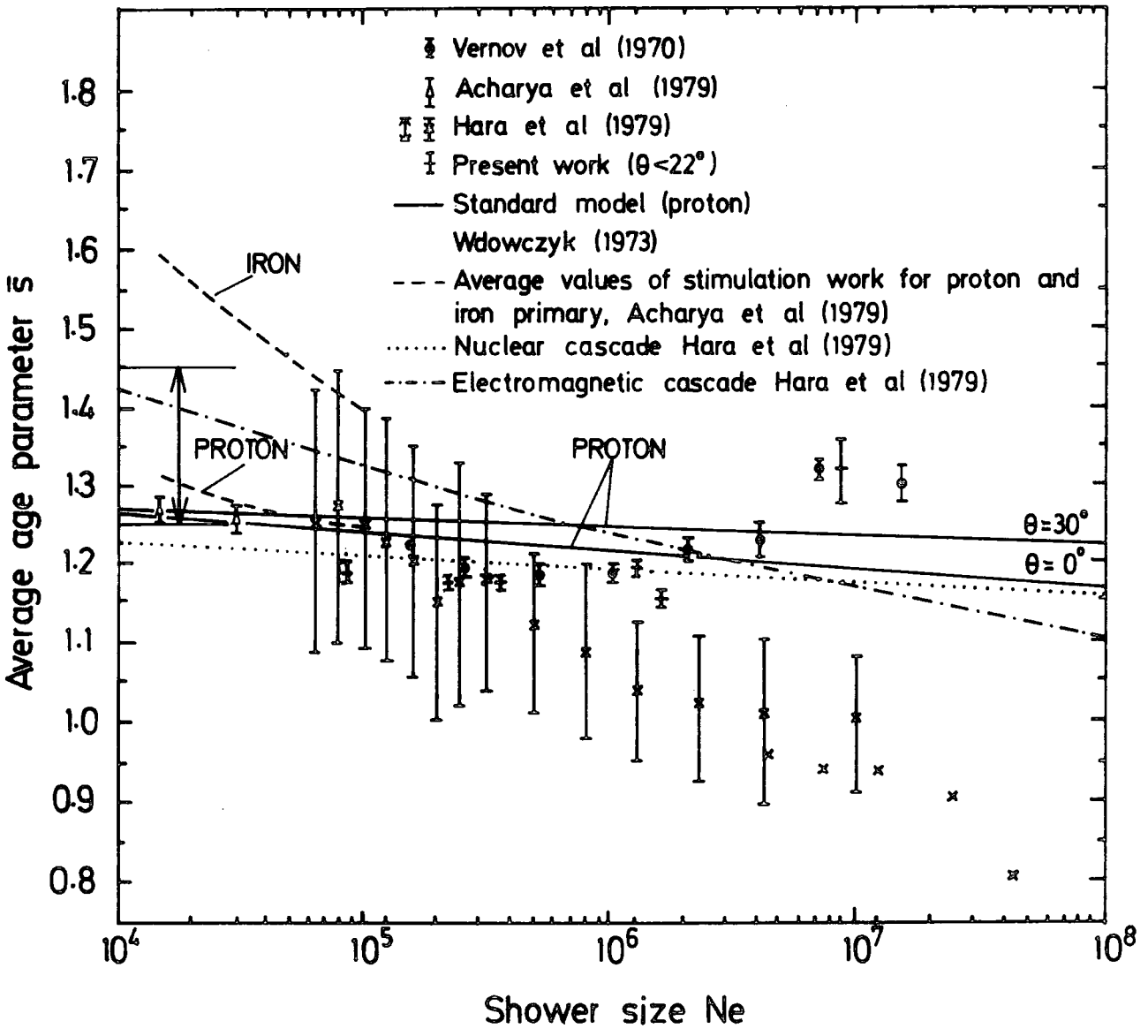

Figure 4.19b : Similar to Figure 4.19a except that the preliminary results obtained using the Japanese Akano EAS array (atmospheric depth 927 $g.cm^{-2}$) are also shown.

(a) Inner ring trigger

Size range	No.of showers analysed	$\sigma_{\bar{s}}$	σ_s	$\bar{N}$	$\bar{r}$
$7.1.10^4$ - 10^5	133	1.182 ± 0.018	0.24 ± 0.013	$(8.4 \pm 0.04).10^4$	18.4 m
10^5 - 6.10^5	659	1.165 ± 0.008	0.24 ± 0.007	$(2.41 \pm 0.32).10^5$	31.4 m
6.10^5 - 8.10^6	125	1.188 ± 0.019	0.22 ± 0.014	$(1.37 \pm 0.08).10^6$	57.1 m

(b) Outer ring trigger

Size range	No.of showers analysed	$\sigma_{\bar{s}}$	σ_s	$\bar{N}$	$\bar{r}$
$2.3.10^5$-5.10^5	134	1.17 ± 0.01	0.191 ± 0.017	$(3.54 \pm 0.05).10^5$	37 m
5.10^5-5.10^6	186	1.15 ± 0.01	0.224 ± 0.012	$(1.65^{+}-0.57).10^6$	65 m
5.10^6-5.10^7	21	1.32 ± 0.05	0.24 ± 0.04	$(8.65 \pm 0.6).10^6$	87 m

Table 4.2 : The measured mean age parameter and the standard deviation of the age parameter distribution about the mean value for showers with zenith angle of $< 22^{\circ}$ in different ranges of shower size of inner ring and outer ring respectively. The mean shower size $\bar{N}$ and the mean core distance $\bar{r}$ of the showers from the central detector of the Durham E.A.S. array is also shown.

parameter on zenith angle was also considered by dividing the showers into two ranges of less than and greater than 22^{0} for the six ranges of shower size. The results show that the average age parameter is independent of θ in the limit of statistical error. It is of interest to mention that at a different altitude and different range of shower size a similar result has been found by Aguirre et al (1973) at 5200 metres above sea level for showers of size $>3.10^{7}$ particles in the zenith angle ranges of $\theta < 20^{0}$, $20^{0} \leqslant \theta \leqslant 40^{0}$ and $40^{0} < \theta \leqslant 60^{0}$.

4.7 CONCLUSION

For a given shower size at sea level both the mean age parameter and standard deviation of the age parameter distribution are independent of zenith angle. The result obtained for the standard deviation is larger than the result quoted by Wdowczyk (1973) $\frac{\sigma_s}{s} = 0.09$. The mean age parameter of E.A.S. is found to increase significantly in value over the size range 10^{6}-10^{7} particles. This observation is either a real effect which is representative of the whole shower or due to the fact that density samples at increasing core distance are used to determine the age parameter as the size increase implying that the age parameter increases with core distance. Monte Carlo simulations need to be carried out before a firm conclusion can be made. If correct, the increase in age parameter indicates that the position of the maximum development of E.A.S. does not move down in the atmosphere as the primary energy increases as is expected from cascade shower theory assuming the chemical composition of the primaries does not change throughout the energy range studied. Since heavy primaries are expected to produce a greater average age parameter than primary protons, it is possible that the chemical composition of the highest energy primary radiation studied in the present

work contains a greater percentage of heavy nuclei. However, as measurements of the primary energy spectrum show no significant change in slope in this energy range, it is thought that a more likely explanation is a change in characteristic of the nucleon-nucleon interaction at an energy of $\sim 5.10^{16}$eV.

Appendix to Chapter 4

The results presented in table 4.2 are believed to give the correct result for the variation of the mean age parameter of EAS with shower size but the results given for the standard deviation of the age parameter distribution σ_s(measured) are all too large as they have not been corrected for the effects of measurement errors. Factors which contribute to the error in s are electron density sampling fluctuations and a small component due to the fact that the EAS array used two thicknesses of scintillator (2.5 and 5 cm) for recording electron density samples. Hara et al (1979) have shown that there is a significant difference in response of scintillators with thickness 3 mm and 50 mm at distances less than 10 m from the shower core. All the showers were analysed by computer using the CERN MINUIT programme and for each shower the best fit $\hat{s}$ and the error (standard deviation) on s were printed out. Figure 4.20 shows the distribution of the error on s for samples of showers in the relevant size ranges. The mean error $\bar{\Delta}$ on s for samples of showers in the size ranges shown in table 4.2 was calculated and the true width of the s distribution found from

$$\sigma_s^{\,2}(\text{true}) = \sigma_s^{\,2}(\text{measured}) - \Delta^{-2}$$

The result is shown in table 4.3. In figure 4.21 the variation of $\bar{s}$ with N and σ_s(true) with N are compared with the results of Hara et al (1981) and the results quoted by Wdowczyk(1973).

Discussion. The variation of mean age parameter with shower size N is in reasonable agreement with previous work except for showers of size $> 5.10^6$ particles. This observation is either a real effect which is representative of the whole shower or due to the fact that density samples at increasing core distances from the centre of the array are used to determine the age parameter as the size increases implying that

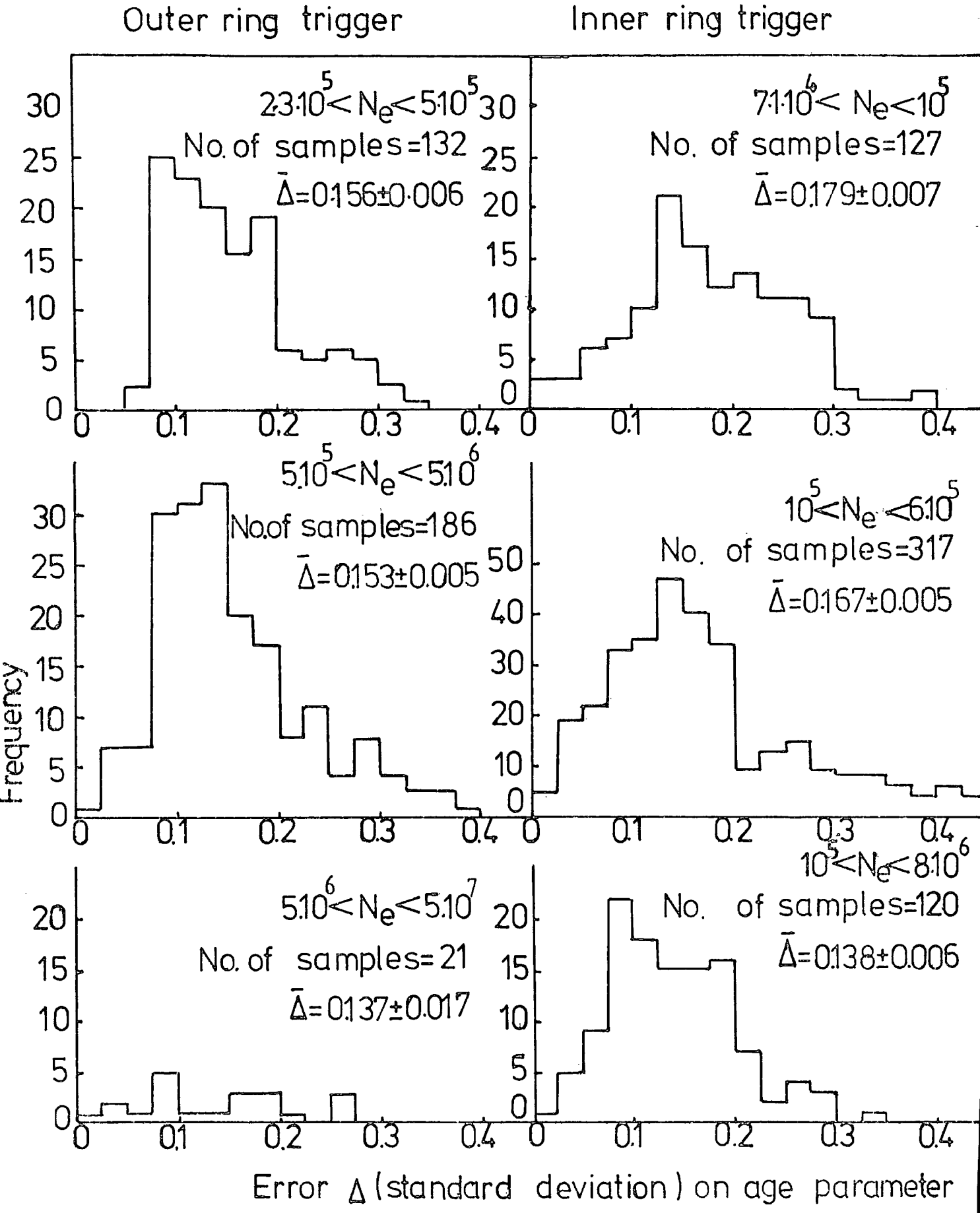

Figure 4.20 : Frequency distribution of the error (standard deviation) on the best fit age parameter of individual showers. $\bar{\Delta}$ is the mean error.

(a) Inner ring trigger

Size range	$\bar{N}$	No. of showers analysed	$\bar{S}$	σ_s (measured)	σ_s (true)	$\frac{\sigma_s \text{ (true)}}{\bar{s}}$
$7.1.10^4 - 10^5$	$(8.41 \pm 0.04).10^4$	133	1.182 ± 0.018	0.24 ± 0.01	0.16 ± 0.02	(0.136 ± 0.015)
$10^5 - 6.10^5$	$(2.41 \pm 0.32).10^5$	659	1.165 ± 0.008	0.24 ± 0.01	0.172 ± 0.011	(0.147 ± 0.008)
$6.10^5 - 8.10^6$	$(1.37 \pm 0.08).10^6$	125	1.188 ± 0.019	0.22 ± 0.01	0.171 ± 0.019	(0.144 ± 0.014)

(b) Outer ring trigger

Size range	$\bar{N}$	No. of showers analysed	$\bar{S}$	σ_s (measured)	σ_s (true)	$\frac{\sigma_s \text{ (true)}}{\bar{s}}$
$2.3.10^5 - 5.10^5$	$(3.54 \pm 0.05).10^5$	134	1.17 ± 0.01	0.191 ± 0.017	0.110 ± 0.031	(0.094 ± 0.005)
$5.10^5 - 5.10^6$	$(1.65 \pm 0.57).10^6$	186	1.15 ± 0.01	0.224 ± 0.012	0.163 ± 0.017	(0.142 ± 0.014)
$5.10^6 - 5.10^7$	$(8.65 \pm 0.61).10^6$	21	1.32 ± 0.05	0.24 ± 0.04	0.197 ± 0.051	(0.149 ± 0.033)

Table 4.3 : Evaluation of the true width (standard deviation) of the age parameter distribution as a function of shower size.

the age parameter increases with core distance. Such an effect has been observed by Atrashkavich et al (1977) who found that in showers of size $1.5.10^7$ particles the lateral distribution function is described by an NKG function with s = 1.33 for core distances >1 Moliere unit (79 m at sea level) but with an NKG function with s = 1.18 at core distances <1 Moliere unit. To check this the variation of age parameter with core distance was investigated for the observed showers in the size range 5.10^6 - 5.10^7 and the result is shown in figure 4.22. It is seen that the mean age parameter observed is 1.38 ± 0.11 for core distances < 80 m from the centre of the array and 1.29 ± 0.06 for core distances > 80 m. The available evidence from the present work although of limited statistical precision thus suggests that the increase in age parameter for $N > 5.10^6$ is a real effect.

From figure 4.21 the variation of σ_s(true) with N is seen to be in reasonable agreement with previous work for $N < 6.10^5$ but diverges considerably at larger sizes. This divergence is presumably correlated with the observed increases of s for $\bar{N} = 8.6.10^6$. If correct the present results are inconsistent with both proton and iron primaries generating the observed showers assuming the expected standard behaviour of high energy hadron interaction. According to Wdowczyk (1973), the expected value of σ_s(true) is 0.04 to 0.08 forproton initiated showers and a quite negligible value for iron initiated showers. The implication of the present measurements of σ_s(true) is that there is a change in the characteristics of high energy interactions over the whole energy range of 10^{15} - 10^{17}eV compared with that expected from the extrapolation of low energy accelerator data.

References

Atrashkevich, V.B., et al (1977), PICCR, Plovdiv, 8, 142.
Hara, T., et al (1981), PICCR, Paris, 6, 52.

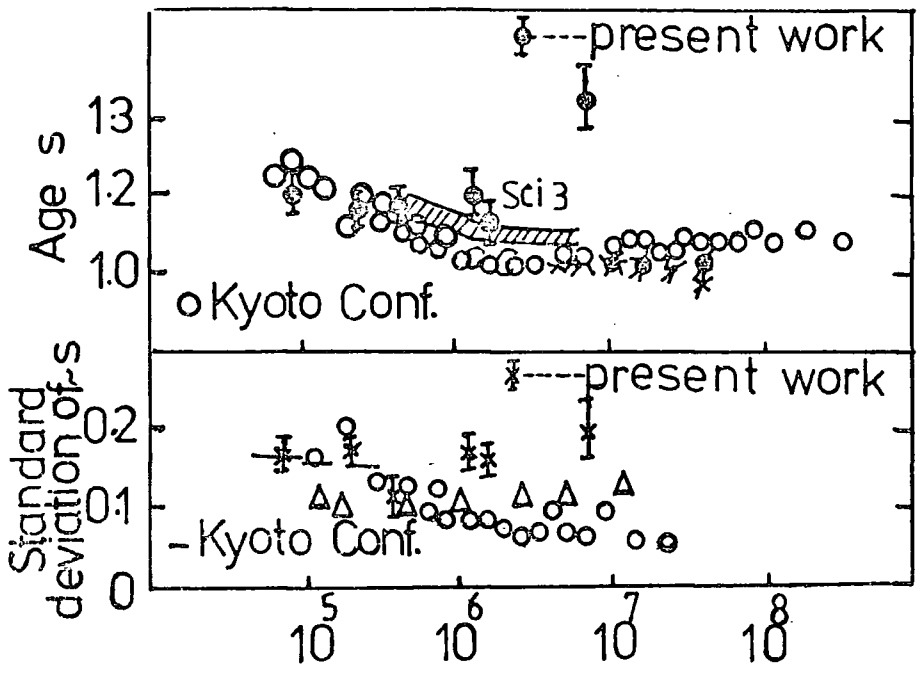

Figure 4.21 : Comparison of the present results for the variation of the mean age parameter and the standard deviation of the age parameter distribution with shower size with the results reported by Harra et al. (1981). The results quoted by Wdowczyk (1973) for the standard deviation of the age parameter distribution are shown by Δ.

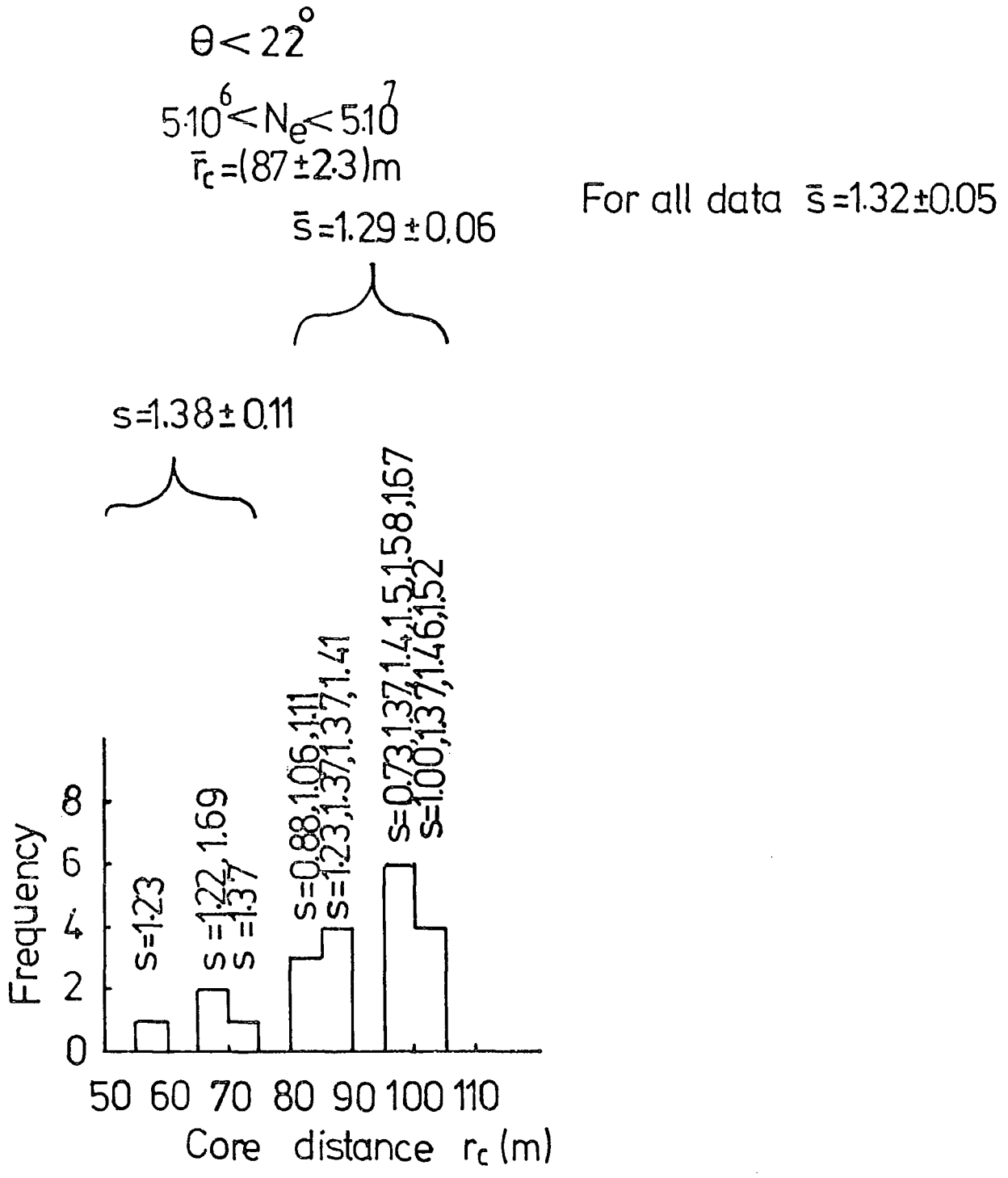

Figure 4.22 : Age parameter of individual showers in different distance ranges for showers in the size range 5.10^6 - 5.10^7.

CHAPTER 5

SIZE SPECTRUM OF E.A.S. AT SEA LEVEL

5.1 INTRODUCTION

The study of the size spectrum (which is sometimes called the number spectrum) is undertaken mainly for the information that it contains on the primary energy spectrum and that in turn gives information which must be explained by any theory of the origin of cosmic rays. However, the conversion of the observed size spectrum to the energy spectrum of cosmic ray primaries is not a straightforward process and is dependent upon the model of air shower development used to derive the relationship between them. This aspect of air showers, which is out of the scope of this work is based on working out the total number of particles produced at sea level caused by the shower in its passage through the atmosphere. The relation between the energy of the primary particle and the observed shower size can be calculated, but this is still the subject of some uncertainty due to a lack of knowledge of the appropriate nuclear physics. In the present work where measurements of the size spectrum are concerned, the air shower parameters including the age parameter and shower size have been evaluated, using the measured size distribution of showers incident at zenith angles of $\leq 30^{o}$. The size spectrum is determined taking the zenith-angle dependence of the showers as

$$I(\theta) = I(0)\cos^{n}\theta \qquad (5.1)$$

The size distribution and the electron lateral distribution are closely connected.

The determination of the shower size (N) and collecting area of a shower is very dependent on the lateral structure function employed, on the shower core location and the goodness of the fit of the region determined experimentally. The shower size can be underestimated and the

collecting area overestimated by assuming a too flat lateral distribution and vice versa for a too steep distribution. The most popular form of f(r) used to fit experimental data is that defined by Greisen (1956) which is dependent on s, the age of the shower. Young showers have a lateral distribution which is steeper than old showers. Although there have been several measurements of the size spectrum of extensive air showers (E.A.S.) at sea level most workers (e.g. Catz et al 1975, Ashton et al 1979, Crouch et al 1980) have assumed all showers have the same electron lateral distribution function in determining the shower size. Only Vernov et al (1968) determined the age parameter of individual showers and hence accurately determined the shower size. The conclusion of their work was that over the size range 10^5 - 10^7 the size spectrum determined in this way has the same shape but a smaller absolute intensity by an average factor 0.77 than the size spectrum determined using an average electron lateral structure function. The present work was undertaken to check this result.

5.2 SOME PREVIOUS MEASUREMENTS OF THE SIZE SPECTRUM

The results of size spectrum measurements, like other measurements in E.A.S. studies, depend upon the altitude at which the experiment is carried out, and measurements have been made at mountain altitudes as well as at sea level. Two different approaches have been used in measuring the size spectrum. The first, which is used in this experiment, is derived from measuring the frequency, size and angular distribution of showers and the second, from measurements on density spectrum which represents the frequency distribution of occurrence of a given particle density at a particular place, irrespective of information concerning the size and location of the axis of the showers responsible for the detected particle density. The results of these studies show that the particle - number spectrum of extensive showers

both at sea level and at high altitudes can not be described by a power law with a single exponent. The simplest description of the observed density spectrum covering a limited range of particle densities has been found to be consistent with a power law integral density distribution of the form

$$N(>\Delta) = K\Delta^{-\gamma}$$

where K is a constant. The exponent γ is not strictly constant, but increases with density. Under the assumption of a fixed lateral distribution of charged particles around the axis of the shower the exponent of the density spectrum can be shown to be equal to that of size spectrum (Cocconi, 1961 and Greisen, 1956). This is a relatively simple way to determine the size spectrum. Over many years, the number spectrum has been measured by many workers with different types of detector and array geometry. Norman (1956) used aproportional counter to measure the integral density spectrum of E.A.S. in the range of Δ = 20 - 1000 m^{-2}. A three-fold coincidence was used as E.A.S. selection. Norman expressed his result for the number spectrum as follows:

$$R(>N) = 2.3.10^{-4}\left(\frac{N}{10^6}\right)^{-1.47\pm0.1} \text{ hr}^{-1}\text{m}^{-2} \text{ for } N<10^6$$

and with evidence of a rapid increase in the exponent for $N \geq 10^6$ particles. Hillas (1970) from his survey of available data concluded that many experiments at sea level and at other altitude, show that the spectrum of shower size, N steepens suddenly at an energy near 3 of 4.10^{15}. The best estimate number spectrum based on measurements of available data of extensive air shower at sea level is formulated as follows:

$$R(\geq N) = 52.0\ N^{-1.5}\ m^{-2}\ sec^{-1}\ st^{-1} \text{ for } N_e < 5.10^5$$

$$R(\geq N) = 36920\ N^{-2.0} m^{-2}\ sec^{-1}\ st^{-1} \text{ for } 5.10^5 < N_e < 3.10^7$$

$$R(\geq N) = 6.76\ N^{-1.5}\ m^{-2}\ sec^{-1}\ st^{-1} \text{ for } N \geq 3.10^7$$

Where $R(\geq N)$ is the integral rate of showers of size more than N particles it is plotted in figure 5.11 (curve 1). Some more recent experiments are summarised by the Australian group, Crouch et al (1980), see figure 5.12. The size spectrum is characterised as:

(i) having a sharp break or "knee" around size 5.10^5 particles at sea level and 2.10^6particles at mountain altitude.

(ii) An increase of the exponent of the slope above the "knee". A determination of the size spectrum from the measured density spectrum has been described by Paravaresh et al (1975). The number spectrum was derived from the density spectrum measured over the density range of 40 $m^{-2} < \Delta < 5000\, m^{-2}$, where the kink was at $\Delta \sim 1000 m^{-2}$. The best estimate of the integral number spectrum at sea level was derived as,

$$R(>N) = 3\, N^{-1.3}\, m^{-2} s^{-1} st^{-1} \qquad N \leq 7.10^5$$

$$R(>N) = 36920 N^{-2} m^{-2} s^{-1} st^{-1} \qquad 7.10^5 \leq N < 3.10^7$$

$$R(>N) = 6.76\, N^{-1.5} m^{-2} s^{-1} st^{-1} \qquad N > 3.10^7$$

The spectrum has approximately the same form as that given by Hillas except for $N_e < 7.10^5$ where a smaller rate is predicted (figure 5.11 (curve 2)). In spite of a suggestion of slope, flattening of the integral number spectrum for $N_e > 10^7$ by Khristiansen et al (1974),it has not been clearly investigated. A change in the slope of the density and number spectrum reflects a sharper change in the form of the primary energy spectrum in the energy interval $E \sim 10^{15}$- 10^{16}eV. Around the break, the exponent of the slope changes from -1.7 to -2.3. Two possible interpretations of the sharp break in the energy spectrum may be (a) a break in the energy spectrum of primary cosmic ray itself (i.e. a genuine change) or (b) a sudden change in the nature of nuclear

interactions at an energy of around 5.10^{15}eV. Generally, the form of the primary energy spectrum is of particular interest from the point of view of the theory of the origin of the cosmic radiation.

5.3 EXPERIMENTAL ARRANGEMENT AND DATA ANALYSIS

Extensive air showers were selected by the inner and outer ring triggers of the Durham E.A.S. array (see chapter two). A total number of 2608 showers detected by the inner ring trigger and 1200 showers detected by the outer ring trigger were analysed (see table 5.1). The shower size, and core distance distributions obtained in figures 5.1, 5.2 and 5.3. The exponent (n) of the angular variation of E.A.S. was calculated to be n = 8.0 for inner ring triggers and 8.25 for outer ring triggers. The orthogonal core distance from the central detector C is given with a comparison with the (X,Y) plane core distance in figure 5.3. In determining the size spectrum the dependence of collecting area on shower age is of importance. For showers with zenith angle less than 30^{o}, the data was grouped into approximately three equinumber ranges of age parameter with mean ages of S = 0.95, 1.2 and 1.45, where each age range was subgrouped into three zenith angle ranges of $0\text{-}10^{o}$, $10\text{-}20^{o}$ and $20\text{-}30^{o}$. The dependence of collecting area on shower size for inclined showers is shown in figures 5.4, 5.5 and 5.6. The structure function considered is the structure function relevant to the age parameter of individual showers. To obtain the vertical differential size spectrum R(N,0) from the experimental data it was assumed that the differential size spectrum at zenith angle θ is given by

$$R(N,\theta) = R(N,0)\ \cos^{n}\theta\ m^{-2}sec^{-1}st^{-1}/\text{unit } N_e$$

The number of showers X of size N/unit N traversing the effective collecting area $A(\theta)$ in the horizontal plane in time t is given by

$$X = \int_0^{\theta} R(N,\theta).A(\theta)\cos\theta\ t\ 2\pi\ \sin\theta\ d\theta \text{ from which}$$

$$R(N,0) = \frac{X}{t2\pi \int_0^{\theta} A(\theta)\cos^{n+1}\theta\sin\theta\ d\theta} \qquad (5.2)$$

E.A.S. Selection	Run time (hrs.)	Total no. of triggers	Trigger rate (hr^{-1})	Total no.of analysable showers	No. of showers with $0<\theta<30^{o}$ and $r_c \leq 95$ m for inner ring and $r_c \leq 105$ for outer ring
Inner ring trigger : $\Delta_c(>4m^{-2})$ $\Delta_{11}(>2m^{-2})$, $\Delta_{31}(>2m^{-2})$, $\Delta_{51}(>2m^{-2})$	128	2683	20.96±0.4	2608	1618
Outer ring trigger : $\Delta_c(>4m^{-2})$ $\Delta_{13}(>2m^{-2})$, $\Delta_{33}(>2m^{-2})$, $\Delta_{53}(>2m^{-2})$	293.02	1317	4.5±0.09	1200	638

Table 5.1 : Summary of experimental data used in the analysis

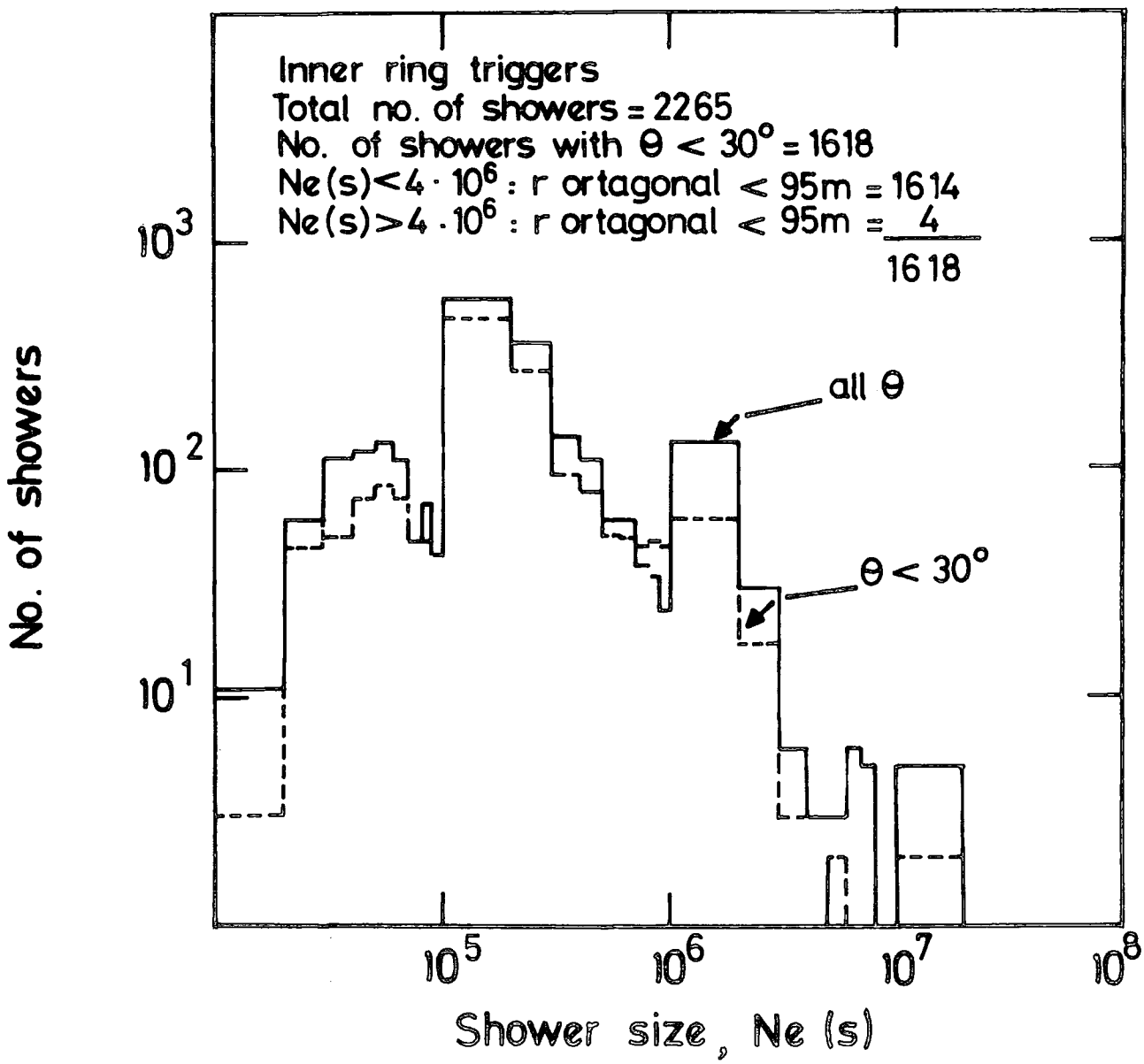

Figure 5.1 : The size distribution of all showers and those with $\theta<30^{o}$ used in the data analysis.

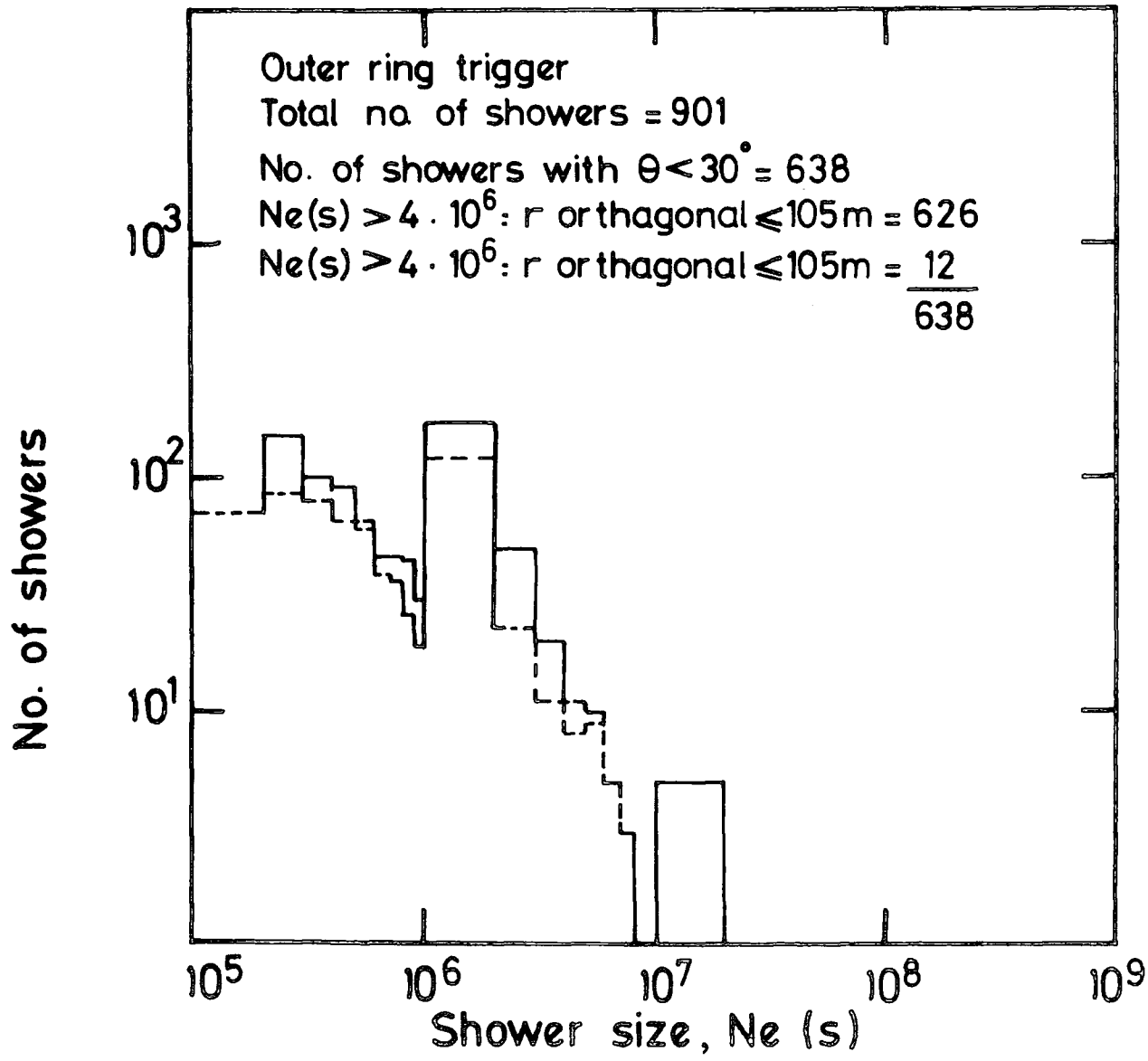

Figure 5.2 : The size distribution of all showers and those with $\theta < 30^{0}$ used in the data analysis.

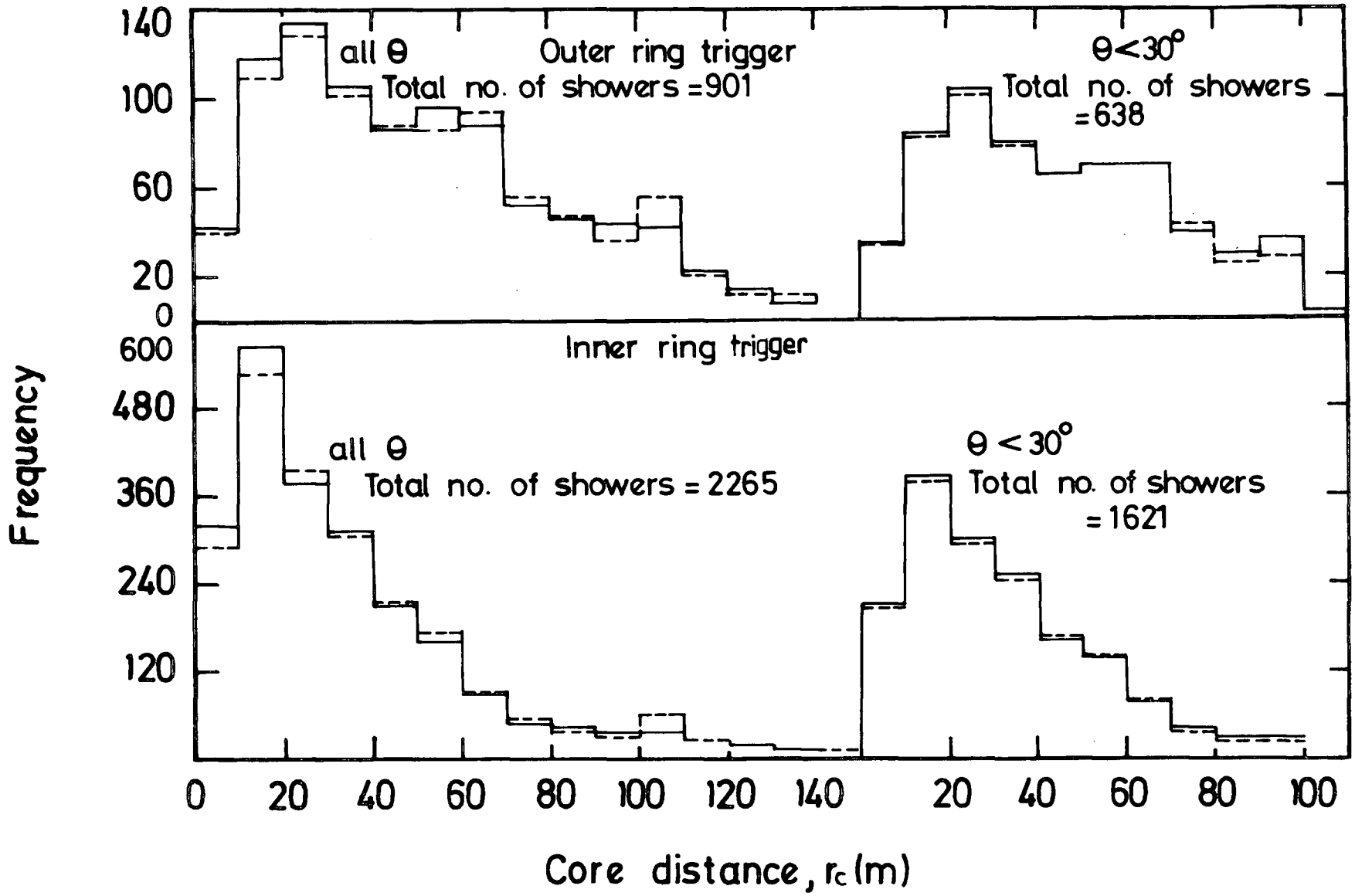

Figure 5.3 : A comparison between the distribution of orthogonal and (X,Y) plane core distance from the central detector C.

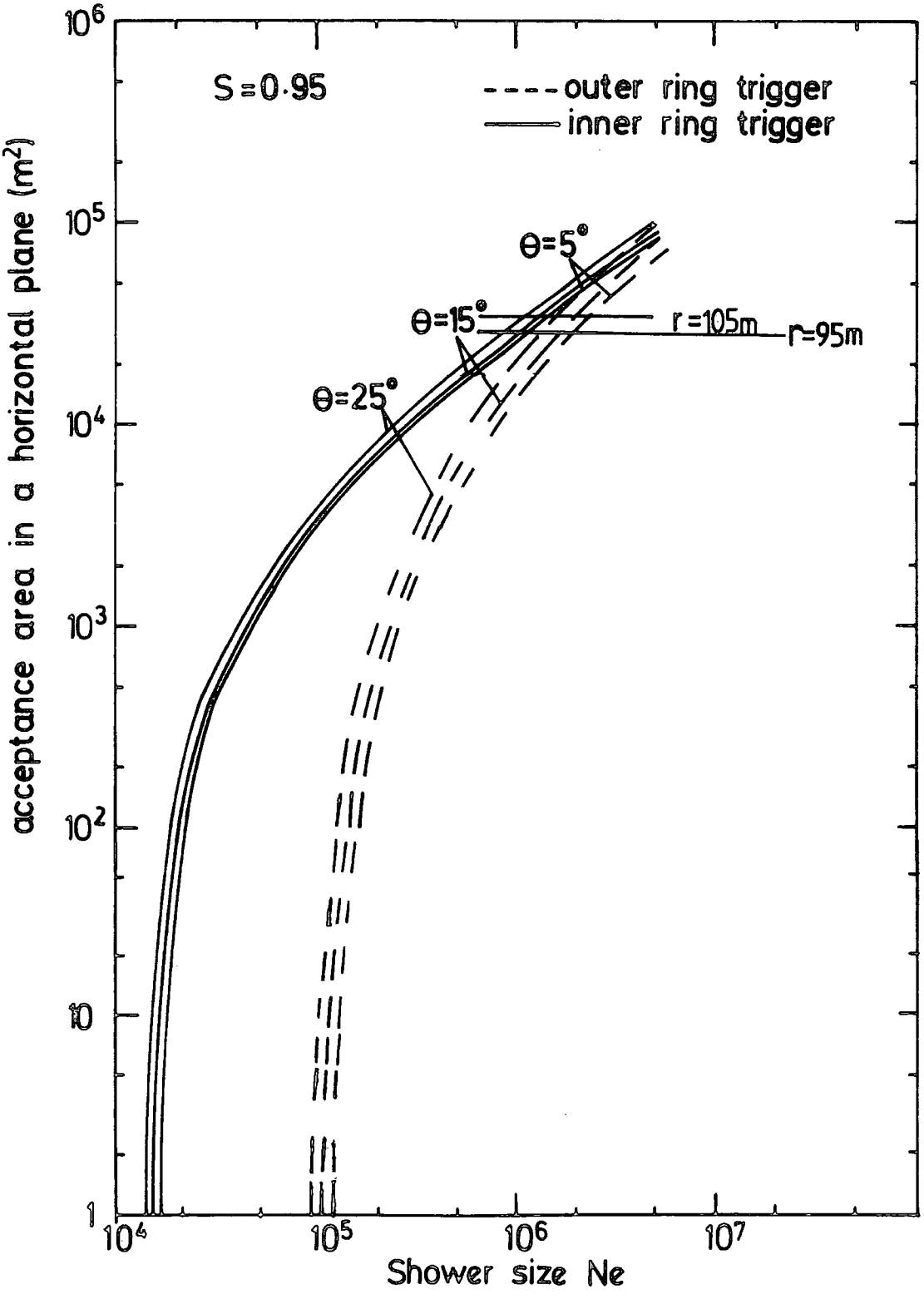

Figure 5.4 : The dependence of collecting area on shower size for showers with age parameter s = 0.95 and different values of zenith angle.

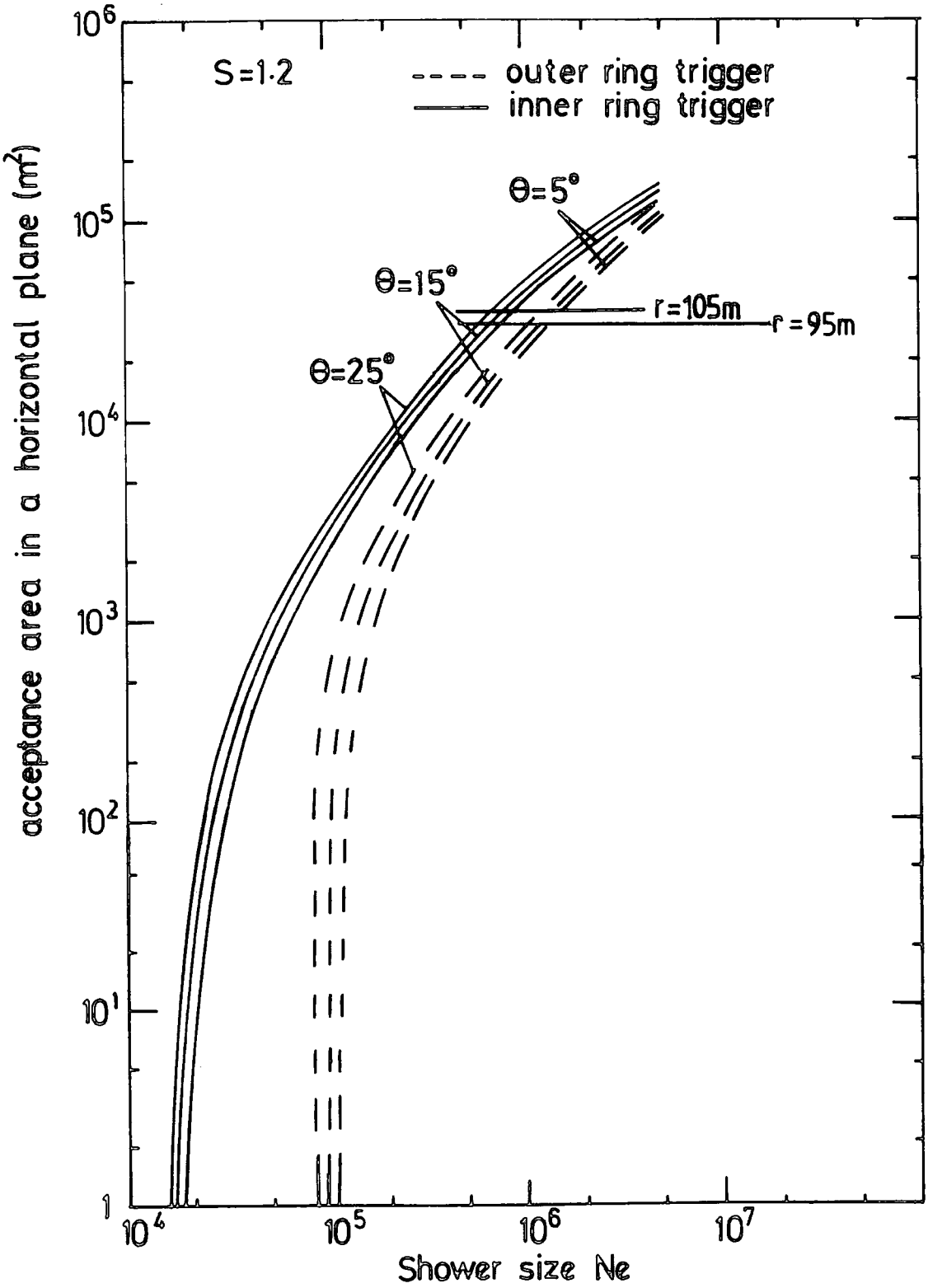

Figure 5.5 : The dependence of collecting area on shower size for showers with age parameter s = 1.2 and different values of zenith angle.

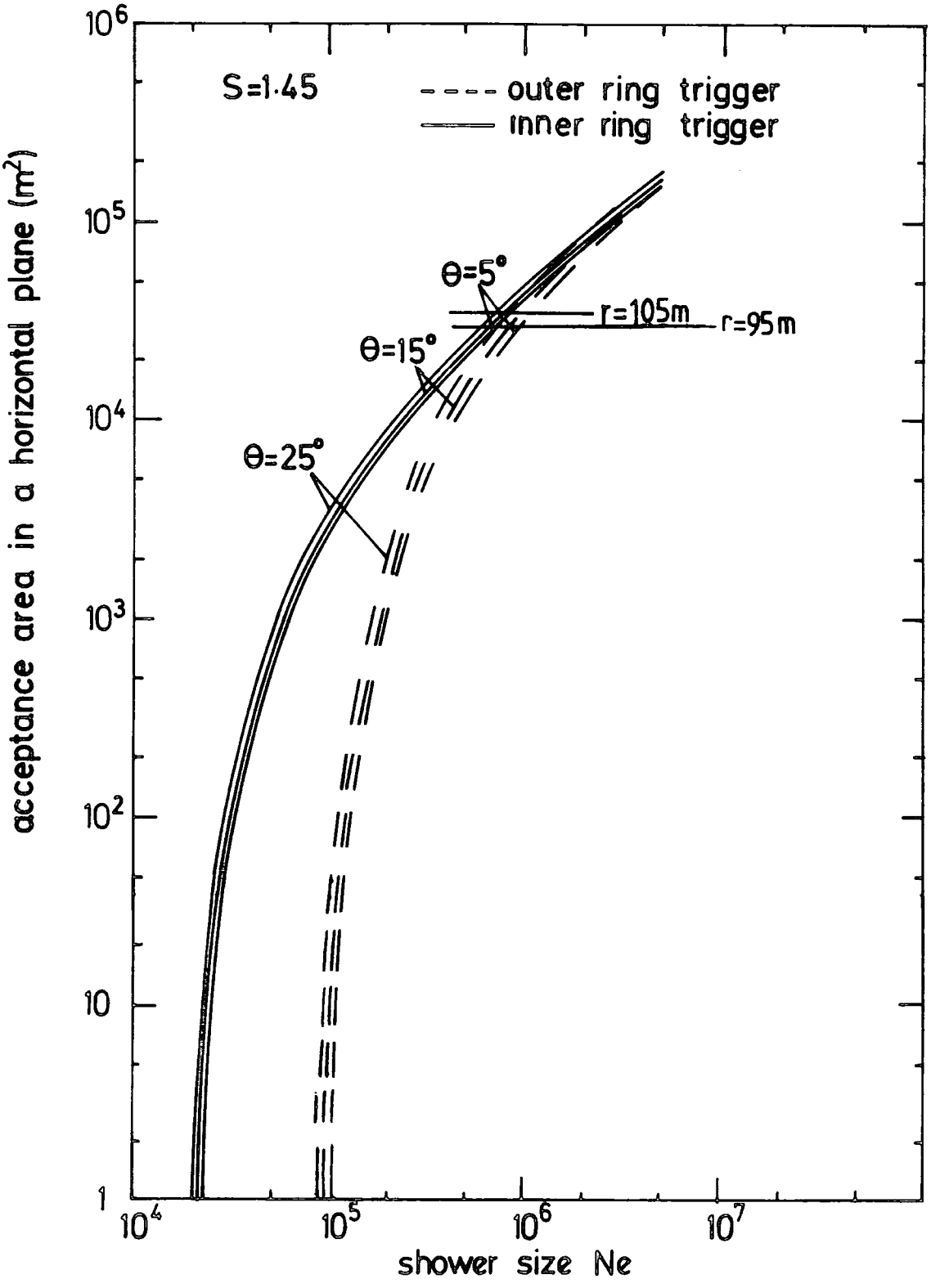

Figure 5.6 : The dependence of collecting area on shower size for showers with age parameter s = 1.45 and different values of zenith angle.

Using the shower size and age dependence of $A(\theta)$ obtained from the curves of figures 5.4, 5.5 and 5.6 and using n = 8.0 and 8.25 for the inner and outer ring triggers, equation 5.2 was evaluated for showers in the three stated age parameter ranges. Adding the three resulting rates together gives the total differential rates of showers of size N/unit N incident vertically at sea level. This was done when $N_e(s)$ was used for showers with zenith angle less than 30^o. For near vertical showers where $A(\theta) = A$ = a constant, equation (5.2) becomes

$$R(N,0) = \frac{X}{t.2\pi\ A\ \{\frac{1-\cos^{n+2}\theta}{n+2}\}}$$

5.4 THE COLLECTING AREA OF E.A.S. AND THE SHOWER AGE

To determine the size spectrum, the collecting area for the detection of E.A.S. (this is the area within which the shower axes have to fall to be detected) has been found. To detect E.A.S. particles, a number of detectors are arranged over a certain area, these are calibrated,such that the density of particles in each detector exceeds a certain level. The number of particles per square metre in a given detector is given by $\Delta(r,s) = Nf(r)$ where f(r) is the lateral structure function normalized so that

$$\int_0^\infty f(r)2\pi r\,dr = 1$$

N as the number of particles in a given E.A.S. Since the density represented in the above equation depends on s, the distance from the axis r is a function of N, Δ and s. Hence the collecting area depends on s and can be represented as $\pi r^2(N,s)$ for a given triggering density Δ. In the present work the collecting area has been plotted for the three groups of showers having age parameter ranges of $0.6<S<1.1$, $1.1<S<1.3$, $1.3<S<1.8$ with means of 0.95, 1.2 and 1.45. Figure 4.3 also shows that the density at small core distance ($r\leqslant 20$ m)

in a shower of small age is larger than for showers with a bigger value of s, whereas at larger core distances the reverse is true. This can be seen in the plots of the dependence of collecting area on age parameter shown in figures 5.4, 5.5 and 5.6. For fixed large shower sizes the collecting area of the shower increases with its age.

5.5 CORRECTIONS

There are several effects that introduce systematic errors in the size spectrum determination. These will now be discussed.

5.5.1 Effect of Zenith Angle on Collecting Area

Each scintillator in the array is calibrated by determining the average pulse height $\bar{v}$ produced by relativistic muons traversing it at normal incidence. If a pulse height V is produced by a shower of particles traversing a scintillator of area S at normal incidence, the particle density Δ is given by

$$\Delta = \frac{V}{\bar{v}S} \ m^{-2} \qquad (5.3)$$

Consider the same particle density traversing the scintillator at zenith angle θ. The actual number of particles that traverse the scintillator is $\Delta.S.\cos$ but each particle will produce a larger pulse height $v/\cos\theta$ because of its longer track length in the phosphor. The pulse height produced is thus, $\Delta S\cos\theta \ . \frac{\bar{v}}{\cos\theta} = \Delta . S\bar{v} = V$ from equation 5.3. Thus if a pulse height V is observed from any detector and $\bar{v}$ is the average pulse height produced by normally incident muons, the particle density at the detector is correctly given by $\frac{V}{\bar{v}}$ for any incident zenith angle.

Consider a detector of area S situated at O as shown in figure 5.7 and initially assume showers can only fall anywhere along the line OX. If an electronic requirement of $\geq n$ particles m^{-2} is

required for triggering then vertical showers of size N will only trigger the detector if they fall at distance $\leq r$ from O in the direction of OX where r is found from solving the equation $Nf(r) = n$, where $f(r)$ is the electron lateral distribution function. For showers of size N incident at A at zenith angle θ their orthogonal core distance from O is not r but the smaller value $r\cos\theta$. Only at the larger distance $r/\cos\theta$ from O is their orthogonal core distance from O equal to r as illustrated in figure 5.7b. Thus the maximum distance from O along the line OX at which showers of size N can trigger the detector at O increases as their zenith angle increases. In the case of three triggering detectors situated in a plane they will be simultaneously triggered by a shower of size N, only if it falls in an arca (collecting area) which is approximately given by

$$A = \pi(r-d)^2 \text{ for vertical showers} \qquad (5.4a)$$

$$B = \pi(r/\cos\theta - d)^2 \text{ for inclined showers} \qquad (5.4b)$$

where d is the distance of an outer detector from C (assumed to be the same for all three triggering detectors) and r is the maximum core distance that a shower of size N incident vertically can fall from a triggering detector to satisfy the electron density triggering requirements, (see figure 5.8). For the outer ring trigger, the distance $d \sim 58$ m for a collecting area, say $10^2 m^2$, r is found from equation 5.4a to equal 63.6 m. For the same shower incident at an angle θ the maximum distance that this core can fall in the horizontal plane to satisfy the electron density criteria is increased from r to $r_1 = r/\cos\theta$. For $\theta = 15^o$, $r = 65.42$ m which from equation (5.4b) gives collecting area $1.72.10^2 m^2$. This shows the collecting area is increased by a factor of 1.72 if the shower is incident with $\theta = 15^o$. It is seen that the importance of this effect is very large close to the triggering threshold but becomes less important as the collecting area (shower size) increases. The variation of collecting area with shower size

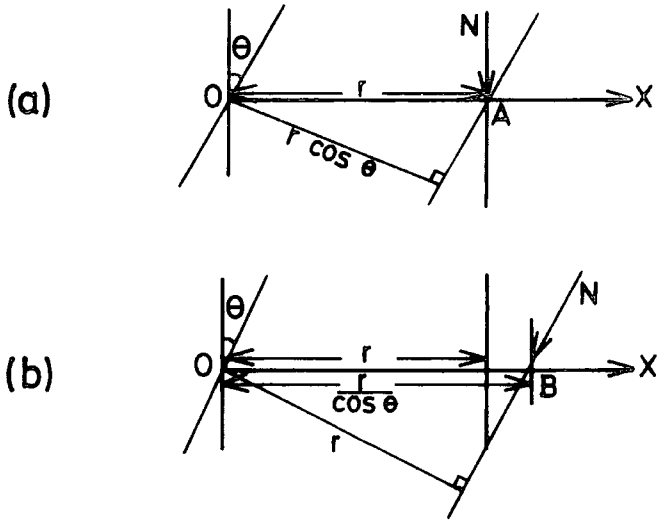

Figure 5.7 : To be detected by a given local density detector situated at O the maximum distance from O along OX at which showers of a given size can fall is r as shown in Fig.(5.7a) if the showers are incident vertically. For showers incident at zenith angle θ the maximum distance is r/cosθ as shown in Fig.(5.7b).

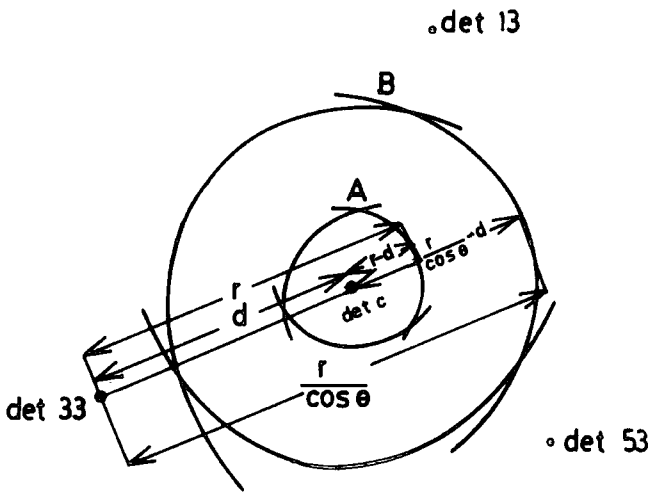

Figure 5.8 : The dependence of collecting area on zenith angle for showers of a given size. A is the collecting area for a vertical shower and B is the collecting area for the same shower incident at zenith angle θ.

for different zenith angles are shown in figures 5.4, 5.5 and 5.6 for the inner and outer ring triggers of E.A.S. array.

5.5.2 The Effect of Sampling Density Fluctuations on the Collecting Area

Investigation of this effect is given in appendix (B) where the sampling density fluctuations at the detector has been taken into account and assumed to be Poissonian. The effect of fluctuations was found to be small when averaged over the whole collecting area.

5.6 RESULTS AND CONCLUSION

In attempting to measure an unbiased size spectrum, the measurements most accurately made through studying individual showers, using their age parameter. Since the collecting area is a function of the incident angle of the shower front, this zenith angle has been taken into account. In general, the shower density at a detector is underestimated if all showers are assumed to fall vertically. Hence the data has been divided into these with $\theta<30^{o}$ and these with $\theta>30^{o}$. It can be seen from the shower size distribution that the array is useful for detecting showers over the range of sizes from 10^{4} to 2.10^{7} particles. The size spectrum using $N_e(s)$ for three stated ranges of age parameter has been found - figure 5.9. The result as a final size spectrum is given in table 5.2 and is also shown in figure 5.10 where the work of Hillas (1970) curve (1) and Parvarach (1975) curve (2), are also plotted for comparison. From these figures it is evident that with the exception of small and very large shower size spectra obtained using $N_e(s)$ is consistent with the previous work of Paravarch. The result for the integral size spectrum is shown in figures 5.11 and 5.12 where it is compared with some recent measurements (Catz et al 1975, Ashton et al 1979,and Crouch et al, 1980). The difference at the two

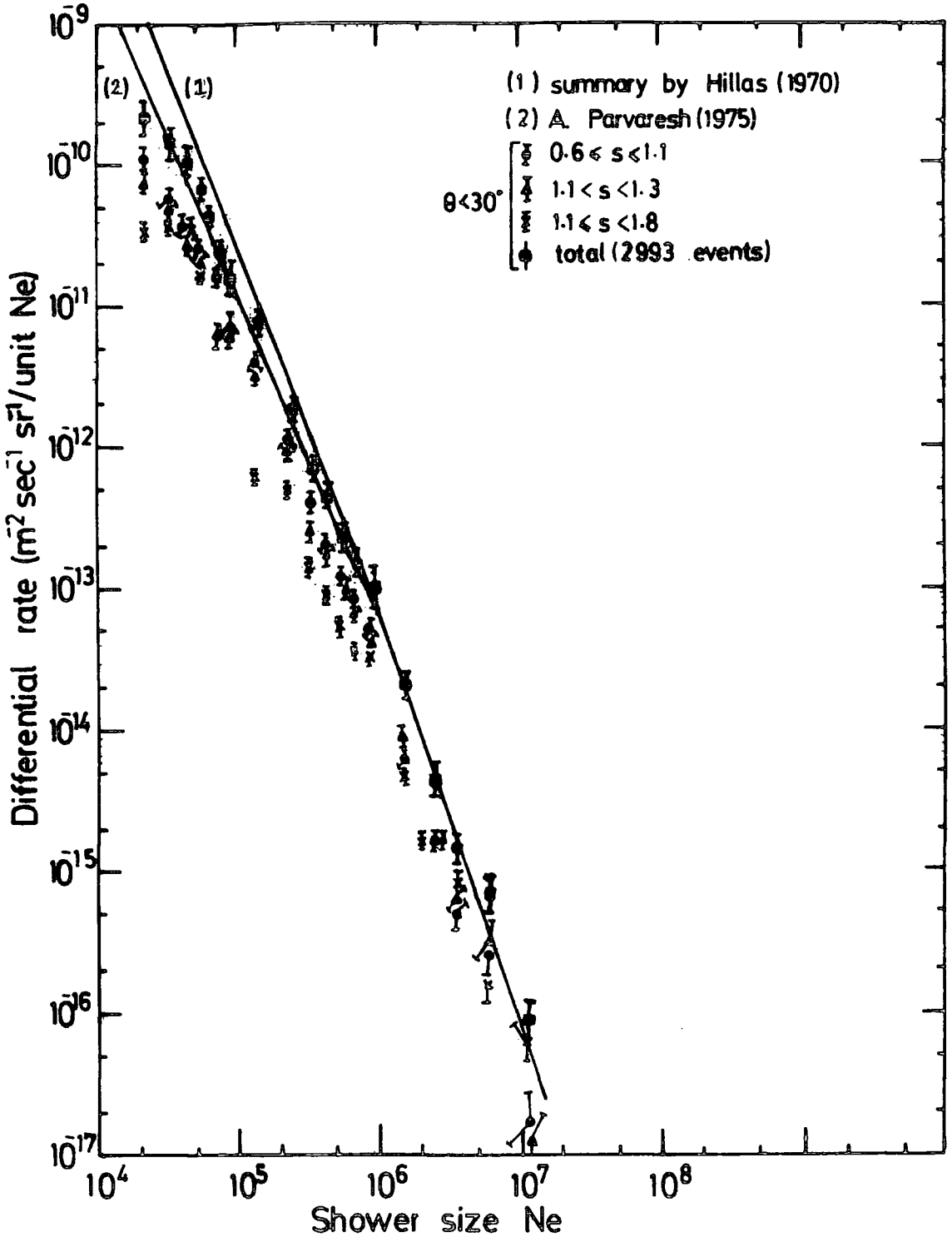

Figure 5.9 The vertical differential size spectrum of E.A.S. at sea level for showers with different values of the age parameters. The total rate for showers of all age parameter is also shown. The work of Hillas (1970) and Parvaresh (1975) are also plotted for comparison.

Shower size range	Core dist-ance range	$\bar{N}$	Total No. of showers with $\theta<30$		Average R(N,O) for inner & outer ring triggers									Final R(N,O) for all $s(m^{-2}sec^{-1}st^{-1}$Unit N^{-1})
					$0.6<s<1.1$	No. of showers		$1.1<s<1.3$	No. of showers		$1.3<s<1.8$	No. of showers		
			Inner ring	Outer ring		Inner ring	Outer ring		Inner ring	Outer ring		Inner ring	Outer ring	
$(2-3)\cdot10^4$		$2.5.10^4$	45		$1.06.10^{-10}$	31		$7.73.10^{-11}$	10		$3.72.10^{-11}$	4		$(2.205\pm0.89).10^{-10}$
(3-4)	<95m	3.5	50		$5.44.10^{-11}$	33		$5.09.10^{-11}$	13		$3.53.10^{-11}$	4		$(1.41\ \pm0.52).10^{-10}$
(4-5)		4.5	73		$3.8\ .10^{-11}$	39		$2.9\ .10^{-11}$	17		$3.9\ .10^{-11}$	17		$(1.06\ \pm0.1\ ).10^{-10}$
(5-6)		5.5	86		$3.186.10^{-11}$	46		$2.76.10^{-11}$	25		$1.87.10^{-11}$	15		$(7.8\ \pm0.5\ ).10^{-11}$
(6-7)		6.5	73		$2.34.10^{-11}$	40		$1.347.10^{-11}$	16		$1.39.10^{-11}$	17		$(5.1\ \pm1.0\ ).10^{-11}$
(7-8)		7.5	46		$1.826.10^{-11}$	39		$2.7\ .10^{-12}$	4		$1.11.10^{-12}$	3		$(2.2\ \pm0.7\ ).10^{-11}$
(8-9)		8.5	48		$1.37.10^{-11}$	33		$0.7\ .10^{-11}$	13		$0.5\ .10^{-12}$	2		$(2.145\pm0.46).10^{-11}$
(9-10)		9.5	41		$8.05.10^{-12}$	23		$7.59.10^{-12}$	16		$6.75.10^{-13}$	2		$(1.63\ \pm0.84).10^{-12}$
$(1-2)\cdot10^5$	<105m	$1.5.10^5$	433	71	$4.18.10^{-12}$	205	37	$3.1\ .10^{-12}$	153	29	$1.21.10^{-12}$	75	5	$(8.49\ \pm0.84).10^{-12}$
(2-3)		2.5	271	83	$1.33.10^{-12}$	122	33	$0.96.10^{-12}$	93	34	$0.49.10^{-12}$	56	16	$(2.75\ \pm0.27).10^{-12}$
(3-4)		3.5	92	80	$4.26.10^{13}$	39	33	$2.55.10^{-13}$	32	30	$1.38.10^{-13}$	21	17	$(8.19\ \pm1.59).10^{-13}$
(4-5)		4.5	81	67	$2.21.10^{-13}$	32	21	$1.88.10^{-13}$	31	33	$8.38.10^{-14}$	18	13	$(4.9\ \pm0.76).10^{-13}$
(5-6)		5.5	53	60	$1.183.10^{-13}$	20	14	$1.19.10^{-13}$	23	29	$2.6\ .10^{-14}$	10	17	$(2.88\ \pm0.74).10^{-13}$
(6-7)		6.5	49	38	$8.57.10^{-14}$	17	12	$7.6\ .10^{-14}$	23	16	$3.27.10^{-14}$	9	16	$(1.94\ \pm0.484).10^{-13}$
(7-8)		7.5	37	36	$7.1\ .10^{-14}$	16	9	$5.1\ .10^{-14}$	14	17	$2.4\ .10^{-14}$	7	10	$(1.4\ \pm0.38).10^{-13}$
(8-9)		8.5	34	26	$5.58.10^{-12}$	13	5	$4.15.10^{-12}$	11	18	$3.5\ .10^{-12}$	10	3	$(1.32\ \pm0.49).10^{-13}$
(9-10)		9.5	24	19	$0.45.10^{-13}$	9	3	$0.27.10^{-13}$	11	8	$0.125.10^{-13}$	4	8	$(0.79\ \pm0.28).10^{-13}$
$(1-2)\cdot10^6$		$1.5.10^6$	58	112	$6.0.\ 10^{-13}$	12	26	$9.7.\ 10^{-13}$	30	50	$5.93.10^{-13}$	16	36	$(2.16\ \pm0.37).10^{-14}$
(2-3)		2.5	17	23	$1.68.10^{-15}$	1	11	$1.67.10^{-15}$	11	3	$1.52.10^{-15}$	5	9	$(4.87\ \pm1.36).10^{-15}$
(3-4)		3.5	3	11	$0.48.10^{-15}$	0	3	$0.56.10^{-15}$	1	3	$0.73.10^{-15}$	2	5	$(1.77\ \pm0.48).10^{-15}$
(4-7)		4.5	2	11	$2.4\ .10^{-16}$	1	3	$4.2\ .10^{-16}$	1	3	$1.44.10^{-16}$	0	5	$(8.1\ \pm3.69).10^{-16}$
$(7-2)\cdot10^7$		$1.1.10^7$	2	1	$1.94.10^{-17}$	0	1	$1.39.10^{-17}$	1	0	$5.92.10^{-16}$	1	0	$(9.25\ \pm3.0\ ).10^{-17}$
			1618	638		771	211		549	273		298	154	

Table 5.2 : Final differential size spectrum of showers with $\theta<30^0$ for all values of age parameters

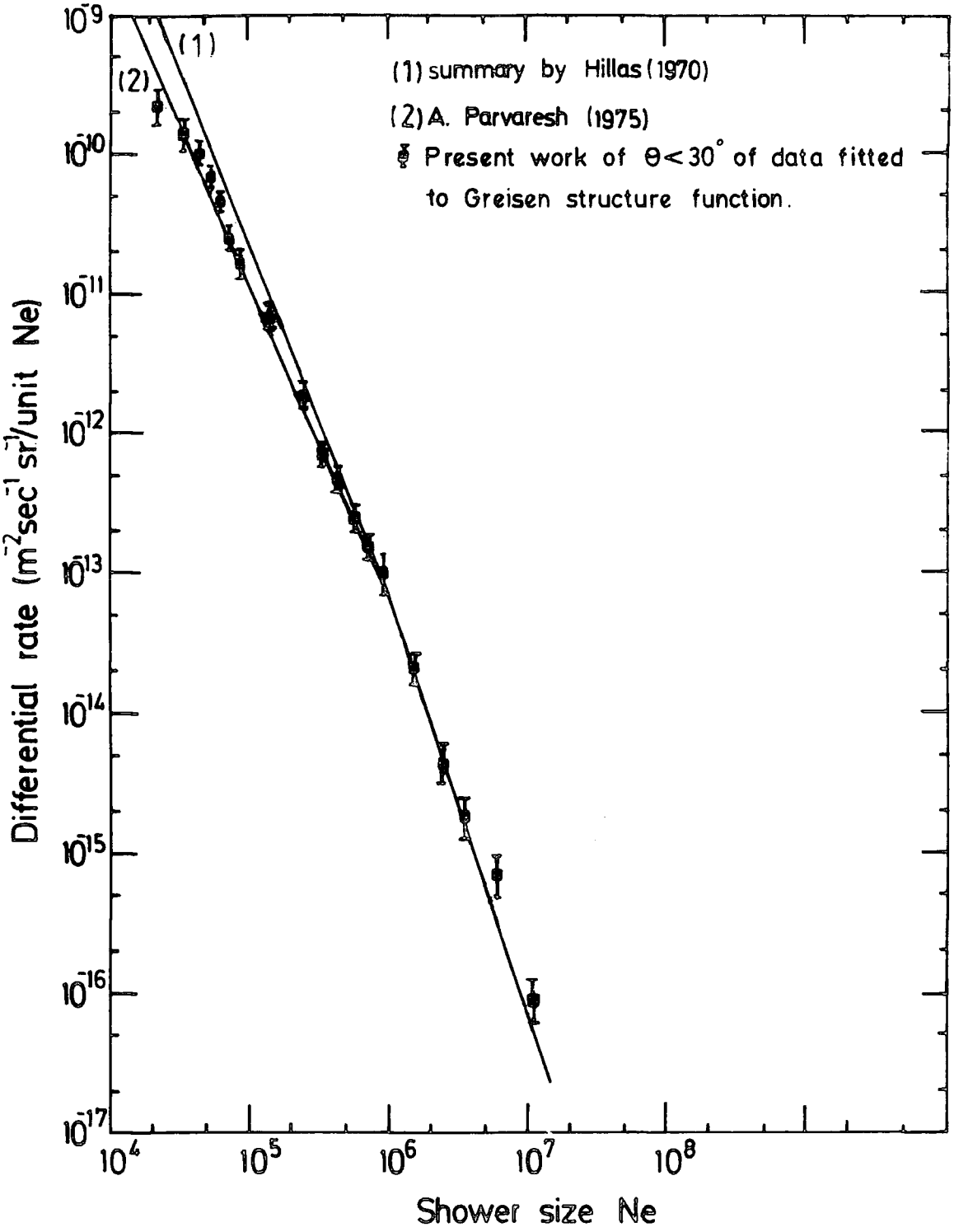

Figure 5.10 : The vertical differential size spectrum of E.A.S. at sea level taking the age parameter of individual showers into account. The full lines are the previous work of the Hillas (1970) and Parvaresh (1975).

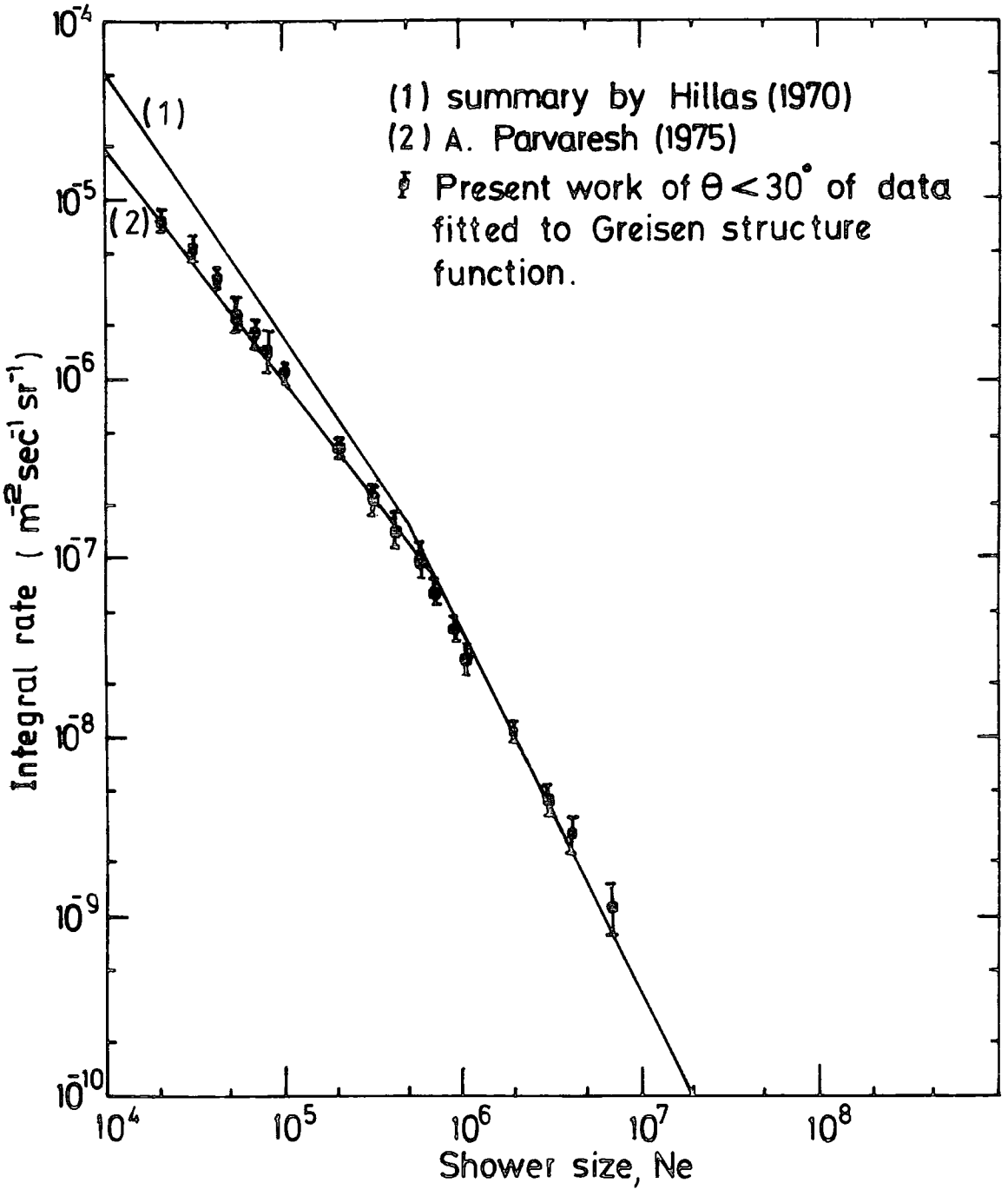

Figure 5.11 : The vertical integral size spectrum of E.A.S. at sea level taking the age parameter of individual showers into account. The full lines are the previous work of Hillas (1970) and Paravaresh (1975).

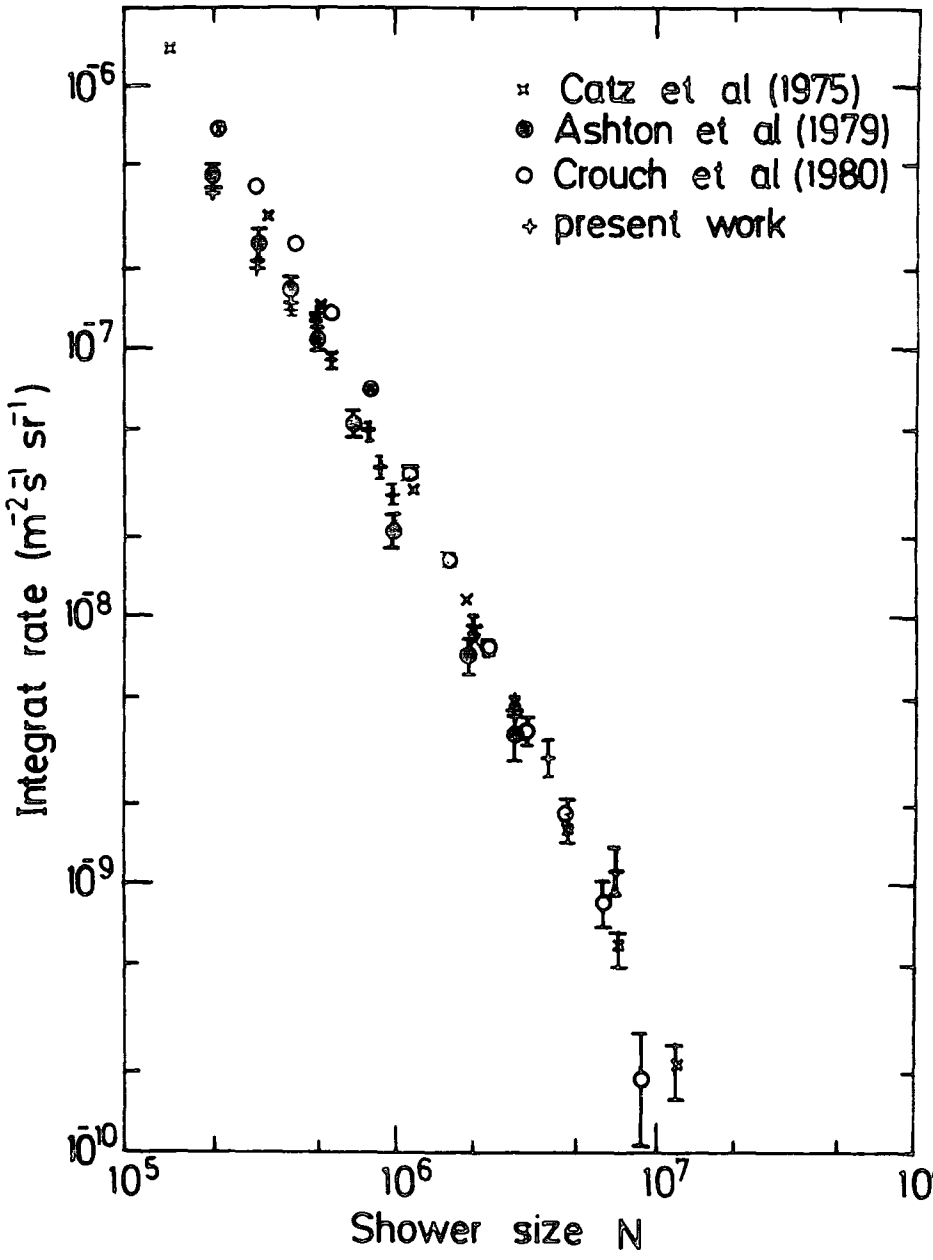

Figure 5.12 : Comparison of the vertical integral size spectrum of E.A.S. at sea level taking into account the age parameter of individual showers with other recent measurements.

largest shower sizes is associated with an increase in age parameter with shower size which is such that sizes determined using the Greisen average lateral structure function are less than those determined when the age parameter of individual showers is taken into account.

CHAPTER 6

THE ARRIVAL DIRECTIONS OF E.A.S. IN GALACTIC COORDINATES

6.1 INTRODUCTION

Much attention has been focussed in the past on the distribution of the arrival directions of the primary particles. This is because a significant anisotropy in the cosmic ray flux, observed at the earth, would provide a very important key to understanding the origin of cosmic rays by reflecting the whereabouts in space of the cosmic ray sources. The absence of any anisotropy however, suggests that the sources of cosmic rays are uniformly distributed in the galaxy or are extragalactic. An isotropy has been established by the many experiments already carried out, and the search is continuing in the belief that improved statistics will reveal the small variation and to make sure that it exists. The distribution of the arrival direction can be determined directly from observation of E.A.S. This arises because the general direction of motion of the secondary particles in a large shower is practically the same as the arrival direction of the primary. The arrival direction of a shower can be roughly established by merely noting the sidereal time of its occurrence. This defines the celestial hemisphere from which the primary must have come. As the earth rotates, a band of declination centred on the observer's latitude is scanned once per sidereal day and the distribution of the arrival directions of the primaries is measured, in a somewhat smeared out form, as the distribution of the rate of detecting E.A.S. in sidereal time.

Any broad anisotropy of the primaries would be revealed as a periodic variation in this rate with a period of one sidereal day and thus would reflect the existence of point sources. Time variations of E.A.S. may also be produced by changes in atmospheric temperature and

pressure. Only the effect of atmospheric pressure will be discussed since the effect due to the temperature is negligible.

6.2 PREVIOUS ANISOTROPY MEASUREMENTS

Efforts have been made by many workers to find any significant anisotropy of the primary flux in sidereal time. It is a long time since the discovery of cosmic rays was achieved. In such a varied history the search for a genuine galactic anisotropy of cosmic rays was frustrated in the period prior to about 1975. Many of the promising positive indications were superseded by more precise measurements showing little or no sign of the hoped for anisotropy. However, these measurements kept improving and were of great value in putting some restrictions on the condition of the anisotropy, such as origin and propagation models. The indication of anisotropy for primary energy below 10^{12} eV shows uncertainty as such measurements can be modified by the solar wind. In recent years the first strong experimental evidence of an anisotropy based on studies of extensive air showers were carried out at ground level and was given by Gombasi et al (1975) and Nagashima et al (1977). The energies of the primaries of the showers detected in these experiments were between 10^{13} and 10^{14} eV where the effect of the interplanetary magnetic field is very small and it is difficult to think of explanations in terms of other than genuine effects. Continuing to higher energies in the range of (10^{14}-10^{17}) eV a review paper by Linsley and Watson (1977) also gave positive evidence for an anisotropy. Another review paper given by Edge et al (1978) supported the claim of positive results where the shower primary energy range of 6.10^{16}-10^{20}eV was investigated. In these experiments the anisotropy was measured by the amplitude of the first harmonic which was fitted to the observed sidereal variation.

Summarising, the claim for the detection of genuine galactic anisotropies have been made by Kiraly et al (1979) and the result is shown in figure 6.1. The significance of this analysis comes in understanding the nature and origin of cosmic rays. As is shown in figure 6.1 there are two features, first, the increase of the anisotropy with the energy and the second feature, is the change of slope of anisotropy versus energy at around 3.10^{15} eV where the primary energy spectrum also has a change of slope. More recently, an excess of extensive air showers from the general direction of the crab pulsar of galactic latitude of $b"=(-6^{o})$ and galactic longitude of $\ell"=(184^{o})$ has been found on the level of about 4 standard deviations (Dzikowski, T. et al, 1981).

6.3 PRESENT WORK

6.3.1 Experimental Arrangement

The Durham E.A.S. array was described in chapter two and has been used in the present experiment to detect E.A.S. using both the inner and outer ring triggering modes.

The array is capable of measuring shower sizes in the range of $(10^{5}- 10^{6})$ particles, which covers particle energies around 3.10^{15} eV which is the energy region in which the primary energy spectrum changes slope.

Apart from the shower size, the zenith (θ) and a zimuthal (ϕ) angles of a primary particle are derived from the geometry of the detector array and the relative times of arrival of the shower front at the detectors. Following the determination of ϕ and θ the arrival direction of the primary, referred to celestial coordinates (right ascension, RA, and declination, δ), can be calculated from the

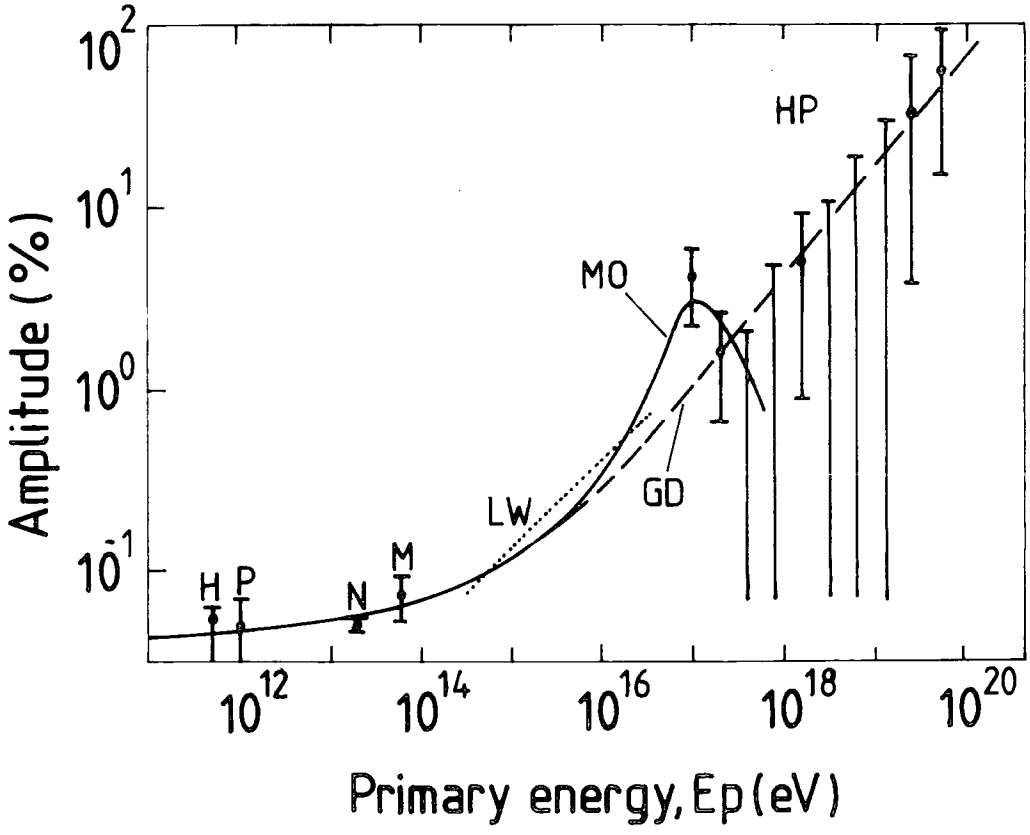

Figure 6.1 : Amplitude of 1st-harmonic analysis versus primary energy (After Kiraly et al, 1979).

relationships given by Prescott (1977) which are as follows :

$$\text{(a)}\quad \text{Sin}\delta = \sin\delta_0\cos\theta + \cos\delta_0 \sin\theta \cos\phi$$

$$\text{(b)}\quad \text{Sin H} = \frac{\text{Sin}\theta \sin\phi}{\cos\delta} \qquad (6.1)$$

$$\text{(c)}\quad \text{RA} = \gamma + \text{H}$$

$$\text{(d)}\quad \text{cosH} = \frac{\cos\theta - \sin\delta_0 \sin\delta}{\cos\delta_0 \cos\delta}$$

where δ_0 = latitude of the array (54.75^0)

γ = local sidereal time

H = Hour angle

A more meaningful picture of these parameters and their relationship is illustrated in figure 6.2.

The measured right ascension and declination of individual showers have been converted into galactic coordinates (latitude and longitude) and the following formulae given by Lang (1974) were used:

$$\text{(a)}\quad \sin b'' = \sin\delta \cos 62.6^0 - \cos\delta \sin(\text{RA}-282.25^0)\sin 62.6^0$$

$$\text{(b)}\quad \sin(\ell''-33) = \frac{\cos\delta\sin(\alpha-282.25^0)\cos 62.6^0 + \sin\delta \sin 62.6^0}{\cos b''} \qquad (6.2)$$

$$\text{(c)}\quad \cos(\ell''-33) = \frac{\cos\delta\cos(\alpha - 282.25^0)}{\cos b''}$$

where ℓ'' = galactic longitude

b'' = galactic latitude

To obtain the right ascension, it is seen from equation (6.1c) that it is necessary to record solar time and convert it into sidereal time, this is discussed in the next section.

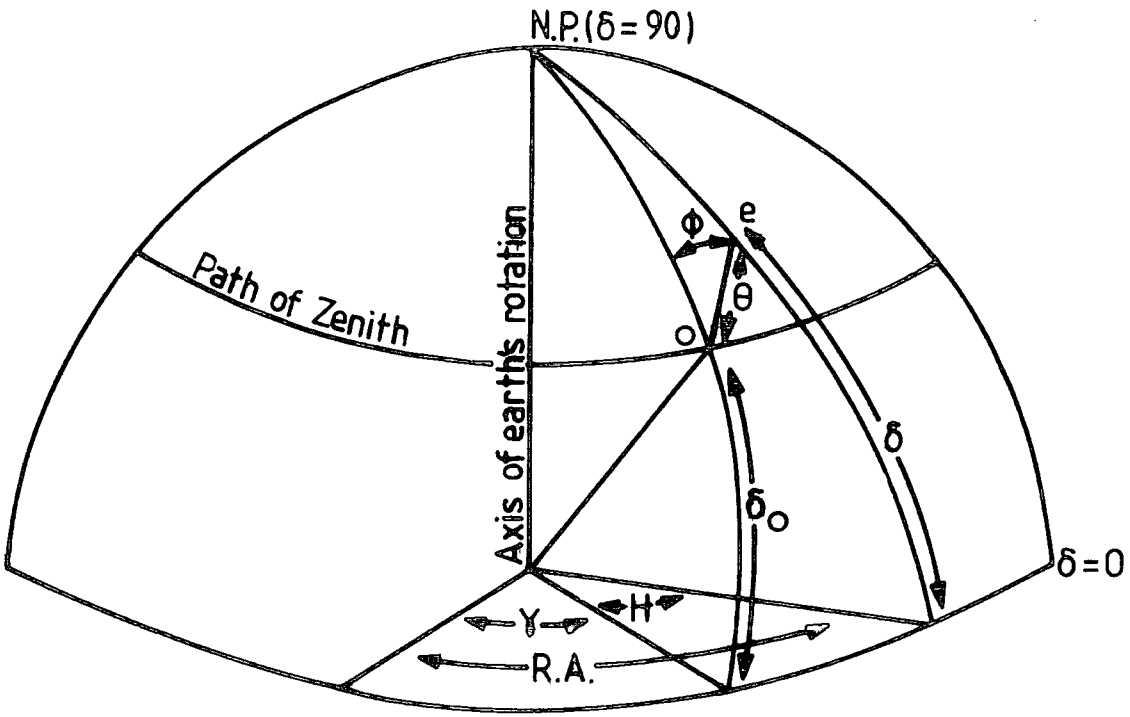

Figure 6.2 : Presentation of the arrival direction of an event e in celestrial coordinates where o is the projection of the array.

6.3.2 Conversion of Local Solar Time to Local Sidereal Time

The E.A.S. used in the present analysis were recorded during the period March to July 1977. For each event the local time of its occurrence was recorded. During the period March 21st to October 23rd 1977 local time was British summer time which is one hour ahead of Greenwich mean time. Having established the Greenwich mean time (which is also called universal time) of each event the local sidereal time of its occurrence was found using the Astronomical Ephemeris for 1977. The procedure is best illustrated by an example.

Example : What is the local mean sidereal time of an E.A.S. observed on March 28th 1977 at 18 hr 26 min 43 sec. local time.

18 hr 26 min 43 sec local time = 17 hr 26 min 43 sec Greenwich mean time (GMT)

Zero hours GMT on March 28th 1977 = 12 hr 21 min 10.889 sec

Sidereal time at Greenwich (see page 13 of 1977 Astronomical Ephemeris)

	17 hr 26 min 43 sec
Add 17 hr 26 min 43 sec	
	29 hr 47 min 53.889 sec
Add 2 min 51.946 sec for gain of Sidereal time on GMT in 17 hr 26 min 43 sec. See page 515 of 1977 Astronomical Ephemeris.	2 min 51.94 sec
	29 hr 50 min 45.835 sec
Subtract 24 hours to give the local mean sidereal time at Greenwich	24 hr
	5 hr 50 min 45.835 sec
subtract 6 min 17.2 sec to give the local mean sidereal time at Durham which is at a longitude $1^{o}34.3$ west of Greenwich	6 min 17.200 sec
	5 hr 44 min 28.635 sec
local mean sidereal time of the E.A.S.	

6.3.3 Method of Calculating the Expected Number of Showers in Galactic Coordinates Assuming they are isotropically Distributed in Space

Having obtained the measured number of showers arriving from different cells of galactic coordinates, it is required to calculate the expected numbers assuming that the occurrence of an E.A.S. is uniformly probable in sidereal time. To obtain such expected numbers the following procedures were performed:

(a) The probability of a shower arriving with zenith angle θ and azimuthal angle ϕ.

$p(\theta,\phi)$ was calculated as follows,

Assume $I(\theta) = I(0)\cos^n\theta\, m^{-2}s^{-1}st^{-1}$ for a horizontal collecting area A in time t.

No. of events with $\theta \to \theta+d\theta$ $= I(\theta)A\cos\theta.2\pi\sin\theta d\theta.t$

$= I(0)\cos^n\theta.A\cos\theta.2\pi\sin\theta d\theta.t$

$= I(0).A.2\pi t\cos^{n+1}\theta\sin\theta d\theta$

$= \text{const.}\cos^{n+1}\theta\sin\theta d\theta$

The probability that a shower of given zenith angle has ϕ in range $\phi \to \phi + d\phi = \frac{d\phi}{2\pi}$. The probability that a shower has zenith angle in the range $\theta \to \theta + d\theta$ and ϕ in the range $\phi \to \phi + d\phi$ is thus

$$p(\theta,\phi)d\theta d\phi = \text{const.}\cos^{n+1}\theta\sin\theta d\theta\frac{d\phi}{2\pi}$$

$$= K\cos^{n+1}\theta\sin\theta d\theta d\phi$$

Requiring $\int_0^{\pi/2}\int_0^{2\pi} p(\theta,\phi)d\phi d\phi = 1$

$$K\int_0^{\pi/2}\int_0^{2\pi}\cos^{n+1}\theta.\sin\theta\, d\theta d\phi = 1$$

$$K\int_0^{\pi/2}\cos^{n+1}\theta.\sin\theta d\theta\int_0^{2\pi} d\phi = 1$$

$$\int_{\cos\theta=0}^{\cos\theta=1}\cos^{n+1}\theta\, d(\cos\theta).2\pi = 1$$

$$K \left[\frac{\cos^{n+2}\theta}{n+2} \right]_{\cos\theta=0}^{\cos\theta=1} \cdot 2\pi = 1$$

$$K \left[\frac{1}{n+2} \right] .2\pi = 1 \rightarrow K = \frac{n+2}{2\pi}$$

$$p(\theta,\phi)\, d\theta d\phi = \frac{n+2}{2\pi} \cos^{n+1}\theta . \sin\theta d\theta d\phi$$

The probability of a shower being incident at θ, ϕ.

$$p(\theta,\phi) = \frac{n+2}{2\pi} \cos^{n+1}\theta . \sin\theta \quad \text{radian}^{-2}$$

(b) For N showers randomly distributed in a total sensitive time T_s of sidereal time the number expected in an interval t to t+dt of sensitive time t_s is $N.t_s/T_s$. For these showers the number $n(\theta,\phi)d\theta d\phi$ expected in the zenith angle range θ to $\theta+d\theta$ and ϕ to $\phi+d\phi$ is

$$n(\theta,\phi)\, d\theta d\phi = \frac{n+2}{2\pi} \cos^{n+1}\theta . \sin\theta\, d\theta\, d\phi .N.t_s/T_s$$

Converting from azimuthal angle, zenith angle, sidereal time to right ascension and declination and then to galactic coordinates the expected number of showers in different ranges of galactic coordinates can be calculated. Most of the calculation was carried out by computer. The computer printout shown in appendix C gives the expected number of these events that should have the galactic coordinates shown. With similar information for the whole 24 hours period of sidereal time, the total expected number of events in given cells of galactic longitude and latitude can be calculated and this is how the expected number of E.A.S. shown in brackets in figures 6.13 , 6.14 and 6.15 have been calculated.

6.4 ANALYSIS OF THE DATA AND RESULTS

A total of 3575 showers were detected in the time period March to July 1977. Showers were selected initially using an inner ring trigger and later the outer ring trigger where the record of the events with relatively greater shower size range was found. Although the periods of reliable operation heppened to be chosen like that, the possibility of the existence of time variations in the rate of detecting E.A.S. and point sources have been investigated.

The size distribution and the measured θ and ϕ distribution for all the data, the outer ring trigger data and the inner ring trigger are given in figures 6.3 to 6.7, where the measured zenith and azimuthal angle distributions are also shown in the figures. For the measured θ distribution the function of the form $I(\theta) = I(0)\cos^{n}\theta$ where $I(0)$ is the vertical intensity and $I(\theta)$ the intensity at zenith angle θ was fitted to the date. The best values of n were calculated to be 8.2 for all the data, 8.5 for the outer ring trigger data and 8.0 for the inner ring trigger data.

For these data, the operational times were determined and used to construct frequency distributions of the detector operational time in both solar and sidereal times. Figures 6.8, 6.9 and 6.10 show these distributions. The dotted lines are the expected distribution in sidereal time. X^2 probability tests between the measured and expected number of events in different intervals of sidereal time showed that they are not far from being randomly distributed. An interesting point arises from the comparison of the inner ring data (events with $\bar{N}e = 3.9.10^5$ pts) with the outer ring trigger data (events with $\bar{N}e = 1.11.10^6$ pts). The X^2 test shows that the probability of the data in the two samples is consistent with a uniform distribution in the sidereal time decrease from 30% to 5% as N_e increases from $3.9.10^5$ to $1.11.10^6$. Thus the measurements suggest an anisotropy of primary particles in sidereal time which

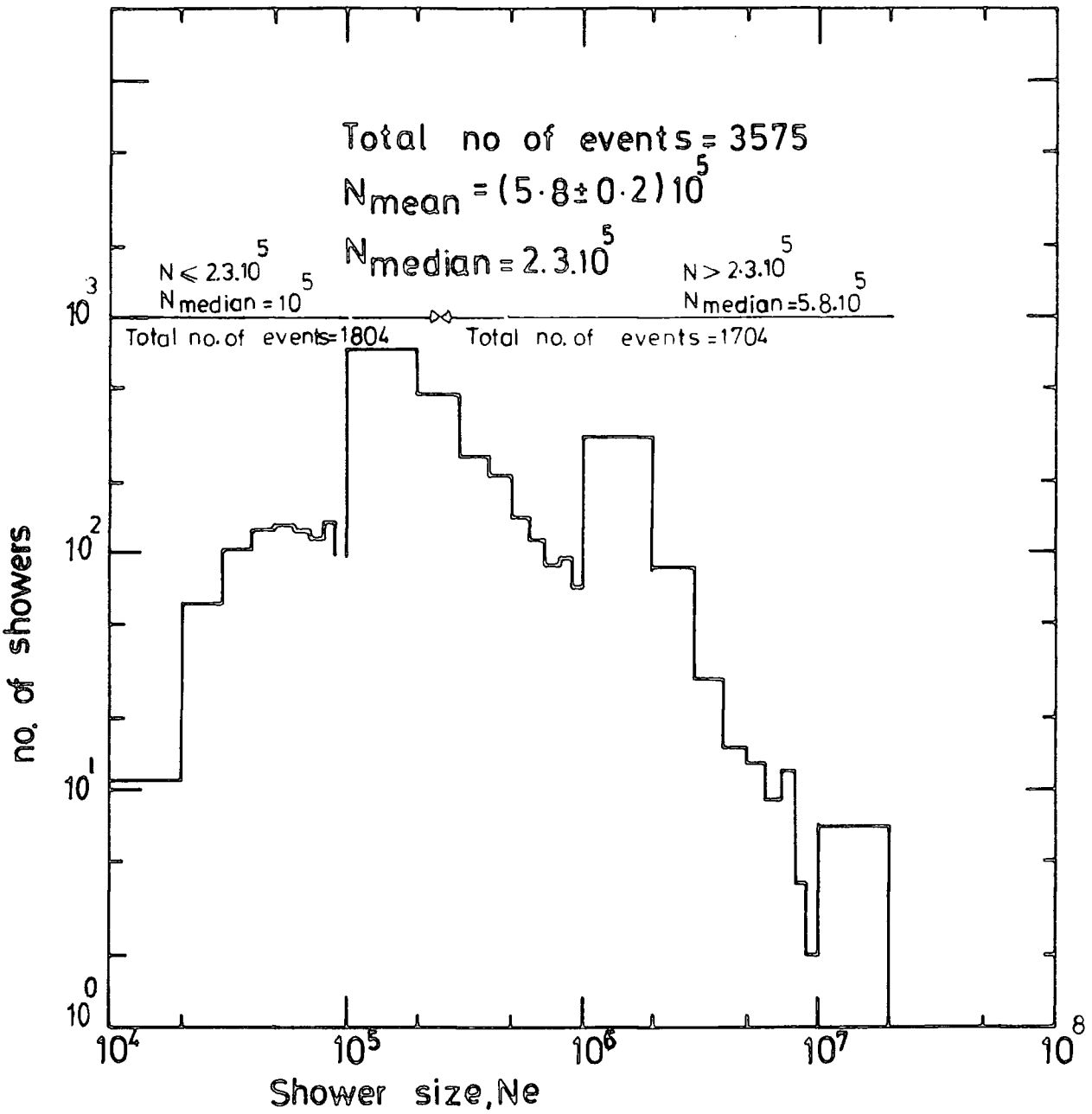

Figure 6.3 : Shower size distribution of all the data.

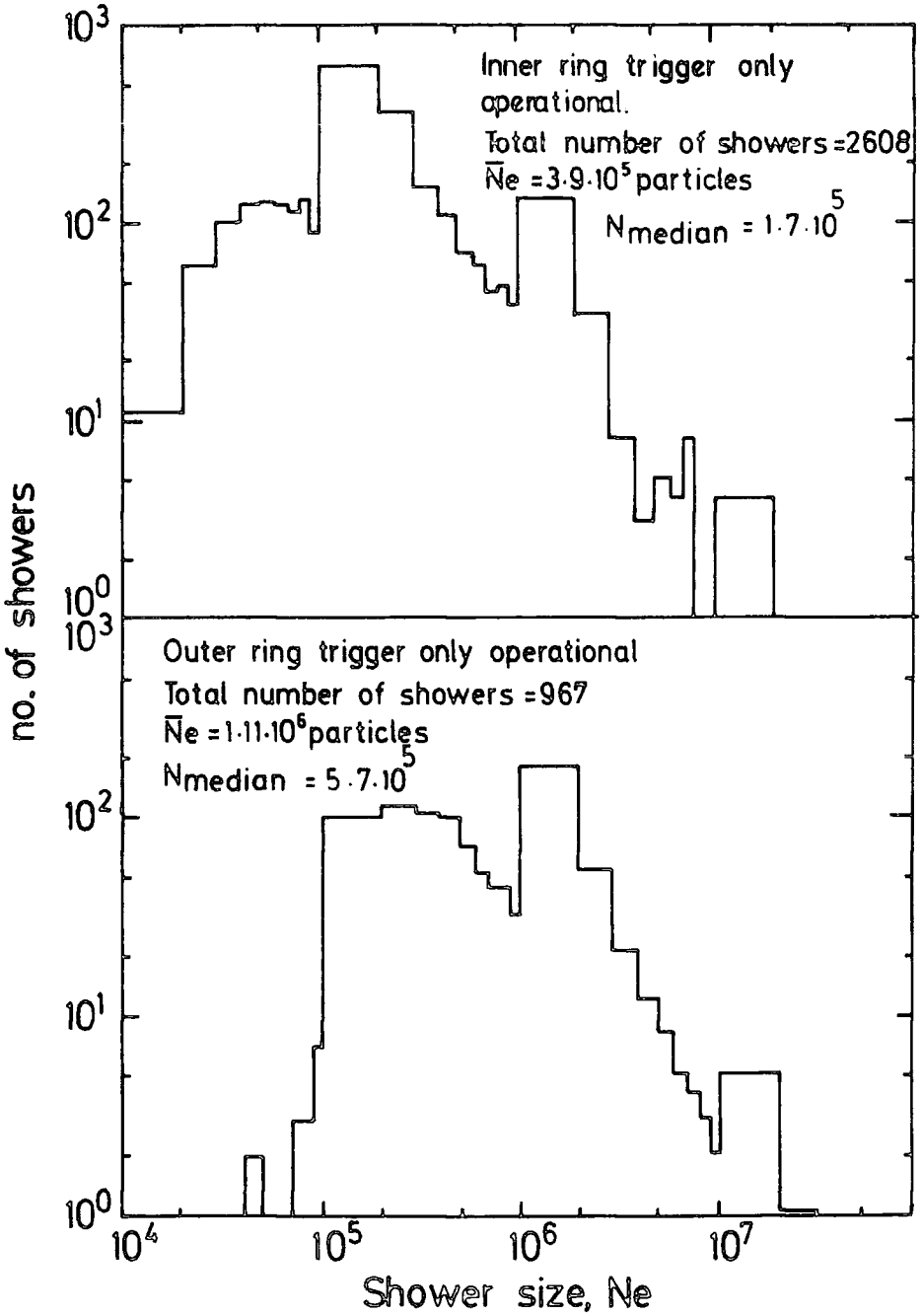

Figure 6.4 : Shower size distributions for different triggering systems

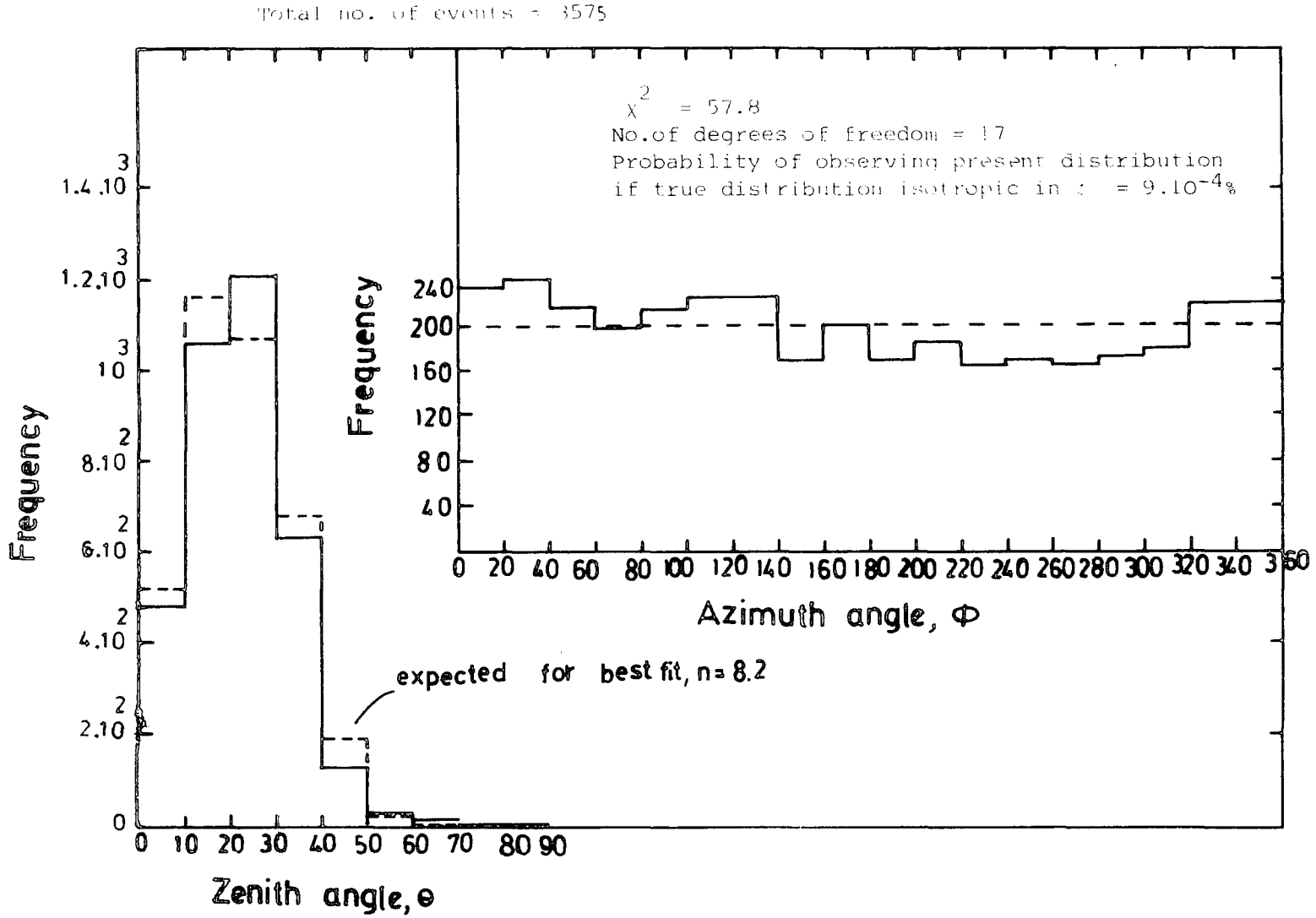

Figure 6.5 : Zenith and azimuth angle distributions of all the data.

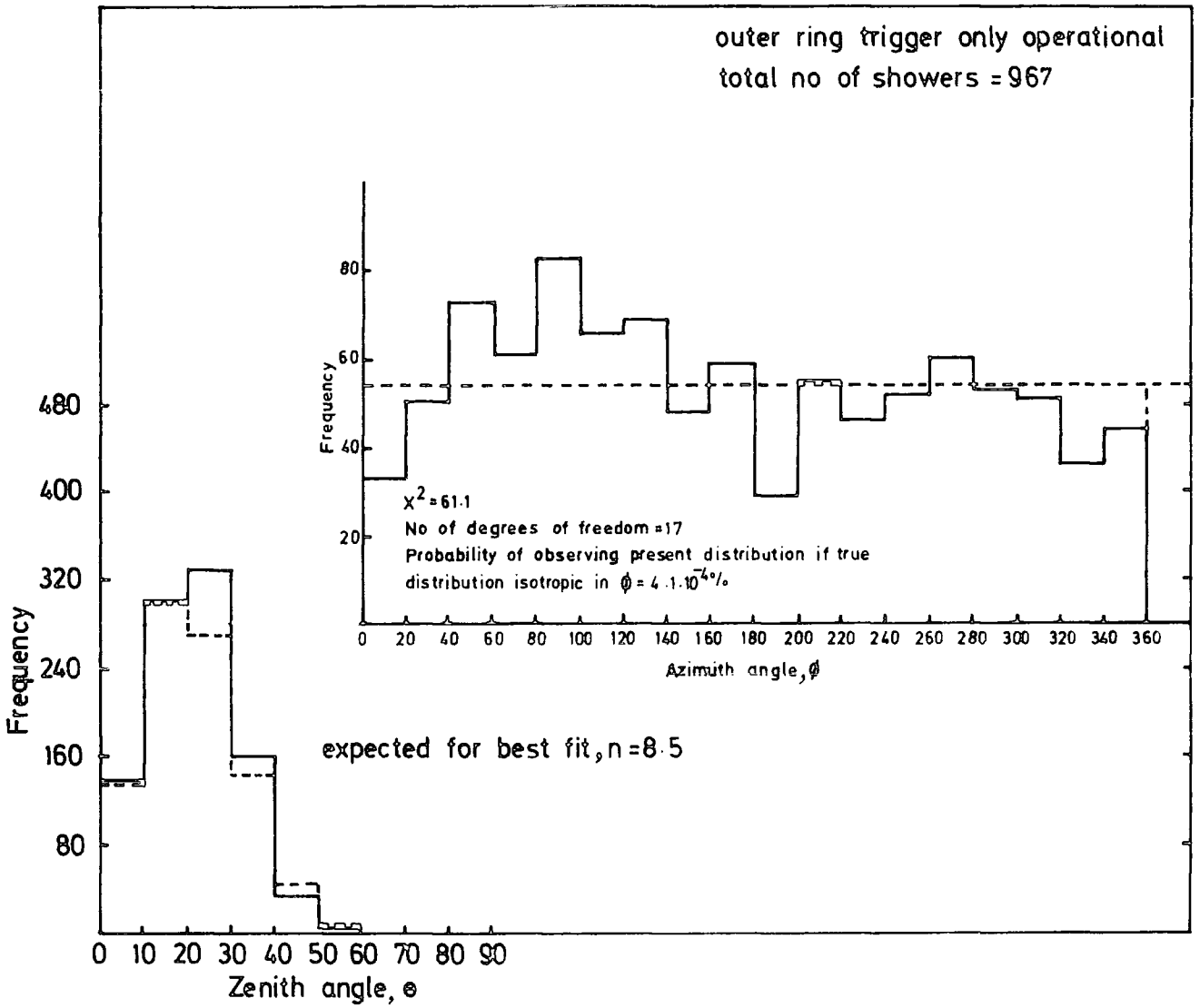

Figure 6.6 : Zenith and azimuth angle distribution of showers selected by the outer ring trigger. Dotted lines are the predicted distribution.

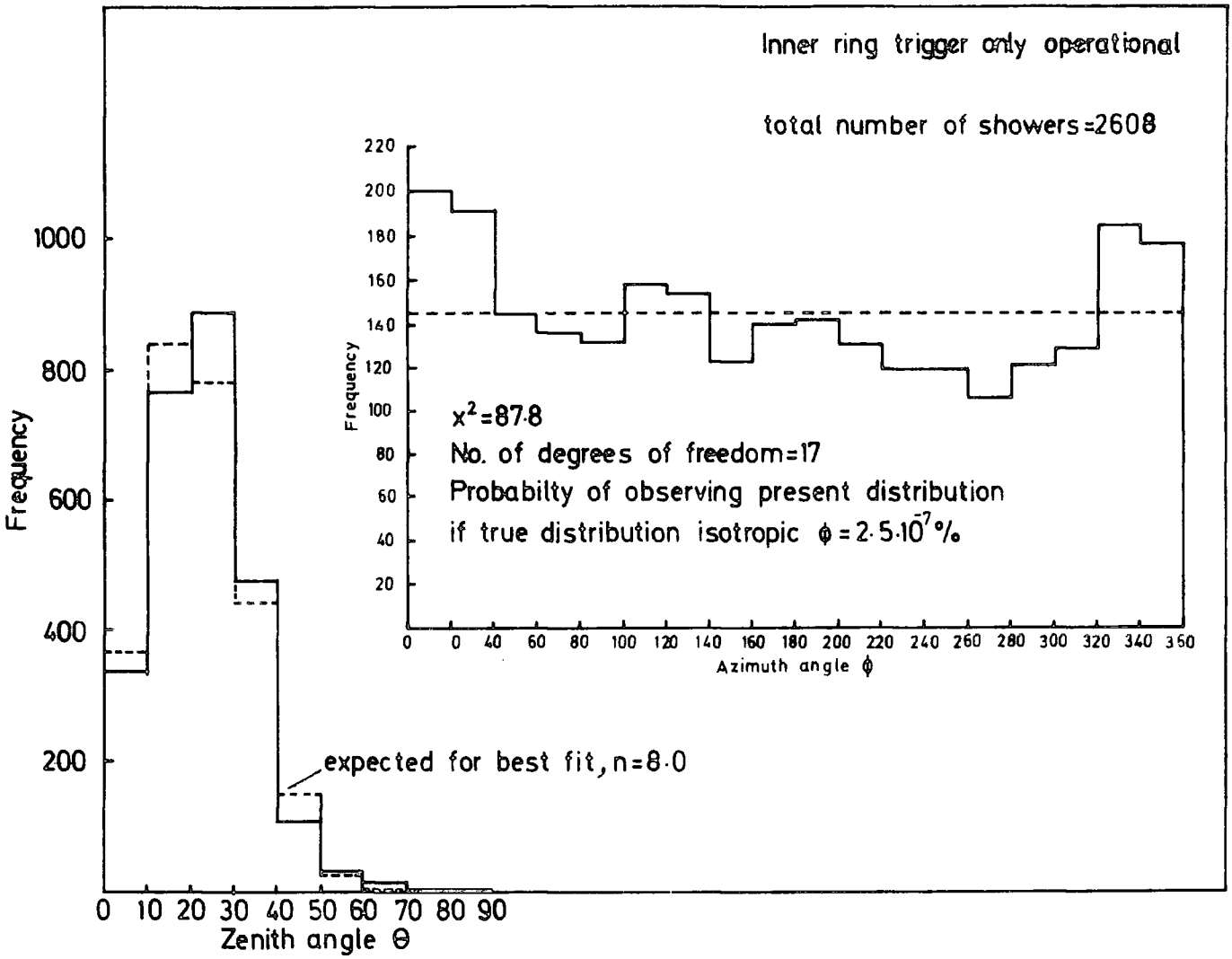

Figure 6.7 : Zenith and azimuth angle distribution of showers selected by the inner ring trigger. Dotted lines are the predicted distributions.

$\chi^2_0 = 23$ probability of a value χ^2 this value or

χ^2 arising by chance = 15%

running time = 337.57 hrs

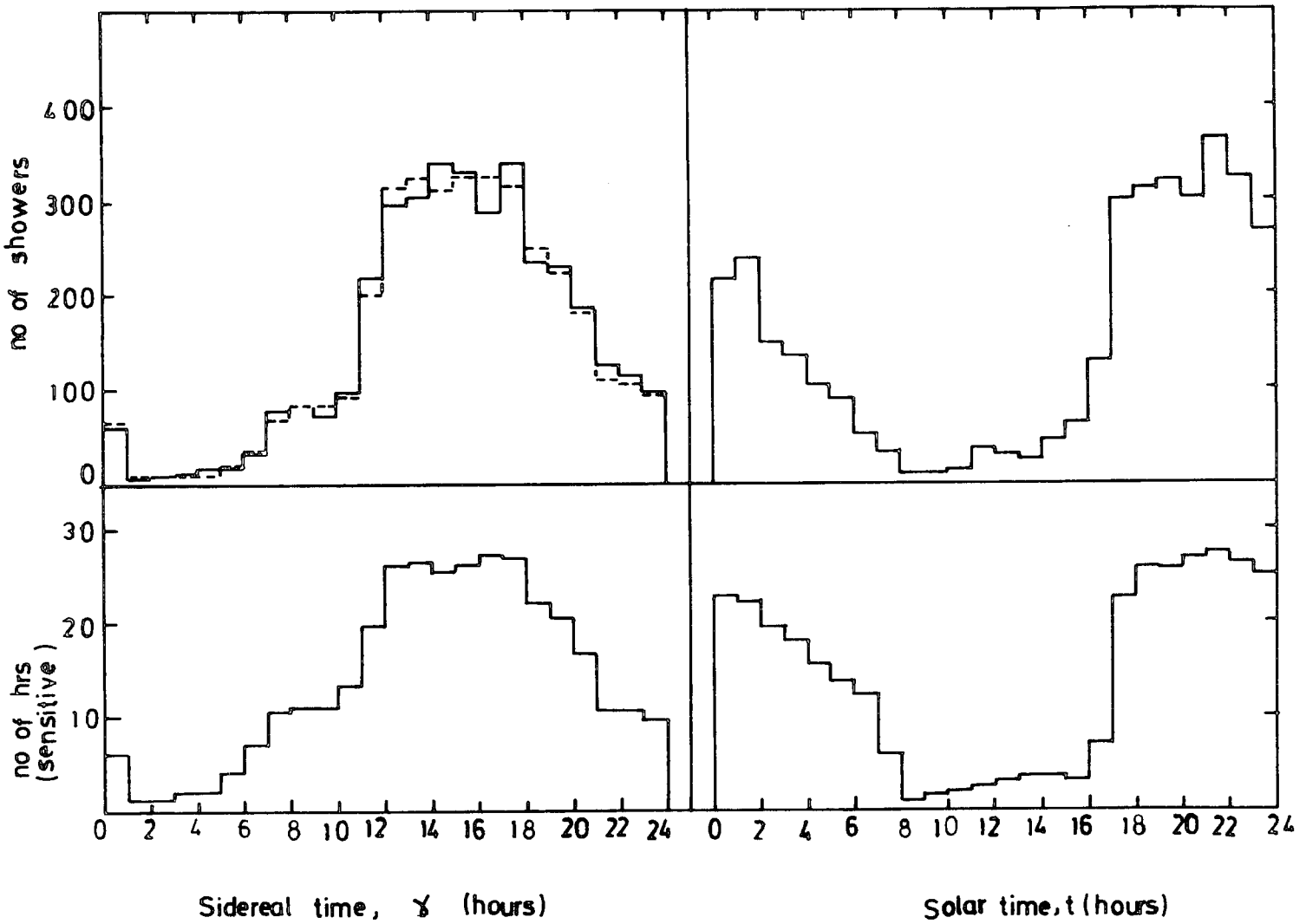

Figure 6.8 The operational time distributions and frequency time variations of E.A.S. in solar and sidereal time for all the data. Dotted line is predicted distribution if it is isotropic in sidereal time.

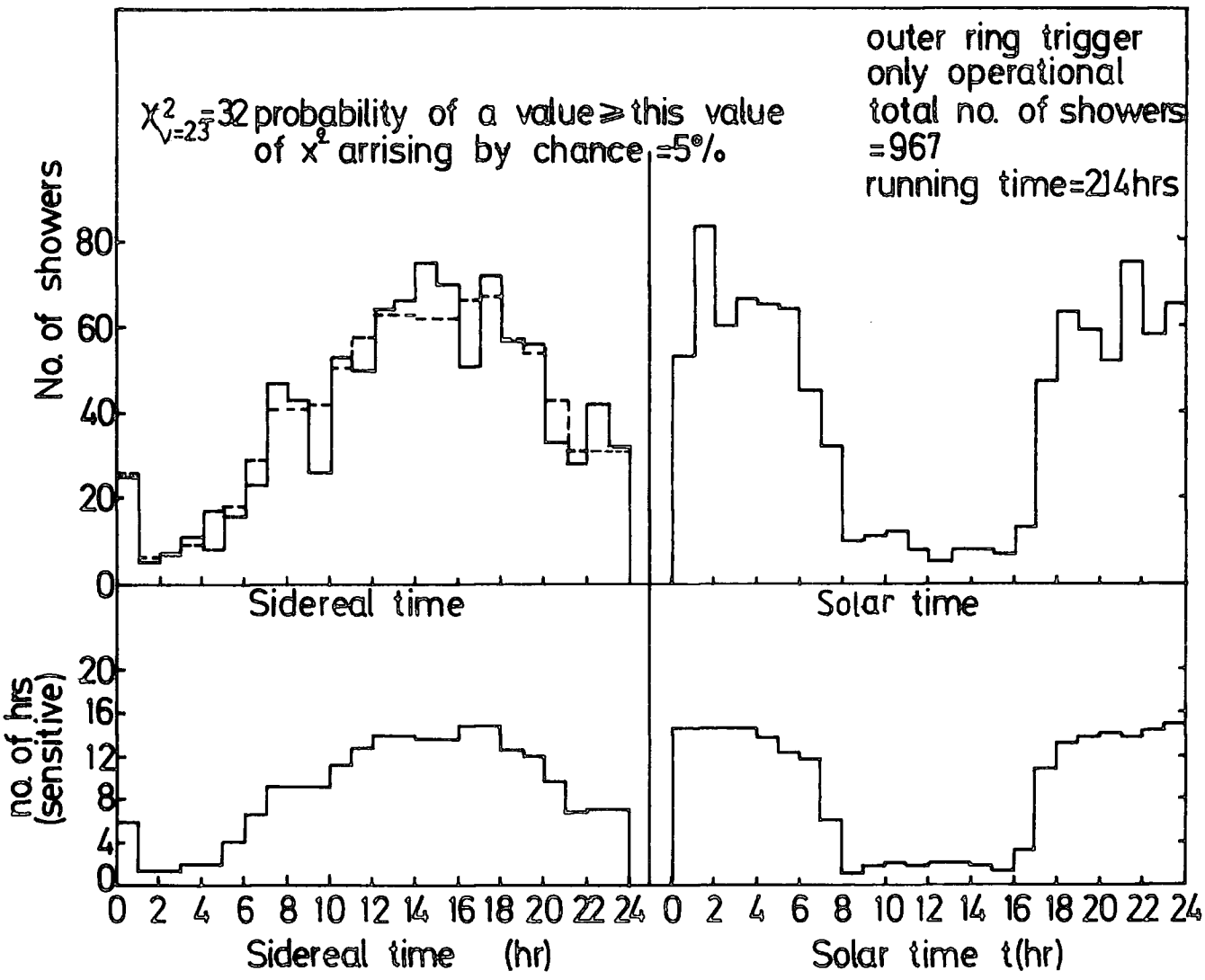

Figure 6.9 : The operational time distributions and frequency-time variations of E.A.S. in solar and sidereal time for outer ring triggers. Dotted line is predicted distribution if it is isotropic in sidereal time.

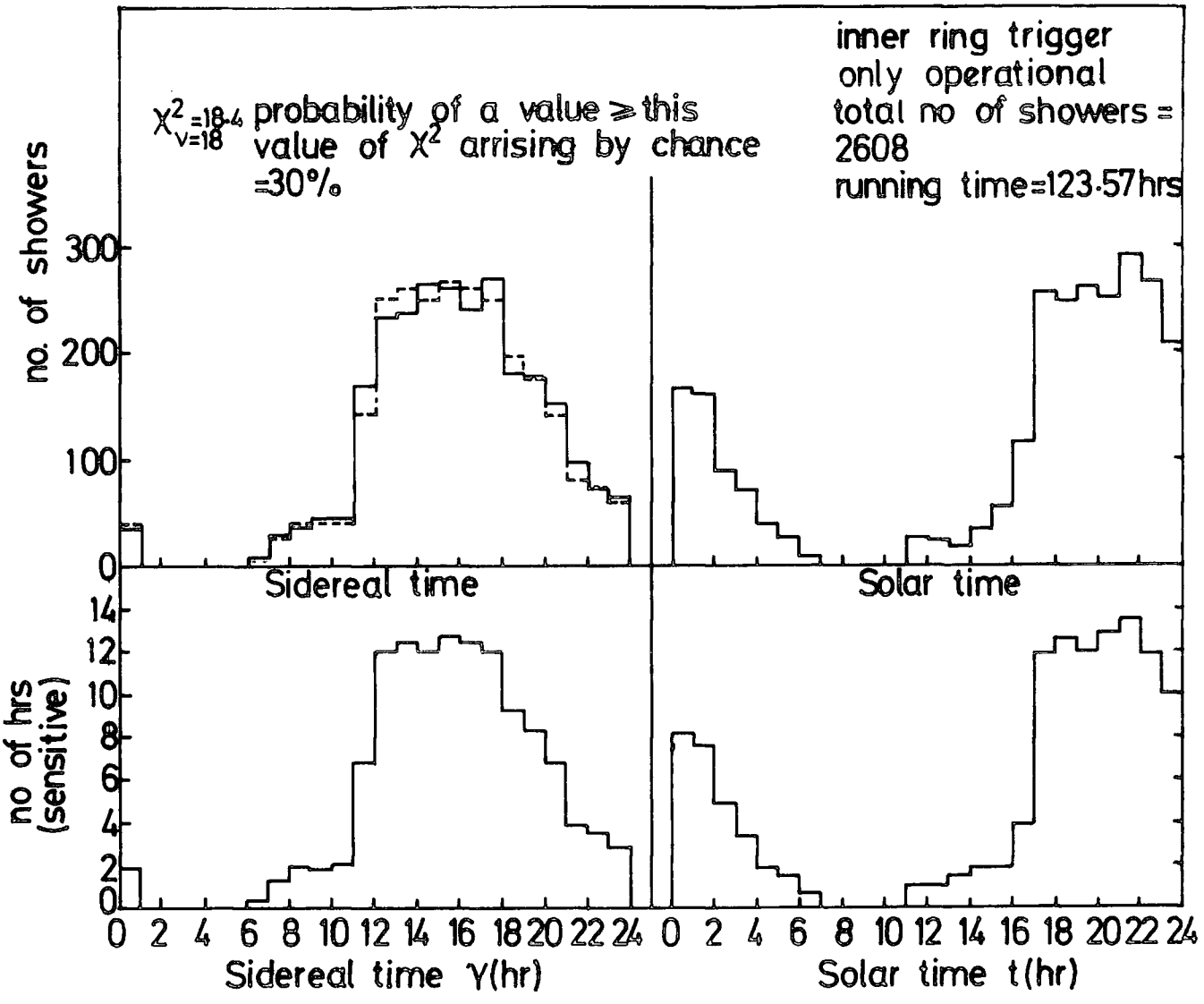

Figure (6.10) : The operational time distributions and frequency-time variation of E.A.S. in solar and sidereal time for inner ring trigger. Dotted line is predicted distribution if it is isotropic in sidereal time

increases with their primary energy. The next step was the analysis of the data in galactic coordinates. From the sidereal time distribution simulation data sets were derived. A computer programme using these data and the result of determining the probability of an expected shower arriving with zenith (θ) and a zimuthal (ϕ) angles in half hour sidereal time intervals is given in the appendix C. The results of the computer programme were plotted (represented in brackets)in pictorial form as galactic longitude versus galactic latitude, so that any clustering of events in 20^{o} x 30^{o} rectangles can be recognised. The galactic latitude and longitude of showers were obtained from the declination and right ascension of figures 6.11 and 6.12 producing the galactic frequency distribution of observed showers and these are shown in figures 6.13, 6.14 and 6.15. Inspection of figures 6.13 which is based on all the 3575 observed showers, shows that overall there is a good agreement between observation and expection assuming a uniform distribution in sidereal time except for the cell marked Δ. The observed number of events 222 exceeds the expected number 171.8 by 3.4 standard deviations. Also the data was split into two shower size categories, 1804 showers of $N_e \leq 2.3.10^5$ and 1771 showers of $N_e > 2.3.10^5$ to see if the excess previously mentioned was due to small or large size showers. The measured θ distribution, the function $I(\theta) = I(0)\cos^n\theta$ was fitted to the data and for showers of $N_e \leq 2.3.10^5$ n = 8.15 and for showers of $N_e > 2.3.10^5$ n is found to be 8.3. It is found from the analysis that the major contribution to the excess comes from the inner ring data, such that the observed number of showers of that particular cell exceeded the expected number by 4.6 standard deviationswhereas using only inner ring data this figure is found to be 4.4 standard deviations. The same data is also presented graphically in figures 6.22 to 6.27. Finally plots in galactic coordinates of pulsars, X, γ ray sources and quasars have been made. Only pulsars and quasars show sources in the general direction in which a possible increase in cosmic ray intensity is observed.

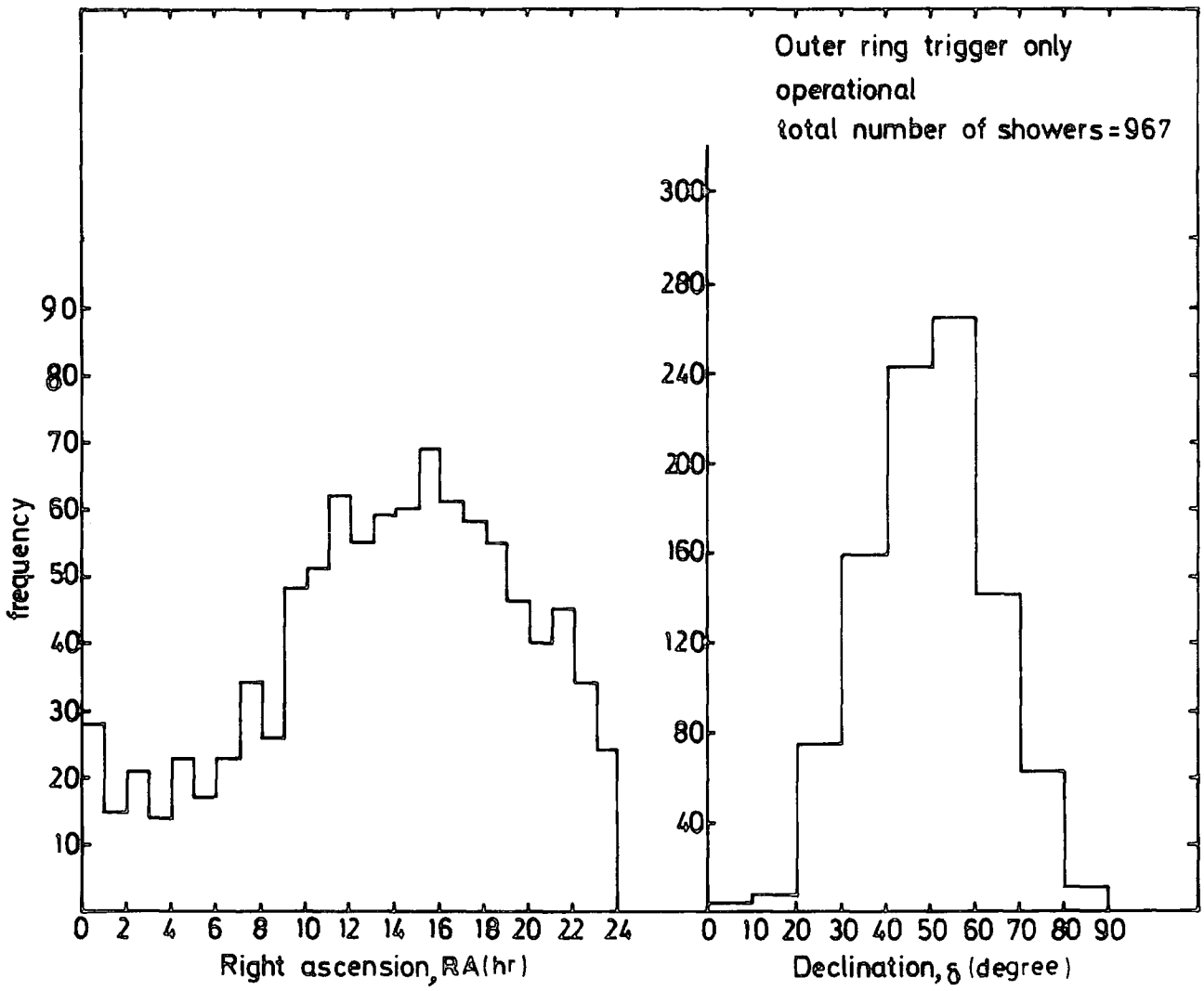

Figure 6.11 : Distribution of E.A.S. in celestial coordinates for outer ring triggers.

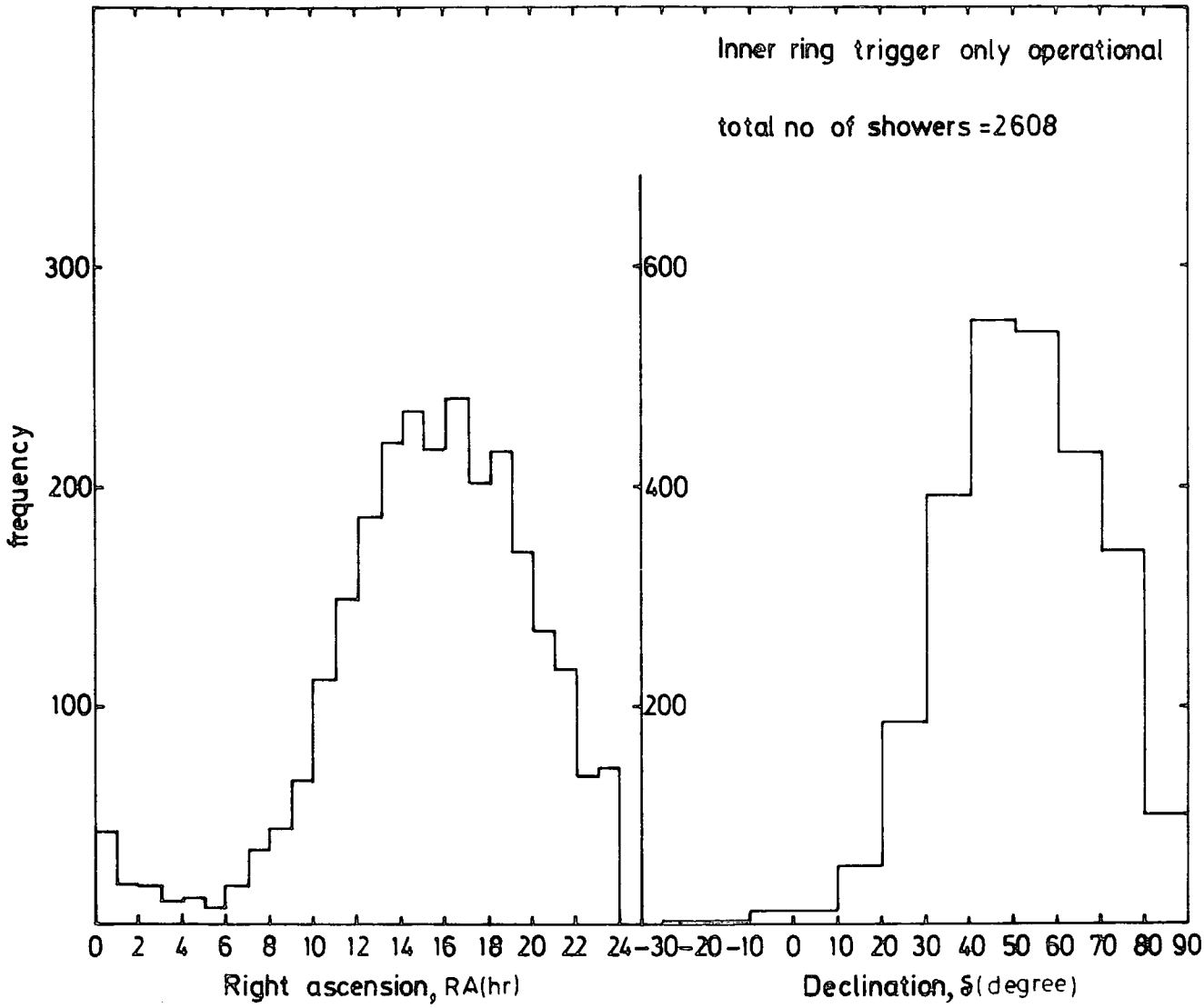

Figure 6.12 : Distribution of E.A.S. in celestial coordinates for inner ring trigger.

Figure 6.13 : The observed and expected frequency distribution of E.A.S. in galactic coordinates for all the data . The expected number is calculated assuming an isotropic distribution in the galaxy and is shown in brackets. Prob. of obtaining value of X^2 = 21.43 and ν = 53 if true distribution is isotropically distributed in galactic coordinates = 99.5%.

Total no. of events = 3575
observed (expected)
atmospheric pressure in mb.

Inner and Outer ring triggers

Galactic latitude, b° (degree)	30	60	90	120	150	180	210	240	270	300	330	360	
90	13(8.74) 1004.88	29(32.1) 1005.77	43(39.34) 1005.18	46(54.45) 1005.53	47(35.4) 1006.35	25(31.67) 1004.08	22(27.89) 1005.01	14(4.03) 1006.43	4(7.7) 1004.7	9(5.3) 998.75	5(6.81) 1006.87	5(6.25) 1008.4	262(259.71)
70	9(19.88) 1007.39	72(76.09) 1004.39	150(179.9) 1004.3	209(224.9) 1004.38	188(175.14) 1004.82	108.(105.5) 1005.75	44(46.39) 1002.77	12(10.82) 1006.3	4(2.82) 1005.3	1(0.51) 1009.3	1(0.47) 1007	4(2.73) 1004.95	802(845.15)
50	7(6.82) 1008.7	93(96.47) 1005.16	285(294.62) 1004.25	345(331.77) 1006.34	Δ 222(171.82) 1005.28	105(123.9) 1006.63	34(38.24) 1006.65	3(3.76) 1007.45	2(0.14) 995.6	0(0.0) -	1(0.0) 1011.2	3(0.0) 1009.3	1100(1067.54)
30	5(1.45) 1007.99	39(55.72) 1005.64	280(266.4) 1004.31	292(284.8) 1005.04	65(84.58) 1005.3	71(71.8) 1005.9	16(19.29) 1008.8	3(1.16) 1005.9	0(0.0) -	0(0.0) -	0(0.0) -	0(0.0) -	771(783.84)
10	0(0.19) -	14(19.36) 1004.33	147(155.88) 1006.48	166(170.19) 1006.66	63(44.9) 1006.04	21(25.63) 1005.68	3(4.68) 1006.3	0(0.094) -	0(0.0) -	0(0.0) -	0(0.0) -	0(0.0) -	414(420.04)
-10	2(7.6.10^{-3}) 999.4	3(2.51) 999.7	43(45.67) 1005.82	93(76.7) 1005.4	41(37.55) 1005.61	8(7.68) 1007.36	1(1.06) 1004.2	0(0.0027) -	0(0.0) -	0(0.0) -	0(0.0) -	0(0.0) -	191(171.19)
-30	0(0.0)	2(0.14) 1000.2	3(2.0) 1001.75	20(13.52) 1005.91	7(7.1) 1005.68	0(1.16) -	0(0.016) -	1(0.0) 1001.	0(0.0) -	0(0.0) -	0(0.0) -	1(0.0) 999	34(26.20)
-50	0(0.0) -	0(5.6.10^{-3}) -	0(0.12) -	1(0.78) 1001.1	0(0.38) -	0(0.03) -	0($<10^{-3}$) -	0(0.0) -	0(0.0) -	0(0.0) -	0(0.0) -	0(0.0) -	1(1.32)
-70													3575(3575)

Galactic longitude, ℓ ° (degree)

Figure 6.13:

Figure 6.14 : The observed and expected frequency distribution in galactic coordinates for events of shower size $\leq 2.3.10^5$ particles and also the figure shows the average barometer reading.

Total no. of events = 1804
observed (expected)
atmospheric pressure in mb

Events of shower size $\leq 2.3.10^5$ particles

Galactic latitude, b" (degree)	30	60	90	120	150	180	210	240	270	300	330	360	
90	6(4.7) 1002.34	16(16.6) 1005.67	29(21.95) 1005.03	24(23.34) 1007.97	17(15.02) 1006.92	16(17.29) 1006.24	7(14.1) 1002.55	5(2.09) 1006.38	3(3.87) 1004.33	4(2.85) 1006	2(3.65) 1012.25	3(2.45) 1006.4	132(127.94)
70	8(10.73) 1007.2	43(42.14) 1005.5	82(90.71) 1004.02	105(118.4) 1004.49	87(89.04) 1003.94	46(49.61) 1005.38	17(21.95) 1004.3	7(5.08) 1006.88	2(1.41) 1005.35	1(0.27) 1009.3	0(0.25) -	3(1.48) 1006.27	401(431.07)
50	5(3.71) 1010.68	57(53.6) 1005.67	131(157.9) 1005.06	190(173.8) 1006.16	Δ 140(85.42) 1006.23	43(55.3) 1007.2	12(15.4) 1005.64	2(1.7) 1006.8	1(0.06) 994	0(0.0) -	1(0.0) 1011.2	1(0.01) 1012.2	583(546.89)
30	4(0.45) 1007.83	20(30.4) 1005.39	140(138.8) 1003.8	181(149.9) 1004.75	39(38.44) 1006.86	23(25.9) 1006.14	5(6.78) 1008.37	3(0.47) 1005.9	0(0.0) -	0(0.0) -	0(0.0) -	0(0.0) -	415(391.11)
10	0(0.1) —	8(10.4) 1002.2	63(81.13) 1007.35	74(93.14) 1006.94	24(22.86) 1007.51	6(5.65) 1006.63	1(1.45) 1006.4	0(0.024) -	0(0.0) -	0(0.0) -	0(0.0) -	0(0.0) -	176(214.47)
-10	1(0.004) 999.5	2(1.28) 999.77	19(23.3) 1006.39	42(37.33) 1005.85	11(15.29) 1005.85	5(2.2) 1005.48	1(0.26) 1004.2	0(0.001) -	0(0.0) -	0(0.0) -	0(0.0) -	0(0.0) -	81(79.67)
-30	0(0.0) -	0(0.0) -	3(0.15) 1001.75	7(6.85) 1010.11	5(2.96) 1004.66	0(0.3) -	0(0.006) -	0(0.0) -	0(0.0) -	0(0.0) -	0(0.0) -	0(0.0) -	15(12.26)
-50	0(0.0) -	0(0.0028) -	0(0.05) -	1(0.36) 1001.1	0(0.17) -	0(0.01) -	0(0.0) -	0(0.0) -	0(0.0) -	0(0.0) -	0(0.0) -	0(0.0) -	1(0.59)
-70													1804(1804)

Galactic longitude, ℓ " (degree)

Figure 6.14 :

Figure 6.15 : The observed and expected frequency distribution of E.A.S. in galactic coordinates for events of shower size $>2.3.10^5$ particles and also the figure shows the average barometer reading.

Total no. of events = 1771
Observed (expected)
atmospheric pressure in mb.

Events of shower size $>2.3.10^5$ particles

Galactic latitude, b" (degree)	30	60	90	120	150	180	210	240	270	300	330	360	
90 to 70	7(4.04) 1008.44	13(15.5) 1006	14(17.39) 1005.9	22(31.11) 1003.82	30(20.38) 1004.98	9(14.38) 1002.88	15(13.79) 1005.83	9(1.94) 1006.55	1(3.83) 1003.2	5(2.45) 991.5	3(3.16) 1001.5	2(3.8) 1009.4	130(131.77)
70 to 50	1(9.15 1008.3	29(33.95) 1003.44	68(89.19) 1004.6	104(106.5) 1004.31	101(86.1) 1005.69	62(55.89) 1006.04	27(24.44) 1001.97	5(5.74) 1005.58	2(1.41) 1005.25	0(0.24) -	0(0.22) -	2(1.25) 1003.63	401(414.08)
50 to 30	2(3.11) 998.8	36(42.8) 1004.5	154(136.72) 1003.86	155(157.97) 1006.21	82(86.4) 1003.49	62(68.6) 1005.7	22(22.84) 1007.29	1(2.06) 1008.1	1(0.08) 997.2	1(0.0) -	0(0.0) -	2(0.0) 10064	517(520.65)
30 to 10	1(0.45) 1008.5	19(25.32) 1006.07	140(127.6) 1004.76	111(134.16) 1005.34	26(46.14) 1003.69	48(45.9) 1005.8	11(12.51) 1009.08	0(0.69) -	0(0.0) -	0(0.0) -	0(0.0) -	0(0.0) -	356(392.73)
10 to -10	0(0.09) -	6(8.96) 1006.1	84(74.15) 1005.41	92(77.05) 1006.48	39(22.04) 1005.09	15(19.98) 1005.21	2.(3.23) 1006.2	0(0.07) -	0(0.0) -	0(0.0) -	0(0.0) -	0(0.0) -	238(205.57)
-10 to -30	1(3.6.10^{-3}) 999.3	1(1.23) 999.5	24(22.37) 1005.46	51(39.37) 1005.009	30(22.26) 1004.8	3(5.48) 1012.05	0(0.8) -	0(0.0017) -	0(0.0) -	0(0.0) -	0(0.0) -	0(0.0) -	110(91.52)
-30 to -50	0(0.0) -	2(0.14) 1000.2	0(1.85) -	13(6.67) 1003.97	2(4.14) 1006-7	0(1.13) -	0(0.01) -	1(0.0) -	0(0.0) -	0(0.0) -	0(0.0) -	1(0.0) -	19(13.94)
-50 to -70	0(0.0) -	0(2.8.10^{-3}) -	0(0.07) -	0(0.42) -	0(0.21) -	0(0.02) -	0(5.10^{-4}) -	0(0.0) -	0(0.0) -	0(0.0) -	0(0.0) -	0(0.0) -	(0.73)
													1771(1771)

Galactic longitude, ℓ " (degree)

Figure 6.15 :

6.5 THE BAROMETRIC EFFECT

It is well known that the intensity of any secondary cosmic ray component varies with atmospheric pressure at the level of observation. This variation can be expressed as follows:

$$I = I_o \exp-\beta(p-p_o)\ m^{-2}sec^{-1}st^{-1}$$

where I is the cosmic ray intensity at pressure p, I_o is the intensity at standard atmospheric pressure p_o (1000 mb). The barometric pressure at Durham during the time this experiment was running varied over the range 990-1022 mb with a mean of 1010 mb (figure 6.16), which corresponds to a mean atmospheric depth of 1029.3 $g.cm^{-2}$ (one $g.cm^{-2}$ = 1000 mb/g where g is the acceleration due to gravity in cm sec^{-2}). The above equation of the barometric pressure coefficient, β, with average barometer reading corresponding to the observed showers were used to correct the measured intensity to standard atmospheric pressure and these are shown in figures 6.17, 6.18 and 6.19. The measured intensity variation due to the pressure was found to be very small. Because of different observed shower sizes, it is found that the trigger rate is variable for both the inner and outer ring triggers. In the present work, β, is the barometric coefficient defined as the percentage change in the intensity with pressure as calculated, for all the data. $\beta = 15 \pm 2.7\ cm^{-1}.Hg^{-1}$ for all showers and $14 \pm 3.1\ cm^{-1}.Hg^{-1}$ for showers of $N_e > 2.3.10$ particles and $13.4 \pm 0.56\ cm^{-1}.Hg^{-1}$ for showers of $N_e \leqslant 2.3.10^5$ particles. These results are shown in figure 6.20. The measurements do not agree with theoretical predictions for photon-electron cascades that the barometric coefficient is expected to become progressively smaller as the shower size increases. However, in practice, figure 6.21 shows that the barometric coefficient of extensive showers in the lower atmosphere (below 650 $g.cm^{-2}$) is approximately constant and equal to about 10 per cent $cm^{-1}.Hg^{1}$ pressure over quite a wide

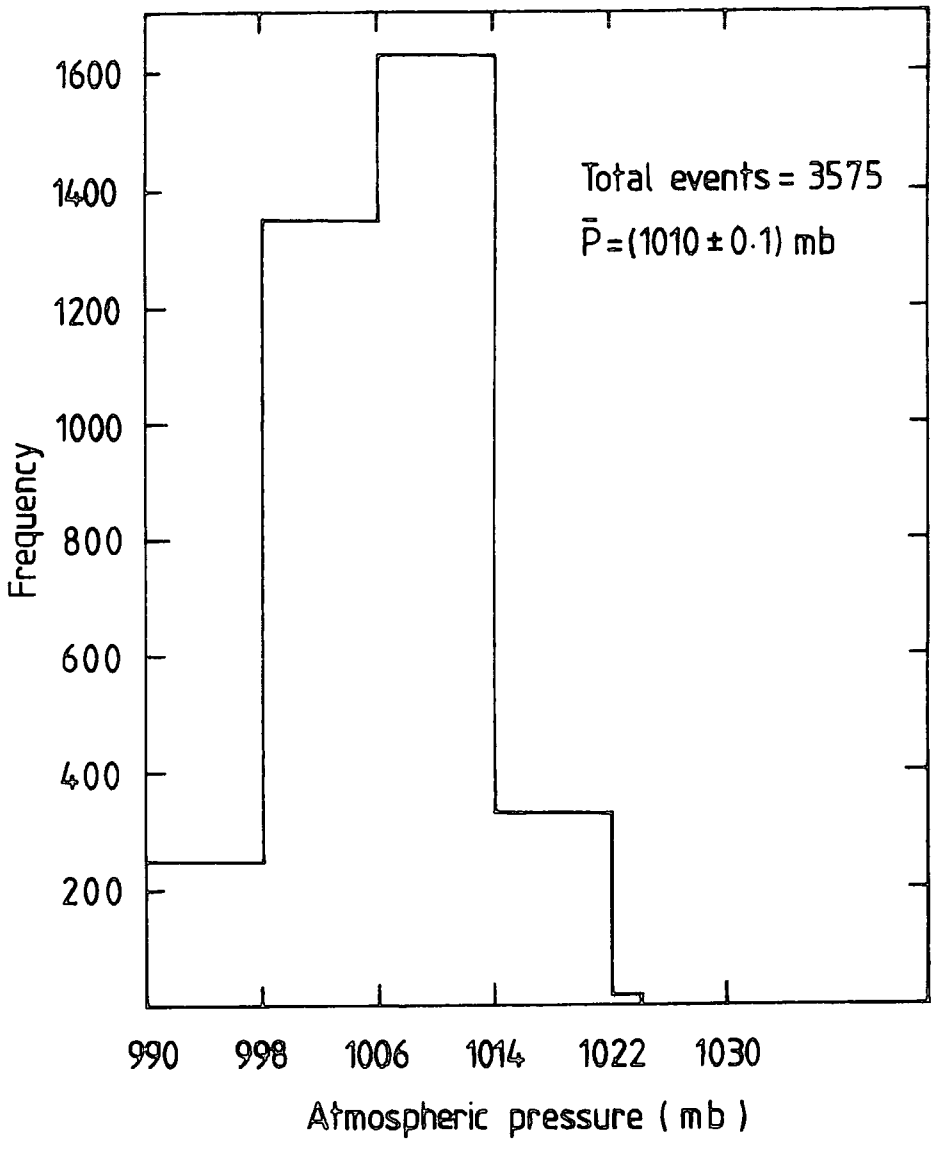

Figure 6.16 : Distribution of atmospheric pressure recorded at the times that E.A.S. were detected.

Figure 6.17 : The observed and expected frequency distribution of E.A.S. in galactic coordinates for all the data. Data are corrected due to the atmospheric pressure variation. The expected number is calculated assuming an isotropic distribution in galaxy and is shown in brackets.

Prob. of obtaining value of $X^2 = 21.63$ and $\nu = 49$ if true distribution is isotropically distributed in galactic coordinates = 99.5%.

Total no. of events = 3575
observed (expected)

Inner and Outer ring triggers

Galactic latitude, b" (degree)	30	60	90	120	150	180	210	240	270	300	330	360	
90 to 70	13(8.77)	29(31.93)	43(39.4)	46(54.3)	47(34.98)	25(32.1)	22(28)	14(3.98)	4(7.76)	9(5.72)	5(6.7)	5(6.04)	262(259.73)
70 to 50	9(19.42)	72(76.9)	150(182)	209(227.3)	188(176.2)	108(105)	44(47.8)	12(10.7)	4(2.8)	1(0.5)	4(0.46)	4(2.74)	802(851.81)
50 to 30	7(6.6)	93(96.7)	285(298.3)	345(327.9)	222(172) Δ	105(122.1)	34(37.7)	3(3.7)	2(0.16)	0(0.0)	1(0.0)	3(0.0)	1100(1064.9)
30 to 10	5(1.4)	39(55.5)	280(269.5)	292(285)	65(84.6)	71(71.3)	16(18.5)	3(1.15)	0(0.0)	0(0.0)	0(0.0)	0(0.0)	771(787)
10 to -10	0(0.2)	14(19.6)	147(153.2)	166(167.6)	63(44.5)	21(25.5)	3(4.63)	0(0.1)	0(0.0)	0(0.0)	0(0.0)	0(0.0)	414(415.43)
-10 to -30	2(0.008)	3(2.68)	43(45.4	93(76.6)	41(37.4)	8(7.5)	1(1.07)	0.(0.002)	0.(0.0)	0(0.0)	0(0.0)	0(0.0)	191(170.7)
-30 to -50	0(0.0)	2(0.14)	3(2.08)	20(13.4)	7(7.1)	0(0.16)	1(0.02)	1(0.0)	0(0.0)	0(0.0)	0(0.0)	1(0.0)	34(23.98)
-50 to -70	0(0.0)	0(5.6.10^{-3})	1(0.13)	1(0.82)	0(0.4)	0(0.032)	0(<10^{-3})	0(0.0)	0(0.0)	0(0.0)	0(0.0)	0(0.0)	1(1.39)
													3575(3575)

Galactic longitude, ℓ" (degree)

Figure 6.17 :

Figure 6.18 : The observed and expected frequency distribution of E.A.S. in galactic coordinates for events of shower size $\leqslant 2.3.10^5$ particles. The expected number in brackets are corrected due to the atmospheric pressure variations.

Total no. of events = 1804
observed (expected)

Events of shower size $\leq 2.3.10^5$ particles

Galactic latitude, b" (degree)	30	60	90	120	150	180	210	240	270	300	330	360	
90													
70	6(4.85)	16(16.6)	29(22.1)	24(22.8)	17(14.8)	16(17.2)	7(14.5)	5(2.07)	3(3.92)	4(2.84)	2(3.41)	3(2.43)	132(127.47)
50	8(11.1)	43(42.2)	82(92.2)	105(119.7)	87(90.5)	46(49.7)	17(22.2)	7(5.02)	2(1.41)	1(0.27)	0(0.25)	3(1.47)	401(435.96)
30	5(3.52)	57(53.5)	131(158.7)	190(172.8)	Δ 140(84.8)	43(54.4)	12(15.4)	2(1.68)	1(0.1)	0(0.0)	1(0.0)	1(0.01)	583(544.9)
10	4(0.44)	20(30.5)	140(141.3)	181(151.1)	39(37.9)	23(25.8)	5(7.2)	3(0.47)	0(0.0)	0(0.0)	0(0.0)	0(0.0)	415(394.09)
-10	0(0.1)	8(10.76)	63(79.7)	74(91.8)	24(22.4)	6(5.6)	1(1.44)	0(0.024)	0(0.0)	0(0.0)	0(0.0)	0(0.0)	176(211 .72)
-30	1(0.004)	2(1.38)	19(23.1)	42(37.2)	11(14.9)	5(2.22)	1(0.26)	0(0.0)	0(0.0)	0(0.0)	0(0.0)	0(0.0)	81(79.16)
-50	0(0.0)	0(0.0)	3(0.16)	7(6.54)	5(2.98)	0(0.32)	0(0.006)	0(0.0)	0(0.0)	0(0.0)	0(0.0)	0(0.0)	15(10.0)
-70	0(0.0)	0(0.003)	0(0.05)	1(0.35)	0(0.2	0(0.01)	0(0.0)	0(0.0)	0(0.0)	0(0.0)	0(0.0)	0(0.01)	1(0.59)
													1804(1804)

Galactic longitude, ℓ" (degree)

Figure 6.18 :

Figure 6.19 : The observed and expected frequency distribution of E.A.S. in galactic coordinates for events of shower size $>2.3.10^5$ particles. The expected number in brackets are corrected due to the atmospheric pressure variations.

Total no. of events = 1771
observed (expected)

Events of shower size $> 2.3.10^5$ particles

Galactic latitude, b" (degree)	30	60	90	120	150	180	210	240	270	300	330	360	
90 to 70	7(3.9)	13(15.34)	14(17.23)	22(31.51)	30(20.4)	9(14.72)	15(13.67)	9(1.91)	1(3.9)	5(2.83)	3(3.28)	2(3.63)	130(132.3)
70 to 50	1(8.84)	29(34.5)	68(89.6)	104(107.3)	101(85.5)	62(55.3)	27(25.3)	5(5.7)	2(1.4)	0(0.24)	0(0.22)	2(1.27)	401(415.2)
50 to 30	2(3.3)	36(43.1)	154(138.4)	155(156)	82(87.8)	62(68.1)	22(22.3)	1(1.99)	1(0.087)	0(0.0)	0(0.0)	2(0.0)	517(521.4)
30 to 10	1(0.43)	19(25.04)	140(127.9)	111(133.7)	26(46.8)	48(45.52)	11(11.98)	0(0.73)	0(0.0)	0(0.0)	0(0.0)	0(0.0)	356(392.19)
10 to -10	0(0.09)	6(8.86)	84(73.9)	92(75.9)	34(22.03)	15(19.9)	2(3.2)	0(0.07)	0(0.0)	0(0.0)	0(0.0)	0(0.0)	238(203.91)
-10 to -30	1(0.004)	1(1.31)	24(22.2)	51(39.4)	30(22.3)	3(5.05)	0(0.84)	0(0.008)	0(0.0)	0(0.0)	0(0.0)	0(0.0)	110(91.15)
-30 to -50	0(0.0)	2(0.15)	0(1.95)	13(6.75)	2(4.04)	0(1.13)	0(0.01)	1(0.0)	0(0.0)	0(0.0)	0(0.0)	1(0.0)	19(14.09)
-50 to -70	0(0.0)	0($2.8.10^{-3}$)	0(0.07)	0(0.42)	0(0.21)	0(0.02)	0(0.0)	0(0.0)	0(0.0)	0(0.0)	0(0.0)	0(0.0)	0(0.77)
													1771(1771)

Galactic longitude, ℓ " (degree)

Figure 6.19 :

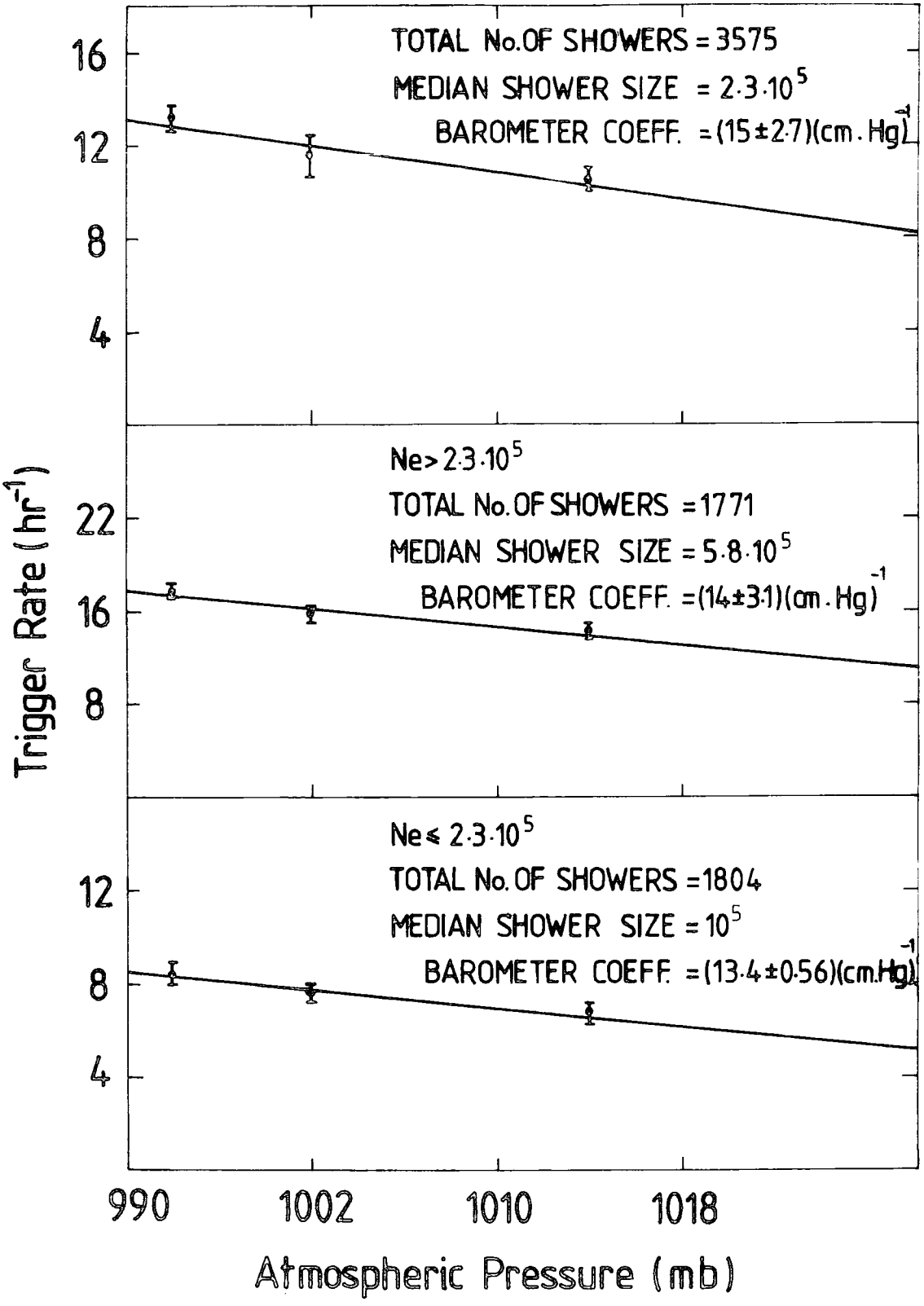

Figure 6.20 : The variation of trigger rate of observed showers with atmospheric pressure.

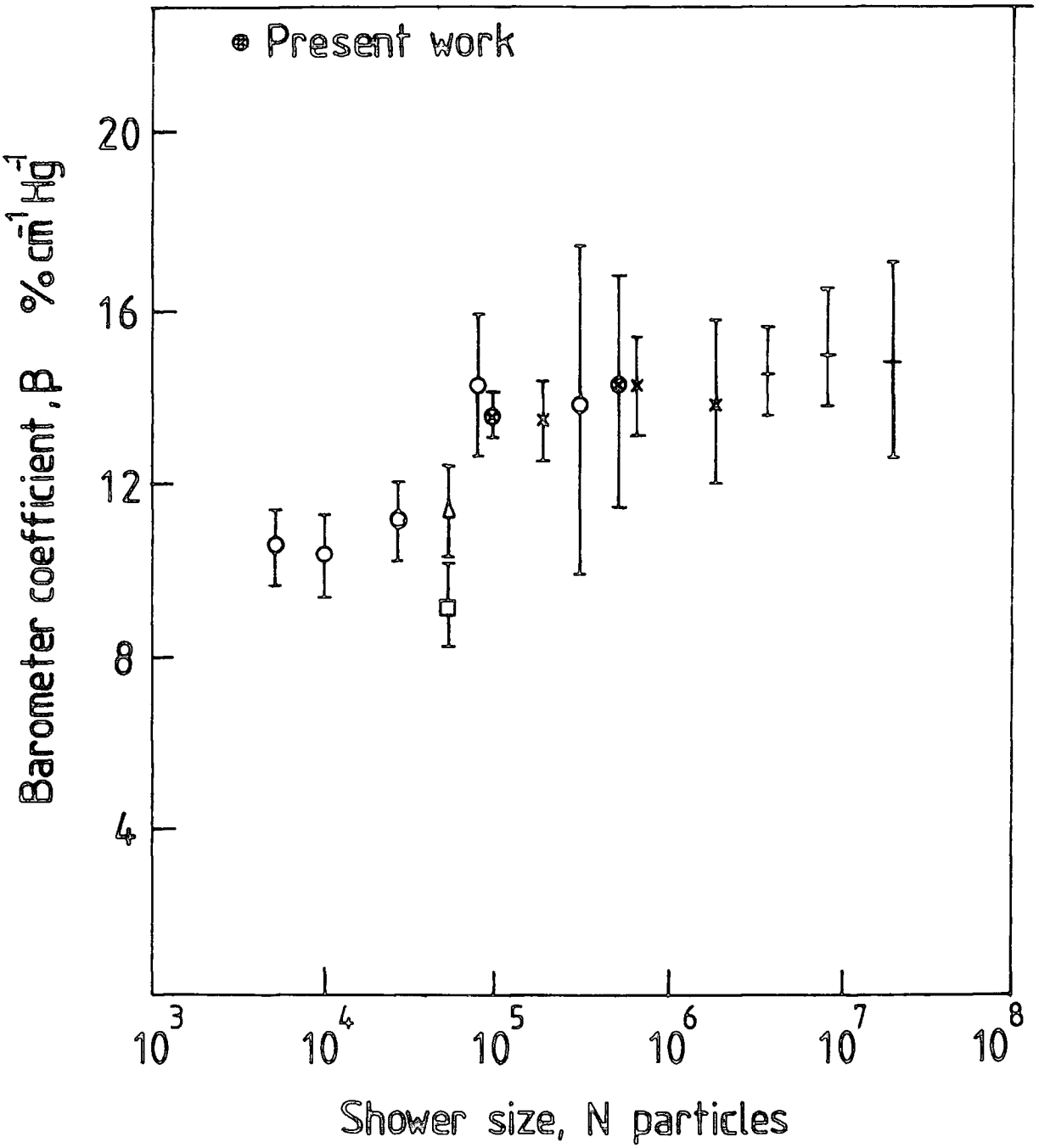

Figure 6.21 : Experimental measurements of the barometer coefficient of air showers (After Galbraith, 1958).

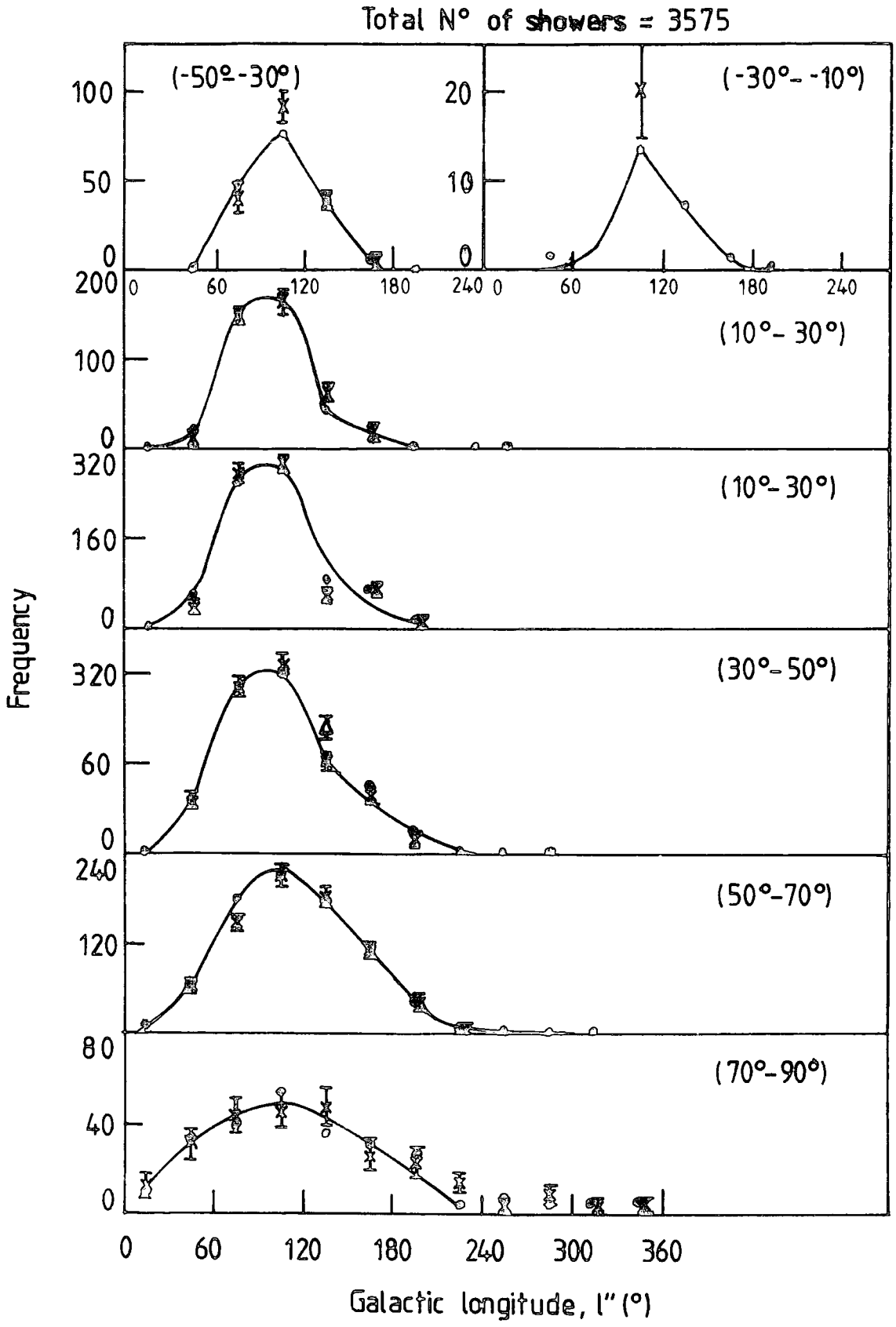

Figure 6.22 : Variation of the expected number of showers with galactic longitude for different ranges of galactic latitude. The observed number of events in cells containing ⩾10 are plotted.

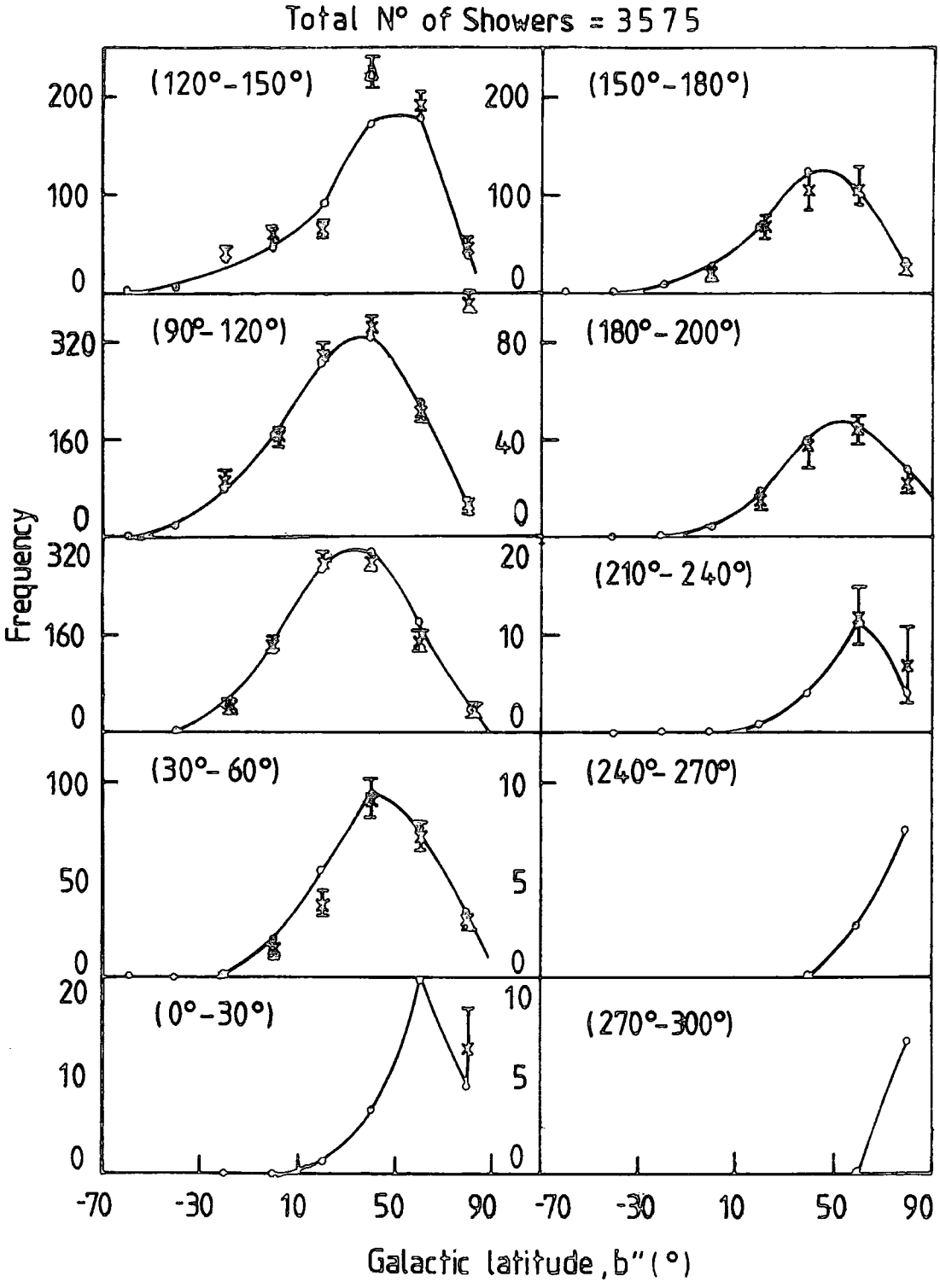

Figure 6.23 : Variation of the expected number of showers with galactic latitude for different ranges of galactic longitude. The observed number of events in cells containing ≥10 showers are plotted.

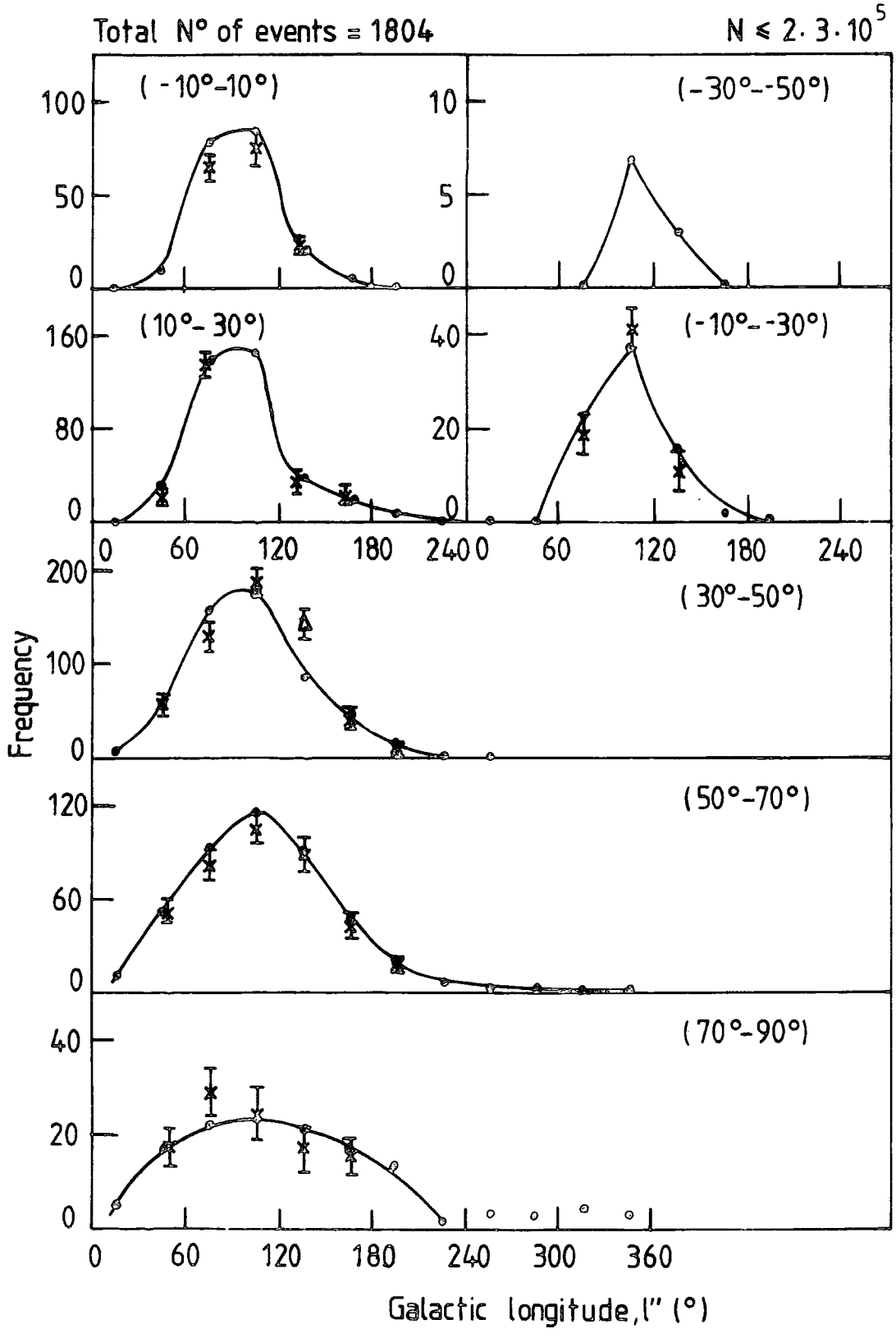

Figure 6.24 : Variation of the expected number of showers with galactic longitude for different ranges of galactic latitude. The observed number of events in cells containing ≥10 showers are plotted.

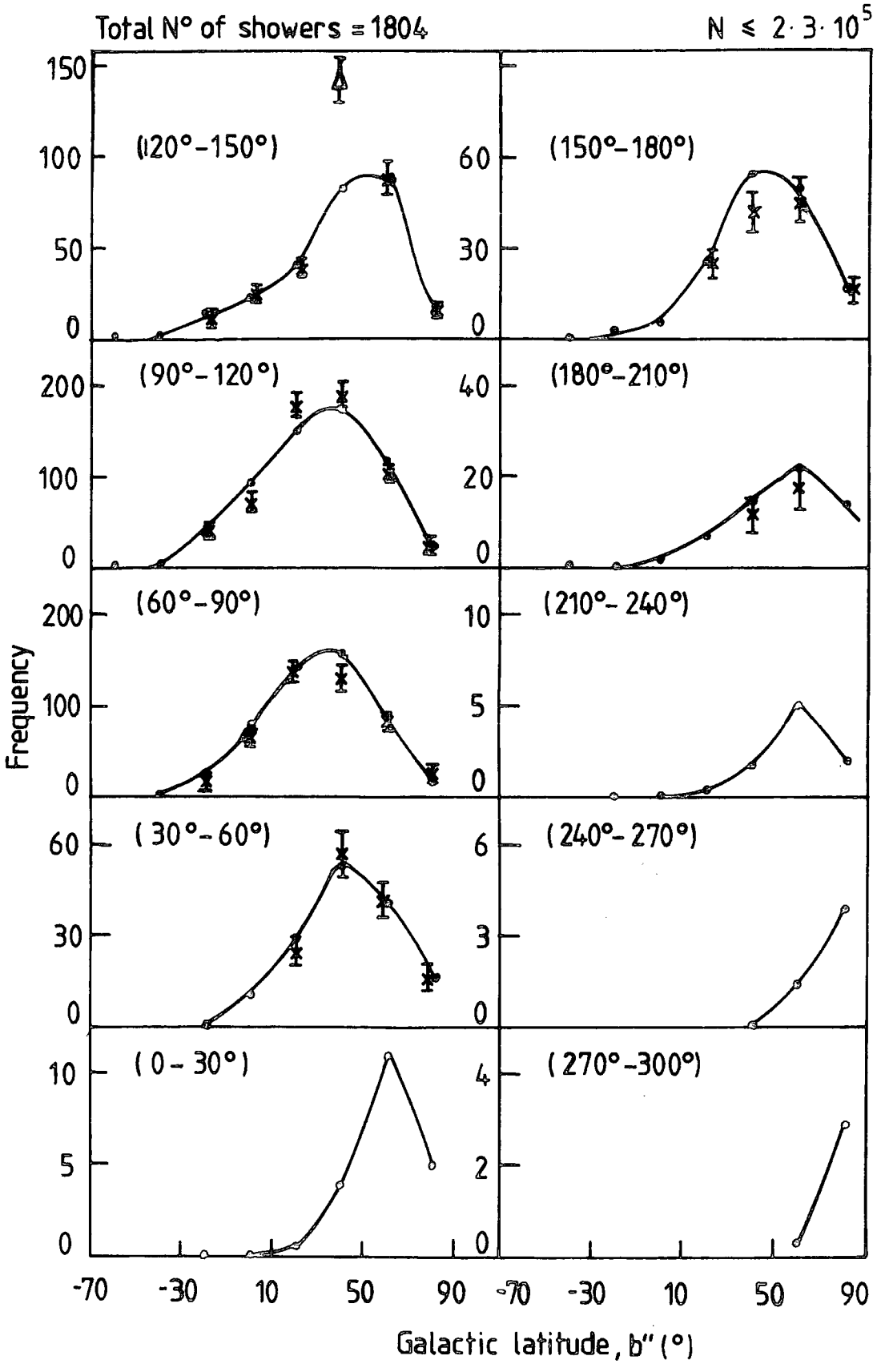

Figure 6.25 : Variation of the expected number of showers with galactic latitude for different ranges of galactic longitude. The observed number of events in cells containing ≥10 showers are plotted.

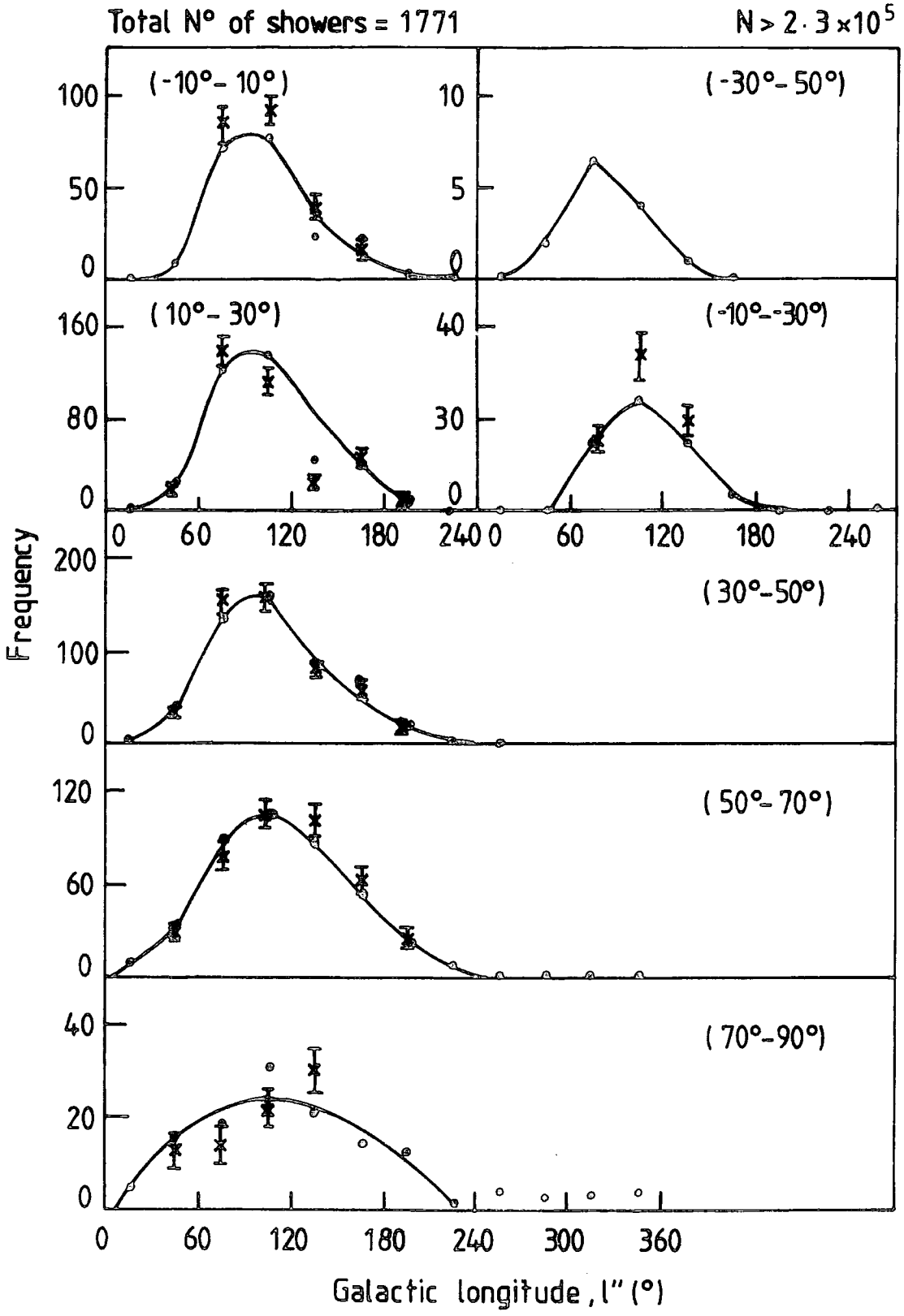

Figure 6.26 : Variation of the expected number of showers with galactic longitude for different ranges of galactic latitude. The observed number of events in cells containing ≥10 showers are plotted.

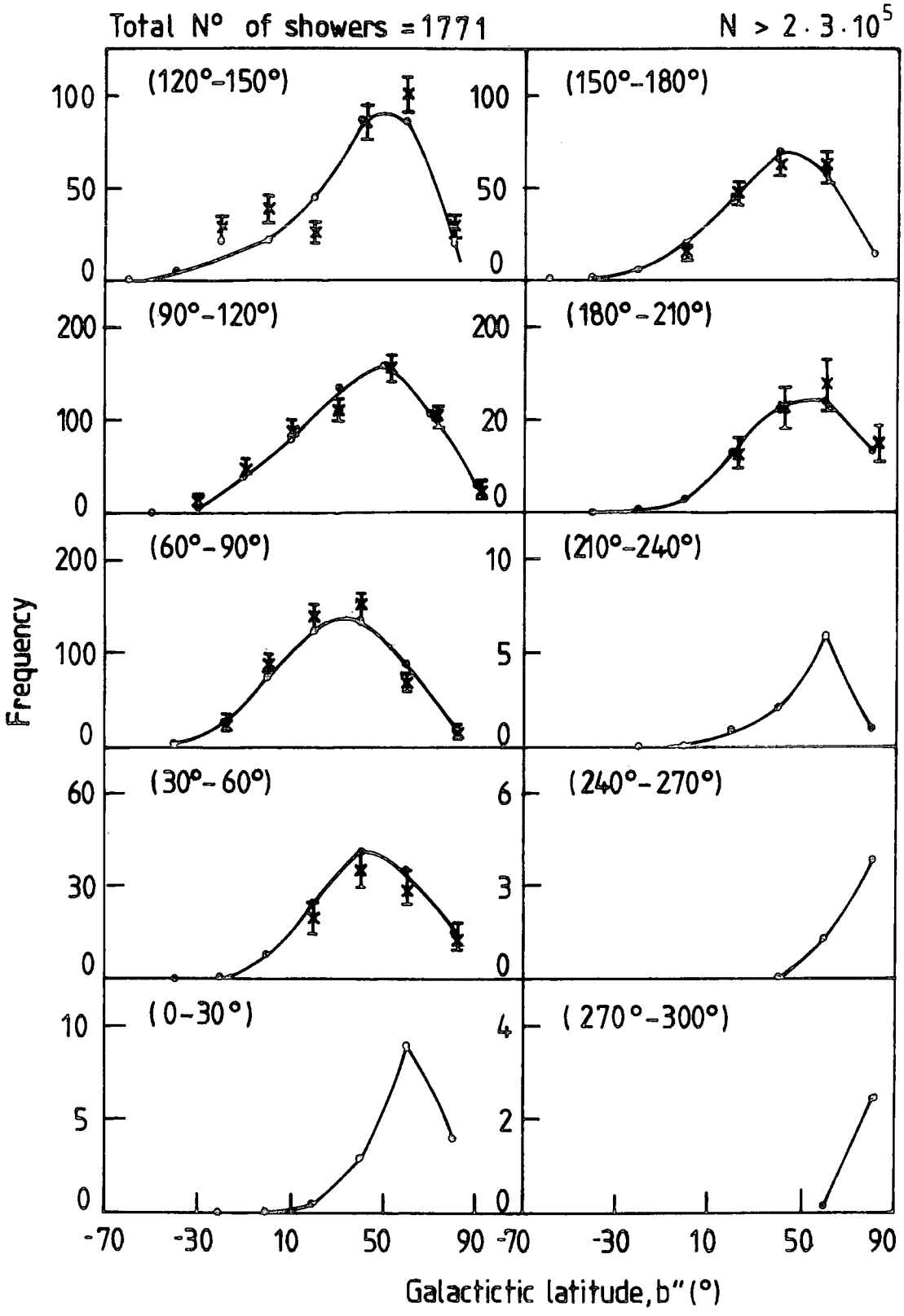

Figure 6.27 : Variation of the expected number of showers with galactic latitude for different ranges of galactic longitude. The observed number of events in cells containing ⩾10 showers are plotted.

range of shower size, but the accuracy of measurements does not permit definite conclusion to be made about possible variation in the barometer coefficient with shower size. Some measurements suggest that the barometer coefficient of showers increases with shower size and for showers containing more than 10^7 particles is significantly greater than 10 per cent $cm^{-1}.Hg^{-1}$.

6.6 CONCLUSION

It appears from the analysis on the time variation that the arrival direction of E.A.S. seem to be predominantly isotropically distributed in space. Some evidence is found for a possible increase in intensity of low energy shower of size $2.3.10^5$ particles from the range of galactic longitude and latitude (135 ± 15^0, 40 ± 10^0). The galactic coordinates of the galactic cell shown in figure 6.13 which contain a significantly larger number of events than expected have been compared with the galactic coordinates of supernova remants, pulsars, quasars, X and γ-ray sources which are shown in figures 6.28 to 6.32. It is seen from the figures that there are no observed X, γ or supernova remants (they are mostly in the galactic plane) in our excess region of events (represented by squares). However, there is some correlation with pulsar and quasar sources. The properties of these sources have been investigated in spite of not every pulsar or quasar having all the required information at the present time. The ones known are shown in figures 6.33 and 6.34. The correlated excess of quasars show no sign of any anomalous property whereas the pulsar (P0809 + 74) shows the interesting property of having one of the longest ages and shortest distances from the earth of known pulsars.

94, supernova remnants

anomalous region

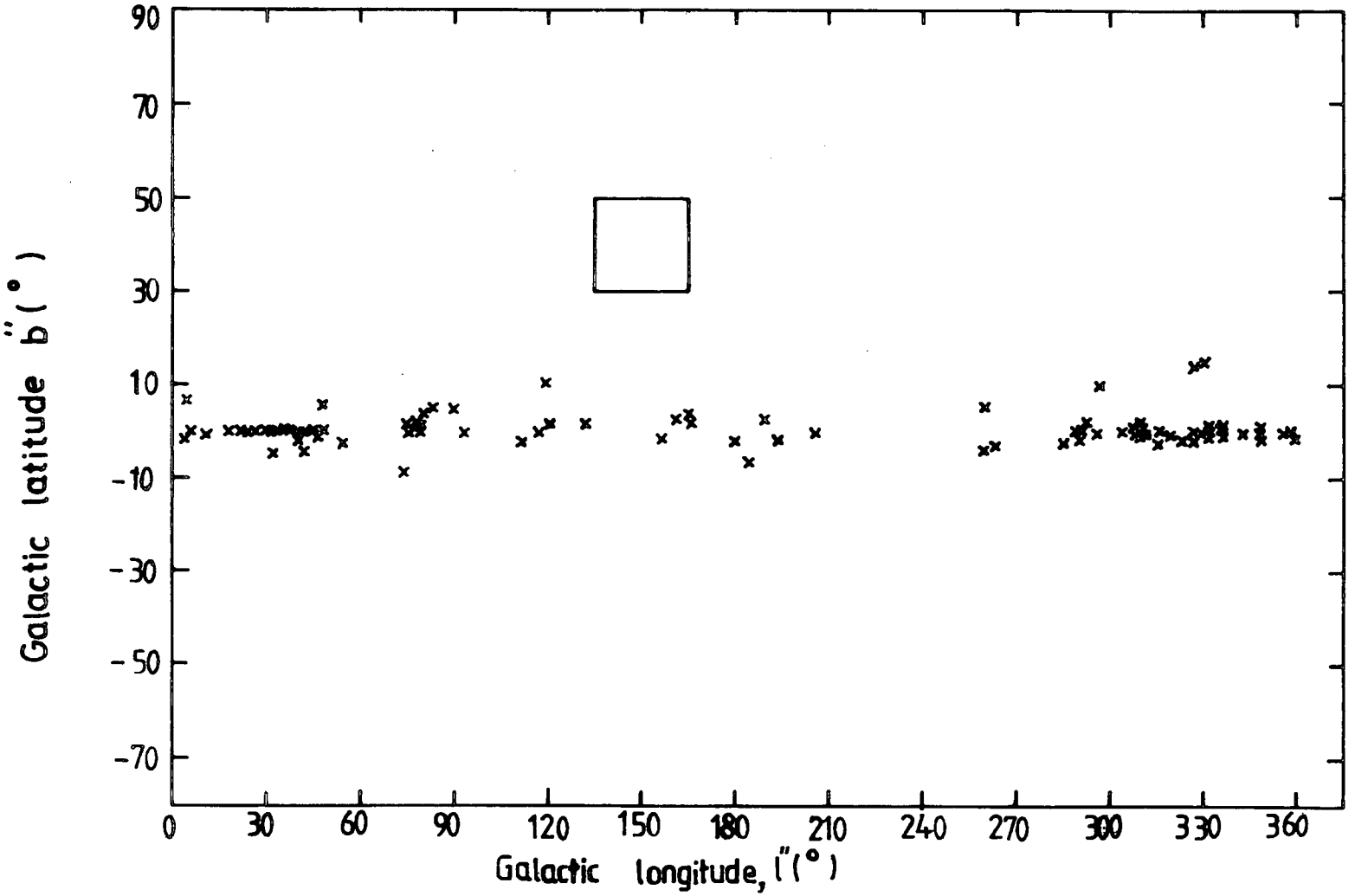

Figure 6.28 : Known supernova remnants in galactic coordinates,
(From "Astrophysical Formulae", Lang (1974).

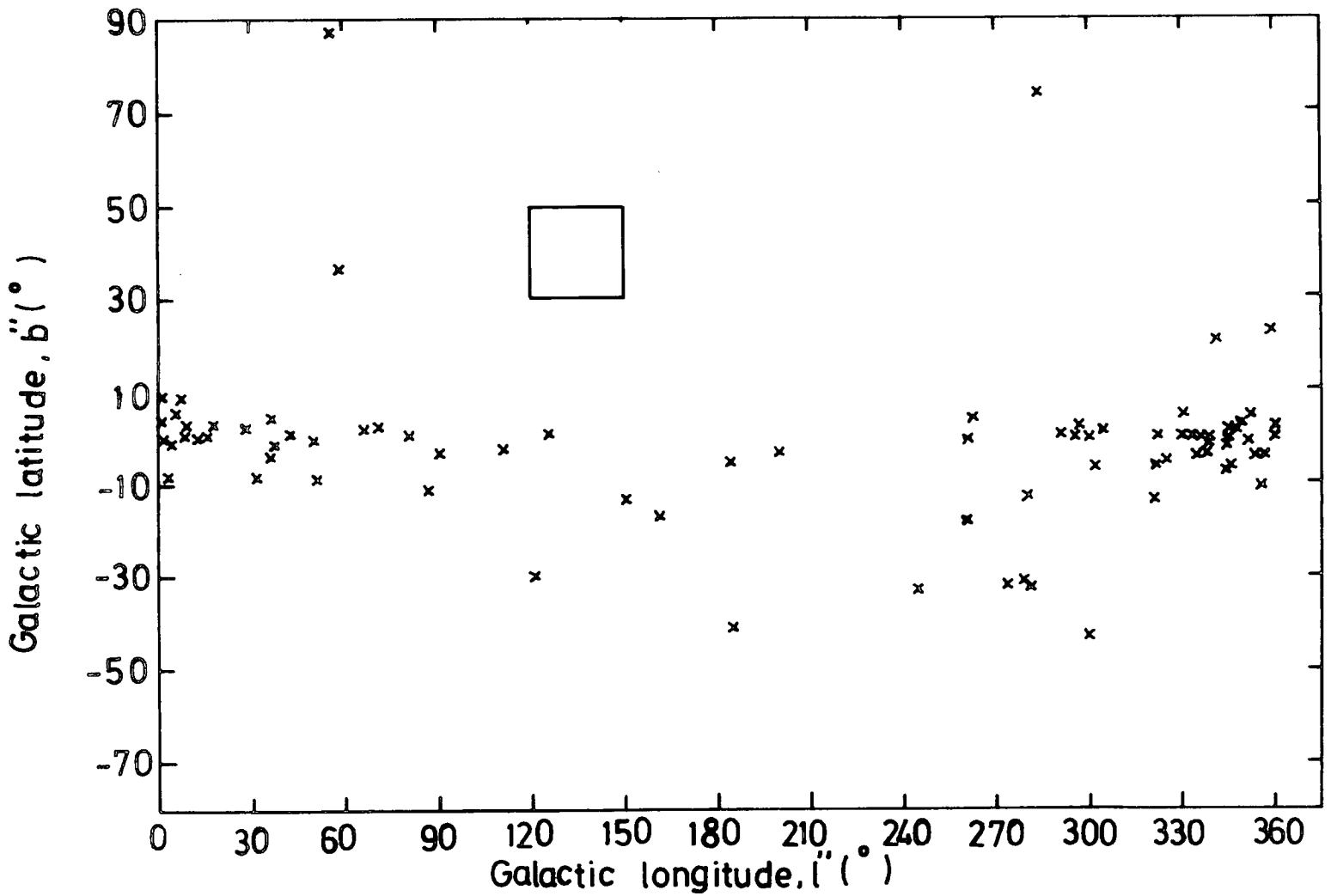

Figure 6.29 : 79 X-ray sources in galactic coordinates, (From the Fourth URURU Catalogue of X-Ray sources, Forman (1978)).

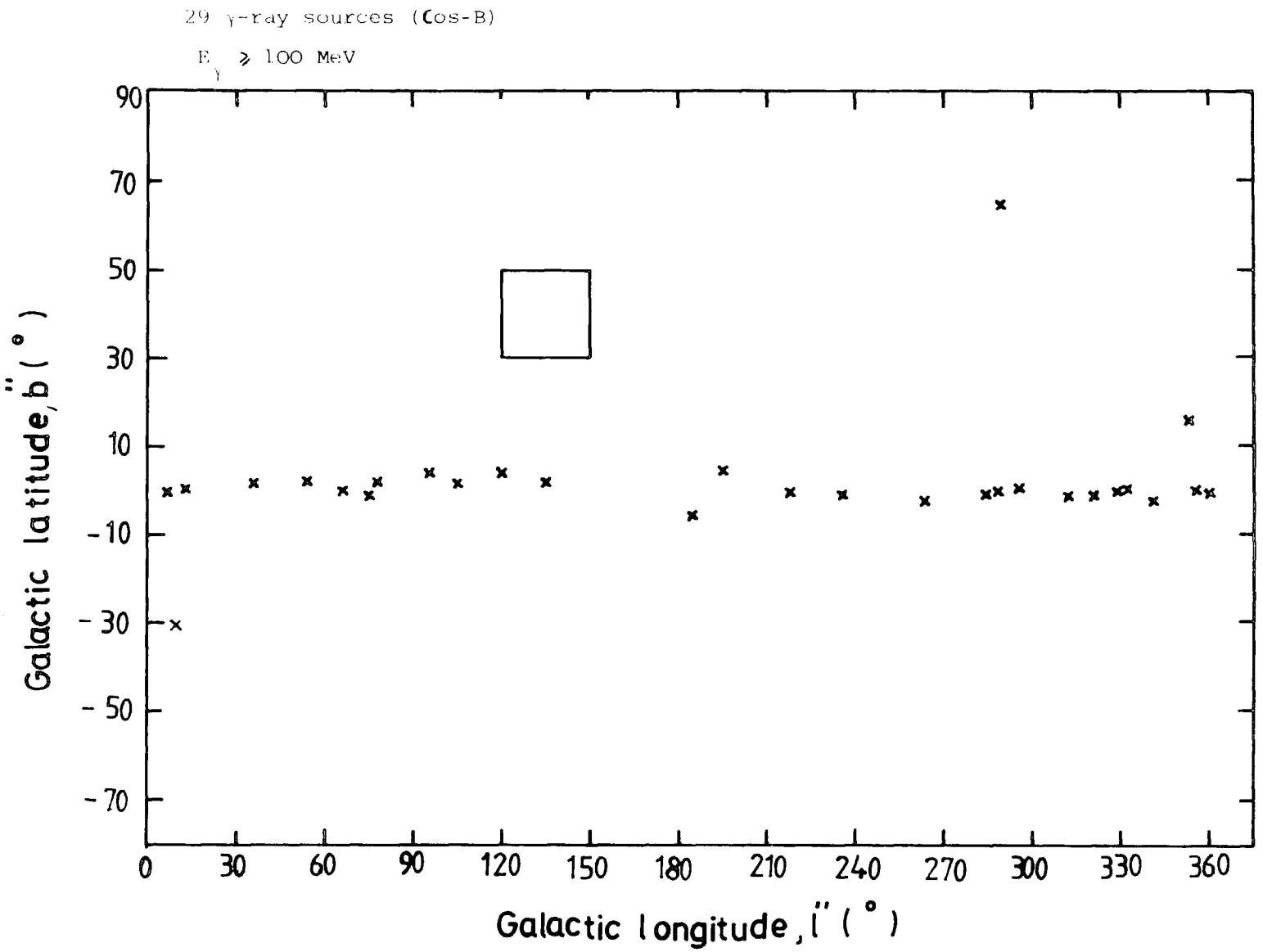

Figure 6.30 : Known γ ray sources in galactic coordinates, (Europhysics Study Conference, (1979), Gamma ray Astronomy after Cos-B).

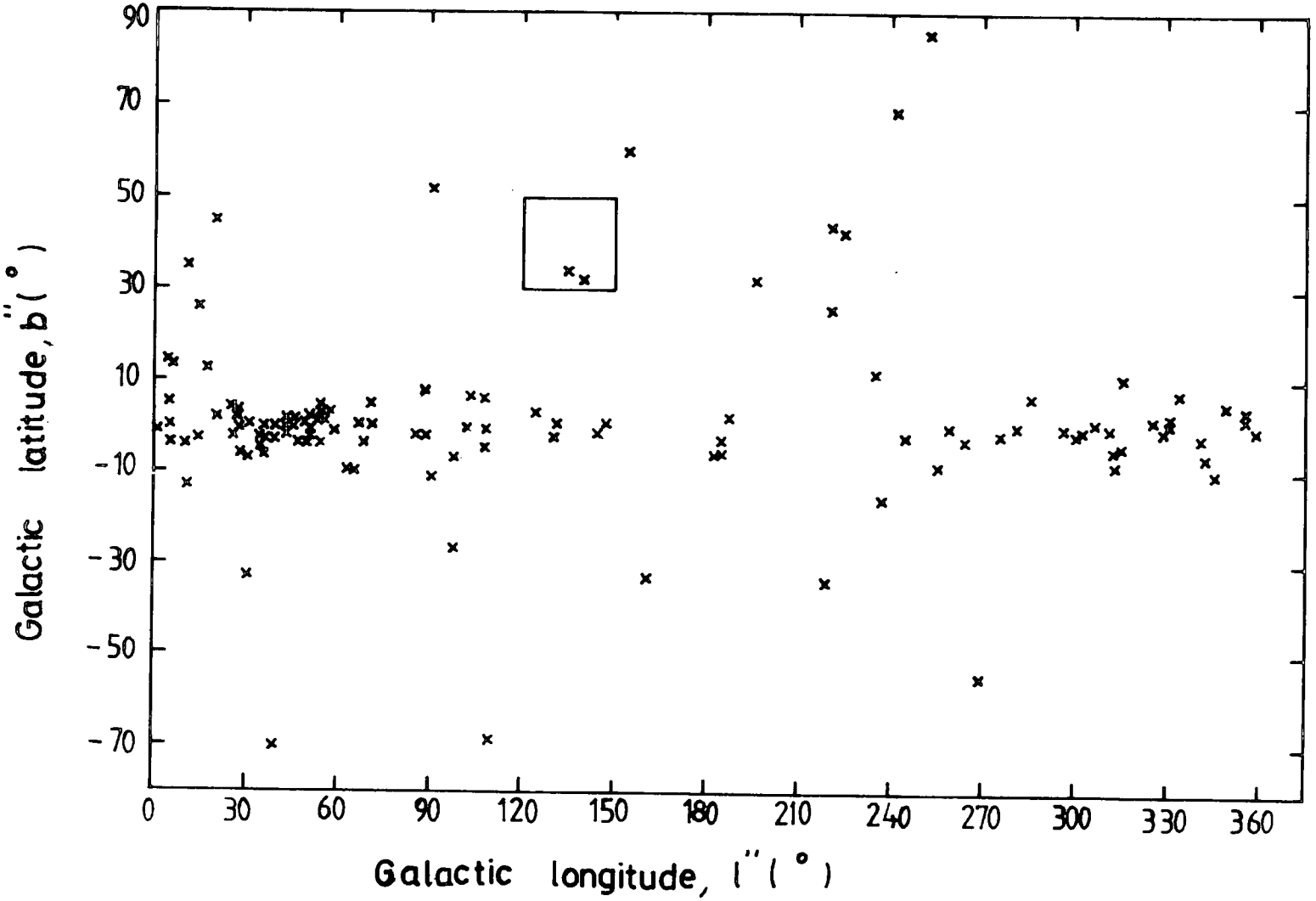

Figure 6.31 : Known pulsars in galactic coordinates (from "Pulsars", Manchester et al, (1977))

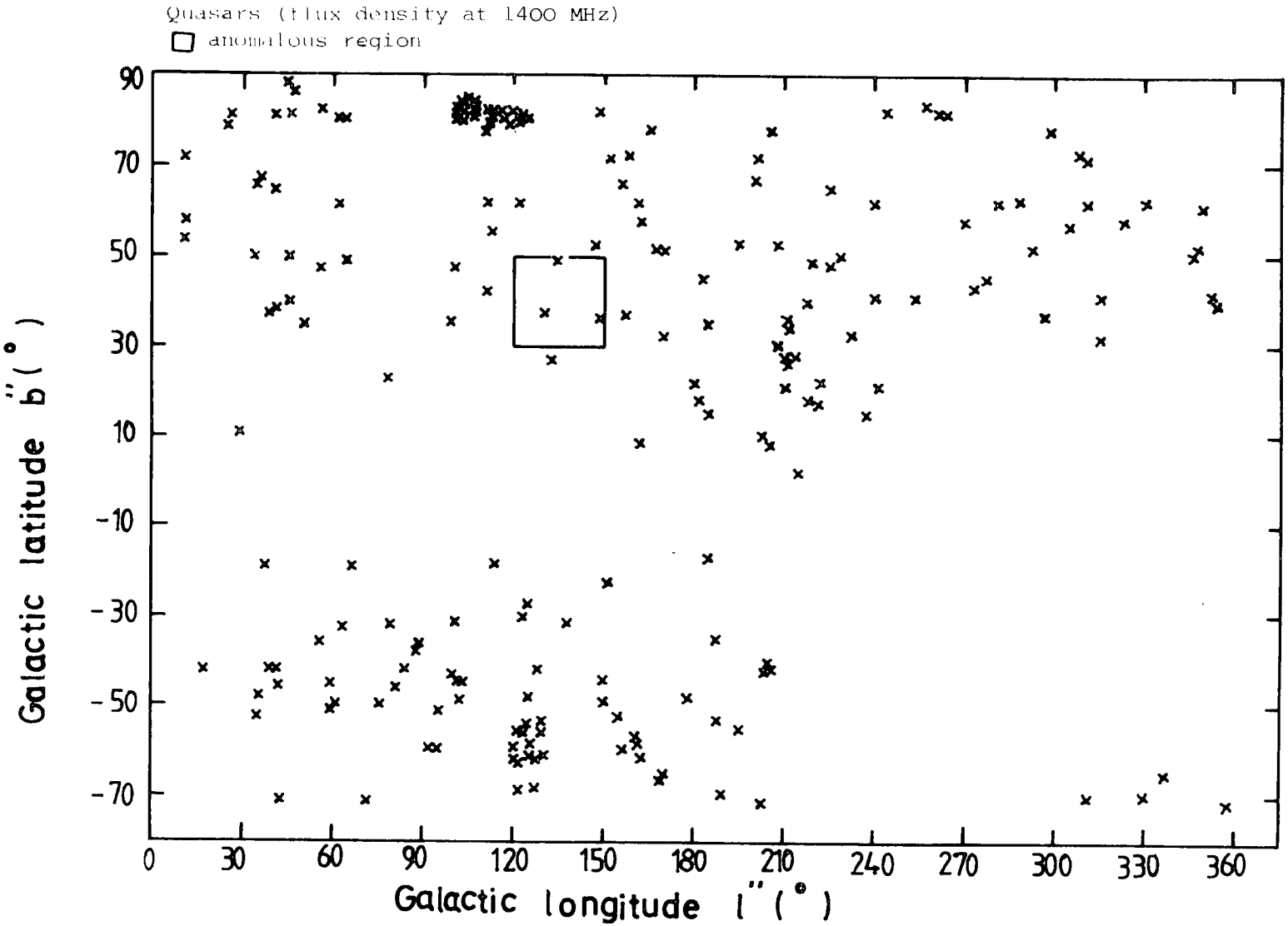

Figure 6.32 : Known quasars in galactic coordinates, (from "Astrophysical Formulae", Lang (1974)).

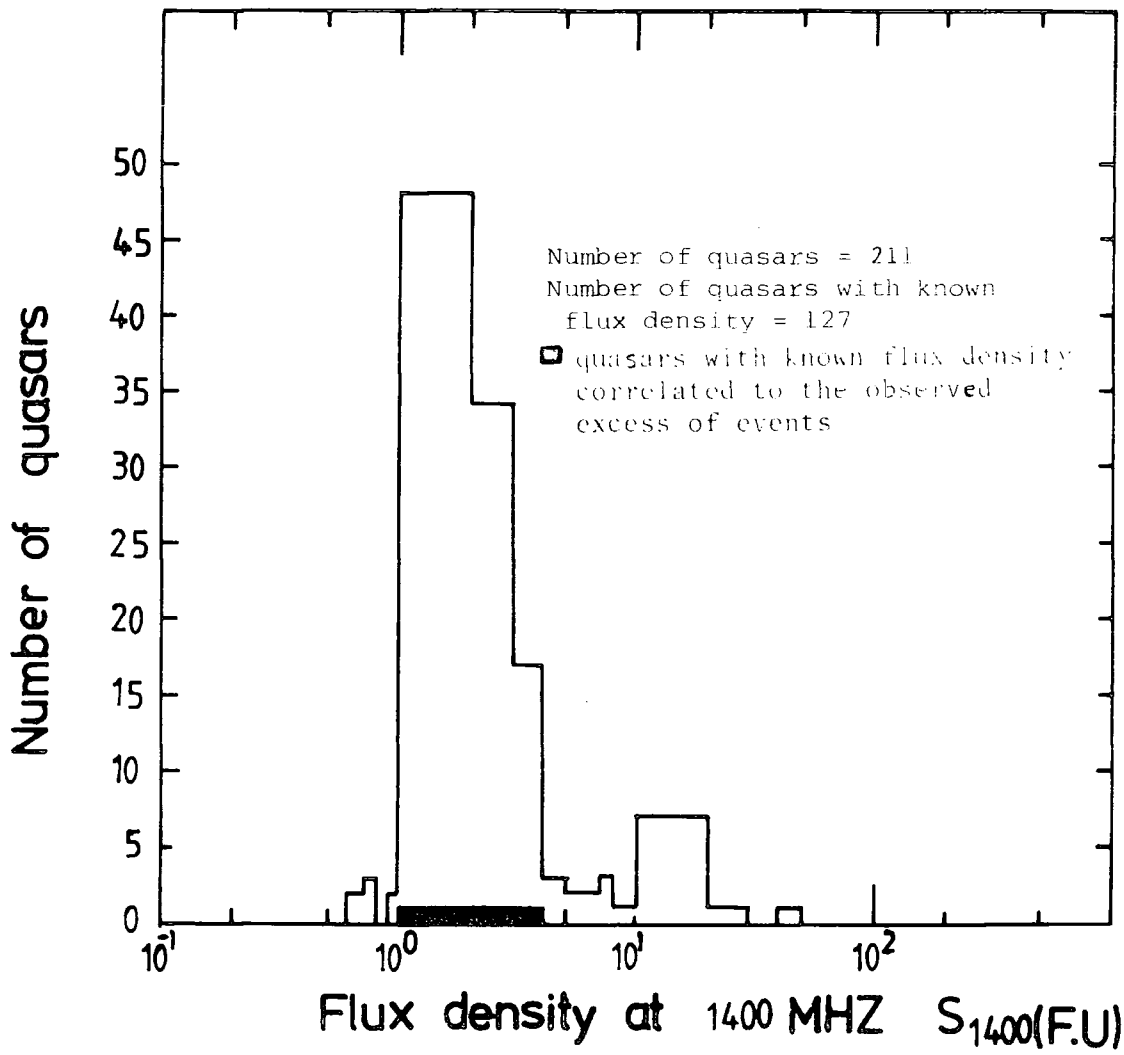

Figure 6.33 : Flux density distribution of known quasars (from "Astrophysical Formulae", Lang (1974)).

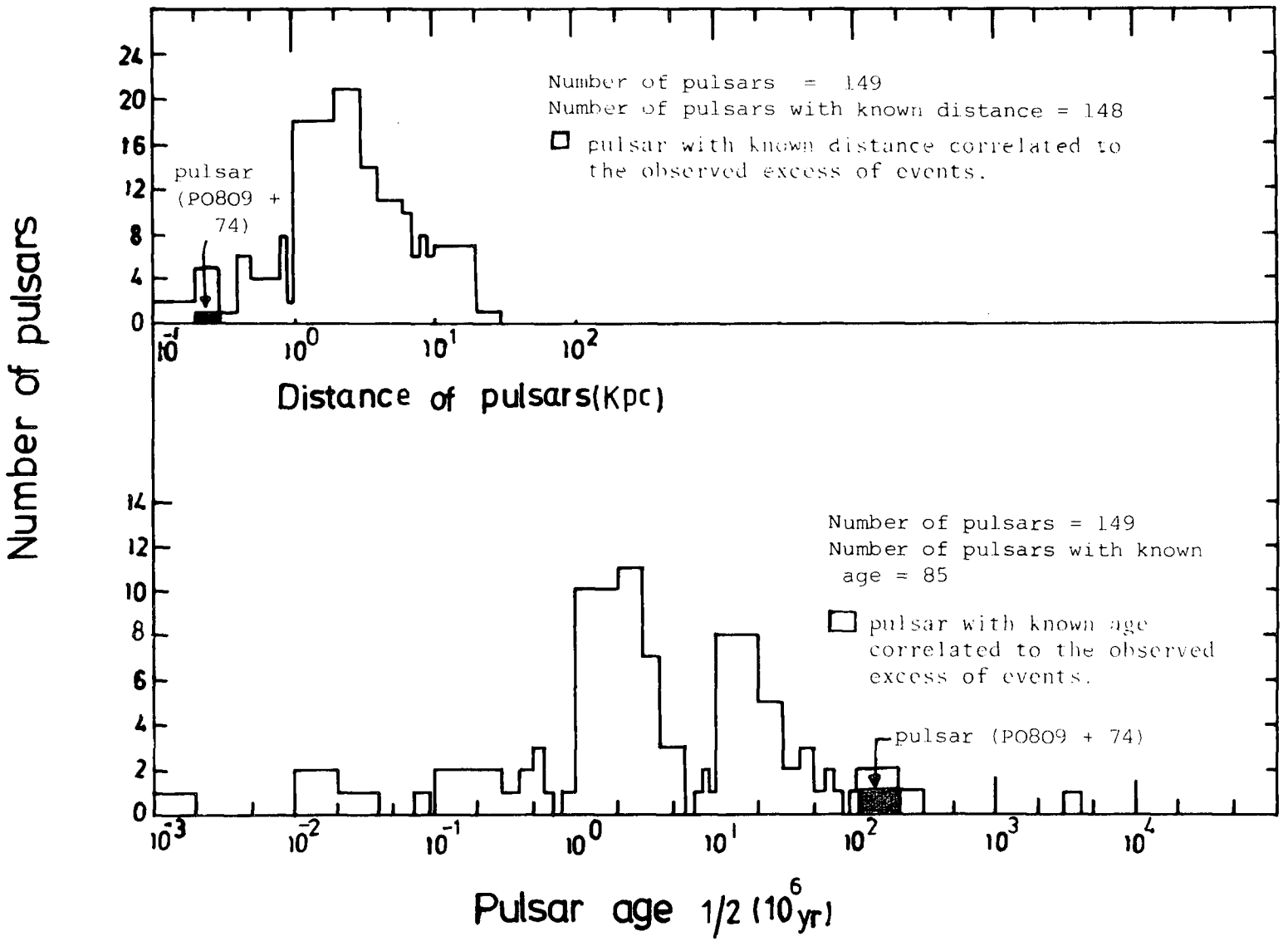

Figure 6.34 : Age and Distance Distributions of Known Pulsars (from "Astrophysical Formulae", Lang (1974)).

Appendix to Chapter 6

Shower rates in solar time and testing whether the observed number distribution in solar time is isotropic

1. Outer ring trigger (total number of showers = 967) - see figure 6.9

Solar time interval	No.of hrs sensitive	Observed no. of showers	Expected no. of showers for isotropy	Trigger rate (hr^{-1})
0 - 2 hr	29.0 hr	136	131.2	4.7 ± 0.4
2 - 4	29.3	126	132.3	4.3 ± 0.4
4 - 6	26.2	129	118.4	4.9 ± 0.4
6 - 8	17.9	77	80.8	4.3 ± 0.5
8 - 10	3.4	19	15.4	5.6 ± 1.3
10 - 12	3.8	19	16.7	5.1 ± 1.2
12 - 14	3.8	14	17.2	3.9 ± 0.9
14 - 16	2.9	15	13.1	5.2 ± 1.3
16 - 18	13.7	60	62.1	4.4 ± 0.6
18 - 20	26.8	122	121.2	4.6 ± 0.4
20 - 22	27.7	127	125.2	4.6 ± 0.4
22 - 24	29.5	123	133.3	4.2 ± 0.4

$X^2_{\nu=11} = 4.5$ Probability of a value $\geq$ this value of X^2 arising by chance = 95.3%

2. Inner ring trigger (total number of showers = 2608) - see figure 6.10.

Solar time interval	No.of hrs. sensitive	Observed no. of showers	Expected no. of showers for isotropy	Trigger rate (hr^{-1})
0 - 2	15.9 hr	328	334.8	20.6 ± 1.1
2 - 4	8.4	161	177.3	19.6 ± 1.6
4 - 7	3.9	73	81.7	18.9 ± 2.2
7 - 11	0	0	0	0
11 - 14	3.3	72	68.9	20.4 ± 3.0
14 - 16	4.0	87	84.4	21.8 ± 2.3
16 - 18	15.9	367	336.3	23.0 ± 1.2
18 - 20	24.3	509	512.9	20.8 ± 0.9
20 - 22	26.1	540	551.6	20.5 ± 0.9
22 - 24	21.8	471	459.9	21.6 ± 1.0

$X^2 = 6.12$ probability of a value $\geq$ this value of X^2 arising
$\nu = 8$
by chance = 66.6%

3. Combined outer ring and inner ring trigger data (total number of showers = 3,575) see figure 6.8

The data contained in figure 6.8 is the sum of the data contained in figures 6.9 and 6.10. Because it is the sum of data obtained with 2 different triggers which both have a different variation of the number of hours sensitive as a function of solar time the trigger rate derived from the data in figure 6.8 is physically meaningless and is not expected to be constant in solar time. However, the expected number of showers in different solar time intervals can be calculated from the results given in section 1 and 2 and the result is shown in the table.

Solar time interval	No.of hrs sensitive	Observed no. of showers	Expected no. of showers for isotropy
0 - 2 hr	44.9 hr	464	466.0
2 - 4	37.7	287	309.6
4 - 7	41.9	247	253.3
7 - 11	11.5	63	52.0
11 - 14	8.9	93	94.1
14 - 16	6.9	102	97.5
16 - 18	29.6	427	398.4
18 - 20	51.1	631	634.1
20 - 22	53.8	667	676.8
22 - 24	51.3	594	593.2

$X^2 = 7.18$ probability of a value $\geq$ this value of X^2 arising
$\nu = 9$
by chance = 62%

Figure 6.35 shows the rate of EAS detected by the inner ring trigger and outer ring trigger for different solar time intervals. The overall conclusion is thus that the 3575 EAS detected in the present work are isotropically distributed in solar time.

Reasons for and consequences of the asymmetry in the azimuthal angle distributions shown in figures 6.5, 6.6, and 6.7

The asymmetry in azimuthal angle (measured in a clockwise direction from the local geographic N-S line - see figure 6.2) for both showers detected by the inner ring and outer ring triggers is believed to be caused by (a) the rleative geometry of the 4 scintillation counters used to select EAS and (b) by the presence of local absorbing material. At the

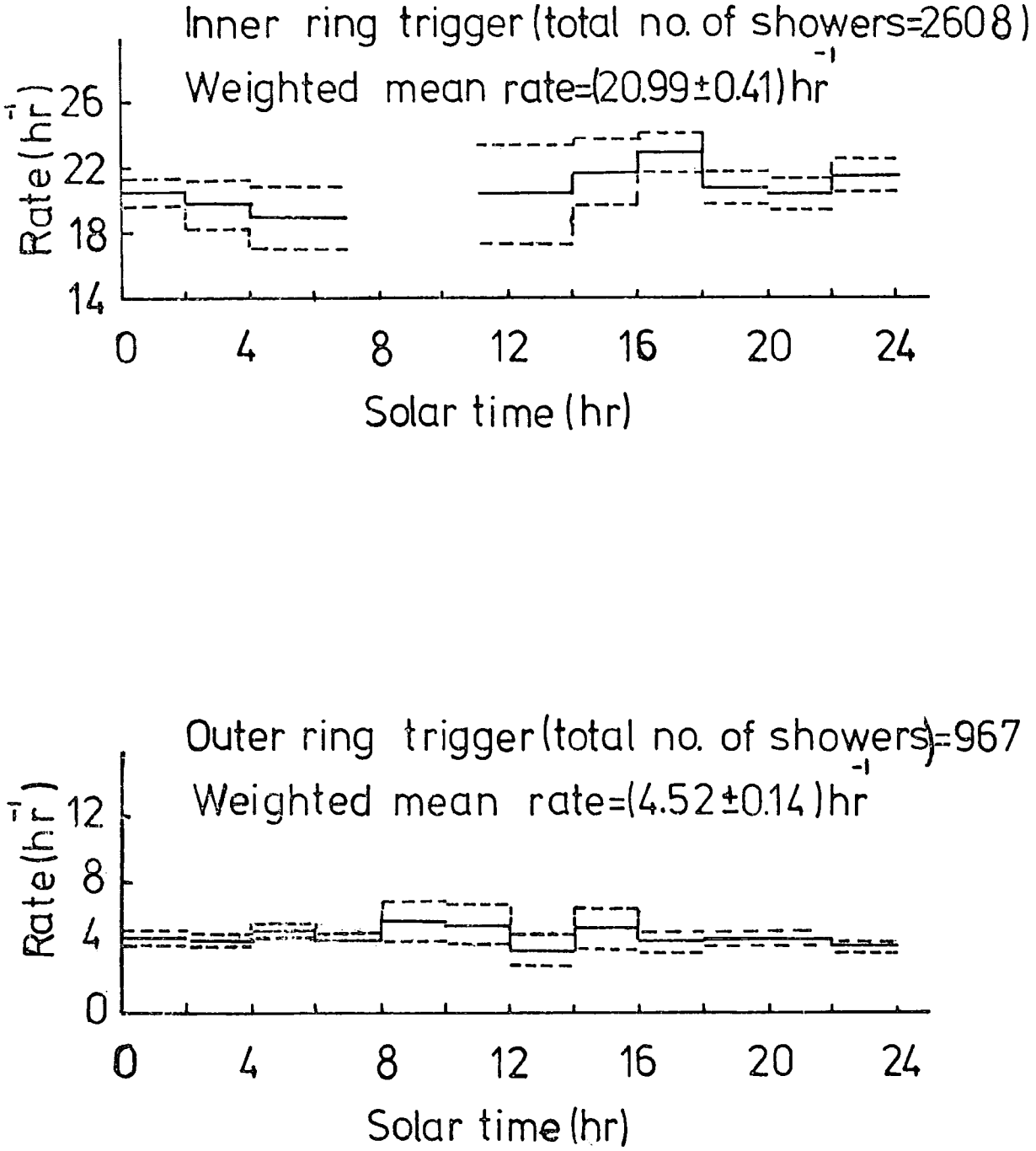

Figure 6.35 : The rate of EAS detected by the inner ring trigger and the outer ring trigger for different solar time intervals. The dashed lines represent the ± 1 standard deviation limits.

time of writing the relative contribution of (a) and (b) to the observed asymmetry is not clear. However, calculations are being made to assess the effect of (a).

The consequence of the observed asymmetry in azimuthal angle for all the showers shown in figure 6.5 is that the expected number of showers in different cells of galactic coordinates shown in figures 6.13 to 6.19 are not exactly correct as an isotropic distribution in ϕ was assumed in calculating the expected numbers. A calculation is being carried out to obtain the expected number of showers using the observed distribution in ϕ.

CHAPTER 7

SEARCH FOR TACHYONS

7.1 INTRODUCTION

For many decades now the view has prevailed that no particle could possibly travel with a velocity greater than the velocity of light in a vacuum $c = 3 \times 10^8 m\ sec^{-1}$. It is generally held that this limitation is a direct consequence of the special theory of relativity. However, several workers have investigated the possibility that the velocity of light does not represent a barrier but a limit approachable from below and above. Some theoreticians found they were able to conclude that Eistein's equation relating mass to energy, velocity and other kinematic variables in principle permit the existence of particles with velocities greater than the velocity of light (Bilaniuk, 1962, Feinberg 1967, Recami, 1974, Feldman, 1974). Such particles would speed up as they lose energy and would never be observed with $v \leq c$. Many experiments were carried out to detect such particles not only through their ionization in conventional particle detectors, but also through their production of Cherenkov radiation in vacuum. In this chapter I will present a brief discussion of the theory behind the possibility of the existence of particles that travel faster than light and also a summary of some of the experiments which have already been carried out by other workers.

The discussion presented here is a summary of some points discussed mainly by Feinberg (1967). In his paper, he described the properties that such particles would have if they exist within the context of the special theory of relativity.

The relations between energy momentum and speed that must be satisfied by any object obeying the special theory of relativity is

given by the following equations :-

$$E = \frac{m_0 c^2}{(1-v^2/c^2)^{\frac{1}{2}}} \qquad (1)$$

$$p = \frac{m_0 v}{(1-v^2/c^2)^{\frac{1}{2}}} \qquad (2)$$

where m_0 is the rest mass.

A result of the above equations is that for a particle being accelerated from below c to a value approaching c their energy and momentum will approach infinity as their velocity approaches the speed of light in a vacuum. Since this energy must be supplied by whatever is accelerating the particle, an infinite source of energy would be needed to speed up a particle to the speed of light from any lower speed. However, no such infinite energy source is available, and so it is impossible to make a particle go from less than c to $\geq c$. In addition, to accelerate a particle from a speed less than c to one greater than c, their energy and momentum would have to be imaginary which has no physical meaning. Hence the velocity of light is a limit which may not be crossed. So far we conclude that if a particle is at one time moving with $v < c$, it can not be made to move with $v \geq c$. However, this does not mean that particles that always travel faster than light could not exist because particles, already traveling faster than light, avoid the need for accelerating them through the light barriers with the attendant expenditure of infinite energy. Consider photons or neutrinos, they do travel with a velocity equal to the speed of light without ever having being accelerated from a slower speed. In fact there are no slow photons or neutrinos. When they are created in atomic or nuclear processes they take off right away with the velocity of light. Conversely, the only way to slow them down is to make them disappear. For this reason for particles which travel faster than light v^2/c^2 is greater than one

and consequently equations (1) and (2) might be rewritten as follows -

$$E = \frac{\mu_0 c^2}{(v^2/c^2 - 1)^{\frac{1}{2}}} \tag{3}$$

$$p = \frac{\mu_0 v}{(v^2/c^2 - 1)^{\frac{1}{2}}} \tag{4}$$

and as a result of the above equations, one can write the following equation -

$$c^2 p^2 - E^2 = \mu_0^2 c^4 \tag{5}$$

This would imply that although the rest mass of the particle would be an imaginary quantity, its energy and momentum would remain real. Since the particle could not cross the limiting value of c, then the rest mass being imaginary would not necessarily create a problem. From the above equations, the range of the energy and momentum are given by -

$$0 \leq E \leq \infty, \mu_0 c \leq p \leq \infty$$

These equations also imply that both the energy and momentum are monotonic decreasing function of the velocity, so that faster than light particles (or tachyons) would speed up as they lose energy. A tachyon with $v = \infty$ carries no energy, $E = 0$ and $p = \mu_0 c$ but travels with infinite speed (called transcendental state) so that tachyons of infinite speed in one frame have almost a finite velocity in another frame (the usual velocity transformation laws remain valid). Hence the velocity of a tachyon in both frames is greater than the velocity of light. This formulation of the kinematics of faster than light particles leads to a number of different arguments. These have been advanced for the existence of tachyons such as the one which is already discussed above, i.e. that the tachyons cannot be reduced in velocity to $v < c$ since an infinite amount of energy would be required to traverse the light barrier. The second and third arguments are essentially addressed to the same problem, so both

will be cited before analysing them. The second argument is : the sign of the fourth component of a space like four-vector, the energy, can be changed by an ordinary Lorentz transformation. Hence, a particle which is seen by one observer to have positive energy will have negative energy to another observer. This is validated by the principle of relativity. Therefore faster than light particles can exist in negative-energy states for all observers. From the transformation equations of energy and momentum

$$\bar{E} = \frac{(E-p_x u)}{(1-v^2/c^2)^{\frac{1}{2}}} \tag{6}$$

$$\bar{p} = \frac{(p_x - uE/c^2)}{(1-v^2/c^2)^{\frac{1}{2}}} \tag{7}$$

Since $p_c > E$, one can always choose u so that for instance $\bar{E} = -E$. The occurrence of negative-energy states for particles has always been objected to on the grounds that no other system could be stable against the emission of these negative energy particles, an entirely unphysical behaviour. The third objection is similar to the second, but considers time ordering instead of energy. For particles whose velocity is greater than c, there can be changes in the time ordering of points along its trajectory, in another frame. As already mentioned, the answer to both of these objections is the same as the change in the sign of the energy. That is, it is exactly the same circumstances that produce one effect as the other. For one observer, a process may be interpreted as emission of a positive energy tachyon at one space-time point (1), and absorption of the tachyon at a later space time point (2). For another, Lorentz-transformed, observer the second point may be earlier in time than the first, and the energy of the tachyon may be transformed to a negative value. The observer will interpret the process as the emission of a positive-energy tachyon at point $(\acute{2})$ and its absorption at the later point $(\acute{1})$, rather than require the introduction of negative-energy states.

This may be called a reinterpretation principle for tachyons. It is related to the ideas of Dirac on positrons as electrons going backwards in time. If tachyons carry charge or baryon number, the reinterpreted particles will be antitachyons. However, it must be also pointed out that Newton (1970) contradicted the possibility of tachyon existence. He concluded that it is impossible for tachyons to exist, but that if they did, then either relativity theory or the basic rules of quantum mechanics would be incorrect, or else some very fundamental assumptions of the essential controllability of events would have to be abandoned. This argument is based on a "closed causal cycle". That is, if a signal can travel faster than the speed of light it might in one frame appear as though the effect preceded the cause. In other words, if two events are causally connected, the definition for the earlier event as the cause and the later event as the effect.

7.2 THE ENERGY OF A TACHYON

The behaviour of the energy and momentum of particles obeying the special theory of relativity as velocities are increased can be seen in figure 7.1. The figure clearly illustrates the following points:-

1) Since the E-β and p-β relationships are asympototic in the region $\beta = 1$, a particle travelling slower than light can never travel faster than light, and a particle travelling faster than light can never travel slower than light.

2) Also illustrated in figure 7.1 is that for ordinary particles (tardyons) as their speed increases, their energy also increases. However for tachyons, in contrast both the energy and momentum are monotonic decreasing functions of the velocity, an increase in speed resulting in a decrease in energy. Hence a tachyon that was losing energy by interacting with matter or by radiating light would speed up, whereas a tachyon

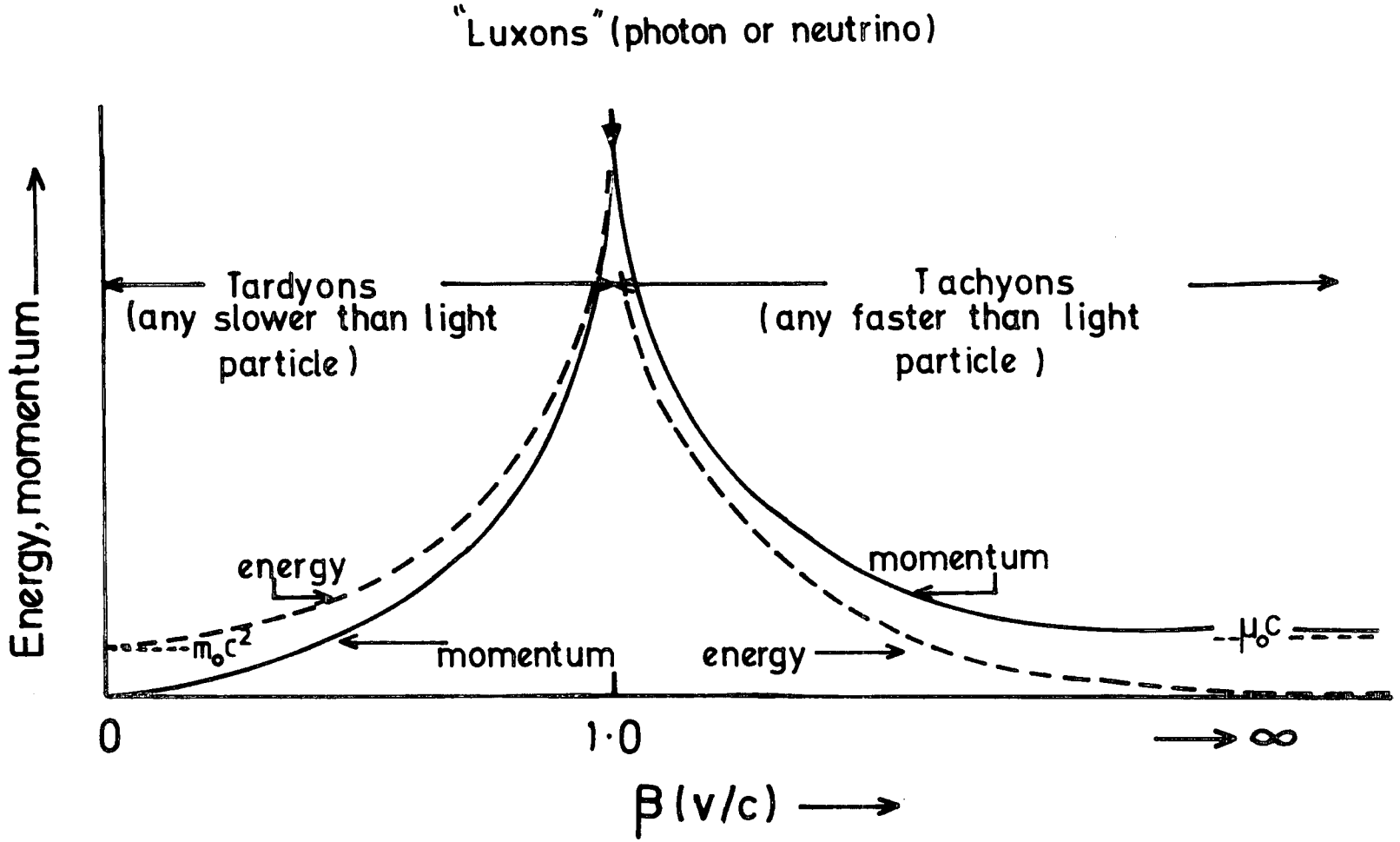

Figure 7.1 : Energy-momentum dependence as a function of velocity β(v,c) for three classes of particles, where v is the velocity of the particle and c is the velocity of light.

that was gaining energy from some outside source would slow down and its speed would approach c from above rather than below. The speed of light c acts as a limiting speed for tachyons also, but the limit is a lower limit rather than the upper limit that it is for ordinary objects.

In the limiting case of a tachyon moving at infinite speed its total energy would be zero, although its momentum would remain finite. For an ordinary particle with non zero mass the total energy can never vanish. Also shown in the figure is that the energy of tachyons is always less than its momentum multiplied by c. This ambivalence does not apply to ordinary particles.

7.3 TACHYONS AND EXPERIMENTAL PHYSICS

The possible existence of a class of particles with a space like four-momentum, which presumably travel faster than light in a vacuum, has led to considerable discussion about superluminal entities. Since there seems to be no argument strictly forbidding tachyons, these particles are allowed by relativistic quantum mechanics. Theoretical controversies regarding their existence rests on experimental questions. Many elementary particles were discovered in the cosmic radiation before their existence was suspected or proved to be a theoretical necessity. Although it is not quite certain which properties of this particle are most amenable to the experimentalist, several searches were made, soon after their postulation using laboratory particle sources and high energy cosmic rays.

The experimentalists searching for free tachyons are faced with the following two related problems.

A) How do tachyons interact with normal matter?

B) What sort of detector is needed to search for tachyons?

One possible approach that could detect tachyons in a way similar to ordinary particles has been suggested. The technique involves the detection of Cherenkov radiation emitted by the tachyons in a vacuum. A search for charged tachyons was carried out by Alvager and Kreisler (1968). The experiment was based on the assumption that a free charged tachyon (if it exists) exhibits normal electromagnetic interaction with bradyonic matter. The experiment was an attempt to detect this process. The first problem in such an experiment is to design it in such a way as to allow the Cherenkov light to be detected but for no other process to cause background radiation. This requirement was met in their experiment by allowing a particle beam which was assumed to contain charged tachyons to traverse lead shielding. The tachyon then passed into the detector, which consisted of two parallel plates between which an electrostic field was maintained, and a photomultiplier was located to view the area between the plates. The plates were in a vacuum of $\sim 10^{-6}$torr. The tachyons were hoped to be produced in pairs from a γ-ray source of 5-mCi of caesium -C_s^{134}. It was expected that the tachyons would produce a peak in the pulse height spectrum obtained from the photomultiplier. However, no such peak was obtained. From this and similar experiments using different γ-ray sources they were able to quote a figure of $<2.10^{-3}cm^2$ as an upper limit for the photoproduction cross section of tachyons. Another possibility is to look for tachyons produced in the high energy reactions of bradyons using the missing mass plot of bubble chamber interaction techniques. The negative results of searching for charged tachyons did not rule out the possible existence of neutral tachyons. Several searches have been carried out and these searches have made use of the defining property of tachyons : their space like four momenta. To recognize the possible production of a tachyon without the need for the detection of the tachyon after production Baltay et al,

(1970) performed such an experiment using a bubble-chamber. They investigated the reactions.

$$\bar{K} + p \rightarrow \Lambda^0 + t^0$$

$$\rightarrow \Lambda^0 + t^0 + \bar{t^0}$$

$$\bar{p} + p \rightarrow \pi^+ + \pi^- + t^0$$

$$\rightarrow \pi^+ + \pi^- + t^0 + \bar{t^0}$$

These reactions have been selected in order to get only a small contamination of events due to m^2 (missing mass squared) in the tachyon region. Both the $\bar{K}$ and the $\bar{p}$ were captured at rest in hydrogen. The incoming energy and momentum (zero) were known, the energy and momentum of the resultant ordinary particles ($\Lambda^0, \pi^{\pm}$ pairs) were measured. The energy E and momentum p of the remaining neutrals could be calculated, using energy and momentum conservation. If these neutrals were made up of "ordinary particles" i.e. velocity less than the speed of light, then $E^2 - p^2 > o$; the presence of a tachyon or tachyon pair would have been indicated by $E^2 - p^2 < o$ (a negative missing mass squared, where $m^2 = E^2 - p^2$). These measurements of missing mass would show up as a spike in the plot, but this was unlikely. From theoretical considerations (Feinberg 1972) pair production of tachyons seem more likely (i.e. reactions (ii) and (iv)). The negative missing mass squared method of searching for pairs of tachyons then only covers a small section of the spectrum available for this parameter when two neutral tachyons are produced. The advantage of a search such as this is that no assumption regarding the behaviour and/or properties of the tachyons need to be made. The main experimental problem is a background of events in which the missing neutral is one or more π^o's. They were able to conclude that they had seen no evidence for tachyon production. They interpreted their experiment by giving an upper limit for the production

of either one or two tachyons. The upper limit was of order 10^{-3} of typical strong-interaction processes.

Another type of experiment to detect tachyons was performed by Murthy using cosmic ray extensive air showers (Murthy, 1971). The principle of the experiment is that in the development of an extensive air shower, the "shower front" travels through the atmosphere nearly at the speed of light. Tachyons, on the other hand, would precede this shower front since they travel faster than light. Murthy estimated $\frac{v_t}{c} \sim 1.4$ and for a height of production of 2 Km. gives a 2 μs interval between the arrival of the tachyon and the extensive air shower. Basically his experiment consisted in searching for tachyon signals in one of two detectors followed within 20 μs by the arrival of an extensive air shower. The signals were generated from (i) a photomultiplier viewing at liquid scintillator of dimensions of 75 x 75 x 22 cm^3 and (ii) a second detector based on the principle as used by Alvager and Kreisler (1968). This was an air gap between two flat electrodes with a suitable magnitude of electric field applied between them. This was viewed with two pairs of photomultipliers to detect any Cherenkov light of a tachyon that might be produced in it. To detect the extensive air shower, he used 4 x 0.26 m^2 chronatron scintillators arranged in a square array of side 10 m and placed symmetrically about the tachyon detector. A coincidence of $>1m^{-2}$ in each scintillator provided the trigger. Each coincidence triggered an oscilloscope on which the times of occurrence of the potential tachyon signal and the extensive air shower were recorded. However, the results were negative in that (i) the observed number was not more than the expected number of events due to chance and (ii) the frequency distribution of the separation times showed that they were randomly distributed in the region 0-20 μs. He concluded that the frequency of occurrence of tachyons (T^0, T^+, T^-)

in E.A.S. was less than 3.10^{-4} to 10^{-5} relative to that of electrons.

Another experiment was carried out by Ashton et al (1970). This experiment was to determine the velocity of a tachyon by measuring its time of flight over a certain distance and look for values exceeding the speed of light. They used two large ($1m^2$) scintillation counters separated by 5.3 m and viewed by single photomultiplier tubes. These authors found no evidence for the presence of particles travelling with velocities >1.6 c in cosmic rays at sea level. Ashton et al were able to place an upper limit of less than $2.2 \times 10^{-5} cm^{-2} s^{-1} sr^{-1}$ at 90% confidence level on the flux of tachyons in the incoherent sea level cosmic radiation. The above discussion is based on experiments prior to the publication of Clay and Crouch and subsequent experiments.

Clay and Crouch (1974)

These authors set up an experiment similar in many ways to that of Murthy. They detected showers with the fast timing part of an air shower array and used plastic scintillators ($1\ m^2 \times 5$ cm) positioned at the corners and centre of an array of area 900 m^2. Extensive air showers were detected by a coincidence between the centre detector and any of three of the outer detectors. This gave a trigger rate of showers of $7.2\ hr^{-1}$ corresponding to shower of energy $> 2 \times 10^{15}$eV. The output from an additional photomultiplier viewed one of the four outer scintillators and was recorded on a transient recorder. Their method of analysis was to record the time of arrival of pulses in the 100 μs time interval preceding the arrival of the air shower front. Comparing the measured arrival time distribution for 1,307 air showers with a randomly generated set of arrival times gave a X^2 probability of 10^{-4} that the test data and E.A.S. data were from the same distribution. They concluded from this result they had observed non-random events preceding the arrival of extensive air

showers and that this was the result of particles travelling with an apparent velocity greater than that of light. Since the publication of Clay and Crouch's article several similar experiments have been performed. Perhaps the most interesting is one performed by P.J. Robinson, J.D. Kuhlmann and D.F. Liebing at Adelaide - reported in a paper by J.R. Prescott (1975). They essentially repeated Clay and Crouch's original experiments, with the original apparatus. They found that the time distribution of events was consistent with a uniform distribution. Prescott also discussed what might have been the reason for the non random distribution initially found by Clay and Crouch. Apparently the main contribution to the X^2-test comes from low counting rates in the first channel (earliest in time) of the interval scanned. If events in this channel were systematically low, then the overall results might no longer be significant. Fegan et al (1974, 1975) have also carried out a search for tachyons. Following Clay and Crouch they used 2.5 m^2 x 5 cm plastic scintillators positioned at the vertices of an equilateral triangle of side 20 m. The criterion for triggering was a three-fold coincidence, at a signal level slightly higher than the single particle level in each scintillator. To search for a potential tachyon signal a fourth scintillator viewed by a pair of photomultiplier tubes, was located at the array centre. The outputs from both photomultiplier tubes were fed into discriminators and standard logic pulses generated. Coincidences between the two outputs were also generated. A 200 bit shift register was used to delay the pulses up to 800 μ sec. A master pulse inhibited the register 380 μ s after an air shower arrival was obtained. The discrimination settings were set well below the single muon level. Two sets of data were obtained and histograms representing the data for just one pulse, and coincidence pulses were plotted. A statistical analysis based on a X^2 test for either data set were performed and showed no significant deviation from random expectation.

Yet another group inspired to search for tachyons in extensive air

showers were workers at the University of Tasmania (Emery et al, 1975). This search used the same technique as used by Clay and Crouch but using Geiger counters and liquid scintillators. The frequency distribution of the precursive times in the 108 μs preceding the arrival of the E.A.S. shower fronts showed no detectable non-random pulses.

The most recent experiment to search for tachyons associated with E.A.S. at energies $E > 3 \times 10^{16}$ eV has been made by D.J. Fegan (1981). The tachyon detector was an 0.5 m^2 area plastic scintillator of thickness 0.025 m and the top surface of the plastic scintillator was viewed by two photomultiplier tubes of 12.5 cm diameter. The detector was located at the centre of an equilateral triangle with sides of length 20 m and three circular plastic scintallators were located at the vertices. Fegan in his experiment used two different approaches. Firstly, the tachyon detector was shielded by 25 cm concrete and an additional 15 cm of lead. Secondly, the trigger threshold energy was larger than previously used so as to reduce the dilution effect of a large number of background pulses. The minimum shower energy required to trigger the system was 10^{16}eV, while the most probable shower energy was 3×10^{16}eV which corresponds to a shower detection rate of 0.17 $hr.^{-1}$ In his analysis, the record of the detector output amplitude for the 480 μs prior to the arrival of the shower front were recorded. The resulting histogram showed an excess of events in the 48 to 60 μs region prior to the arrival of the air shower front. Fegan claimed the excess is not due to tachyons but is caused by the disintegration of cosmic-ray nuclei in the field of solar photons leading to the production of correlated showers in the atmosphere, the arrival time of one of the showers at the earth being later in time than the other.

7.4 PRINCIPLE OF THE PRESENT EXPERIMENT

The principle of the experiment which is now described is to search for tachyons associated with cosmic ray showers of primary energies in the region of 10^6 Gev. Tachyons, if they exist, could be produced high in atmosphere (20 Km to 30 Km above sea level) by the interaction of primary cosmic ray nucleons via $p + p \rightarrow p + p + \pi^+ + \pi^- + t + \bar{t}$, which finally leads to the generation of an extensive air shower. The other assumption held is that at least some of any produced tachyons with $v > c$ (i.e. $\beta > 1$ where $\beta = v/c$) should survive for long enough to reach sea level. Such tachyons would arrive some time before the air shower. The magnitude of that earlyness depends on the height of the point of the production, the tachyon velocity, the energy loss of tachyons in air and their proper mass. For a vertical shower a tachyon will be detected at a time (60-80 μs), and for inclined showers of zenith angle 60^o(1% of all showers at sea level have zenith angles $>60^o$) 120 μs prior to the arrival of the shower front. In the present work a study of particles traversing a 2 m^2 scintillation counter in the time domain 0-264 μs before the arrival of air shower front of size $>2.5.10^5$ particles at sea level has been made.

7.5 EXPERIMENTAL ARRANGEMENT

The present search was made assuming that if a tachyon reaches sea level then it will interact in some way that provides an output from a scintillator-photomultiplier combination which is sufficiently large to be distinguishable above photomultiplier noise - at least in a statistical sense. Detector 31 of the Durham E.A.S. array (see figure 2.1 of Abdullah et al 1979) is an unshielded plastic scintillator of area 2 m^2 was used as a tachyon detector. The electrical signals from each photomultiplier of tachyon detectors are summed and amplified in a mixer-amplifier at the detector (figure 2.6) before being sent down to the laboratory. The signals are recorded and interpreted in terms of shower front parameters

at the signal processing units which is shown in figure 7.2. To select extensive air showers a four-fold coincide of the form $\Delta_c (\geq 20.2\ m^{-2})$, $\Delta_{13} (\geq 4.2\ m^{-2})$, $\Delta_{33} (\geq 4.6\ m^{-2})$, $\Delta_{53} (\geq 4.6\ m^{-2})$ was used.

Air showers were recorded at a rate of 4.3 hr^{-1} (corresponding to a minimum shower size of 2.5 x 10^5 particles), if the density of particles in each detector exceeded the numbers in brackets. The calculated distribution of shower size and core distance, relative to detector 31, for the air shower trigger is found to be similar to the result given in figure 3 of Ashton et al (1977). Figure 7.3 shows the electronic system used to display pre-shower pulses of delay time ~ 20 μs, occurring in the tachyon detector. Because of the large attenuation of pulses in the delay line, it is split into three sections of Hackthall HH 1600 delay cable giving an overall delay of 264 μs. Figure 7.4 shows the attenuation of a 2 μs square pulse after transmission down 80 μs of delay-line which has a delay of approximately 1 μs per foot. The overall gain of the display system between input and output was arranged to be unity by using amplifiers between delay line sections. Figure 7.5 shows the amplifier units used. The output from the delay lines is fed into a Textronisc oscilloscope. This, together with a digital clock, is photographed using a standard type of camera. A typical trace as observed on the oscilloscope is shown in figure 7.6a. The E.A.S. front pulse is preceded by a hump pulse of width 80 μs and a region of high frequency oscillation which extends for a region of 20 μs prior to the arrival of the E.A.S. front pulse and both are instrumental in nature. More of these traces are shown in figures 7.6b, c and d. During the course of the present measurements the whole E.A.S. array was not operational but figure 7.7 shows the integral density distribution of particles measured in detector 31 in a separate experiment which used the same E.A.S. coincidence requirement. It is seen that the median particle density is 26 m^{-2}

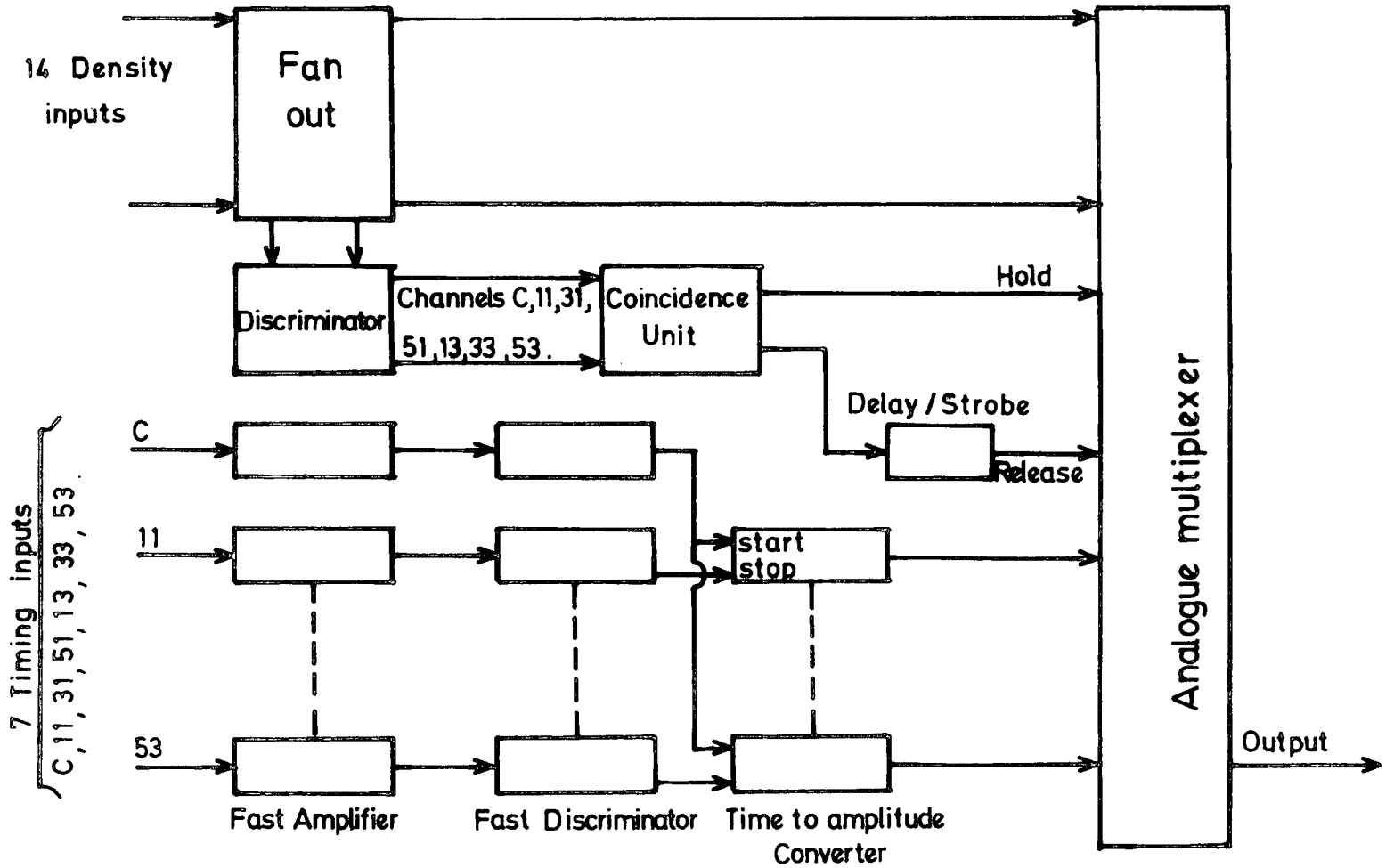

Figure 7.2 : Block diagram of signal processing units.

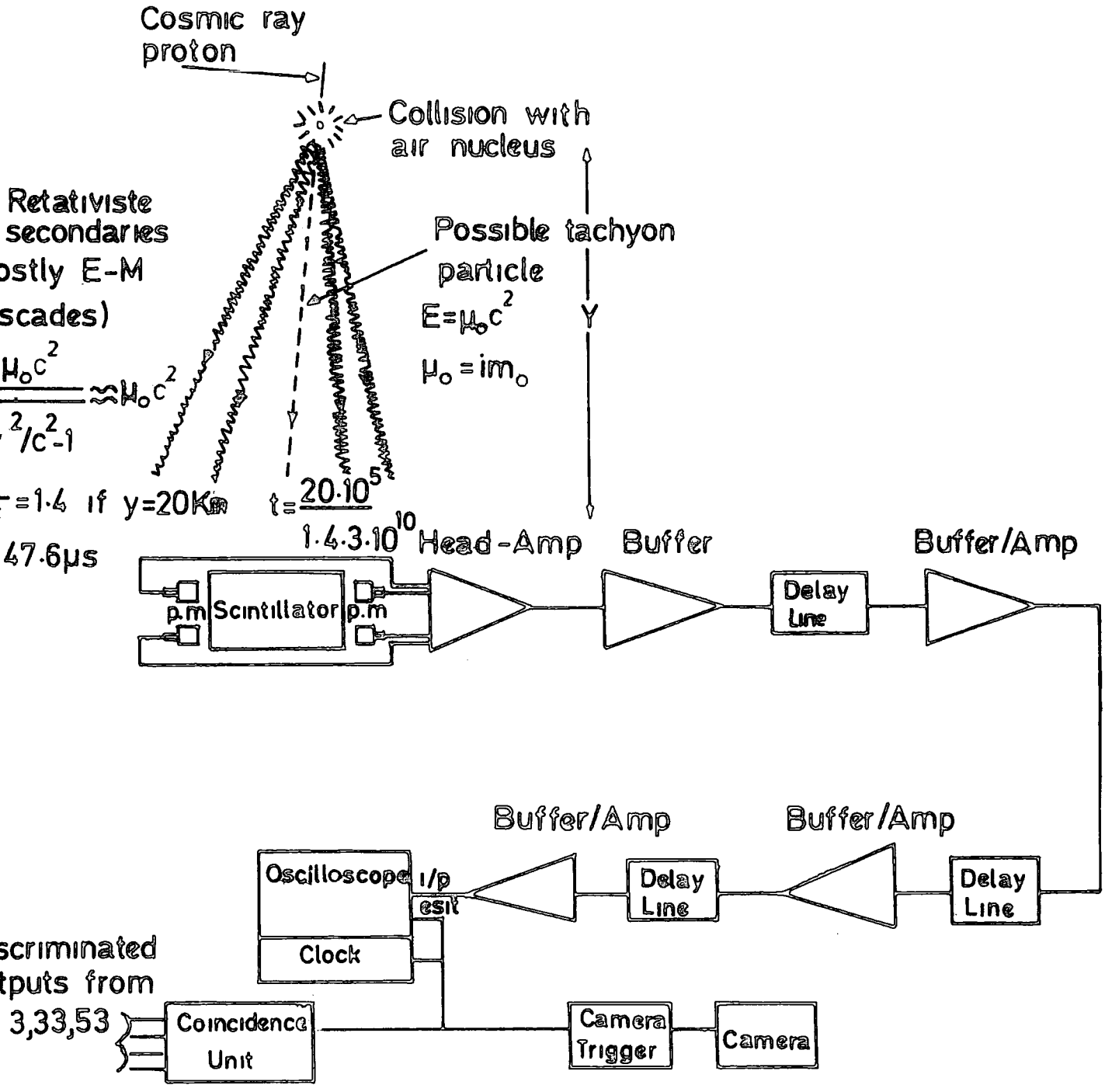

Figure 7.3 : Block diagram of electronics used in the tachyon experiment

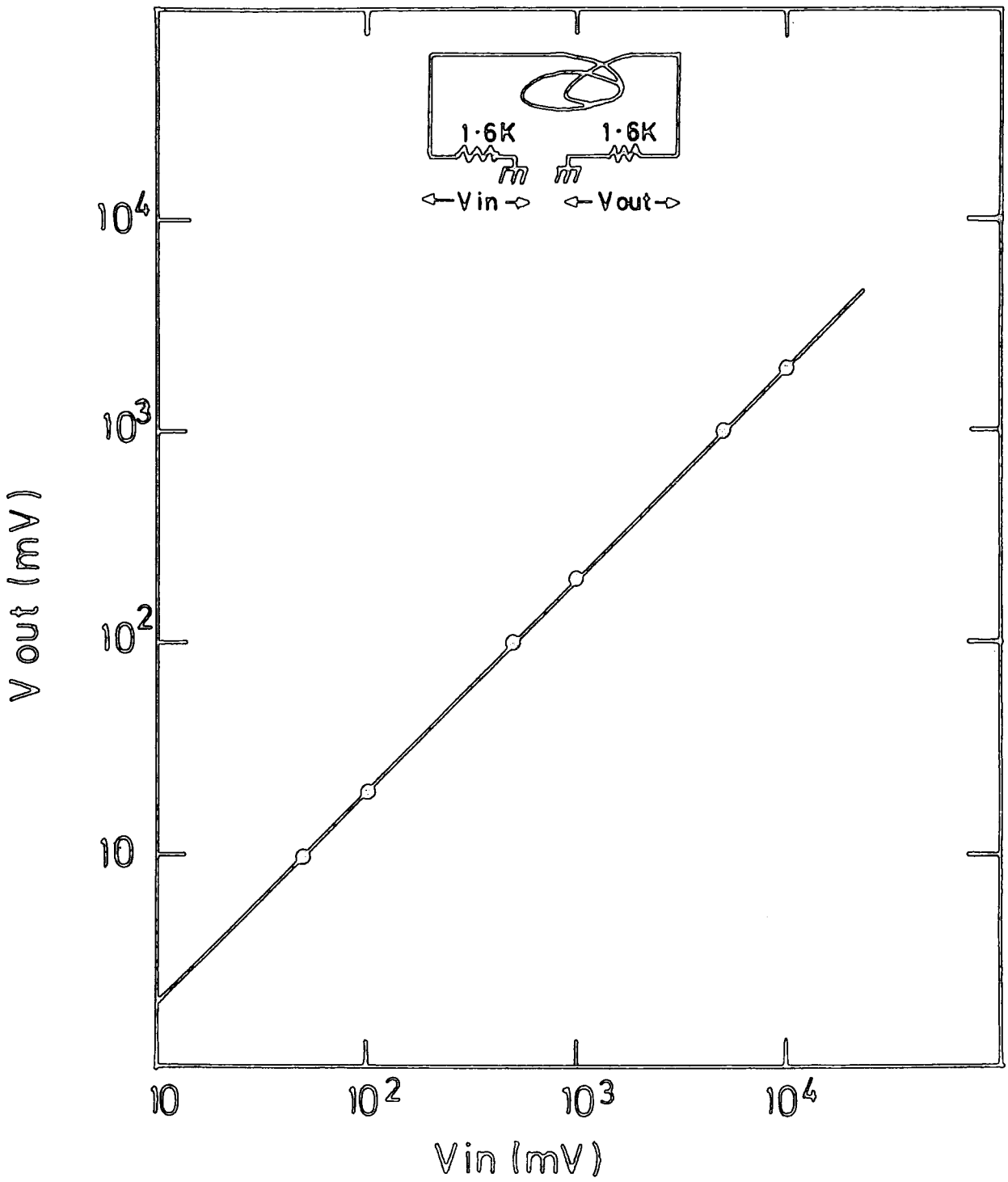

Figure 7.4 : The attenuation of a 2 μs square pulse after transmission down 80 μs of Hackethall HH 1600 delay line.

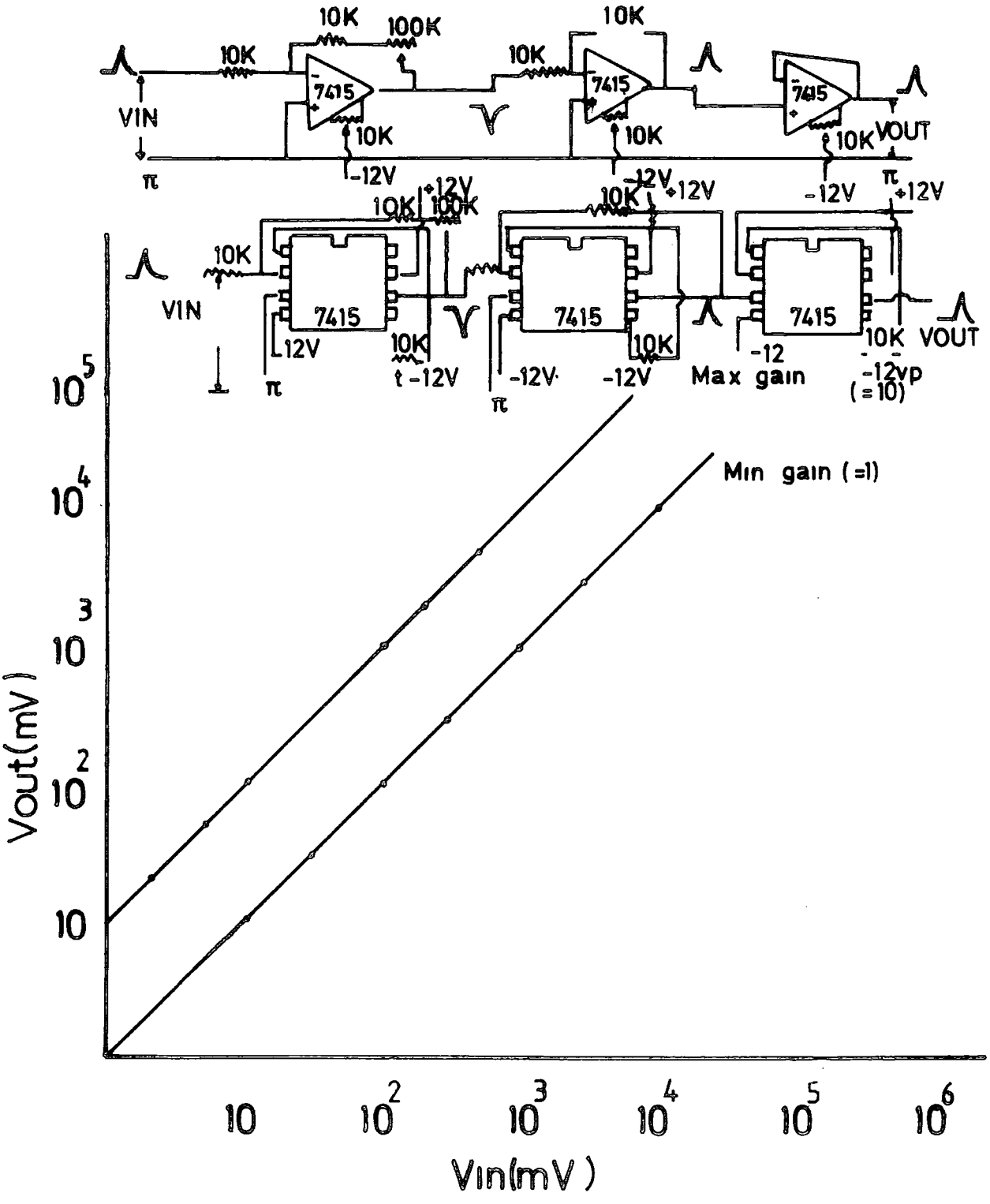

Figure 7.5 : Amplifier unit used in the tachyon experiment.

Figure 7.6 :

(a) One tachyons type pulse

(b) Two pulses preceding the shower front (the first one is in the region of tachyon (120 μs)).

(c) Pulse before the start of the scan.

(d) The pre-shower front hump pulse.

These are typical oscilloscope photographs showing a tachyon type pulse. Normally the air shower front pulse height is off scale. The pre-shower front hump pulse and the oscillation is instrumental in nature. Tachyon pulses are expected to occur in the 120 μs time domain preceding the E.A.S.

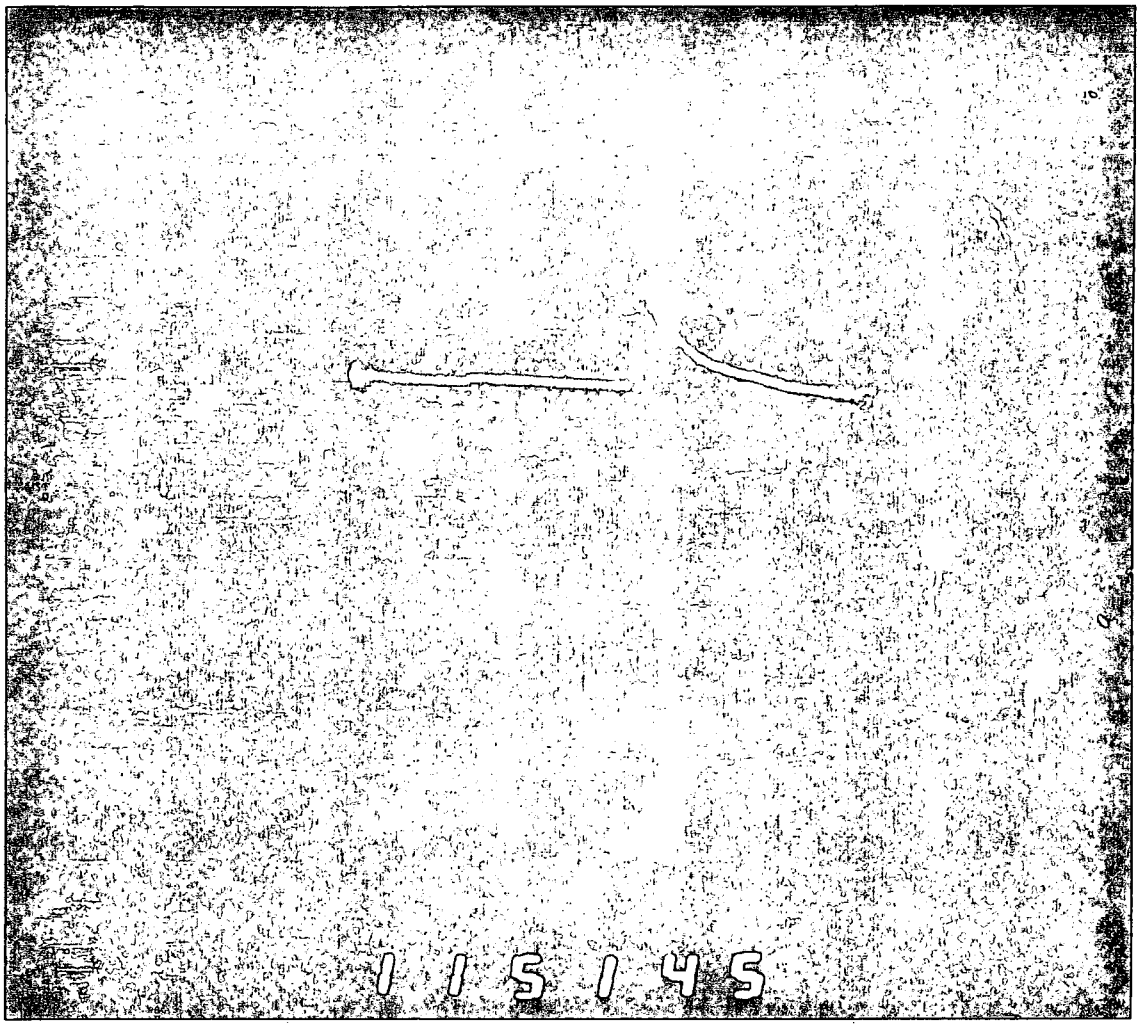

Figure 7.6a :

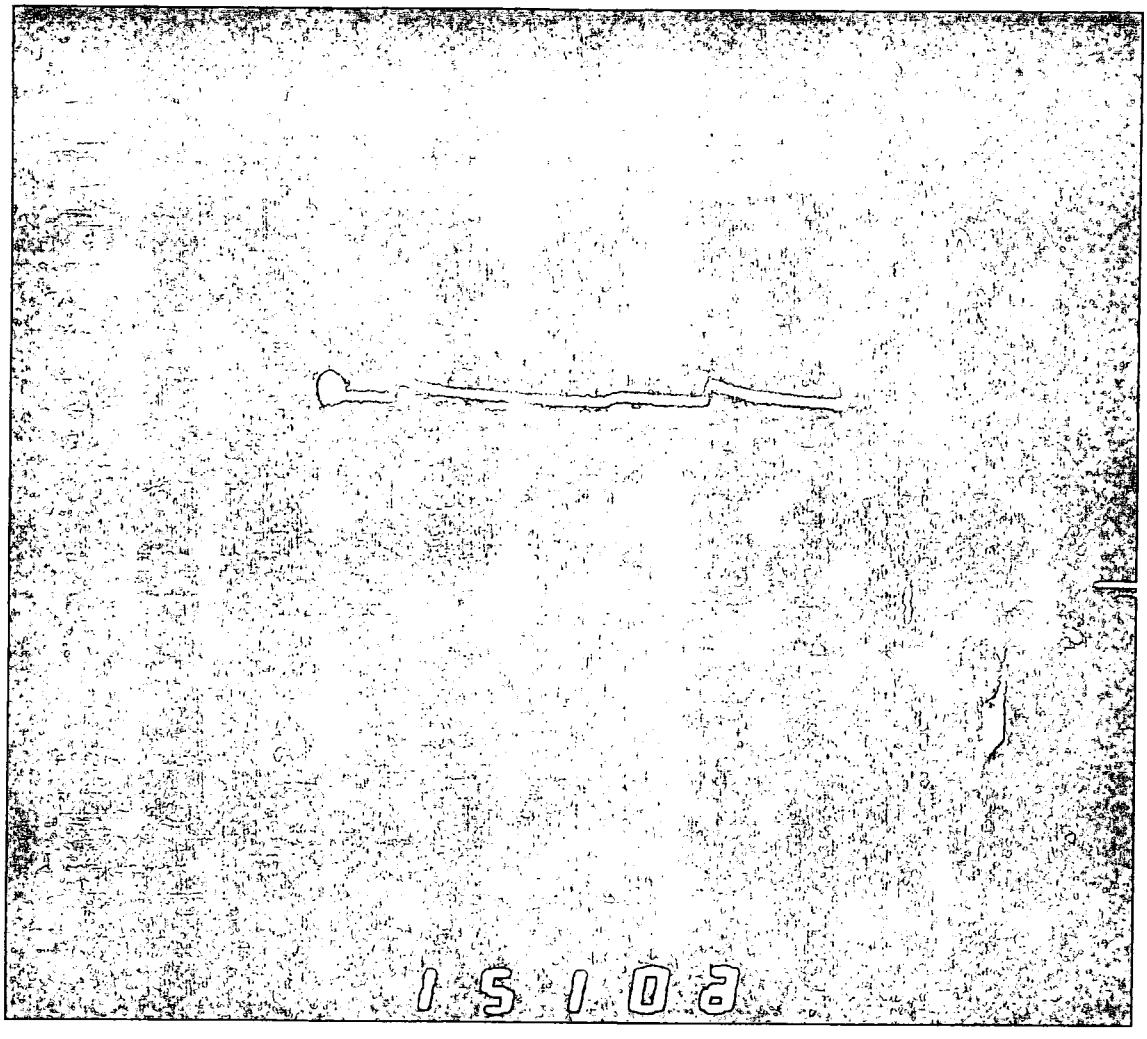

Figure 7.6b :

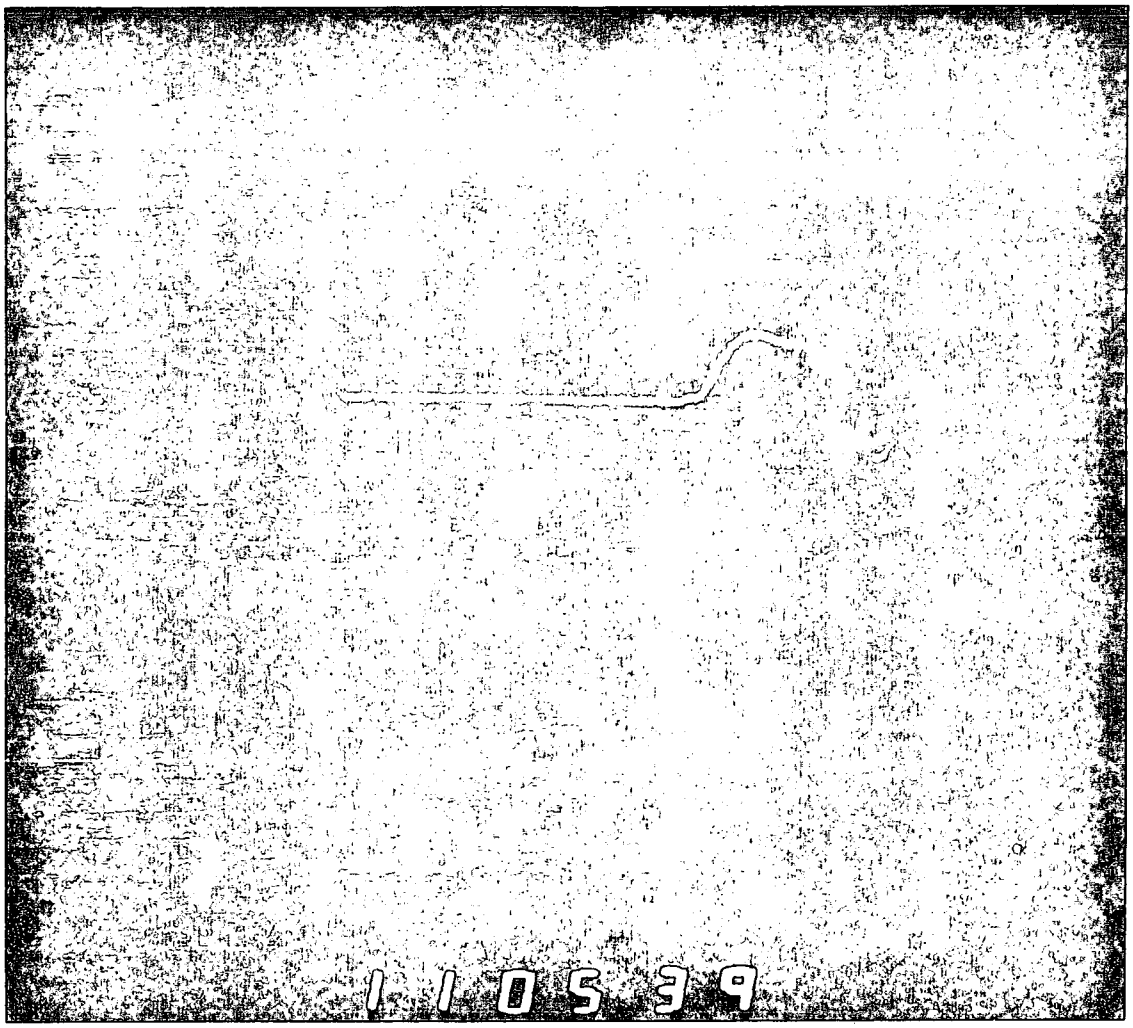

Figure 7.6d :

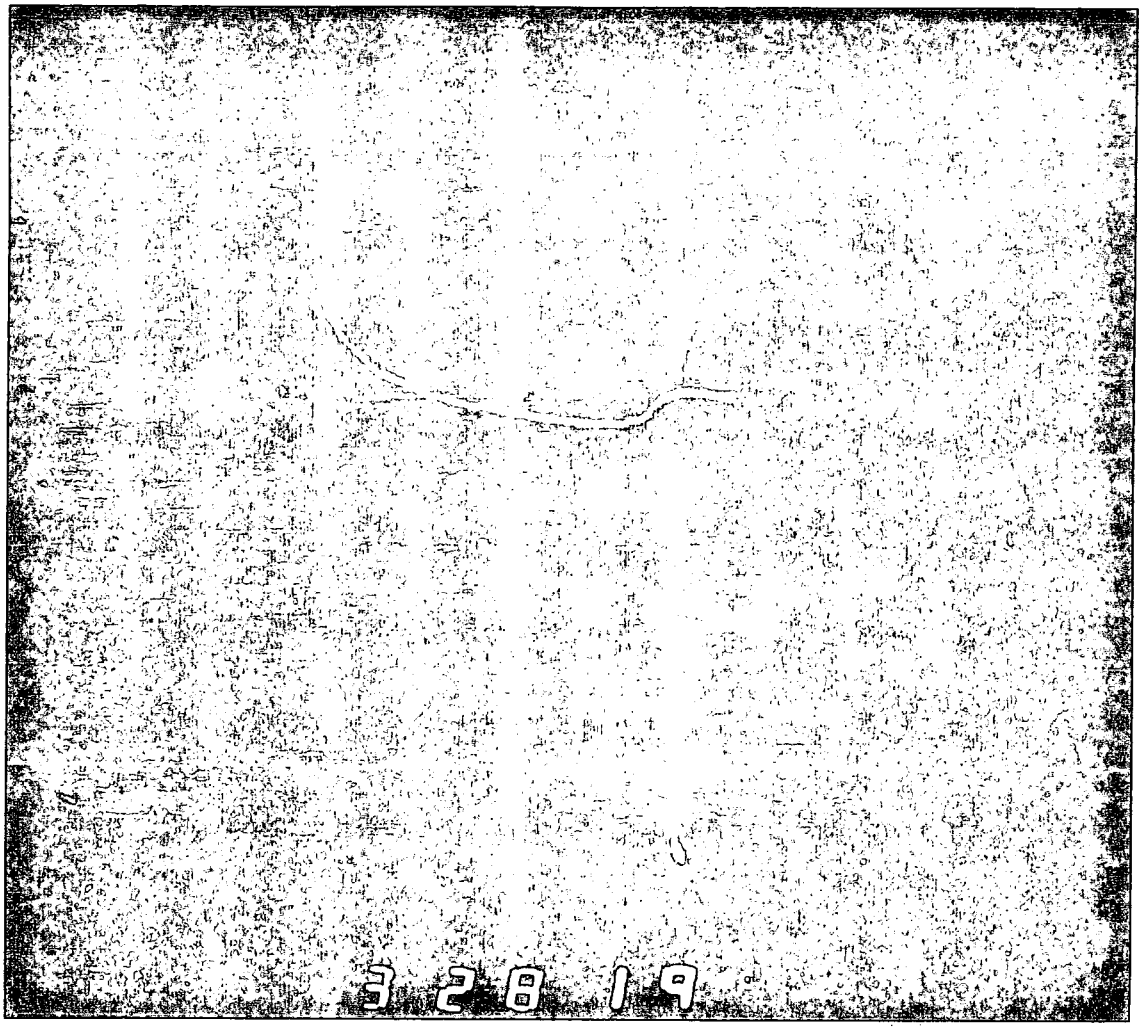

Figure 7.6c :

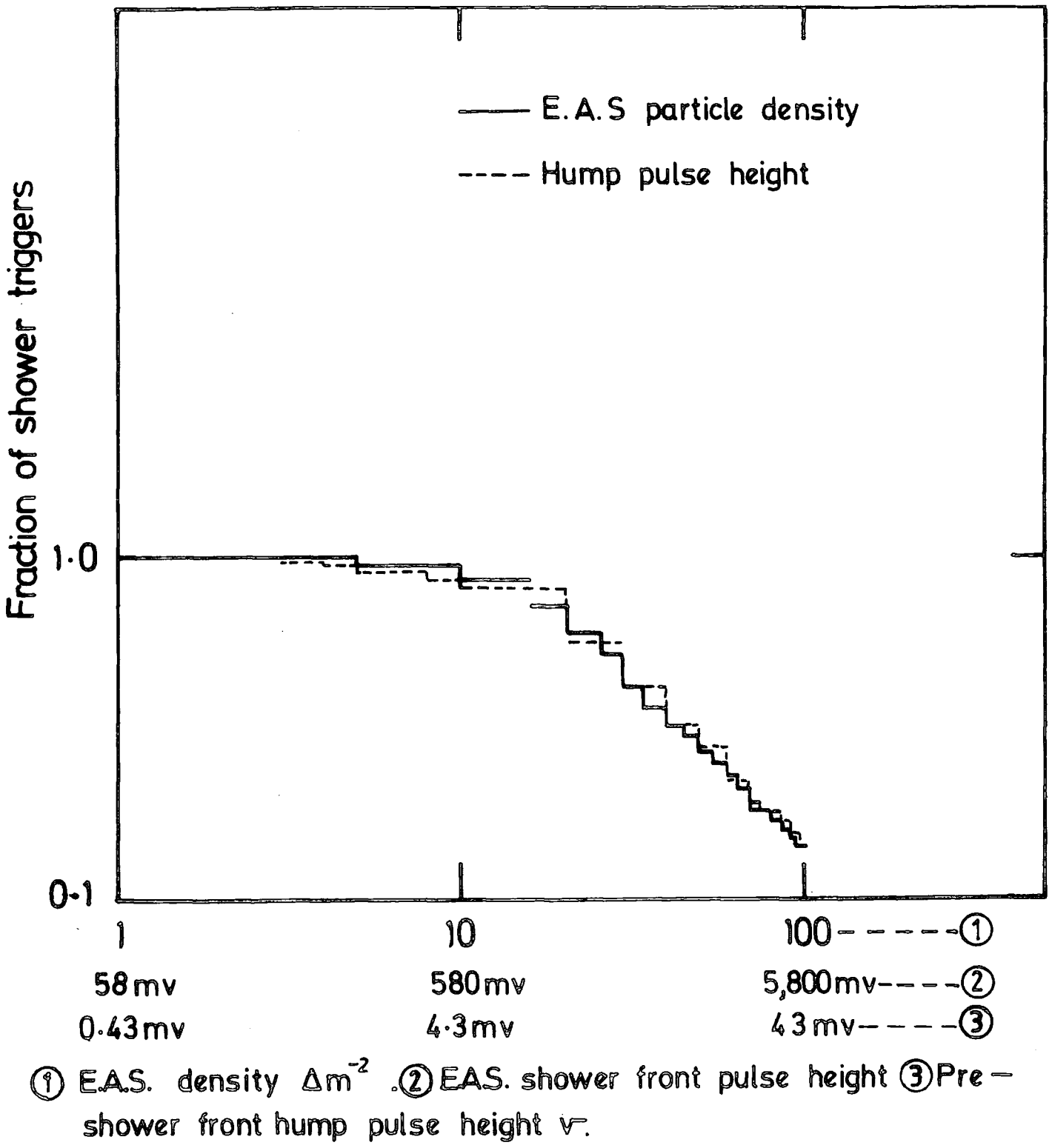

Figure 7.7 : Fraction of shower triggers that produce a density > Δm^{-2} in the tachyon detector for the air shower selection requirement. Equivalent pulse heights at the input to the recording oscilloscope are shown on the figure. Also shown is the fraction of showers that produce a pre-shower front hump pulse height of height > v on the tachyon oscilloscope film.

corresponding to 52 particles traversing the detector of area 2 m^2. In the present experiment the average pulse height produced by relativistic particles traversing the detector 31 at normal incidence is found to be 28.7 mV. Using this figure to change figure 7.7 to a graph of the fraction of pulses of height $>V$ versus V and comparing the result with the measured integral hump distributions agree quite well if the hump height is assumed to be $7.4.10^{-3}$ of the height of the E.A.S. front pulse as shown in figure 7.7. Although the hump is not serious in reducing the efficiency of detecting previous particles the high frequency oscillation which occupies the 20 μs time domain prior to the E.A.S. front pulse is and this will be discussed in more detail later. It is to be noted that using shielding to cover the detector just sufficient to absorb the electron photon component of E.A.S. would certainly reduce the E.A.S. front pulse by a large factor and hence also the amplitude of the oscillation enabling efficient measurements to be made in the 20 μs time domain prior to the E.A.S. front pulse with the present equipment. A further check on the operation of the experiment was to plot the frequency of time intervals between detected showers. The integral plot is shown in figure 7.8. Fitting this by $n(>t) = N_0 \exp(-\frac{t}{T})$ gives a value for T of 15.2 min, which is to be compared with the measured value of 15.2 min, this indicating that the distribution easily approximates a Poisson distribution.

Also the signal to noise ratio of the detector was investigated. The rate of pulses above for a given threshold was determined with both the photo-multiplier tubes unmasked and masked, using an amplifier, discriminator and scaler, the result being shown in figure 7.9.

7.6 RUNNING THE EXPERIMENT

As mentioned earlier, during the course of the present measurements the whole E.A.S. array was not operational. The tachyon detector 31 and some other triggering detectors (C,13,33 and 53) were involved. A number of calibration

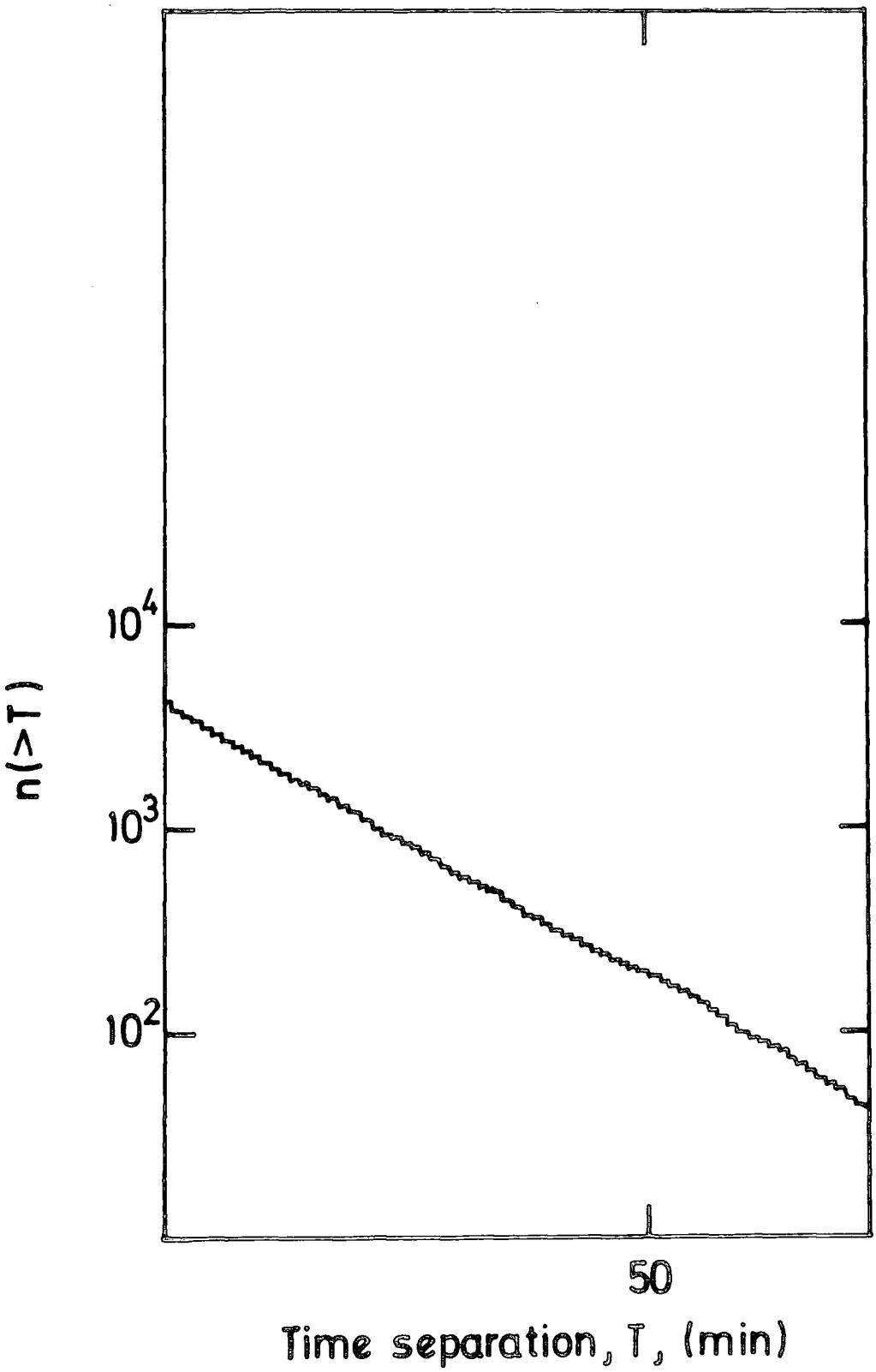

Figure 7.8 : Integral plot of time separation of E.A.S. triggers. A linear regression analysis gives the slope as 15.2 i.e. provided the distribution is Poissonian. The mean time separation is 15.2 min.

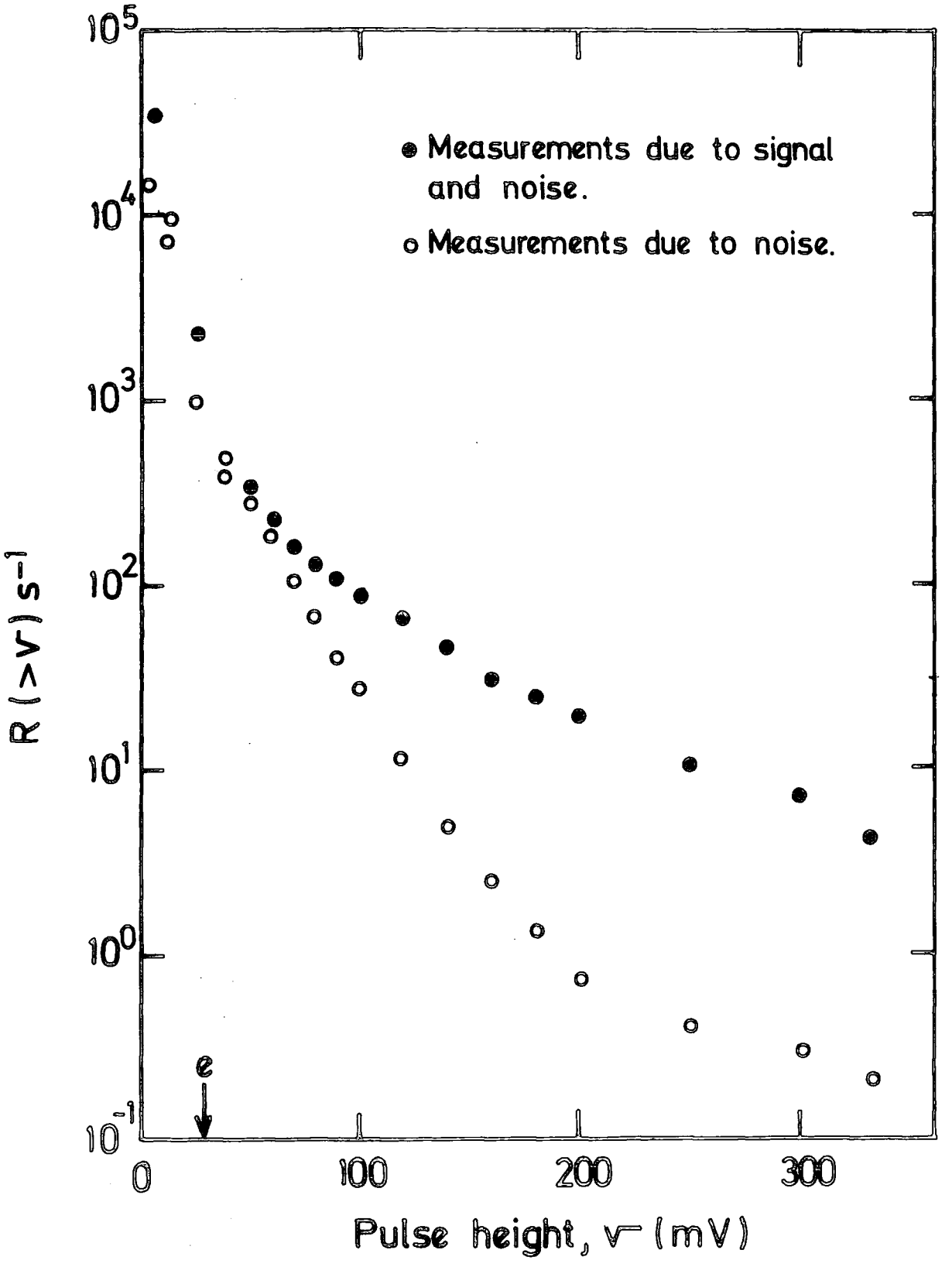

Figure 7.9 : Rate of pulses of height >V versus V for (i) output of tachyon detector (i.e. Signal and noise) (ii) output of tachyon detector with phototubes masked (i.e. noise). Rate obtained using a discriminator and scalor.

checks were made during the running of the experiment.

(1) The gain of the amplifier units and the rates of each of the triggering detectors was checked.

(2) Calibration of the triggering detectors was carried out by gating detector pulses, using a scintillator telescope and pulse height analyser (P.H.A).

(3) Camera output was always checked after a running time of the order of 3-4 days giving a total of 35 ft of film. This was then scanned by eye for events of interest and then analysed according to the quality of the data. The rate of events greater than a certain threshold was checked and a plot of the observed frequency distribution against a random distribution was checked also.

7.7 DATA ANALYSIS AND RESULT

In a total of 6,461 triggers 3,439 were observed to show a measurable pulse preceding the arrival of the air shower. Figure 7.10 shows the time distribution of these events relative to the arrival time of the shower front for different threshold energy losses in the detector. It is seen that there is a depletion of events observed in the 20 μs period prior to the arrival of the E.A.S. front and this is due to obscuration produced by the high frequency oscillation already discussed. Neglecting this time domain, the distribution of events is expected to be flat over the region 20-260 μs; if all events are produced by background (i.e. thermal noise from the phototubes at small pulse height and cosmic ray muons not associated with the air shower trigger at large pulse height) and to show an excess of events in the region 20-120 μs, if a significant tachyons flux is associated with the air shower triggers. For small

URE 7.10: OCCURRENCE TIME DISTRIBUTION OF PULSES CORRESPONDING TO DIFFERENT THRESHOLD ENERGY LOSSES IN THE TACHYON DETECTOR OBTAINED FROM A SAMPLE OF 6461 SHOWER TRIGGERS. $P(x^2)$ REFERS TO THE TIME INTERVAL 20-260μs, $P(x_1^2)$ TO THE TIME INTERVAL 20-140μs AND $P(x_2^2)$ TO THE TIME INTERVAL 140-260μs. $P(x^2)$ IS THE PROBABILITY THAT THE OBSERVED VALUE OF x^2 COULD HAVE OCCURRED BY CHANCE IF THE TRUE DISTRIBUTION IS CONSTANT IN TIME. THE AVERAGE PULSE HEIGHT e PRODUCED BY RELATIVISTIC MUONS TRAVERSING THE DETECTOR AT NORMAL INCIDENCE IS 28.7mV

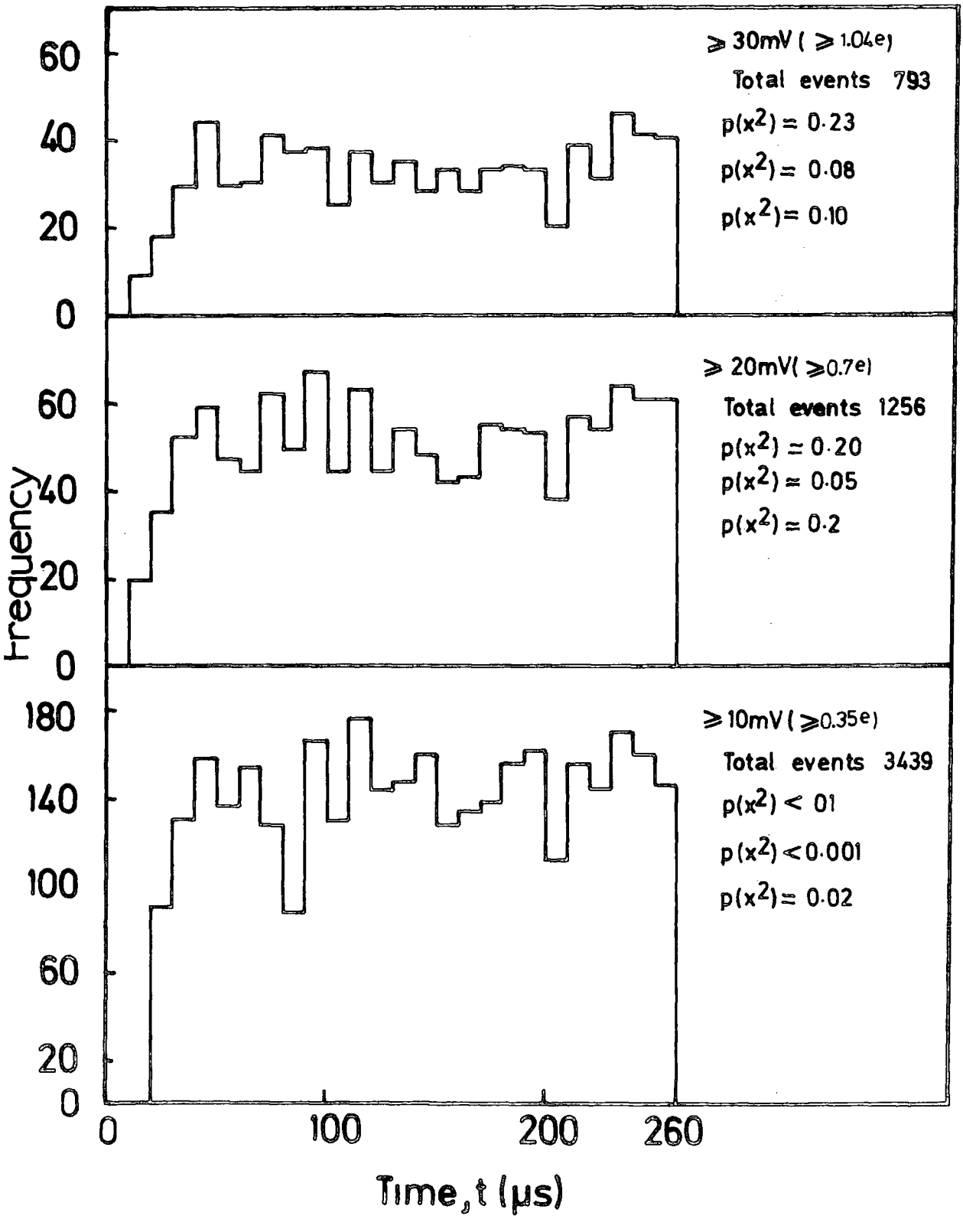

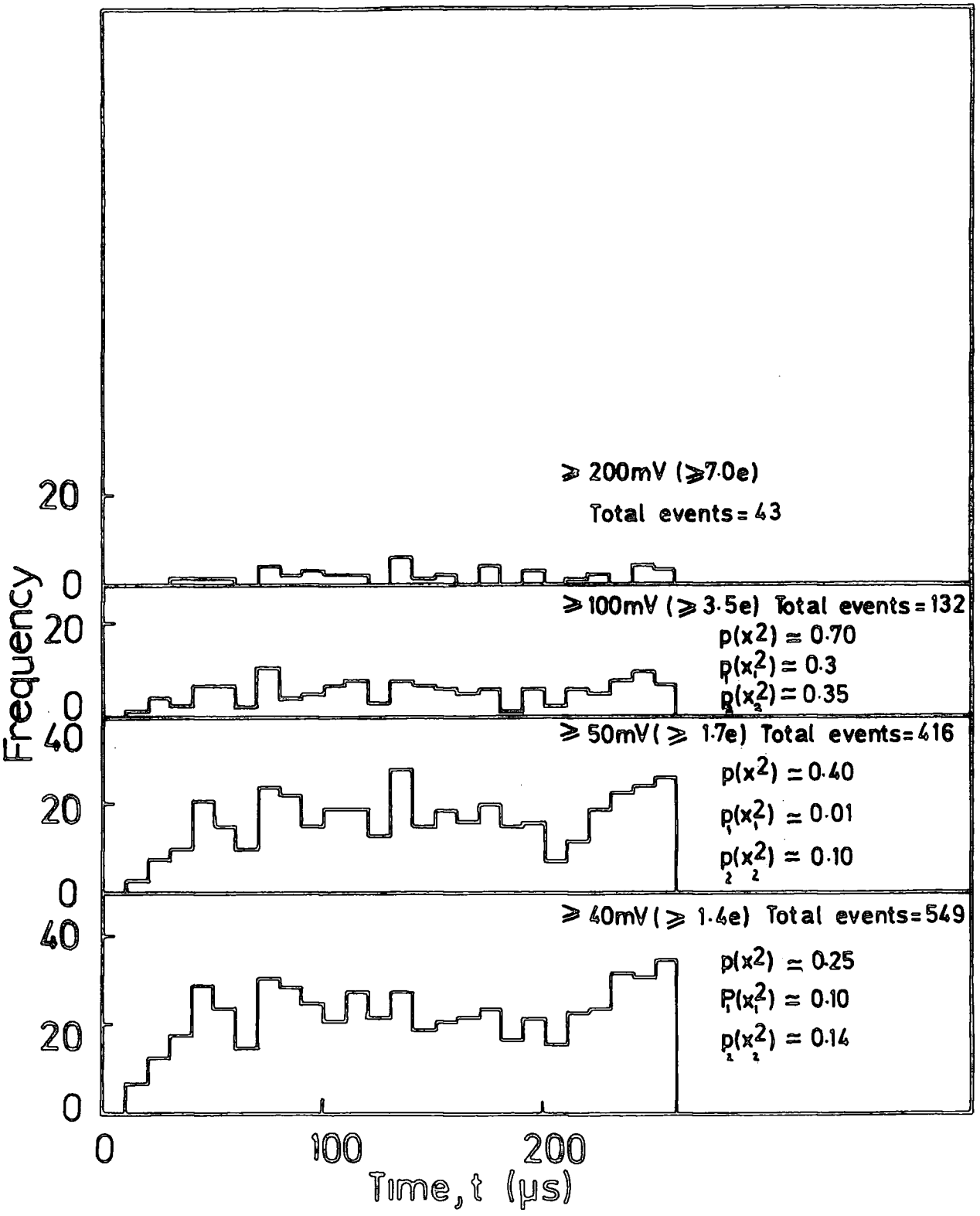

Figure 7.10 : Continued

threshold energy losses in the detector ($\lesssim$ 1.7e) there are sufficient events to test whether the distributions are flat using an X^2 test and both X^2 and the probability p of such a value of X^2 arising by chance if the distributions are really flat. There are also shown in figure 7.10. In addition the test was applied to each half of the distribution i.e. 20 μs - 140 μs and 140 μs - 260 μs, their respective X_1^2, X_2^2, p_1, p_2 being shown in the figure. With the possibility that tachyonic pulses might have predominately similar heights, time distributions were also drawn for pulses in particular height bands. These are shown in figure 7.11. It is seen that in all cases there is no evidence for a significant number of events being produced by tachyons. For large energy losses in the detector (> 7.0e) there are insufficient statistics to apply an X^2-test. However, comparing the number of events observed in the region 20 - 140 μs with the number observed in the region 140 - 260 μs there is no evidence for a significant excess of events in the first 120 μs interval where real tachyons are expected to occur. It is noted that the distribution involving pulses in the 10 mV - 20 mV range give very low probabilities of a true uniform distribution. This is due to the difficulty of measuring such small pulses especially on the leading edge of the hump. This is shown by the large dip in the distribution of pulses of height greater than 10 mV, at 80 μs.

Another way of testing the data to see whether there is evidence for a significant tachyon flux is to compare the rate of pulses of height >v produced by the detector using an amplifier, discriminator and scaler with that obtained from the oscilloscope measurements. If n (>v) pulses of height >v are measured in the time domain 20 - 260 μs during 6,461 triggers then $R(>v) = \frac{n(>v)}{240\times10^{-6}.6461}$ sec^{-1}. Figure 7.12 shows such a comparison where the agreement between the two methods of measuring R(>v) is seen to be good, indicating that the vast majority of measured

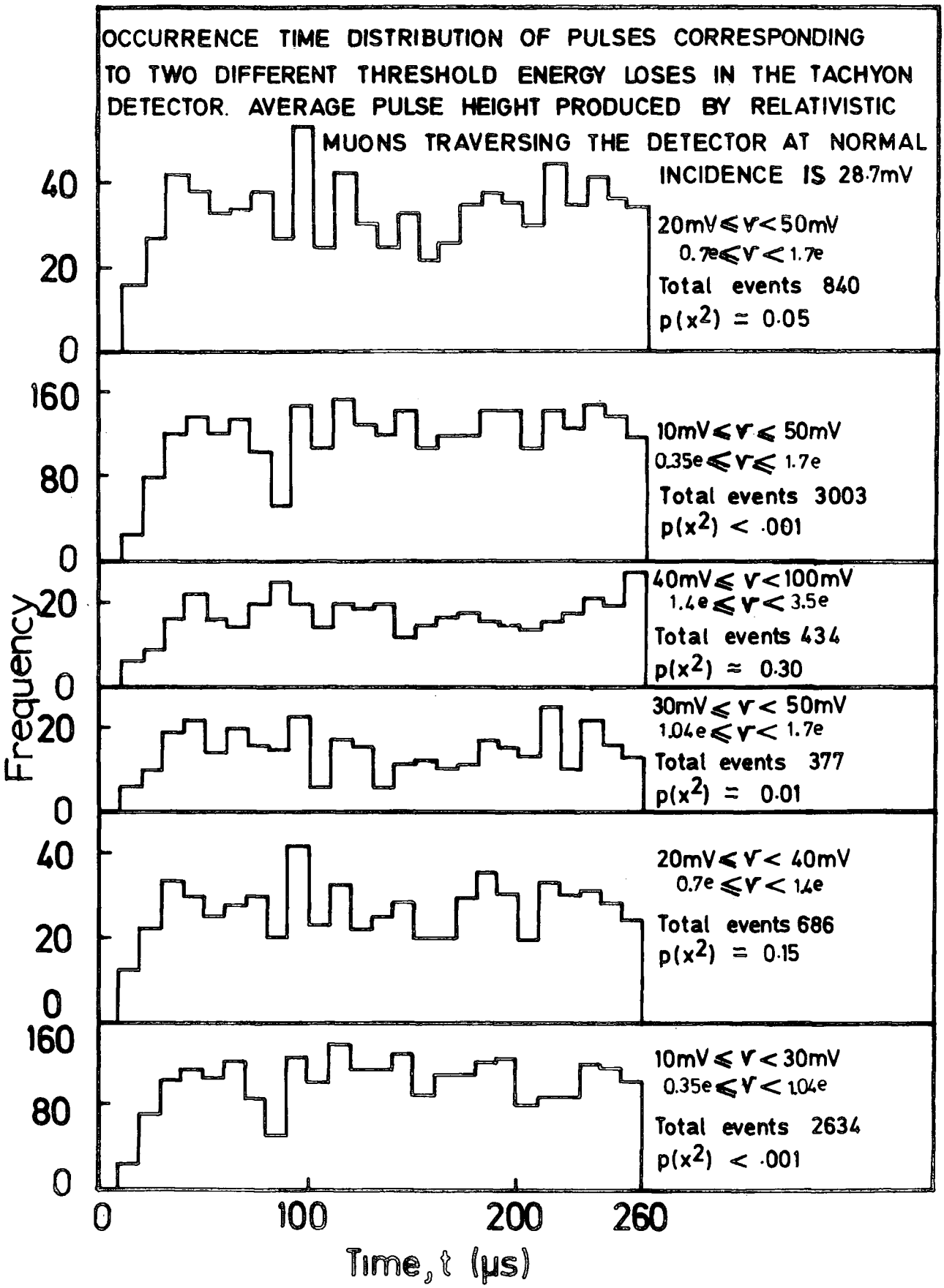

Figure 7.11 : Occurrence time distribution of pulses corresponding to two different threshold energy losses in the tachyon detector. The average pulse height produced by relativistic traversing the detector at normal incidence is 28.7 mV.

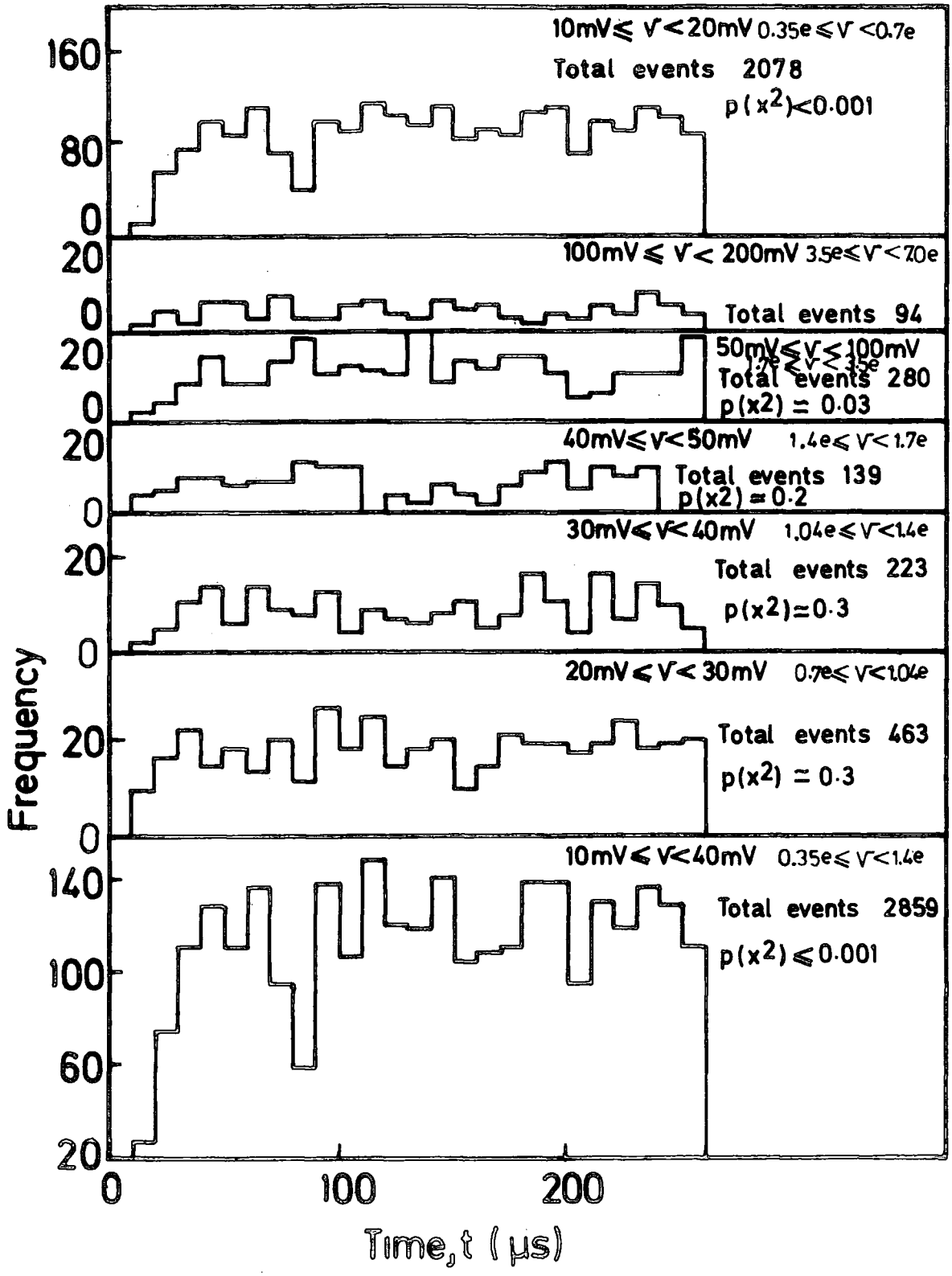

Figure 7.11 : continued.

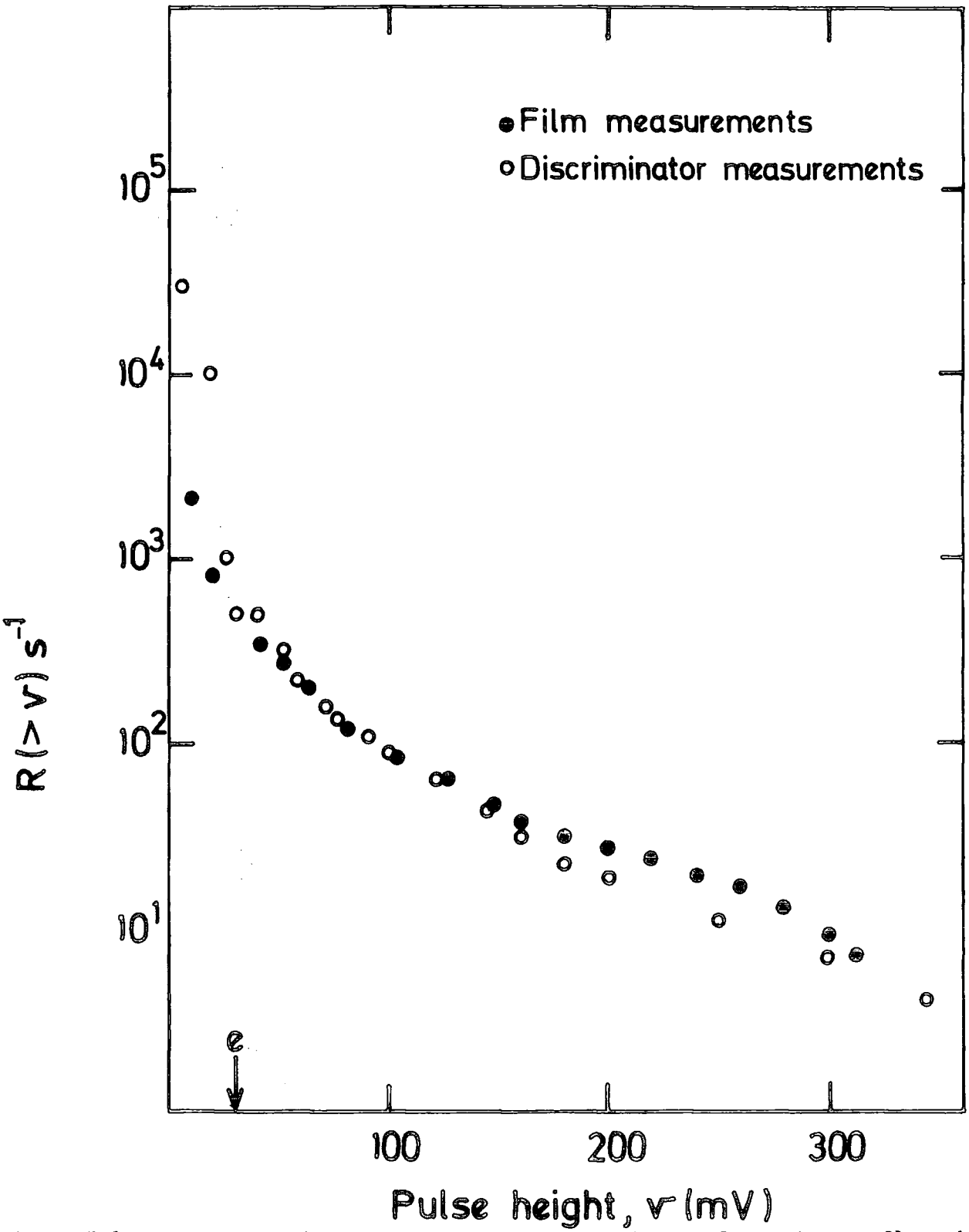

Figure 7.12 : Response of the tachyon detector to the total cosmic ray flux. Integral rate of pulses of height >v millivolts (measured at the input to the recording oscilloscope) versus pulse height v. The average pulse height produced by relativistic muon traversing the detector at normal incidence is 28.7 mV and is indicated by e on the graph.

pulses are due to background.

Finally, multiple pulse events were investigated. A significant number of events have been observed in which more than one previous pulse is observed in the time domain 20 - 260 μs preceding the air shower front pulse. If for a given threshold energy loss the average number of early pulses observed is z. then the probability of observing r, p(r) is expected to be Poisson (i.e. $p(r) = e^{-z}z^r/r!$) if the pulses are randomly related. Table 7.1 shows a comparison between the observed and expected number for different threshold energy losses. If a tachyon signal is present in the data then an excess of observed events having 2 early pulses can be expected as a real early tachyon pulse associated with some showers would mean that both early pulses are not randomly related with respect to the shower front pulse. It is seen from table 7.1 that an excess is observed for small threshold energy losses (<0.7e) in the detector, but the excess is not statistically significant.

For larger threshold energy losses (> 0.7e) the agreement between the observed and expected number of double pulse events is remarkably good, indicating no evidence for a real tachyon signal.

7.8 CONCLUSION

Using an unshielded plastic scintillator of area $2m^2$ and thickness 2.5 cm as a tachyon detector no evidence has been found for a significant flux of tachyons (if tachyons ionize at a rate of >24% that of a relativistic muon) in a sample of 6461 E.A.S. at sea level generated by primary cosmic rays of energy $2.5.10^{15}$ev. Although no tachyon evidence has been found, this does not mean that there are no tachyons. Failure to observe any tachyons in the experiment obviously implies that either they do not exist or the production and interaction characteristics of tachyons are such that they could not have been detected in the experiment. In

Table 7.1 : Number of triggers showing n pulses in the tachyon detector in the time domain 20-260 μs prior to the arrival of an E.A.S. shower front pulse for different threshold energy losses in the tachyon detector. The number of events with n = o increases with threshold energy loss because the rate of the background pulses decreases rapidly with increasing threshold energy loss. n_o is the observed number of events and n_e is the expected number assuming the expected number obeys a Poisson distribution.

Threshold ≥ 0.35e				Threshold 0.70e			
n	n_o	n_e	n_o-n_e	n	n_o	n_e	n_o-n_e
0	3780	3786.7		0	5309	5310.3	
1	2027	2023.2		1	1053	1041.4	
2	556	540.5	+16.5	2	86	102.1	-16.1
3	84	96.3		3	11	6.7	
4	11	12.9		4	1	0.3	
5	2	1.4		5	1	0.0	
6	0	0.1		6	0	0.0	
7	1	0.0					
8	0	0.0					

Threshold ≥ 1.04e				Threshold ≥ 1.4e			
n	n_o	n_e	n_o-n_e	n	n_o	n_e	n_o-n_e
0	5708	5706.8		0	5913	5908.1	
1	709	708.4		1	518	528.5	
2	40	44.0	-4.0	2	30	23.6	+6.4
3	3	1.8		3	0	0.7	
4	1	0.1		4	0	0.0	
5	0	0.0		5	0	0.0	

Threshold ≥ 1.7e				Threshold ≥ 3.5e			
n	n_o	n_e	n_o-n_e	n	n_o	n_e	n_o-n_e
0	6056	6072.2		0	6337	6335.2	
1	369	376.9		1	127	124.5	
2	16	11.7	+4.3	2	0	1.2	-1.2
3	0	0.2		3	0	0.0	
4	0	0.0		4	0	0.0	

Threshold ≥ 7.0e			
n	n_o	n_e	n_o-n_e
0	6422	6422.1	
1	39	38.8	
2	0	0.1	-0.1
3	0	0.0	

the case of using a shielded plastic scintillator, the claim of Fegan (1981) has yet to be confirmed. The excess of events in the region 48 - 60 μs prior to the shower front, is thought by Fegan to be due to the disintegration of cosmic-ray nuclei caused by the solar-radiation photons leading to the detection of correlated air showers. The energy of the disintegrated nuclei is found to be of the order 10^{16} eV per nucleus and their flux of order of 10^{-4} to 10^{-3} km^{-2} hour^{-1} sr^{-1}.

CHAPTER 8

CONCLUSION

Cosmic rays, these energetic particles, electrons and the nuclei of atoms moving at velocities very close to the speed of light, bombard the solar system continuously from all directions. The kinetic energies of some of these particles far exceed anything achieved in the largest man-made accelerator. On entry to the atmosphere, the higher-energy nuclei soon collide with molecules of air, creating a shower of secondary particles, which can be detected on the ground. The sun is an important source of low-energy cosmic rays. The main source of the more energetic particles is unknown, but it is believed that pulsars, supernova, active galaxies and quasars all contribute.

The Durham E.A.S. array which consists of fourteen plastic scintillator was used to study extensive air showers. These studies are mainly related to primary cosmic rays of energy $>10^{12}$eV as the observation of E.A.S. provides a unique method for the detection of such particles with relative ease. The primaries with the forementioned energies are rare, thus their direct detection at the top of the atmosphere is impractical. The information about the size spectrum and arrival direction of primary cosmic rays may lead us to understand elementary particles, nuclear interactions and also the nature and origin of high energy cosmic rays.

One method involved in determining air shower parameters is based on the intersecting loci curve. However, this technique cannot handle large quantities of data for which case an analysis using a computer numerical minimization technique has been discussed. In order to have confidence in the results obtained by the two methods, the error in core location is checked, and found to be on average about $\pm$ 6 m. A method of determining the arrival direction of showers (θ & ϕ) is also discussed, the overall uncertainty in zenith angle is $\pm$ 2.0^{o} and that of the azimuthal is $\pm$ 6.0^{o}.

The study of the electron component and the age parameter, s, of individual E.A.S. in the size range 10^4- 10^7 particles showed that they do not all obey the same structure function. The lateral electron density distributions used in the analysis are due to Greisen (1960) and Catz et al (1975). These two distributions agree well except in the region below 20 metres from the shower core where the Catz lateral distribution is steeper. The mean age parameter and the standard deviation of the age parameter distribution of the showers showed that on average they are independent of zenith angle. In the investigation of the age parameter of individual E.A.S., the mean was found to increase significantly in value over the size range 10^6 - 10^7 particles which is in contradiction with cascade shower theory. Further studies of this effect need to be done.

A measurement of the sea level shower size spectrum was made in the region 2.10^4 - 210^7 particles, and the result showed that it is not quite consistent with previous work. The differences at the two largest shower sizes is associated with an increase in age parameter with shower size which is such that sizes determined using the Greisen average lateral structure function are less than those determined when the age parameter of individual showers is taken into account.

From the analysis of the arrival direction of E.A.S. possible sources of cosmic rays have been studied. A possible excess of events from one direction in galactic coordinates which correlates with the directions of some pulsars and quasars has been found at the level of about three standard deviations. In the search for tachyons associated with air showers, the suggestion is that if tachyons are produced in high energy cosmic ray interactions, then they should be produced high in the atmosphere (20 Km - 30 Km) above sea level. For any produced tachyon with $v > c$ (i.e. $\beta > 1$) it would arrive some 60 - 120 μs before the air shower. The search has produced no evidence for the existence of tachyons.

APPENDIX A

EVALUATION OF THE NISHIMURA - KAMATA - GREISEN (N.K.G.) LATERAL DISTRIBUTION FUNCTION

Greisen (1956) produced a simplified formula representing the lateral distribution of all charged particles in E.A.S. at sea level of size N and the result is known as the N.K.G. formula (i.e. Nishimura, Kamata, Greisen) which is given as

$$\Delta(r) = N \frac{f(r/r_1)}{r_1^2} \quad \text{where}$$

$$f\left\{\frac{r}{r_1}\right\} = C(s)\left\{\frac{r}{r_1}\right\}^{s-2}\left\{1+\frac{r}{r_1}\right\}^{s-4.5}$$

s is the shower age parameter and is a measure of the stage of development of the shower, r is the distance to the shower axis, r_1 is the Moliere unit having a value of 79 metres at sea level and C(s) is a normalization factor such that

$$\int_0^\infty 2\pi\, f(x)x\,dx = 1 \quad \text{where} \quad x = \frac{r}{r_1}$$

and can be approximated by (Greisen, 1956)

$$C(s) = 0.443\, s^2\,(1.09-s) \quad \text{for } s < 1.6 \qquad (1)$$

$$C(s) = 0.366\, s^2\,(2.07-s)^{5/4} \quad \text{for } s < 1.8 \qquad (2)$$

$$C(s) = \frac{1}{2\pi}\left(\frac{\Gamma(s)\Gamma(4.5-2s)}{\Gamma(4.5-s)}\right)^{-1} \quad \text{for } s \leq 2.25 \qquad (3)$$

Exact values of C(s) are given in table A.1 and they are shown in figure A.1

Values of C(s) for $0.6 < s < 1.8$ were used in the data analysis.

To calculate the electron density in a shower of unit size, a computer programme was used to evaluate the expression for $\Delta(r)$ for the case N = 1. The result is plotted in figure A.2 and shows how s determines how peaked or flat the structure of the shower is. Figures A.3 and A.4 show both the programme and the output of the programme used in the calculation of $\Delta(r)$. Programmes are given in Fortran (figure A.3) and Basic (figure A.4) for use on both large and small computing systems.

s	0.0	0.2	0.4	0.6	0.8	1.0	1.2	1.4	1.6	1.8	2.0	2.2	2.25
C(s)	0.0	0.045	0.117	0.212	0.312	0.398	0.44	0.437	0.363	0.247	0.12	0.018	0.0

Table A.1 : Exact values of C(s), which are consistent with the last formula (3)

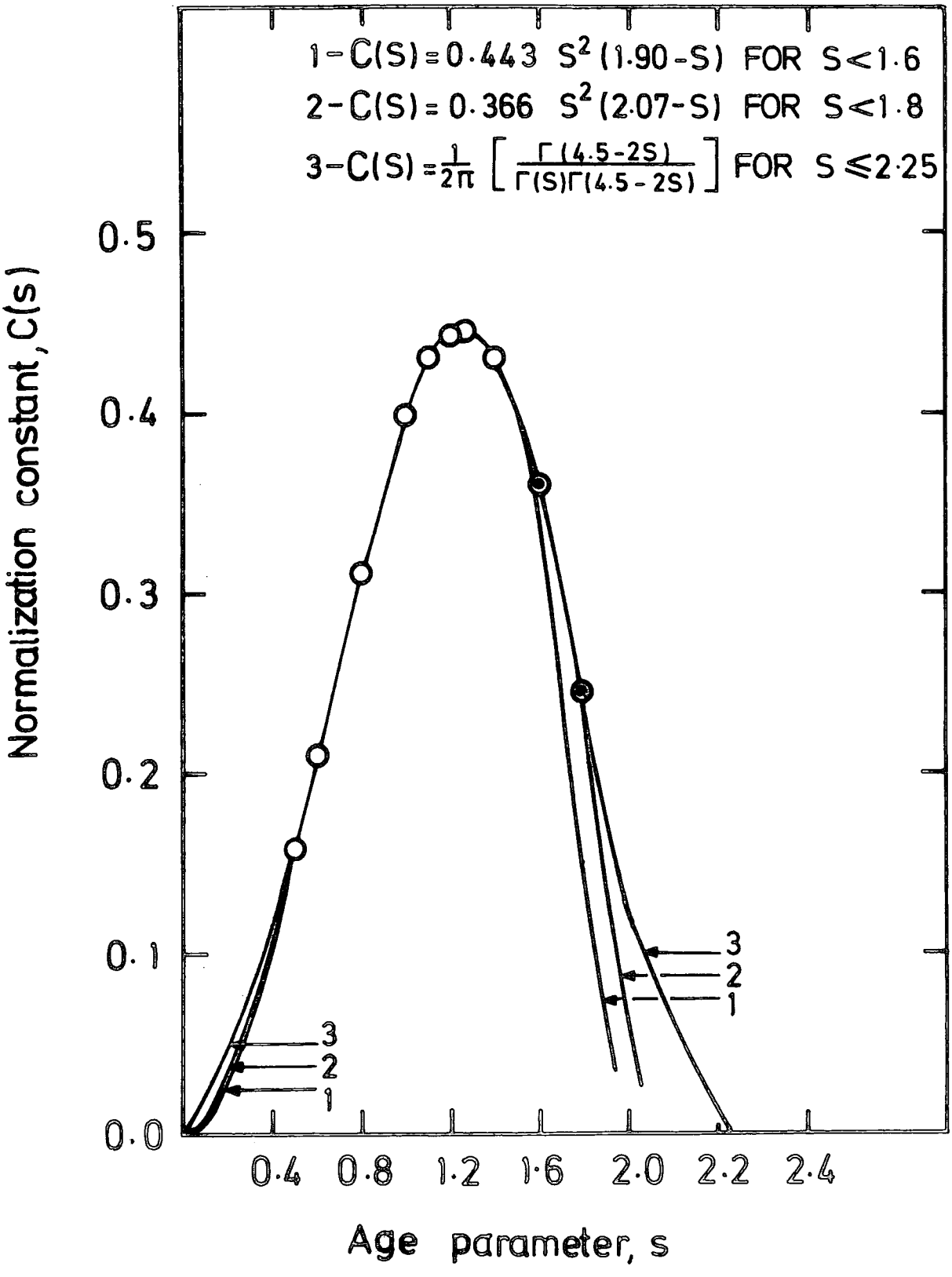

Figure A.1 : Consistency of the values of normalization factor as a function of age parameter.

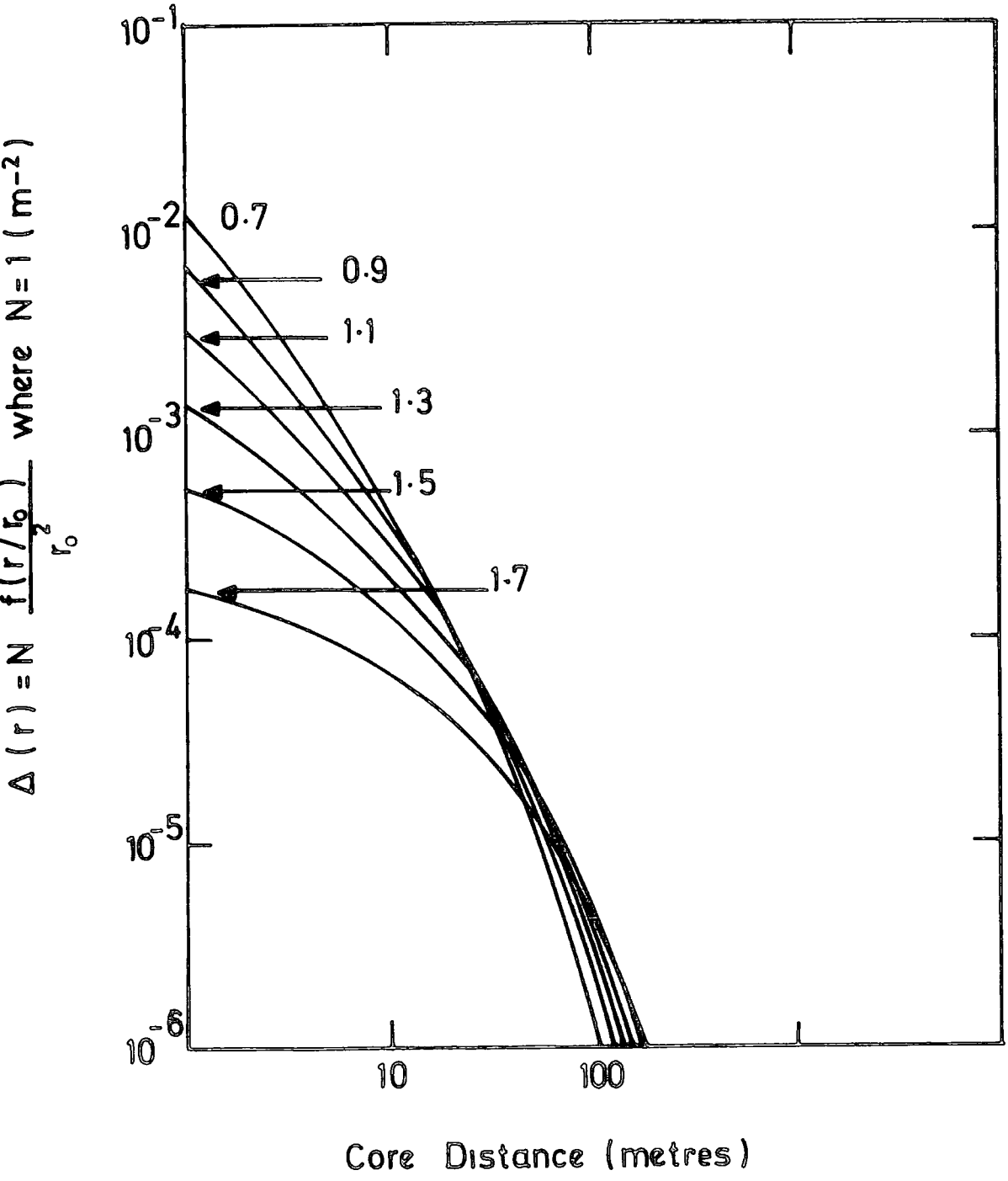

Figure A.2 : Electron density as function of core distance for showers with different age parameter.

```
      INTEGER R
      READ(5,100)S,F
  100 FORMAT (F10.1,F11.3)
      PRINT 30
      PRINT 40
      PRINT 10,S,F
   10 FORMAT (1X,'   S=',F3.1,'   F=',F5.3  '    )
   40 FORMAT (1X,'   AGE PARAMETER DISTRIBUTION    ')
   30 FORMAT (1X,33('-'))
      PRINT 20
      PRINT50
      PRINT 60
   50 FORMAT (1X,'   CORE DIST.    ','   DENSITY (D(R))     ')
   60 FORMAT (1X,'   IN METER      ','   PER SQU.METER      ')
   20 FORMAT (1X,33('-'))
      DO 200  R=1,100,9
      A=ABS((FLOAT(R)/79+1)**(S-4.5))
      B=ABS(F*(FLOAT(R)/79)**(S-2))
      Z=A*B
      DR=Z/(79*79)
      PRINT 66
      PRINT 1952,R,DR
 1952 FORMAT(4X,I3,16X,E10.3)
   66 FORMAT(1X,33('-'))
  200 CONTINUE
      PRINT 66
      RETURN
      END
```

```
   AGE PARAMETER DISTRIBUTION
   S=0.7    F=0.266
```

CORE DIST. IN METER	DENSITY(D(R)) PER SQU.METER
1	0.119E-01
10	0.398E-03
19	0.120E-03
28	0.518E-04
37	0.265E-04
46	0.151E-04
55	0.916/-05
64	0.588E-05
73	0.393E-05
82	0.271E-05
91	0.193E-05
100	0.140E-05

Figure A.3 : N.K.G. Function Programme, using Fortran Language

```
1       OPEN1,4
3       CMD1
5       PRINT"-------------------------"
7        PRINT "AGE PARAMETER DISTRIBUTION"
9        PRINT"-------------------------"
11       INPUT S
13       INPUT F
15       PRINT"      S=  ";S
17       PRINT"  C(S)=  ";F
19       PRINT"------------------------------"
21       PRINT"CORE DIST.(R)""   DENSITY(D(R))  "
23       PRINT"IN METER   ""     PER SQU.METER  "
25       PRINT"------------------------------"
27        FOR R=1 TO 100 STEP 9
29        LET A=ABS((R/79+1)^(S-4.5))
31        LET B=ABS(F*(R/79)^(S-2))
33        LET Z=A*B
35        LET DR=Z/(79*79)
37        PRINT"      ";R;"       ";DR
39        PRINT"------------------------------"
41        NEXT R
43        END
READY.

 1 DATA
 20 .7
 30 .266
READY.

-------------------------
AGE PARAMETER DISTRIBUTION
-------------------------
     S=    .7
  C(S)=    .266
------------------------------
CORE DIST,(R)  DENSITY(D(R))
IN METER       PER SQU.METER
------------------------------
      1        .0119064877
------------------------------
      10        3.97963823E-04
------------------------------
      19        1.19808285E-04
------------------------------
      28        5.18276865E-05
------------------------------
      37        2.65413506E-05
------------------------------
      46        1.50550564E-05
------------------------------
      55        9.16338404E-06
------------------------------
      64        5.87779872E-06
------------------------------
      73        3.92826039E-06
------------------------------
      82       .2.71412149E-06
------------------------------
      91        1.92781746E-06
------------------------------
      100       1.40179369E-06
------------------------------
READY.
```

Figure A.4 : N.K.G Function Programme, using basic language.

APPENDIX B

THE EFFECT OF SAMPLING DENSITY FLUCTUATIONS ON THE COLLECTING AREA FOR SHOWERS OF A GIVEN SIZE FOR A GIVEN E.A.S. SELECTION TRIGGER

Consider the collecting area for showers of size 3.10^5 selected by an outer ring trigger, $\Delta_C(\geq 4\ m^{-2}).\ \Delta_{13}(\geq 2\ m^{-2}).\Delta_{33}(\geq 2\ m^{-2}).\ \Delta_{53}(\geq 2\ m^{-2})$ where the area of detector C is 0.75 m^2 and the areas of detectors 13,33 and 53 are 2 m^2. Suppose the showers are incident vertically and the electron lateral distribution function (s = 1.25). This means that the collecting area is calculated for a minimum number of particles = 3 at C and 4 at the other three triggering detectors, which is the area of the spherical triangle shown in figure B.1. To get a more exact estimate of the collecting area the effect of sampling density fluctuations at the detectors should be taken into account. Taking the fluctuations as Poissonian

$$p(s) = \frac{e^{-z}\ z^s}{s!}$$

where p(s) is the probability of observing s when the mean number expected is z. For any core position (X,Y) in the array at which a shower of size 3.10^5 falls, the core distance from a triggering detector and therefore the average number of particles through it can be calculated.

For the case of the outer ring detectors the probability that sufficient particles traverse the detector to trigger it p(>s) is given by

$$p(\geq 3) = 1 - \{e^{-z}(1 + \frac{z^1}{1!} + \frac{z^2}{2!})\} \text{ for detector c}$$

$$p(\geq 4) = 1 - \{e^{-z}(1 + \frac{z^1}{1!} + \frac{z^2}{2!} + \frac{z^3}{3!})\} \text{ for detectors 13, 33 and 53}$$

Where z is the mean number of particles through the detector and the first term in brackets is the probability of there being zero, the second term being the probability of there being 1, etc. The

Figure B.1 : Scale diagram showing the collecting area for a vertical shower of size 3.10^5 with s = 1.25 selected by an outer ring trigger $\Delta_C(\geq 4m^{-2})$, $\Delta_{13}(\geq 2m^{-2})$ $\Delta_{33}(\geq 2m^{-2})$, $\Delta_{53}(\geq 2m^{-2})$ and assuming no sampling density fluctuations. 20 radius vectors on which the effect of sampling density fluctuations have been studied are also shown in the figure.

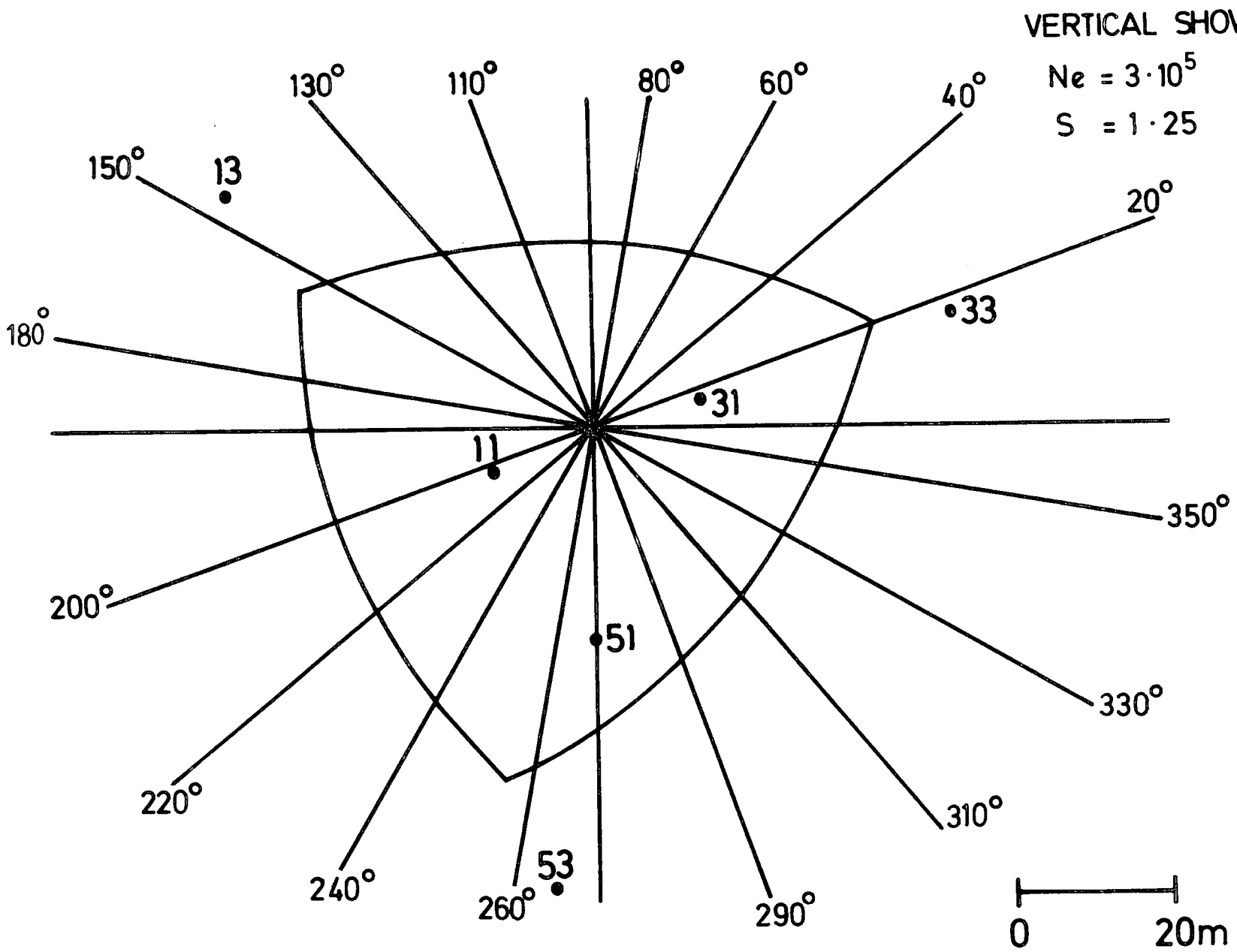
VERTICAL SHOWER
Ne = 3·10^5
S = 1·25
130°
110°
80°
60°
40°
150°
13
20°
180°
33
31
11
350°
200°
51
330°
220°
310°
240°
53
260°
290°
0
20m

Figure B.1 :

detection probability p(r) for a shower falling at the position (X,Y) is the product of all the detector probabilities or

$$p(r) = \prod_i p_i(\geq s) \; : \; i = C,\ 13,\ 33 \text{ and } 53$$

In the present case p(r)-r for each of 20 radius vectors (as shown in figure B.1) was evaluated and the results are given for the case of fluctuations and no fluctuation in figure B.2.

The collecting area A is given by

$$A = \int_{\theta=0}^{2\pi} \int_{r=0}^{\infty} r d\theta \; dr \; p(r)$$

A measure of the effect of fluctuations on the collecting area for each radius vector is

$$\frac{\int_0^{\infty} rdr\ p(r)}{\int_0^{rmax} rdr} = \frac{\int_0^{\infty} rdr\ p(c)}{\frac{r^2 max}{2}} = \frac{\text{fluctuation collecting area}}{\text{no fluctuation collecting area}} = F$$

Table B.1 shows the values of F for the 20 radius vectors together with the mean value of $\bar{F}$ which shows the effect of sampling density fluctuations on collecting area for a shower of size 3.10^5 particles. It is seen that $\bar{F} = 1.005 \pm 0.068$ which indicates the effect is small. The collecting area assuming no sampling density fluctuation for a vertical shower of size 3.10^5 with s = 1.25 is $3.2.10^3 m^2$ (see figure B.3). A more exact estimate of the collecting area taking the sampling density fluctuations factor $\bar{F}$ into account is

$$3.2.10^3 m^2 \times 1.005 = 3.21.10^3 m^2$$

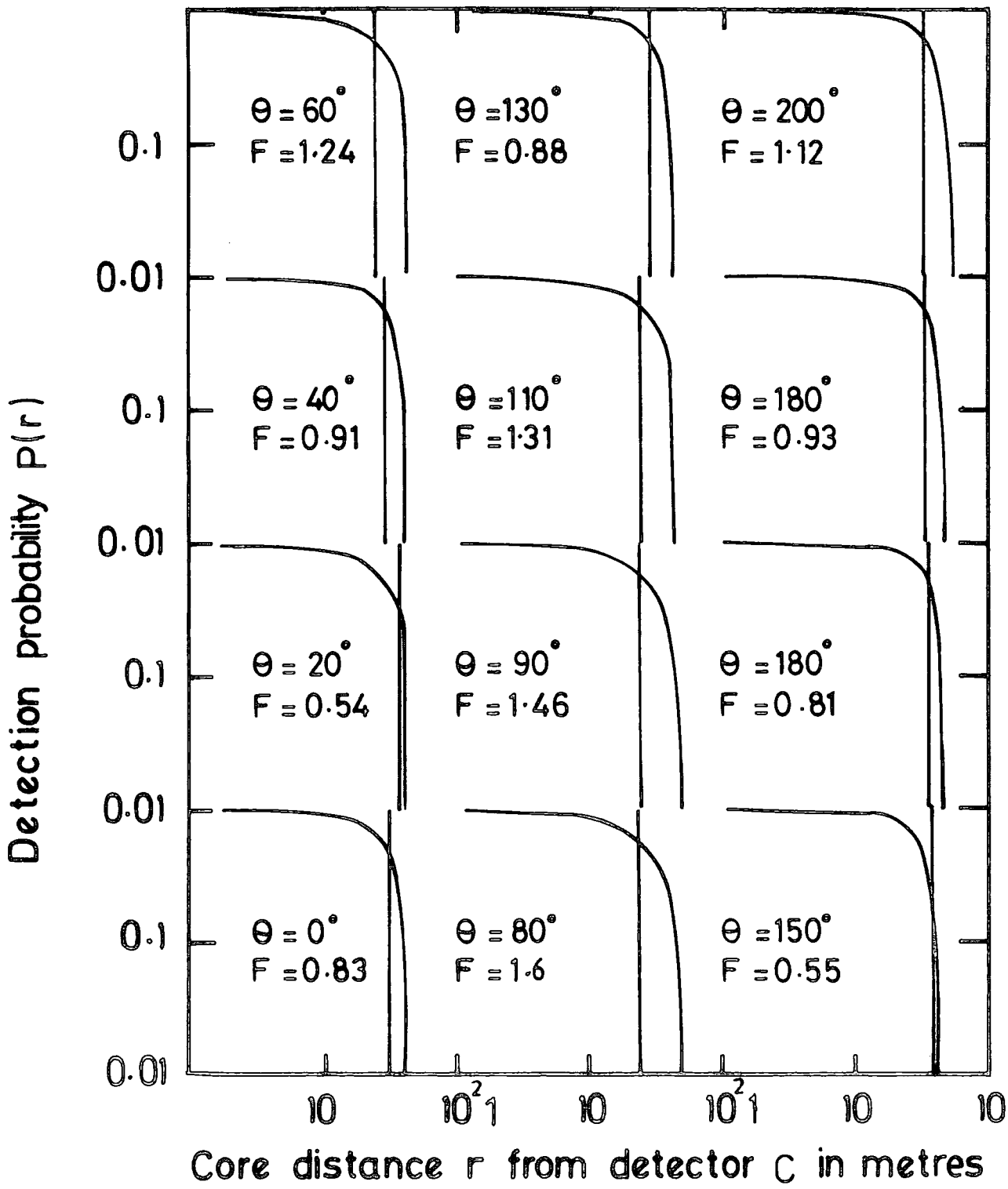

Figure B.2 : Detection probabilities of the outer ring trigger as a function of core distance r from C for a shower of size 3.10^5 particles. The angle refers to different directions of the radius vector as shown in figure B.1.

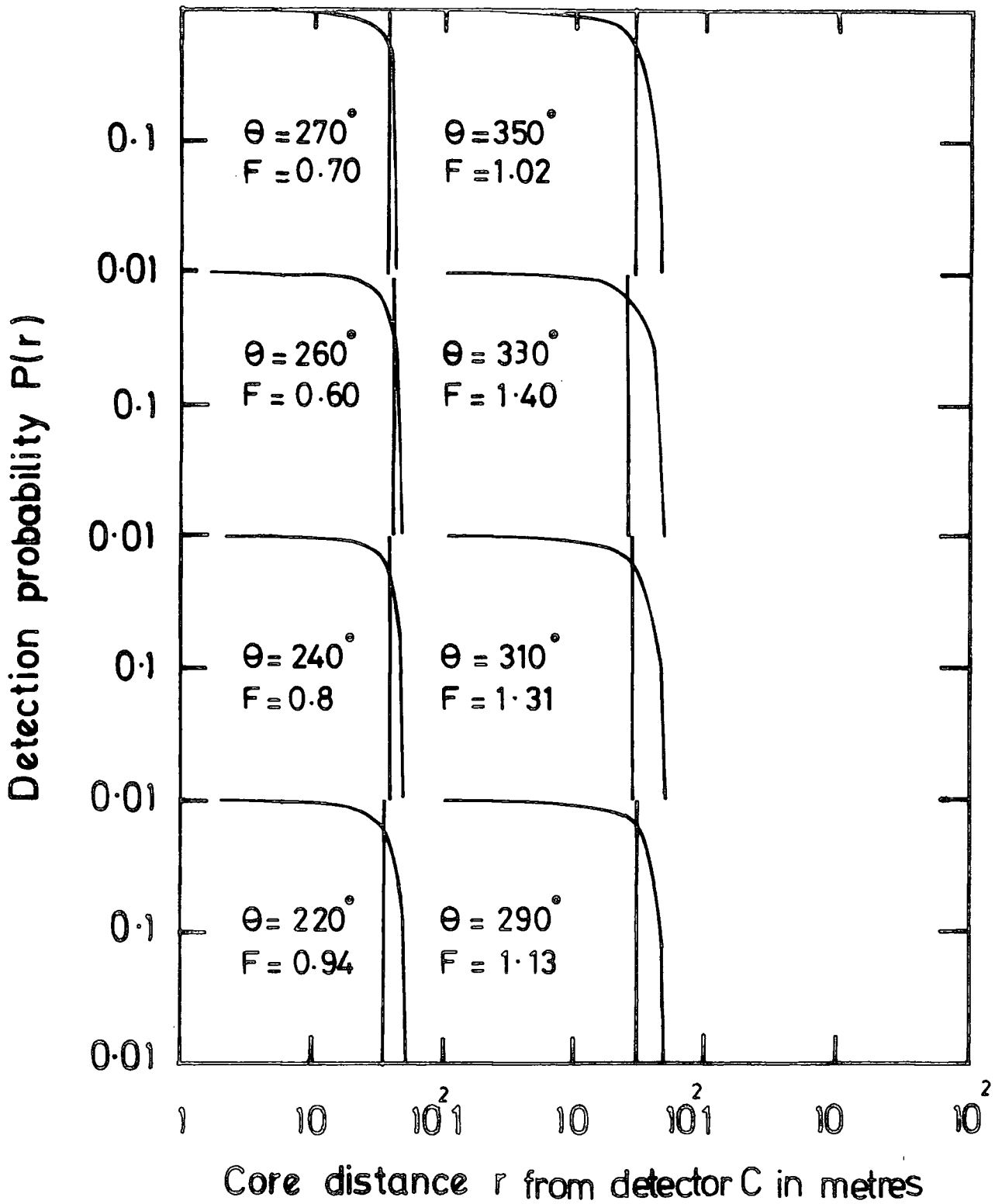

Figure B.2 : continued

$\theta = 0$	$F = 0.83$
$\theta = 20$	$F = 0.57$
$\theta = 40^{o}$	$F = 0.91$
$\theta = 60^{o}$	$F = 1.24$
$\theta = 80^{o}$	$F = 1.6$
$\theta = 90^{o}$	$F = 1.46$
$\theta = 110^{o}$	$F = 1.31$
$\theta = 130^{o}$	$F = 0.86$
$\theta = 150^{o}$	$F = 0.55$
$\theta = 170^{o}$	$F = 0.81$
$\theta = 180^{o}$	$F = 0.93$
$\theta = 200^{o}$	$F = 1.12$
$\theta = 220^{o}$	$F = 0.94$
$\theta = 240^{o}$	$F = 0.8$
$\theta = 260^{o}$	$F = 0.6$
$\theta = 270^{o}$	$F = 0.71$
$\theta = 290^{o}$	$F = 1.13$
$\theta = 310^{o}$	$F = 1.31$
$\theta = 330^{o}$	$F = 1.4$
$\theta = 350^{o}$	$F = 1.02$
	$\bar{F} = 1.005 \pm 0.068$

Table B.1 The value of the radius of fluctuation collecting area to the no fluctuation collecting area F for a shower of size 3.10^5 with s = 1.25 selected by the outer ring selection trigger for the 20 radius vectors shown in figure B.1. The average value of $\bar{F}$ is also given.

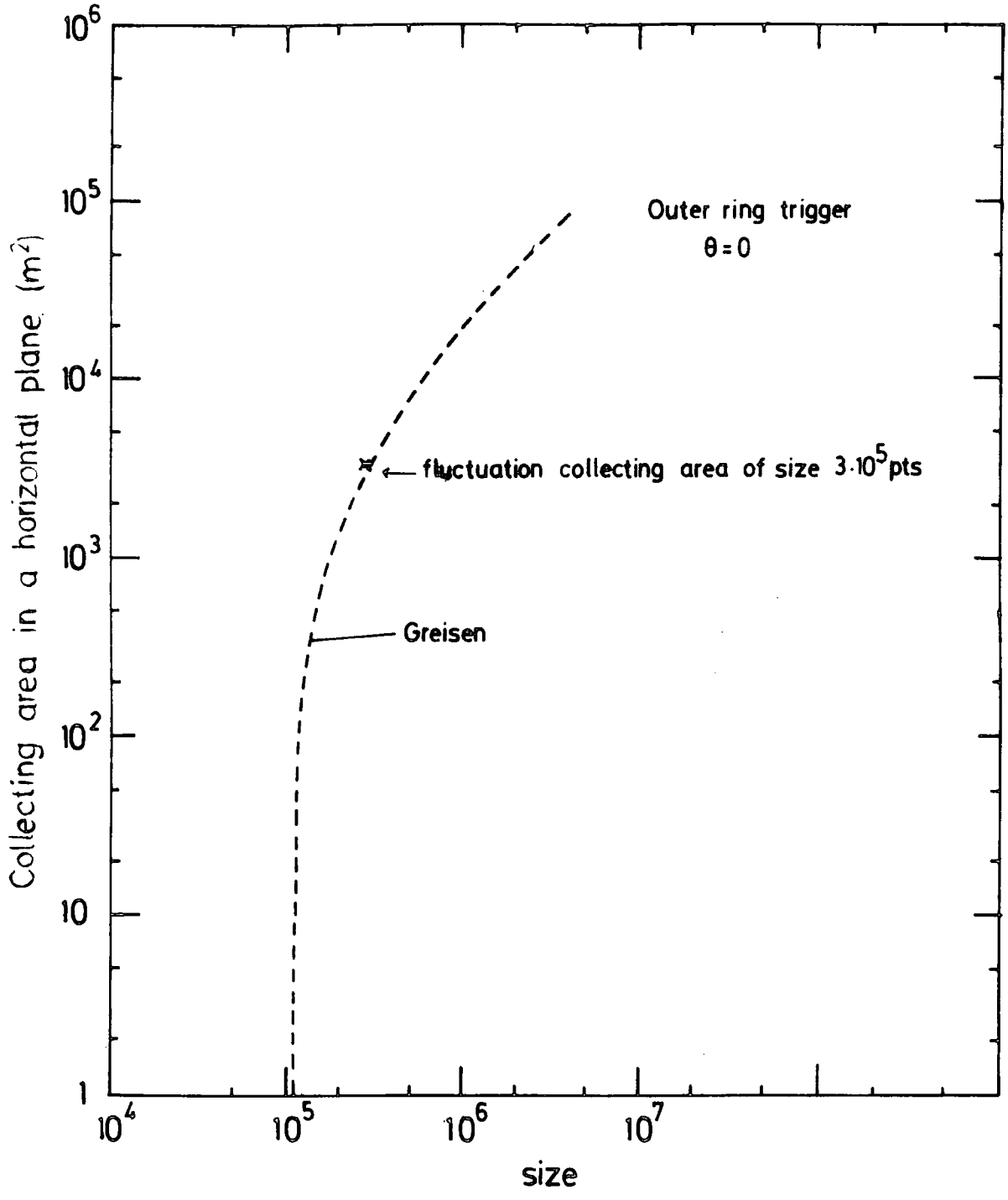

Figure B.3 : The collecting area as a function of shower size for E.A.S. selected by an outer ring trigger. For size 3.10^5 pts the no. fluctuation collecting area as compared with the fluctuation collecting area is marked by a cross.

APPENDIX C

A COMPUTER PROGRAMME USED TO CALCULATE THE EXPECTED NUMBER OF SHOWERS IN GALACTIC COORDINATES

In this programme the formulas given by Presott (1977) were used to determine the right ascension and declination of a shower being incident at zenith (θ) and azimuthal (ϕ) angles. Using these values the galactic longitude and latitude of showers were also carefully determined such that the value and the sign of the relevant angles were fully realized and satisfied table C.1. By knowing the half hour sidereal time simulation data, then, the programme is used to calculate the probability of the shower (which is described in section 6.3.3). Figure C.1 shows the programmes and some of the printout of the expected number of showers in half hour sidereal time intervals. This programme is not fully developed. More commands and ideas could be added to make it more efficient than it is now.

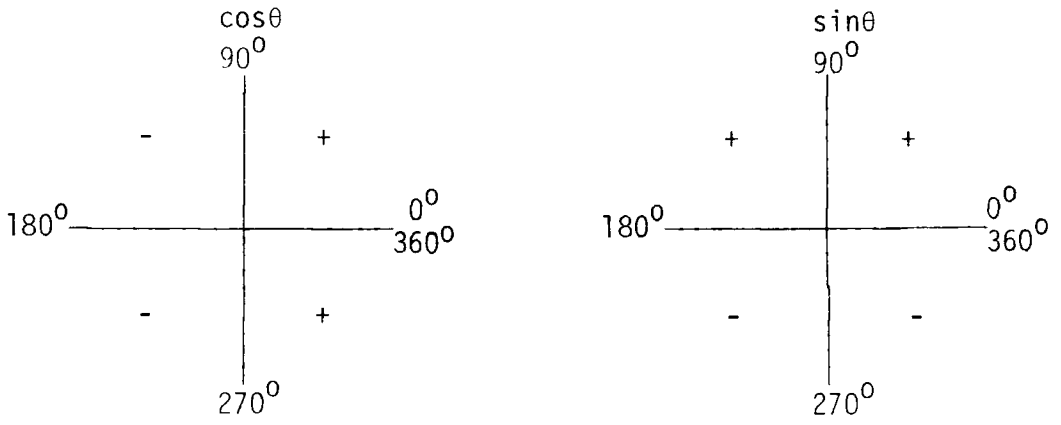

Table C.1.

```
      C *** THIS PROG.CALCULATES THE PROB.OF SHOWER BEING INCIDENT
      C *** AT ZENITH ANGLE THETA AND AZIMUTHAL ANGLE PHI
      C *** DELTA=DECLINATION
      C *** RA=RIGHT ASCENSION
      C *** GLAT=GLACTIC LATITUDE
      C *** GLON=GALACTIC LONGITUDE=Y
      C *** A=PROB.THAT A SHOWER ARRIVES WITH ZENITH ANGLE IN THE RANGE
      C *** THETA->THETA PLUS DELTA THETA AND PHI IN THE RANGE PHI->
      C *** PHI PLUS DELTA PHI
      C *** B=TOTAL NO.OF SHOWERS IN HALF HR.SIDEREAL TIME (ASSUMING SHOWER
      C *** RATE INDEPENDENT OF SIDEREAL TIME)
           DIMENSION XD(48),WAL(48),VAL(13),TAL(19)
           DATA XD/20.12,9.8,0.57,0.31,0.34,0.62,0.69,0.69,0.69,0.62,
          *0.976,1.79,2.0,6.8,9.78,13.78,17.5,16.078,15.85,15.9,16.93,
          *17.54,31.9,68.14,79.3,90.1,87.2,87.2,84.235,84.235,89.0,89.0
          *87.71,87.5,87.2,81.13,71.05,62.07,61.91,58.495,54.9,
          *41.7,28.12,27.38,27.27,24.69,21.76,21.76/
           DO 200 K=1,48,1
           WAL(K)=(K*0.5-0.5)+0.25
           WRITE(6,10)
           WRITE(6,25)WAL(K)
           WRITE(6,30)XD(K)
           WRITE(6,20)
        25 FORMAT(2X,'AVERAGE OF TWO SIDEREAL TIME RANGES(IN HOURS)=',F6.2)
        30 FORMAT(2X,'TOTAL NO.OF SHOWERS IN HALF HR.SIDEREAL TIME=',F8.4)
        20 FORMAT(2X,'PROB..OF SHOWERS BEING INCIDENT AT THETA AND PHI ANGLES
          *')
        10 FORMAT(1X,90( - )
           WRITE(6,40)
           WRITE(6,50)
           WRITE(6,60)
        50 FORMAT(1X,' THETA AVERAGE ',' PHI AVERAGE ',' G.LATIT ','
          *G.LONGI',' PROB.OFSHOWER ',' EXPECTED NO. ')
        60 FORMAT(1X,'I N  D E G R E E S  ','     I N  D E G R E E S
          * ')
        40 FORMAT(1X,90(' -'))
           DO 80 J=1,13,2
           VAL(J)=(J)*5.0
           DO 70 I=1,19,2
           TAL(I)=(I)*18.0
           DELTA=ARSIN(SIN(0.9554)*COS(VAL(J)*0.01745)+COS(0.9554)*
          *SIN(VAL(J)*0.01745)*COS(TAL(I)*0.01745))*57.2956
           H=ARSIN(SIN(VAL(J)*0.01745)*SIN(TAL(I)*0.01745)/
          *COS(DELTA*0.01745))*57.2956
           X=(COS(VAL(J)*0.01745)-SIN(0.9554)*SIN(DEL(A*0.01745))/
          *COS(0.9554)*COS(DELTA*0.01745)
           IF(H .GE. 0.0 .AND. X .GE. 0.0)H=H
           IF(H .GE. 0.0 .AND. X .LE. 0.0)H=180-H
           IF(H .LE. 0.0 .AND. X .LE. 0.0)H=180+ABS(H)
           IF(H .LE. 0.0 .AND. X .GE. 0.0)H=360-ABS(H)
           RA=WAL(K)+H/15
           GLAT=ARSIN(SIN(DELTA*0.01745)*COS(1.0924)-COS(DELTA*0.01745)
          **SIN(RA*15*0.01745-4.9253)*SIN(1.0924))*57.2956
           Y=ARSIN((COS(DELTA*0.01745)*SIN(RA*15*0.01745-4.9253)*
          *COS(1.0924)+SIN(DELTA*0.01745)*SIN(1.0924))/COS(GLAT*0.01745))
          **57.2956
           T=COS(DELTA*0.01745)*COS(RA*15*0.01745-4.9253)/COS(GLAT*0.01745)
           IF(Y .GE. 0.0 .AND. T .GE. 0.0)Y=Y+33
           IF(Y .GE. 0.0 .AND. T .LE. 0.0)Y=213-Y
           IF(Y .LE. 0.0 .AND. T .LE. 0.0)Y=213+ABS(Y)
           IF(Y .LE. 0.0 .AND. T .GE. 0.0)Y=393-ABS(Y)
           IF(Y .BT. 360)Y=Y-360
           A=((10.25/6.2832)*COS(VAL(J)*0.01745)**9.25*(SIN(VAL(J)*0.01745))
          **10.0*0.01745*36.0*0.01745
           B=A*XD(K)
           WRITE(6,90)
           WRITE(6,100)VAL(J),TAL(I),GLAT,Y,A,B
       100 FORMAT(2X,F6.1,12X,F6.1,9X,F6.2,3X,F10.2,5X,F10.4,13X,F6.4)
        90 FORMAT(1X,90('-'))
        70 CONTINUE
           WRITE(6,90)
        80 CONTINUE
       200 CONTINUE
           STOP
           END
```

Figure C.1 : Computer programme used in calculating the expected number of showers in galactic coordinates.

AVERAGE OF TWO SIDEREAL TIME RANGES(IN HOURS)= 0.25
TOTAL NO. OF SHOWERS IN HALF HR.SIDEREAL TIME= 20.1200
PROB..OF SHOWERS BEING INCIDENT AT THETA AND PHI ANGLES

THETA AVERAGE IN DEGREES	PHI AVERAGE IN DEGREES	G.LATIT	G.LONG	PROB.OF SHOWER	EXPECTED NO.
5.0	18.0	-3.03	120.25	0.0150	0.3027
5.0	54.0	-5.14	122.49	0.0150	0.3026
5.0	90.0	-8.17	123.19	0.0150	0.3027
5.0	126.0	-10.96	121.76	0.0150	0.3027
5.0	198.0	-12.03	115.84	0.0150	0.3027
5.0	234.0	-9.89	113.59	0.0150	0.3027
5.0	270.0	-6.85	113.06	0.0150	0.3027
5.0	306.0	-4.08	114.42	0.0150	0.3027
5.0	342.0	-2.62	117.14	0.0150	0.3027
15.0	18.0	6.01	124.54	0.0336	0.6757
15.0	54.0	-0.26	131.24	0.0336	0.6757
15.0	90.0	-9.23	133.15	0.0336	0.6757
15.0	126.0	-17.66	129.45	0.0336	0.6757
15.0	162.0	-22.27	120.95	0.0336	0.6757
15.0	198.0	-20.98	111.17	0.0336	0.6757
15.0	234.0	-14.40	104.46	0.0336	0.6757
15.0	270.0	-5.33	103.12	0.0336	0.6757
15.0	306.0	2.87	107.23	0.0336	0.6757
15.0	342.0	7.22	115.34	0.0336	0.6757
25.0	18.0	15.00	128.97	0.0304	0.6122
25.0	54.0	4.62	139.97	0.0304	0.6122
25.0	90.0	-10.02	143.26	0.0304	0.6122
25.0	126.0	-24.04	137.69	0.0304	0.6122
25.0	162.0	-32.06	123.73	0.0304	0.6122
25.0	198.0	-29.77	105.91	0.0304	0.6122
25.0	234.0	-18.55	94.97	0.0304	0.6122
25.0	270.0	-3.65	93.24	0.0304	0.6122

25.0	306.0	9.77	99.95	0.0304	0.6122
25.0	342.0	17.04	113.45	0.0304	0.6122
35.0	18.0	23.83	133.78	0.0162	0.3262
35.0	54.0	9.38	148.82	0.0162	0.3262
35.0	90.0	-10.50	153.41	0.0162	0.3262
35.0	126.0	-29.94	146.76	0.0162	0.3262
35.0	162.0	-41.79	126.25	0.0162	0.3262
35.0	198.0	-38.32	99.64	0.0162	0.3262
35.0	234.0	-22.21	85.05	0.0162	0.3262
35.0	270.0	-1.87	83.39	0.0162	0.3262
35.0	306.0	16.50	92.37	0.0162	0.3262
35.0	342.0	26.77	111.34	0.0162	0.3262
45.0	18.0	32.68	139.36	0.0051	0.1032
45.0	54.0	13.88	157.90	0.0051	0.1032
45.0	90.0	-10.66	163.58	0.0051	0.1032
45.0	126.0	-35.14	156.90	0.0051	0.1032
45.0	162.0	-51.44	130.08	0.0051	0.1032
45.0	198.0	-46.45	91.73	0.0051	0.1032
45.0	234.0	-25.23	74.63	0.0051	0.1032
45.0	270.0	-0.03	73.56	0.0051	0.1032
45.0	306.0	22.90	84.25	0.0051	0.1032
45.0	342.0	36.66	108.84	0.0051	0.1032
55.0	18.0	41.11	146.09	0.0009	0.0173
55.0	54.0	18.21	167.40	0.0009	0.0173
55.0	90.0	-10.47	173.75	0.0009	0.0173
55.0	126.0	-39.39	168.28	0.0009	0.0173
55.0	162.0	-60.88	135.99	0.0009	0.0173

55.0	198.0	-53.85	81.20	0.0009	0.0173
55.0	234.0	-27.50	63.76	0.0009	0.0173
55.0	270.0	1.81	63.73	0.0009	0.0173
55.0	306.0	29.04	75.31	0.0009	0.0173
55.0	342.0	46.35	105.59	0.0009	0.0173
65.0	18.0	49.03	154.74	0.0001	0.0011
65.0	54.0	21.88	177.26	0.0001	0.0011
65.0	90.0	-10.00	183.89	0.0001	0.0011
65.0	126.0	-42.40	180.90	0.0001	0.0011
65.0	162.0	-69.86	146.73	0.0001	0.0011
65.0	198.0	-59.96	66.62	0.0001	0.0011
65.0	234.0	-28.89	52.53	0.0001	0.0011
65.0	270.0	3.59	53.89	0.0001	0.0011
65.0	306.0	34.32	65.38	0.0001	0.0011
65.0	342.0	55.92	100.94	0.0001	0.0011

REFERENCES

Acharya, B.S., et al (1979), PICCR, Kyoto, 9, 109.

Acharya, B.S., et al (1979), PICCR, Kyoto, 13, 287.

Aguirre, C., et al (1973), PICCR, Denver, 4, 2592.

Alvager, T., et al (1968), Phys. Rev., 171, 1357.

Anderson, C.D., (1932), Science, 76, 238.

Ashton, F., et al (1970), Acta. Phys. Hung., 29, Suppl., 3, 29.

Ashton, F., et al (1973), PICCR, Denver, 4, 2489.

Ashton, F., et al (1977), PICCR, plovdiv, 8, 2, 11, 400.

Ashton, F., et al (1977), PICCR, plovdiv, 12 1.

Bassi, P.C., et al (1953), Phys. Rev., 92, 441.

Baltay, C., et al (1970), Phys. Rev., D1, 759.

Bell, M.C., (1974), Ph.D. Thesis, Durham University.

Berenzinsky, V.S., et al (1969), Phys. Lett. 28B, 423.

Berenzinsky, V.S., et al (1971), Sov.J.Nucl. Phys. 13, 453.

Bilaniuk, O.M., et al (1962), Am.J.Phys. 30, 718.

Bothe, W. and Kalhorter (1929), Z.F.Phys., 56, 751.

Bradt, H., et al (1965), PICCR, London, 2, 715.

Catz, P., et al (1975), PICCR, Munich, 12, 4329.

Chudakov, A.E., et al (1979), PICCR, Kyoto, 8, 217.

Clark, G. W., et al. (1958), Nuovo, Cim. Supp., 8, 623.

Clark, G.W., et al (1961) Phys. Rev., 122, 637.

Clay, J., et al (1927), Proc. Roy. Acad. Amsterdam, 30, 115.

Clay, R.W., et al (1974), Nature, 248, 28.

Cocconi, G., (1961), Handbuch der physik, vol.XLVI/I, 215.

Crouch, P.C., et al (1980), Preprint, University of Adelaide, August, 1980.

De-Beer, T.F., et al (1966), Proc.Phys.Soc., 89, 567.

Dirac P.A.M. (1928), Proc. Roy. Soc. London, A117, 610.

Dixon, H.E., et al (1974), Proc. Roy. Soc., London, A, 339, 171.

Dzikowski, T., et al (1981), PICCR, Paris, 1, 8.

Edge, D.M., et al (1978), J.Phys. G, 4, 113.

Emery, M.W., et al (1975), PICCR, Munich, 2486.

Evans, A., (1971), Ph.D. Thesis, University of Leeds.

Fatemi, J., (1981), Ph.D. Thesis, University of Durham.

Fegan, D.J., et al (1975), PICCR, Munich, 2480.

Fegan, D.J., (1981), PICCR, Paris, 5, 55.

Feinberg, G., (1967), Phys. Rev., 159, 1089.

Feinberg, E.L., (1972), Phys. Rep., 5, 237.

Feldman, L.M., (1974), Am.J.Phys., 42, 179.

Gaisser, T.K., (1974), Nature, 248, 122.

Galbrith, W., (1958), Extensive Air Showers (Butterworths Scientific Publication).

Ginzberg, V.L., et al (1964), The origin of cosmic rays "New York", Pergamon Press.

Gombosi, T., et al (1975), Nature, 255, 687; PICCR, Munich, 2, 587.

Greisen, K., (1956), Prog. In cosmic ray. Phys. III, 1.

Greisen, K., et al (1960), Ann.Rev.Nucl.Sci., 10, 63.

Greisen, K., (1965), PICCR, London, 609.

Greisen, K., (1966), Phys. Rev. Lett., 16, 748.

Hara, T., et al (1979), PICCR, Kyoto, 13, 148.

Hasegawa, H., et al (1962), J. Phys. Soc., Japan, A-III, Supp.17, 189.

Hess, V.F., (1912), Physik., Z, 13, 1084.

Hillas, A.M., (1970), PICCR, Budapest, 3, 539.

Hillas, A.M., (1975), Phys.Rep., 20C, 74.

James, F., et al (1975), Computer Physics communication, 10, 343.

Johnson, H.T., (1932), Phys., Rev., 41, 545.

Julliusson, E., (1975), PICCR, Munich, 8, 2689.

Kamata, K., Nishimura, J., (1952), Prog.Theor.Phys., 1, 185.

Kamata, K., Nishimura, J (1958), Prog.Theor.Phys.Supp.6, 93.

Karakula, S., (1968), See Wdowczyk, J. 1973.

Kempa, J., et al (1974), J.Phys., A, 7, 1213.

Kempa, J., (1976), Nuovo Cimento, 31A, 568.

Kerschenolz, I.M., et al (1971), PICCR, Hobart, 6, 2097.

Khristiansen, G.B., (1972), Preprint, Moscow University.

Khristiansen, G.B., (1974),IZV. Akad, Nauk,SSSR. 38, 1020.

Khristiansen, G.B., (1975), PICCR, Munich, 8, 2801.

Kiraly, P., et al (1979), Nuovo, Cim., 2, N.7,1.

Kitajima, T., et al (1979), PICCR, Kyoto, 11, 158.

Lang, K.R., (1974), Astrophysical Formula, 504.

La-Pointe, M., et al (1968), Can. J.Phys., 46, 568.

Linsley, J., et al (1977), PICCR, Plovdin, 12, 203.

Macleod, G.R., (1956), Nuovo, Cim, III, 118.

McCusker, C.B.A., (1968), Can.J.Phys. 46, 33.

McCusker, C.B.A., (1969), Phys.Rev., 177, 1902.

Meyer, P. et al (1974), Phys.Today, 27, 23.

Miyake, S., et al (1973), PICCR, Denver, 5, 3220.

Nagashima, K., et al (1977), PICCR, plovdiv, 2, 154.

Newton, G.R., (1970), Science, 167, 3925.

Norman, R.J., (1956), Proc. Phys.Soc., 69A, 804.

Paravaresh,A., (1975), Ph.D. Thesis, Durham University.

Peters, B., (1961), Nuovo. Cim., 22, 800.

Powell, C.F., et al (1947), Nature, 160, 453.

Prescott, J.R., (1975), PICCR, Munich, 2474.

Prescott, I.C., (1977), Ph.D. Thesis, Nottingham University.

Ramana, Murthy, P.V., (1971), Lett.Nuovo.Cim., 1, 908.

Recami, E., et al (1974), Rev.De.Nuovo, Cim., 4, 2, 209.

Smart, W.M., (1931), Text book on Spherical Astronomy, University of Cambridge.

Smith, A.C., (1976), Ph.D. Thesis, Durham University.

Smith, A.C., (1978), Nucl.,Inst., and Methods.148, 521.

The Astronomical Ephemeris, 1977, H.M.S.O., London, 526.

The Europhysics Study Conference, (1979), Gamma-ray astronomy after Cos-B, by B.N.Swanenburg.

The Fourth UHURU Catalog of X-ray sources, by W. Forman, (1978) Centre for Astrophysics, No.763, Harvard College Observatory.

Trumper, J., (1969), PICCR, Budapest, Invited papers, 497.

Vernov, S.N., et al (1968), Cana. J.Phys., 46, S197.

Vernov, S.N., et al (1970), Acta. Phys. Hung., 29, Supp., 3, 429.

Wdowczyk, J., et al (1973), PICCR, Denver, 4, 2605.

Wdowczyk, J., (1973), Cosmic Rays at ground level, Ed.Wolfendale, A.W., (Inst.of Physics).

Williams, R.W., (1948), Phys.Rev., 74, 1689.

Wolfendale, A.W. (1973), Cosmic ray at ground level.

Additional references

Abdullah, M.M., et al (1979), PICCR, Kyoto, 8, 258.

Abdullah, M.M., et al (1979), PICCR, Kyoto, 13, 255.

Abdullah, M.M., et al (1981), PICCR, Paris, 6. 151.